Adıyaman University
Journal of Science

Dec. 2020

Volume: 10 Issue: 2

An international peer reviewed journal of science

PHYSIC
SCIENCE
BIOLOGY
CHEMISTRY
MATHEMATICS

ADYU J SCI

ISSN 2147-1630
e-ISSN 2146-586X

An open access, peer reviewed, international journal of science. Biannual (June & December). ISSN 2147-1630 | e-ISSN 2146-586X. Publisher: Adıyaman University.

Publication language: English (with Turkish title and abstract)

Issue published date: 30.12.2020

Privilege owner: On Behalf of Rectorate of Adıyaman University, Prof. Dr. Mehmet TURGUT (Rector)

Web site: EN: https://dergipark.org.tr/en/pub/adyujsci
TR: https://dergipark.org.tr/tr/pub/adyujsci

Table of Contents (İçindekiler)

Volume (Cilt): 10 Number (Sayı): 2
December (Aralık) 2020

BIOLOGY

CHEMISTRY

MATHEMATICS

Adıyaman University Journal of Science
https://dergipark.org.tr/en/pub/adyujsci
DergiPark AKADEMİK
ISSN 2147-1630
e-ISSN 2146-586X

Effect of Angiogenesis Related Growth Factors VEGF-a and FGF-1 on Osteosarcoma Cell Proliferation

Meltem ALPER[1,*]

[1]*Aksaray University, Department of Botanical and Animal Production, Aksaray, Turkey*
meltemalper@aksaray.edu.tr, ORCID: 0000-0001-6359-9979

Received: 12.06.2020 **Accepted:** 10.09.2020 **Published:** 30.12.2020

Abstract

Osteosarcoma is the most common bone tumor in children and adolescents. Alterations in the expression of some genes, cytokines and growth factors are responsible for the development of the malignant phenotype in osteosarcoma. Some members of the VEGF and FGF families have been associated with poor prognosis and the metastasis in various tumor types including osteosarcoma. Among the members of the family, information about effects of VEGF-a and FGF-1 on osteosarcoma cell proliferation is limited.

In the present study, it was aimed to elucidate the effects of VEGF-a and FGF-1 on osteosarcoma cell proliferation. Saos-2 cells, having osteoblastic features, were used for osteosarcoma model. Cells were treated 20 ng/mL VEGF-a and FGF-1 after 24 hours of serum starvation. MTT assay was applied to measure cell viability after incubation for 1-72 hours. Results indicated that VEGF-a promoted cell proliferation for all incubation times. Maximum increase was observed after 48 hours of incubation (1.7 fold) with a statistically important manner. FGF-1 led to very slight increase in Saos-2 cell proliferation. Consequently, these findings can contribute development of new therapy strategies for osteosarcoma.

Keywords: Osteosarcoma; Saos-2; MTT; VEGF-a; FGF-1.

* Corresponding Author DOI: 10.37094/adyujsci.751882

Anjiyogenez Bağlantılı Büyüme Faktörleri VEGF-a ve FGF-1'in Osteosarkoma Hücre Proliferasyonu Üzerine Etkileri

Öz

Osteosarkoma çocuklar ve ergenlerde en sık görülen kemik tümörüdür. Bazı genlerin, sitokinlerin ve büyüme faktörlerinin ekspresyonundaki değişiklikler osteosarkomada malign fenotipin gelişiminden sorumludur. VEGF ve FGF ailelerinin bazı üyeleri, osteosarkomayı da içeren çeşitli tümör tiplerinde kötü prognoz ve metastaz ile ilişkilendirilmiştir. Ailenin üyelerinden VEGF-a ve FGF-1'in osteosarcoma hücre proliferasyonuna olan etkileri hakkında bilgiler sınırlıdır.

Bu çalışmada VEGF-a ve FGF-1'in osteosarkoma hücre proliferasyonu üzerindeki etkilerinin aydınlatılması amaçlanmıştır. Osteosarkoma modeli olarak osteoblastik özelliklere sahip Saos-2 hücreleri kullanıldı. Hücreler, 24 saatlik serum açlığından sonra 20 ng/mL VEGF-a ve FGF-1 ile muamele edildi. 1-72 saat inkübasyon süresinden sonra hücre canlılığını ölçmek için MTT testi uygulandı. Sonuçlar VEGF-a'nın tüm inkübasyon süreleri için hücre proliferasyonunu arttırdığını gösterdi. Maksimum artış, istatistiksel olarak anlamlı bir şekilde, 48 saatlik inkübasyon (1.7 kat) süresinden sonra gözlendi. FGF-1, Saos-2 hücre proliferasyonunda çok küçük bir artışa yol açtı. Sonuç olarak, bu bulgular osteosarkom için yeni tedavi stratejilerinin geliştirilmesine katkıda bulunabilir.

Anahtar Kelimeler: Osteosarkoma; Saos-2; MTT; VEGF-a; FGF-1.

1. Introduction

Osteosarcoma is a highly malignant primary bone tumor characterized by aggressive growth and early metastatic potential, which mainly affects children and adolescents [1-5]. Immature bone or osteoid tissue formation are characteristic features of the osteosarcoma. Lung and bone are the most common metastasis sites [6, 7]. Metastasis leads to poor prognosis for tumor progression. Current therapies have quite a few effects on metastatic osteosarcoma patients [8, 9]. Therefore, elucidation of the molecular mechanisms underlying osteosarcoma pathogenesis and metastasis may be beneficial for developing more effective treatment strategies [10]. Cells with different levels of differentiation lead to heterogeneous tissue formation in bone. Tissue heterogeneity is closely related to the success of the response to treatment. Cytokines can affect cancer formation, progression, and metastasis at different stages [1, 11, 12]. While some cytokines have been used for cancer treatment, some of them contribute to advanced cancer development

[13-16]. Understanding of the cytokine networks in oncogenesis has prognostic importance for the course and progression of osteosarcoma [17].

Vascular endothelial growth factor (VEGF) is a member of a large growth factor family and has a critical function for the induction of the angiogenesis. Angiogenesis is a key regulator for tumor development and metastasis. It has been shown that increased VEGF expression is related to poor prognosis in many tumor types [18-26]. It has been reported that VEGF variants and their receptors were expressed in osteosarcoma cells and promote tumor angiogenesis [27-29].

FGF-1 (Fibroblast Growth Factor) is another important factor related to tumorigenesis, epithelial-to-mesenchymal transition, as well as invasion and metastasis. Dysregulation of the FGF receptors has been reported in many cancer types such as urothelial carcinoma, hepatoma, ovarian cancer, and lung adenocarcinoma. Clinical studies have been indicated that blocking the FGF/FGFR signaling may enable the development of a new strategy for the treatment of various human cancers. Therefore, numerous FGFR inhibitors were developed for therapy [30-33]. The effect of some FGF family members on osteosarcoma progression has been investigated so far. For instance, it has been reported that upregulation of the FGF-5 induces osteosarcoma cell proliferation [34].

Although critical functions of some cytokines have been determined on the pathogenesis of the osteosarcoma, little is known about angiogenesis-related growth factors VEGF-a and FGF-1 on the contribution of osteosarcoma proliferation. The current study is aimed to investigate the antiproliferative effect of these growth factors on osteosarcoma. Saos-2 cell model, displaying osteoblastic features, was used for proliferation studies. Cells were treated 20 ng/mL of VEGF-α and FGF-1 and cell viability was measured using the MTT method. Our findings will provide new insights for the development of new therapeutic approaches for osteosarcoma.

2. Materials and Methods

2.1. Cells and reagents

Saos-2 (Human osteosarcoma) cell line was a gift from Dr. Kenneth Wann (Cardiff, School of Biosciences, Cardiff UK). Cell culture media and reagents; DMEM (Dulbecco's Modified Eagle's Medium) and PBS (Phosphate Buffer Saline) tablets were purchased from Sigma, FCS (Fetal Calf Serum) was purchased from Invitrogen, VEGF-a and FGF-1 were purchased from Peprotech, MTT (Thiazolyl Blue Tetrazolium Bromide) and other chemicals that were used in the study were purchased from Sigma.

2.2 Cell culture and MTT assay

Saos-2 cells were grown in DMEM containing 10 % FCS and 2 mM L-Glutamine and maintained in a humidified incubator at 37˚C containing 5 % (v/v) CO_2 in air. The effect of VEGF-a and FGF-1 on cell viability was assessed by the MTT method. Briefly, Saos-2 cells were plated out in 96-well plastic plates at a concentration of $5x10^4$ cells per well and stimulated with 20 ng/mL of VEGF-a and FGF-1 for 1, 24, 48, and 72 h. Untreated groups were used as control. MTT solution was added to the cells after indicated incubation time intervals. Formazan crystals were solubilized with 200 µl Isopropanol including 0.01% per well and the optical density (OD) at 550 nm was measured with a spectrophotometric microplate reader (Thermo Scientific). The mean OD value of the control groups was subtracted from the OD value of each cytokine treated groups for all incubation times. Experiments were performed for three times [35].

2.2 Statistical analysis

Statistical analyses were performed using Mini Tab 14. Standard deviations and p values were calculated using One-way Anova analysis. Statistical significance was taken as $p \leq 0.05$. Data are representative of average results from independent experiments carried out at least three times and are expressed as the mean ± standard deviation [36].

3. Results

3.1 Effect of VEGF-a and FGF-1 on Saos-2 cell proliferation

To determine the effect of VEGF-a and FGF-1 on osteosarcoma proliferation we used Saos-2 (Sarcoma osteogenic) cell line for *in vitro* model. These cells are well characterized primary osteosarcoma model that is commonly used in bone cancer research for the late osteoblastic differentiation stage [37, 38]. Cells were serum-starved for 24 h using 0.1% BSA before the growth factor treatment to observe the effect more clearly. Saos-2 cells were treated with 20 ng/mL of VEGF-a and FGF-1 for 1-72 hours. MTT analysis was performed as described in Section 2.2 after indicated time intervals. VEGF-a treatment increased Saos-2 cell proliferation for all time intervals. According to statistical analysis, a maximum increase in cell proliferation was observed after 48 hours of incubation (1.7-fold).

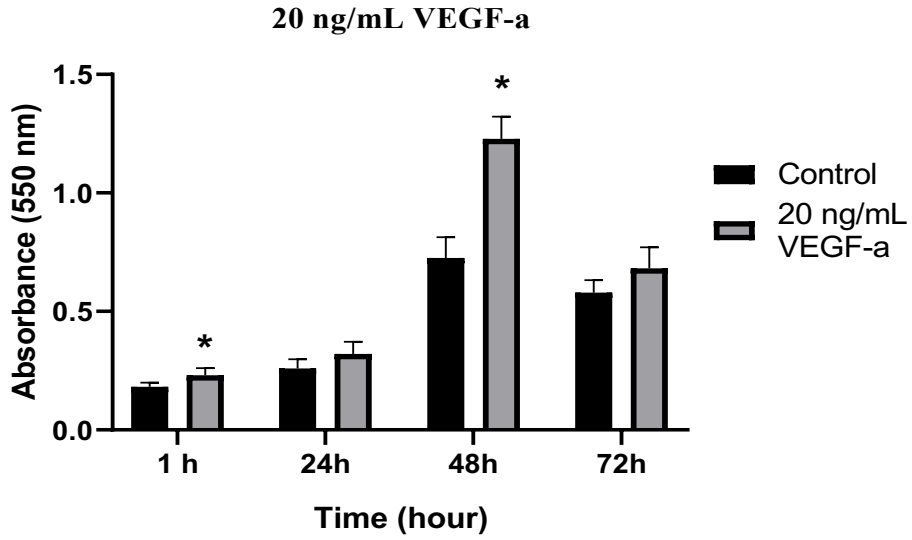

Figure 1: Effect of 20 ng/mL of VEGF-a treatment on Saos-2 cell proliferation. Untreated cells were used as the control for 1, 24, 48, and 72 h. Statistical analysis was carried out by ANOVA (one way) (Statistical significance was taken as * $p \leq 0.05$). The image shown is average results from independent experiments carried out at least three times

We also assessed the proliferative effect of the other angiogenesis-related growth factor FGF-1 on Saos-2 cells by MTT as described above. Treatment of the Saos-2 cell with 20 ng/mL of FGF-1 led to a very slight increase in cell proliferation. A maximum increase was observed after 72 hours of incubation (1.2 fold).

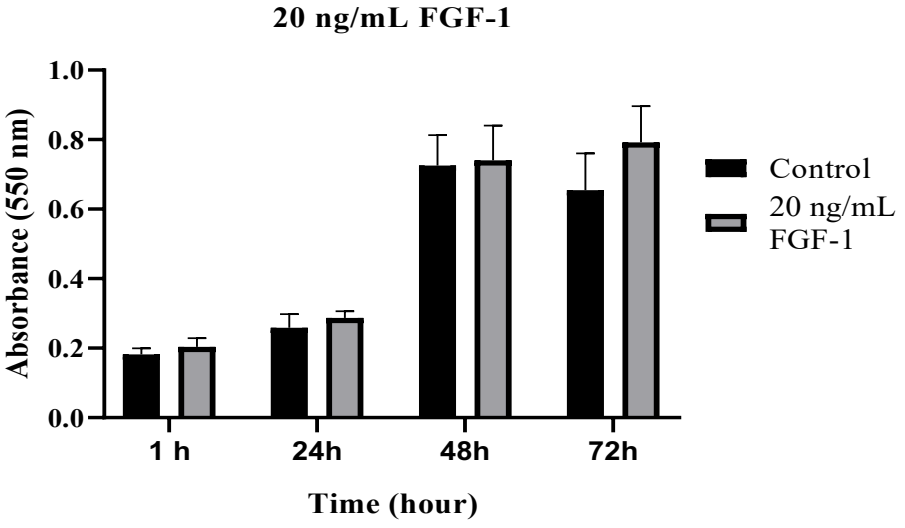

Figure 2: Effect of 20 ng/mL of FGF-1 treatment on Saos-2 cell proliferation. Untreated cells were used as control groups for the indicated time. The p-value was calculated by ANOVA (one way) analysis ($p > 0.05$). The image shown is the average results from independent experiments carried out at least three times

4. Discussion

The development of new blood capillaries is an important issue for tumor growth and metastasis [1]. Angiogenesis involves whole processes of the malignant osteosarcoma. VEGF, aFGF and bFGF are angiogenesis-related growth factors and released from tumor tissues and contribute to tumor progression. They have the ability to stimulate angiogenesis under hypoxic conditions. VEGF promotes cell migration by initiating a variety of signaling pathways. It is also a mediator of vessel permeability and enables endothelial progenitor cells to migrate from the bone marrow to neovascularization sites. It has been reported that increased VEGF production is important in the growth of solid tumors including osteosarcoma. Peng and colleagues were determined that silencing of the VEGF inhibited osteosarcoma growth and angiogenesis in Wistar rat model. Besides, they were established that the silencing of VEGF expression could promote apoptosis in Saos-2 cells [29, 39]. VEGF-a mainly conducts its pro-angiogenic activities through VEGFR-2 (VEGF receptor 2). Because of its critical role in tumor angiogenesis, the VEGF/VEGFR pathway has become a therapeutic target in cancer research [39, 40].

The human FGF family includes 23 members and they are expressed in many tissues. FGFs regulate a broad spectrum of physiological and pathological processes, including development, wound healing and neoplastic transformation. Further, FGFs play important roles in tumorigenesis increasing cell migration and invasion. For instance, FGF2, has angiogenic potential and promote tumor angiogenesis [42]. Shimizu and colleagues have determined that FGF-2 has function maintaining the aggressive profile of the osteosarcoma affecting cellular immaturity They have suggested that blocking of growth factor signaling pathways including FGF-2, might be useful in controlling the aggressiveness of osteosarcoma [1]. Han and colleagues reported a significant upregulation in FGF-5 expression levels in osteosarcoma cell models and patient tissues, compared to control cells and healthy tissues. Further, they presented evidence on FGF5 promoted osteosarcoma cell proliferation [34]. The FGFs promote tumor progression through specific (FGFR) FGF receptor signaling. The expression of *FGFR* genes has been detected in osteosarcoma, such as *FGFR1*, *FGFR2,* and *FGFR3*. However, the expression profile of FGFRs differs among the osteosarcoma cell models. FGFR1 expression is associated with poor response to chemotherapy in osteosarcoma. High expression levels of FGF2 and its receptor FGFR3 have been found in osteosarcoma and are significantly related with poor prognosis [4].

FGF1 has been determined as a proliferative factor for human preadipocytes and IEC-6, Caco-2, and HT-29 cell lines [43]. Although the proliferative effects of FGFs on different cell types have been studied, the effect of FGF-1 on osteosarcoma cell proliferation is unknown.

Because of the critical roles of the VEGF and FGF family on tumor growth and progression antiproliferative effect of these growth factors on the osteosarcoma was assessed. VEGF-a promoted Saos-2 cell proliferation gradually up 1.7 fold for 48 hours. This proliferative effect was started to decrease after 72 hours of incubation. FGF-1 had a slight effect on the proliferation of the osteosarcoma cells. In conclusion, in this work, we demonstrated that treatment of Saos-2 osteosarcoma cell with VEGF-a and FGF-1 in the absence of other growth factors activated cellular proliferation. These effects could contribute to the poor prognosis of osteosarcoma. Overexpression and/or silencing studies will provide more direct evidence for the contribution of these factors to osteosarcoma development.

Acknowledgement

Saos-2 cells were kindly provided by Dr. Kenneth Wann and (Cardiff, School of Biosciences, Cardiff UK).

References

[1] Shimizu, T., Ishikawa, T., Iwai, S., Ueki, A., Sugihara, E., Onishi, N., Kuninaka, S., Miyamoto, T., Toyama, Y., Ijiri, H., Mori, H., Matsuzaki, Y., Yaguchi, T., Nishio, H., Kawakami, Y., Ikeda, Y., Saya, H., Fibroblast growth factor-2 is an important factor that maintains cellular immaturity and contributes to aggressiveness of osteosarcoma, Molecular Cancer Research, 10, 454–468, 2012.

[2] Bielack, S.S., Kempf-Bielack, B., Delling, G., Exner, G.U., Flege, S., Helmke, K., Kotz, R., Salzer-Kuntschik, M., Werner, M., Winkelmann, W., Zoubek, A., Jürgens, H., Winkler, K., Prognostic factors in high-grade osteosarcoma of the extremities or trunk: an analysis of 1,702 patients treated on neoadjuvant cooperative osteosarcoma study group protocols, Journal of Clinical Oncology, 20,776–90, 2002.

[3] Clark, J.C.M., Dass, C.R., A review of clinical and molecular prognostic factors in osteosarcoma, Jornal of Cancer Research and Clinical Oncology,134, 281–97, 2008.

[4] Zhou, W.Y., Zheng, H., Du, X.L., Yang, J.L., Characterization of FGFR signaling pathway as therapeutic targets for sarcoma patients, Cancer Biology and Medicine, 13,260–8, 2016.

[5] Baird, K., Davis, S., Antonescu, C.R., Harper, U.L., Walker, R.L., Chen, Y., Glatfelter, A.A., Duray, P.H., Meltzer, P.S., Gene expression profiling of human sarcomas: Insights into sarcoma biology, Cancer Research, 65, 9226-35,2005.

[6] Xu, C.J., Song, J.F., Su, Y.X., Liu, X.L., Expression of b-FGF and endostatin and their clinical significance in human osteosarcoma, Orthophedic Surgery, 2, 291– 8, 2010.

[7] Berhe, S., Danzer, E., Meyer, P., Behr, G., LaQuaglia, M.P., Price, A.P., Unusual abdominal metastases in osteosarcoma, Journal of Pediatric Surgery Case Reports, 28, 13–16, 2018

[8] Shih, C.H., Chiang, T.B., Wang, W.J., Synergistic suppression of a disintegrin acurhagin-C in combination with AZD4547 and reparixin on terminating development for human osteosarcoma MG-63 cell, Biochemical and Biophysical Research Communications, 492, 513-519,2017.

[9] Mirabello, L., Troisi, R.J., Savage, S.A., International osteosarcoma incidence patterns in children and adolescents, middle ages and elderly persons, International Jornal of Cancer, 125, 229-234, 2009.

[10] Li, Y., Zhang, J., Ma, D., et al., Curcumin inhibits proliferation and invasion of osteosarcoma cells through inactivation of Notch-1 signaling, FEBS Journal, 279(12), 2247–2259, 2012.

[11] Goldszmid, R.S., Trinchieri, G., The price of immunity, Nature Immunology, 13, 932-938, 2012.

[12] Turtle, C.J., Hudecek, M., Jensen, M.C., Riddell, S.R., Engineered T cells for anti-cancer therapy, Current Opinion in Immunology 24, 633-639, 2012.

[13] Dunlop, R.J., Campbell, C.W., Cytokines and advanced cancer, Journal of Pain and Symptom Management, 20 (3) ,214-232, 2000.

[14] Negus, R.P.M., Balkwill, F.R., Cytokines in tumour growth, migration and metastasis, World Journal of Urology, 14,157–165, 1996.

[15] Zumkeller, W., Schofield, P.N., Growth factors, cytokines and soluble forms of receptor molecules in cancer patients, Anticancer Research, 15, 344–348,1995.

[16] Fridman, W.H., Tartour, E., The use of cytokines in the treatment of solid tumours, Haematolgy, Transfusion and Cell Therapy, 39,105–108, 1997.

[17] Savitskaya, Y.A., Rico-Martínez, G., Linares-González, L.M., Delgado-Cedillo, E.A., Téllez-Gastelum, R., Alfaro-Rodríguez, A.B., Redón-Tavera, A., & Ibarra-Ponce de León, J.C., Serum tumor markers in pediatric osteosarcoma: a summary review, Clinical Sarcoma Research, 2, 9, 2012

[18] Koch., S., Claesson-Welsh, L., Signal transduction by vascular endothelial growth factor receptors, Cold Spring Harbor Perspectives in Medicine, 2, a006502, 2012.

[19] Carmeliet, P., Jain, R.K., Angiogenesis in cancer and other diseases, Nature 407, 249–257, 2000.

[20] Folkman, J., Role of angiogenesis in tumor growth and metastasis, Seminars in Oncology, 29, 15–18, 2002.

[21] Ferrara, N., Carver-Moore, K., Chen, H., Dowd, M., Lu, L., O'Shea, K.S., Powell-Braxton, L., Hillan, K.J., Moore, M.W., Heterozygous embryonic lethality induced by targeted inactivation of the VEGF gene, Nature, 380,439-442, 1996.

[22] Ahluwalia, A., Jones, M.K., Matysiak-Budnik, T., Tarnawski, A.S., VEGF and colon cancer growth beyond angiogenesis: does VEGF directly mediate colon cancer growth via a non-angiogenic mechanism?, Current Pharmaceutical Design, 20,1041-1044, 2014.

[23] Hata, K., Watanabe, Y., Nakai, H., Hata, T., Hoshiai, H., Expression of the vascular endothelial growth factor (VEGF) gene in epithelial ovarian cancer: an approach to anti-VEGF therapy, Anticancer Research, 31, 731-737, 2011.

[24] Yu, X.W., Wu, T.Y., Yi, X., Ren, W.P., Zhou, Z.B., Sun, Y.Q., Zhang, C.Q., Prognostic significance of VEGF expression in osteosarcoma: a meta-analysis, Tumor Biology, 35,155-160, 2014.

[25] Zhuang, Y., Wei, M., Impact of vascular endothelial growth factor expression on overall survival in patients with osteosarcoma: a meta-analysis, Tumor Biology, 35, 1745-1749, 2014.

[26] Han, G., Wang, Y., Bi, W., Jia, J., Wang, W., Xu, M., Effects of vascular endothelial growth factor expression on pathological characteristics and prognosis of osteosarcoma, Clinical and Experimental Medicine, 16(4), 577-584, 2016.

[27] Matsumoto, G., Hirohata, R., Hayashi, K., Sugimoto, Y., Kotani, E., Shimabukuro, J., Hirano, T., Nakajima, Y., Kawamata, S., Mori, H., Control of angiogenesis by VEGF and endostatin-encapsulated protein microcrystals and inhibition of tumor angiogenesis, Biomaterials, 35, 1326-33, 2014.

[28] Baptista, A.M., Camargo, A.F., Filippi, R.Z., Oliveira, C.R., Azevedo Neto, R.S., Camargo, O.P., Correlation between the expression of vegf and survival in osteosarcoma, Acta Ortopedica Brasileria, 22, 250-5,2014

[29] Peng, N., Gao, S., Guo, X., Wang, G., Cheng, C., Li, M., & Liu, K., Silencing of VEGF inhibits human osteosarcoma angiogenesis and promotes cell apoptosis via VEGF/PI3K/AKT signaling pathway, American Journal of Translational Research, 8(2),1005–1015, 2016.

[30] Dai, S., Zhou, Z., Chen, Z., Xu, G., Chen, Y., Fibroblast Growth Factor Receptors (FGFRs): Structures and Small Molecule Inhibitors, Cells, 8(6), 614, 2019.

[31] Ramos, C., Becerril, C., Montano, M., Garcia-De-Alba, C., Ramirez, R., Checa, M., Pardo, A., Selman, M., FGF-1 reverts epithelial mesenchymal transition induced by TGF-{beta}1 through MAPK/ERK kinase pathway, American Journal of Physiolgy Lung Cellular and Molecular Physiolgy, 299, L222-31, 2010.

[32] Jouanneau, J., Plouet, J., Moens, G., Thiery, J.P., FGF-2 and FGF-1 expressed in rat bladder carcinoma cells have similar angiogenic potential but different tumorigenic properties in vivo, Oncogene, 14, 671-6, 1997.

[33] Chudzian, J., Szlachcic, A., Zakrzewska, M., Czub, M., Pustula, M., Holak, T.A., Otlewski, J., Specific Antibody Fragment Ligand Traps Blocking FGF1 Activity, International Journal of Molecular Sciences, 19 (9),2470, 2018.

[34] Han, D., Wang, M., Yu, Z., Yin, L., Liu, C., Wang, J., Liu, Y., Jiang, S., Ren, Z., Yin, J., FGF5 promotes osteosarcoma cells proliferation via activating MAPK signaling pathway. Cancer management and research, 11, 6457–6466, 2019.

[35] Tokay, E., Kockar F., Identification of intracellular pathways through which TGF-β1 upregulates URG-4/URGCP gene expression in hepatoma cells, Life Sciences, 144, 121-128, 2016

[36] Kim, H.Y., Analysis of variance (ANOVA) comparing means of more than two groups. Restorative dentistry & endodontics, 39(1), 74–77, 2014.

[37] Fogh, J., Fogh, J.M., Orfeo, T., One hundred and twenty-seven cultured human tumor cell lines producing tumors in nude mice, Journal of the National Cancer Institute, 59(1), 221–226, 1977.

[38] McQuillan, D.J., Richardson, M.D., Bateman, J.F., Matrix deposition by a calcifying human osteogenic sarcoma cell line (SAOS- 2), Bone, 16 (4), 415–26, 1995.

[39] Lu, X., Tao, J., Wei, G., Anti-angiogenesis target therapy for advanced osteosarcoma, Oncology Reports, 38,625-636, 2017.

[40]. Hicklin, D.J., Ellis, L.M., Role of the vascular endothelial growth factor pathway in tumor growth and angiogenesis, Journal of Clinical Oncology, 23, 1011–1027, 2005.

[41] Gazdar, A.F., Kadoyama, C., Venzon, D., Park, J.G., Tsai, C.M., Linnoila, R.I., Mulshine, J.L., Ihde, D.C., Giaccone, G., Association between histological type and

neuroendocrine differentiation on drug sensitivity of lung cancer cell lines, Journal of National Cancer Institute Monographs 13, 191-196, 1992.

[42] Kwabi-Addo, B., Ozen, M., Ittmann, M., The role of fibroblast growth factors and their receptors in prostate cancer, Endocrine-Related Cancer., 11(4):709-724, 2004

[43] Yun, Y.R., Won, J.E., Jeon, E., Lee, S., Kang, W., Jo, H., Jang, J.H., Shin, U. S., Kim, H.W., Fibroblast growth factors: biology, function, and application for tissue regeneration, Journal of tissue engineering, 2010: 218142, 2010.

Adıyaman University Journal of Science
https://dergipark.org.tr/en/pub/adyujsci
DergiPark AKADEMİK
ISSN 2147-1630
e-ISSN 2146-586X

Cloning of ADAMTS2 Gene and Colony Formation Effect of ADAMTS2 in Saos-2 Cell Line Under Normal and Hypoxic Conditions

Sümeyye AYDOGAN TÜRKOĞLU[1,*], Sinem GÜLTEKİN TOSUN[2]

[1]*Balıkesir University, Faculty of Science and Literature, Department of Molecular Biology and Genetics, Balıkesir, Turkey*
saydogan@balikesir.edu.tr, ORCID: 0000-0003-1754-0700
[2]*Erciyes University, Institute of Health Sciences, Faculty of Veterinary Medicine, Department of Genetics, Kayseri, Turkey*
sinemgultekin@outlook.com, ORCID: 0000-0002-3927-0089

Received: 03.05.2020 **Accepted:** 25.09.2020 **Published:** 30.12.2020

Abstract

ADAMTS2 (a disintegrin and metalloproteinase with thrombospondin motifs 2), an N-propeptidase isoenzyme, is an enzyme involved in collagen biosynthesis by providing the amino ends of procollagen to be cut away. ADAMTS2 has anti-angiogenic activity as well as provides the processing of collagen. With this activity, it has become a target in cancer studies. Hypoxic regulation is a process that affects the expression of a large number of genes at the cellular level. Within the scope of our study, the cloning of the ADAMTS2 gene and its expression in Saos-2 (human bone carcinoma) cell line were performed ectopically. For this purpose, the transient transfection of the expression vector containing ADAMTS2 coding sequence was transfected by the calcium-phosphate precipitation method. Recombinant ADAMTS2 mRNA expression was checked by Real-Time PCR in Saos-2 cells. It was observed that there was a 50-fold increase in ADAMTS2 mRNA expression in the transfected Saos-2 cells compared to the control group. Then, the effect of recombinant ADAMTS2 on the colony-forming potential of Saos-2 cells was investigated in both normal and chemically induced hypoxic conditions. Colony formation was reduced in Saos-2 cells, in which ADAMTS2 was expressed ectopically under normal conditions

* Corresponding Author DOI: 10.37094/adyujsci.731430

compared to control group cells. Also, a stronger reducing effect on the colony-formation potential of ectopic expression in hypoxic conditions in Saos-2 cells was determined. In this study, the strong inhibitory effect of ADAMTS2 in hypoxic conditions was determined in Saos-2 cells for the first time.

Keywords: Cloning; ADAMTS2; Saos-2; Hypoxia; Ectopic expression; Colony formation.

ADAMTS2 Geninin Klonlanması ve ADAMTS2'nin Saos-2 Hücre Hattında Normal ve Hipoksik Koşullarda Koloni Oluşumuna Etkisi

Öz

N-propeptidaz izoenzimlerinden ADAMTS2 (a disintegrin and metalloproteinase with thrombospondin motifs 2), prokollajenlerin amino uçlarının kesilip uzaklaştırılmasını sağlayarak kollejen biyosentezinde görev alan bir enzimdir. ADAMTS2, prokollajenlerin işlenmesinin yanı sıra anti-anjiyojenik aktiviteye de sahiptir. Bu aktivitesi ile kanser çalışmalarında bir hedef haline gelmiştir. Hipoksik regülasyon hücresel düzeyde çok sayıda genin ifadesini etkileyen bir süreçtir. Çalışmamız kapsamında ADAMTS2 geninin klonlanması ve ektopik olarak Saos-2 (insan kemik karsinomu) hücre hattında ifadesi gerçekleştirilmiştir. Bu amaçla ADAMTS2 kodlayıcı sekans içeren ekspresyon vektörünün, Saos-2 hücrelerine kalsiyum-fosfat presipitasyonu ile geçici transfeksiyonu gerçekleştirilmiştir. Rekombinant ADAMTS2'nin Saos-2 hücrelerinde ektopik olarak üretilip üretilmediği vektör transfekte edilmeyen hücrelerdeki ADAMTS2 mRNA ifadesi ile kontrol edilmiştir. Transfekte edilen Saos-2 hücrelerinde ADAMTS2 mRNA ifadesi kontrol grubuna kıyasla 50 kat artış olduğu gözlenmiştir. Daha sonra rekombinant ADAMTS2'nin Saos-2 hücrelerinin koloni oluşturma potansiyeli üzerindeki etkisi hem normal hem de kimyasal olarak indüklenmiş hipoksik koşullarda incelenmiştir. Kontrol grubu hücrelerine kıyasla normal koşullarda ektopik ifadenin sağlandığı Saos-2 hücrelerinde koloni oluşumu azalmıştır. Ayrıca Saos-2 hücrelerinde hipoksik koşullarda yapılan ektopik ifadenin hücrelerin koloni oluşturma potansiyellerini üzerinde daha güçlü yönde azaltıcı etkisi tespit edilmiştir. Çalışmamızda, ilk kez ADAMTS2'nin hipoksik koşullarda güçlü inhibe edici etkisi Saos-2 hücrelerinde belirlenmiştir.

Anahtar Kelimeler*:* Klonlama; ADAMTS2; Saos-2; Hipoksi; Ektopik ifade; Koloni formasyon.

1. Introduction

Carcinogenesis occurs with abnormalities in many cellular processes such as cell cycle control, apoptosis, extracellular matrix remodeling (ECM), and metastasis. It is well known that carcinogenesis is associated with ECM remodeling. ECM has a structural and regulatory function

compared to control group cells. Also, a stronger reducing effect on the colony-formation potential of ectopic expression in hypoxic conditions in Saos-2 cells was determined. In this study, the strong inhibitory effect of ADAMTS2 in hypoxic conditions was determined in Saos-2 cells for the first time.

Keywords: Cloning; ADAMTS2; Saos-2; Hypoxia; Ectopic expression; Colony formation.

ADAMTS2 Geninin Klonlanması ve ADAMTS2'nin Saos-2 Hücre Hattında Normal ve Hipoksik Koşullarda Koloni Oluşumuna Etkisi

Öz

N-propeptidaz izoenzimlerinden ADAMTS2 (a disintegrin and metalloproteinase with thrombospondin motifs 2), prokollajenlerin amino uçlarının kesilip uzaklaştırılmasını sağlayarak kollejen biyosentezinde görev alan bir enzimdir. ADAMTS2, prokollajenlerin işlenmesinin yanı sıra anti-anjiyojenik aktiviteye de sahiptir. Bu aktivitesi ile kanser çalışmalarında bir hedef haline gelmiştir. Hipoksik regülasyon hücresel düzeyde çok sayıda genin ifadesini etkileyen bir süreçtir. Çalışmamız kapsamında ADAMTS2 geninin klonlanması ve ektopik olarak Saos-2 (insan kemik karsinomu) hücre hattında ifadesi gerçekleştirilmiştir. Bu amaçla ADAMTS2 kodlayıcı sekans içeren ekspresyon vektörünün, Saos-2 hücrelerine kalsiyum-fosfat presipitasyonu ile geçici transfeksiyonu gerçekleştirilmiştir. Rekombinant ADAMTS2'nin Saos-2 hücrelerinde ektopik olarak üretilip üretilmediği vektör transfekte edilmeyen hücrelerdeki ADAMTS2 mRNA ifadesi ile kontrol edilmiştir. Transfekte edilen Saos-2 hücrelerinde ADAMTS2 mRNA ifadesi kontrol grubuna kıyasla 50 kat artış olduğu gözlenmiştir. Daha sonra rekombinant ADAMTS2'nin Saos-2 hücrelerinin koloni oluşturma potansiyeli üzerindeki etkisi hem normal hem de kimyasal olarak indüklenmiş hipoksik koşullarda incelenmiştir. Kontrol grubu hücrelerine kıyasla normal koşullarda ektopik ifadenin sağlandığı Saos-2 hücrelerinde koloni oluşumu azalmıştır. Ayrıca Saos-2 hücrelerinde hipoksik koşullarda yapılan ektopik ifadenin hücrelerin koloni oluşturma potansiyellerini üzerinde daha güçlü yönde azaltıcı etkisi tespit edilmiştir. Çalışmamızda, ilk kez ADAMTS2'nin hipoksik koşullarda güçlü inhibe edici etkisi Saos-2 hücrelerinde belirlenmiştir.

Anahtar Kelimeler*:* Klonlama; ADAMTS2; Saos-2; Hipoksi; Ektopik ifade; Koloni formasyon

1. Introduction

Carcinogenesis occurs with abnormalities in many cellular processes such as cell cycle control, apoptosis, extracellular matrix remodeling (ECM), and metastasis. It is well known that carcinogenesis is associated with ECM remodeling. ECM has a structural and regulatory function

in cells and tissues. Collagen, fibronectin, laminin, elastin, and proteoglycans are important ECM proteins. Collagen, which is one of the main components of ECM, gains structure by forming a helical structure of three collagen polypeptide subunits [1-4].

During collagen biosynthesis, collagen is synthesized as the precursor molecule and then processed into its mature. First, collagen is synthesized as an intracellular precursor molecule in connective tissue fibroblasts. The first synthesized collagen precursor is pre-procollagen. Then mature collagen fibers are formed undergoing various modifications [5, 6]. Molecules having many protease activities play a role in the proteolytic processing of the extracellular matrix. These molecules are grouped as a large number of protein families according to their domain structure. The first group is serine proteases; tissue plasminogen activator contains thrombin, plasmin, and urokinase. The second group is matrix metalloproteases (MMP); they are highly conserved Zn^{+2} dependent endopeptidases consisting of 23 members. These two groups play a role in ECM destruction and cancer metastasis. The third group is bone differentiation protein 1/tolloid family metalloproteases. The fourth group is transmembrane glycoproteins called ADAM (A Disintegrin and Metalloprotease; Disintegrin Metalloproteases) involved in cell-cell adhesion and proteolysis [7, 8].

Classified as procollagen N-propeptidases, ADAMTS2 (a disintegrin and metalloproteinase with thrombospondin motifs 2), ADAMTS3, and ADAMTS1 are known as procollagen cutting isoenzymes and play an important role in collagen biosynthesis. The ADAMTS2 gene is localized on the long arm (5q35.3) of the 5th chromosome and has 22 exons. It weighs 134 kDa and consists of 1211 amino acids [9]. ADAMTS2, one of the N-propeptidase isoenzymes, has also anti-angiogenic activity as well as the processing of procollagen. The anti-angiogenic activity of ADAMTS2 has been demonstrated by a study in nude mice. Recombinant ADAMTS2 was transfected into cells after tumor formation in mice by HEK cellsand it was observed that tumor formation decreased rapidly when ADAMTS2 was overexpressed. For this reason, tumor vascularization has been decreased and ADAMTS2 has been proven to be directly anti-tumor related. Besides, *in vitro* studies performed as a different step of the study showed that recombinant ADAMTS2 rapidly induced apoptosis of endothelial cells [10].

Hypoxic regulation is a process that affects the expression of a large number of genes at the cellular level. With hypoxia occurring in cells, many genes, especially HIF-1 (Hypoxia-inducible factor-1), are activated. HIF-1 is responsible for detecting changes in cellular oxygen concentration and creating responses. In hypoxic conditions, two main signaling systems are activated in the body: the AMPK pathway (AMP-activated protein kinase; adenosine monophosphate-activating protein kinase) and the HIF pathway (hypoxia-inducible factor;

hypoxia-inducible factor) [11]. When the intracellular ATP level decreases, the AMPK pathway activates and accelerates catabolic processes, and inhibits anabolic processes. HIF creates a cellular response in mammalian cells as a result of oxygen deficiency (hypoxia) [12].

pVHL (von Hippel-Lindau protein) also takes part in the oxygen detection mechanism. HIF-1, which plays a key role in hypoxia, has important functions. HIF-1 consists of the oxygen-sensitive subunit α and the structural subunit β. In hypoxic conditions, HIF-1α escapes proteasomal destruction, accumulates in the cytosol, becomes stable, phosphorylated, and passes to the nucleus, forming a heterodimeric complex. This complex binds to the enhancer region of the hypoxia-inducible genes or binds to the HRE (hypoxia response element), a 50-base pair DNA binding motif, and initiates transcription of target genes [13].

Studies in the literature on ADAMTS2 show that ADAMTS2 protein is important for the cell in the process of cancer as well as in collagen biosynthesis. We investigated the colony formation effect of ADAMTS2 in Saos-2 cells. The colony formation effect of ADAMTS2 was investigated in normal and chemically mimicked hypoxic conditions. The chemical hypoxia model is used to mimic low oxygen conditions in mammalian cells, as it generates a biochemical and molecular response at low oxygen conditions. Cobalt chloride ($CoCl_2$) solution was used while creating the chemical hypoxia model. $CoCl_2$ added to the cell growth medium binds to proline hydroxylases, which inhibits HIF-1 under normal oxygen conditions, and stops their activity. Thus, HIF-1 cannot be hydroxylated and cannot be degraded. It becomes stable like the situation in oxygen deficiency. Thus, HIF-1 increases expression levels by stimulating other genes regulated by hypoxia.

In our study, ADAMTS2, which shows activity in both physiological and pathophysiological processes, has been cloned into the expression vector and transfected into Saos-2 (Osteosarcoma Cell Line). The colony formation effect of ADAMTS2 was investigated in Saos-2 cells in normoxic and hypoxic conditions.

2. Materials and Methods

2.1. Materials

Human sarcoma cell line (Saos-2) was obtained from Dr. Kennent Brown, University of Cardiff, UK. All tissue culture reagents were purchased from Invitrogen and the chemicals were purchased from Sigma-Aldrich. Cloning and expression primers were acquired from Macrogen. Primers were designed and analyzed using the OligoAnalyzer tool from IDT (Integrated DNA Technologies).

2.2. Strategies for the cloning of human ADAMTS2

For primer design, the possible gene region of the human ADAMTS2 gene was first determined using the records in the NCBI. The PCR enhancer components such as Betaine (20%), 7 Deaza GTP (50μM), DMSO (5%) were used in the PCR reaction mixture [14]. The full-length coding sequence (CDS) of the human ADAMTS2 gene variant 2 mRNA sequence was used for designing primers. cDNA of MG-63 (Osteosarcoma cell line) was used as a template and amplified using primers 5'GAATGGATCCGCCGGCGGGAGC'3 and 5'TCAGGCGATCCACCTACCTTGGCC'3 (GenBank accession no. NM_021599). Taq DNA Polymerase (Thermo Scientific) was used for the PCR reaction, and the 1700bp PCR product was cloned into pGEM-T Easy vector (Promega) with TA cloning system and then subcloned into pcDNA 3.1/V5-His A vector at the EcoRI restriction sites. pcDNA 3.1/V5 was dephosphorylated before ligation reaction. A clone was sequenced (REFGEN, Ankara) using ADAMTS2 sequencing primer and cloning primers to confirm the sequence integrity. ADAMTS2 Sequencing primers were 5'-TGG CGC TCA GCA ACT GCG AT-3' and 5'-AAG CCG TCC TCA TGG TTC AG-'3.

2.3. Cell culture and MTT assay

Saos-2 cells were cultured in Dulbecco's Modified Eagle Medium (DMEM) supplemented with 10 % Fetal Calf Serum (FCS) under humidified air at 37°C containing 5 % CO_2. Cell viability was controlled by trypan blue exclusion. 150 μM final concentration of $CoCl_2$ (Cobalt Chloride) was used for the hypoxic treatment of cells [15]. 100 mM of $CoCl_2$ stock solution was prepared in dH_2O and further diluted in cell medium to obtain the final concentration.

Cell cytotoxicity analysis was determined by MTT (3-(4,5-Dimethylthiazol-2-yl)-2,5-Diphenyltetrazolium Bromide) assays [16]. For MTT test, 50000 cells/well were seeded in a 96-well microplate at 37^{o}C. One day after seeding the cells, four different concentrations of samples in a range between 50 μM and 200 μM $CoCl_2$ were treated in the cells for 24 hours. Untreated cells were also included as a comparison. The absorbance was measured with a spectrophotometer (Thermo Scientific) at 550 nm. Independent two experiments were done at least triplicate.

2.4. Transient transfection of the expression vector

pcDNA3.1 expression vector which contained ADAMTS2 gene and SEAP (Secreted Alkaline Phosphatase Plasmid) control (Takara, Clontech) vector were transiently transfected into Saos-2 cells by calcium-phosphate precipitation method [15]. SEAP plasmid was used for internal control of transfection. The secreted SEAP activities in cell medium were measured using Ready

to Glow Secreted luciferase kits (Takara, Clontech) in Luminometer (Thermo, USA). Each transfection was repeated at least three times. For transient transfection assay, 500.000 cells/well were seeded in a 6-well plate at 37ºC. The cell medium was changed 6 hours after transfection and cells were treated with 150 μM $CoCl_2$ for 24 hours. Non-treated cells were used as control cells.

2.5. RNA isolation and quantitative real time-PCR (qRT-PCR)

For RNA analyses, 2000.000 cells/well were seeded in a 25 cm^2 cell culture flask at 37ºC. Cells were treated with 150 μM $CoCl_2$ for 24, 48, and 72 hours. The GeneJET™ RNA Purification Kit was used to extract total RNA according to the manufacturer's recommendation (Thermo Scientific). RNA concentrations were determined by spectrophotometer. Revert Aid Reverse Transcriptase (Thermo Scientific) was used to generate for cDNA synthesis. SYBR Green Master Mix (Roche) was used for Real-Time PCR (Roche LightCycler 480 Instrument) analyses in 96 well-plates in a final volume of 10 μL by adding 1 μL cDNA (synthesized with 1000ng of RNA), 0.5 μL forward primer (100ng/μL), 0.5 μL reverse primer (100ng/μL), 3 μL dH_2O and 5 μL SYBR Green PCR Master Mix. ADAMTS2, HIF1α, and human β2 microglobulin (β2M) gene-specific primers were used. The expression primer sequences for ADAMTS2 were as follows; 5'-CTG TGG CGA CGA GGT GCG-'3 and 5'-GGT GCA CAC ATA GTC CCG TCC-'3. β2M primers were used as an internal control. β2M primer sequences were 5'-TTT CTG GCC TGG AGG CTA TC-'3 and 5'-CAT GTC TCC ATC CCA CTT AAC T-'3 HIF-1α expression primer sequences were 5'-CCA CCT ATG ACC TGC TTG GT-'3 and 5'-TGT CCT GTG GTG ACT TGT CC-'3. Product specificity was analyzed with a melting curve analysis. The results were analyzed with the LIVAK method [17].

2.6. Colony formation assay

For colony formation assay 200 cells/well were seeded in a 6-well plate and transfected with pcDNA3.1 vector containing ADAMTS2. The cell medium was changed 6 hours after transfections and 150 μM $CoCl_2$ were treated to the cells. The medium of the cells was changed every 2 days for normoxic and hypoxic groups and colonies were visualized after 10 days. Cells were plated in a six-well plate at 200 cells per well. Hypoxic stimulation cells were treated with 150 μM $CoCl_2$ and the non-transfected group was used as a control group. The medium of the cells was changed every 2 days and colonies were visualized after 10 days. For this purpose, the plates were fixed with cold methanol for 10 minutes and stained with 0.1% crystal violet for 15 minutes [18]. Plates were photographed and the colony numbers were counted with the Image J program.

2.7. Statistical analysis

One-way analysis of variance (ANOVA) was used for statistical analysis in Minitab, p values of 0.05 or less were accepted for statistical significance of a probability (P).

3. Results

3.1 MTT test for cytotoxic effect of $CoCl_2$

MTT test was done to determine the effect of different $CoCl_2$ concentrations on Saos-2 cells. Saos-2 cells were plated in 96 well-plates counting 50,000 cells into each well. A day after, different concentrations (50 μM, 100 μM, 150 μM, 200 μM) of $CoCl_2$ solution were added to the cells in 96-well plates. The 550 nm absorbance values of the treated cells were compared with the control group cells. No cytotoxic effect of $CoCl_2$ on Saos-2 cells was observed at applied doses (Fig. 1A).

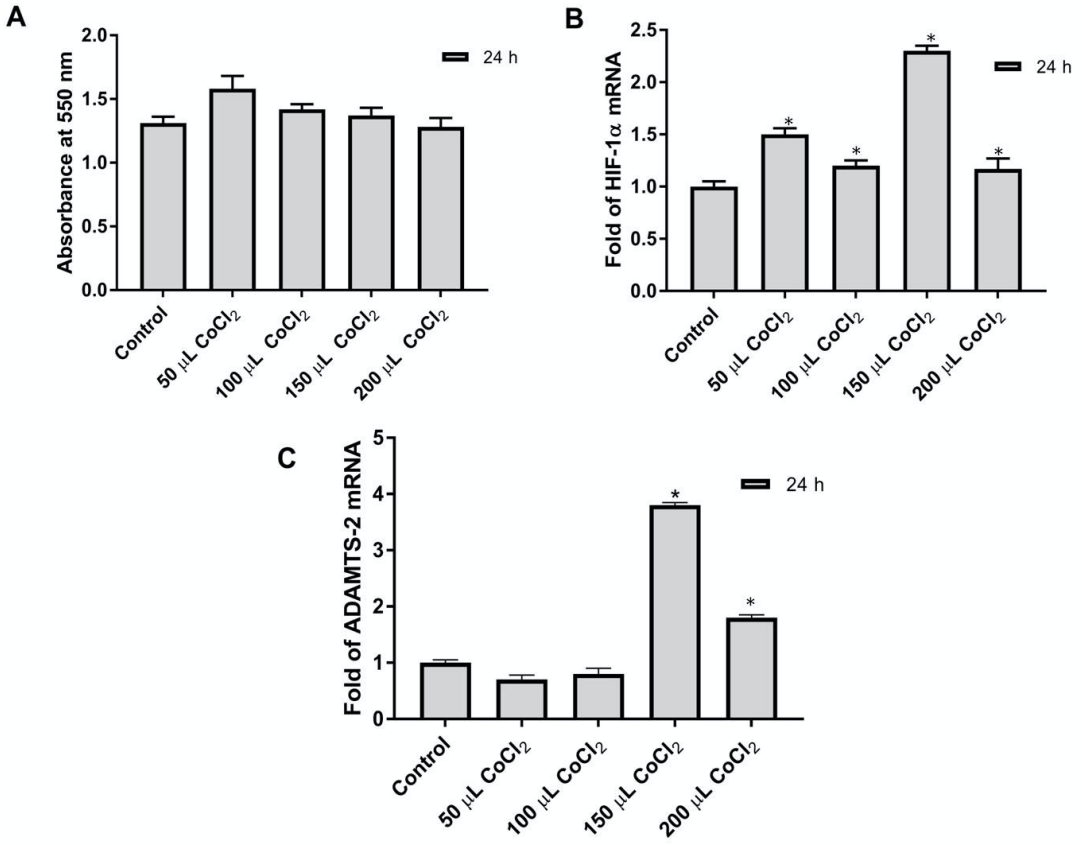

Figure 1: Effects of $CoCl_2$ at different concentrations on cytotoxic and gene expression in Saos-2 cells were shown; (A) MTT Analysis was performed as described above in Saos-2 cells, (B) The relative mRNA expression level of HIF-1α was determined in Saos-2 cells, (C) The relative mRNA level of ADAMTS2 was determined in Saos-2 cells. *p< 0.05

3.2. Verification of hypoxia with q-PCR and detection of ADAMTS2 mRNA level

Saos-2 cells were plated into 25 cm^2 flasks in a 5 ml medium containing 2,000,000 cells. Different concentrations of $CoCl_2$ were added to the cell media of the hypoxia plates the following day. The cells were pelleted at 24h and total RNA was isolated from pellets. cDNA synthesis was performed as 1 µg of total RNA. ADAMTS2, β2M, and HIF-1α mRNA levels were determined in Saos-2 cells at different concentrations of $CoCl_2$. The highest HIF-1α response was detected in 150 µM $CoCl_2$ treated cells (Fig. 1B). Also, the highest ADAMTS2 expression was detected at the same concentration of $CoCl_2$ (Fig. 1C). Consequently, considering both MTT and Real-Time PCR results, it was determined that 150 µM $CoCl_2$ was suitable for hypoxia stimulation.

3.3. The control of transient transfection and ectopic ADAMTS2 expression

Cells were plated in 25 cm^2 flasks and the next day, cells were transfected with pCDNA3.1 (8µg) and SEAP (2µg) vectors using calcium phosphate precipitation method. The SEAP vector was used for transfection control. The cell medium was collected after transfection at 24h, 48h and 72h. Secreted alkaline phosphatase activities were measured. For RNA analysis, cells were centrifuged and RNA isolation was performed from pellets. cDNA synthesis was performed from both control and experimental groups with 1000ng RNA. SEAP activity has reached a detectable level compared to the non-transfected control group. These results showed that the transfection was working. ADAMTS2 mRNA expression was determined by RealTime PCR. β2M mRNA expression was used as an internal control. ADAMTS2 expression was increased 50-fold in the experimental group transfected with pCDNA3.1 vector containing ADAMTS2. This result showed us that ADAMTS2 expression occurred ectopically in Saos-2 cells.

3.4. Colony formation in ADAMTS2 transfected Saos-2 cells

Saos-2 cells were counted with the trypan blue method and plated in 6 well plates. After 24 hours, cells were transfected with the pcDNA3.1 vector containing the ADAMTS2 gene. We compared two transfected groups of cells named transfected in normoxia and transfected in hypoxia. $CoCl_2$ was applied to a transfected group and marked as a hypoxic group. The other transfected group was left under normal conditions and marked as the normoxic group. The medium was replaced with fresh medium every two days, and at the end of 10 days cells medium was removed and the cells were treated with cold methanol for 10 minutes for fixation. After fixation cells were treated for 15 minutes with crystal violet dye. Stained cell colonies in well plates were photographed and the colonies were counted with image J.

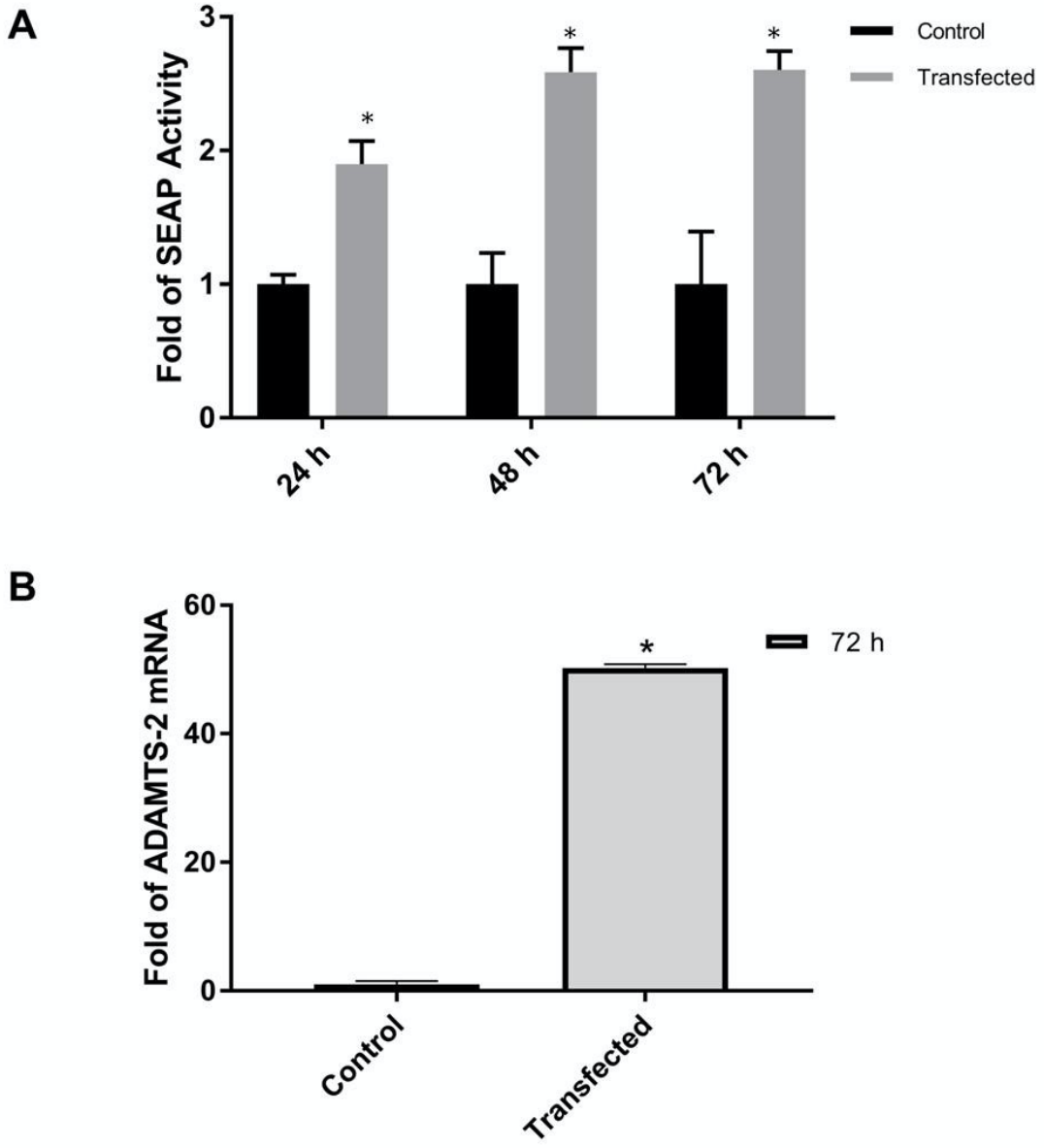

Figure 2: Ectopic ADAMTS2 expression was controlled at the mRNA level (A) Transfection efficiency was controlled using SEAP2 Activity in Saos-2 cells (B) Confirmation of ADAMTS2 Ectopic Expression in Saos-2 cells by Real-Time PCR *p< 0.05

As seen in Fig. 3, when the normoxic transfected group and the hypoxic transfected group were compared, the reducing effect of ADAMTS2 ectopic expression on colony formation in cells under hypoxic conditions was determined.

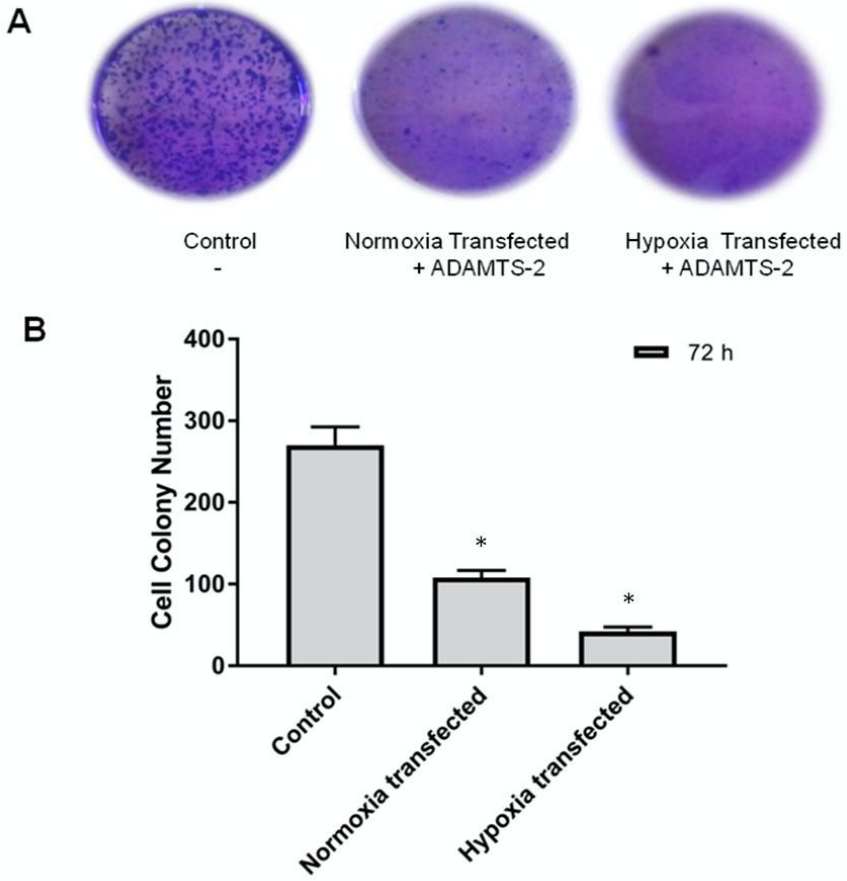

Figure 3: Colony formation effect of ADAMTS2 in Saos-2 cells; Cells were transfected with a pcDNA 3.1 vector containing ADAMTS2. For hypoxic stimulation cells were treated with 150 µm $CoCl_2$. (A) Stained cell colonies photographed in 6 well plates. (B) The colonies counted with Image J and statistically analyzed. *$p< 0.05$

4. Discussion

The primary task of ADAMTS2, defined as amino procollagen peptidase, is to break down the amino propeptides of type I, II, III, and V procollagen. [1, 2, 9]. ADAMTS2 protein is synthesized in an inactive zymogen form and the N-terminal propeptide portion is cut with furin enzyme. This post-translational modification is necessary for the activity of the protein [19]. ADAMTS2 deficiency causes dermatosparaxis (Ehlers – Danlos syndrome type VIIC), a connective tissue disease with recessive inheritance in humans [20, 21]. This hereditary connective tissue disorder occurs as a result of the accumulation of improperly processed amino procollagen, and the main feature of the disease is skin fragility [10, 22]. ADAMTS2 has been found to exhibit antiangiogenic properties via nucleolin in vivo and in vitro, which is associated with the cell membrane [10]. In a study, the anti-angiogenic feature of ADAMTS2 was determined. It was observed that tumor formation rapidly decreased when ADAMTS2 was

overproduced. In vitro studies have shown that recombinant ADAMTS2 rapidly induces apoptosis of endothelial cells [10].

ADAMTS2 has been reported as a tumor suppressor protein due to its anti-angiogenic properties. It has been argued that its function may be impaired by chromosomal rearrangement involving ADAMTS2. It has been thought that rearrangement of the ADAMTS2 gene may be responsible for the production of an active protein [19]. In another study, IL-6 was found to transcriptionally regulate the ADAMTS2 gene in Saos-2 cells and increase the mRNA and protein level of ADAMTS2 [23]. In another regulation study, IL-1α, a proinflammatory cytokine, has been shown to increase gene expression in ADAMTS2 and ADAMTS-3 in Saos-2 and MG-63 cells [24].

Oxygen (O_2) homeostasis is very important for vertebrate life. Expression of many genes related to angiogenesis, glucose metabolism, cell proliferation, and regulation of physiological response is increased by HIF-1 at low O_2 levels [25]. Hypoxic conditions occur in the microenvironment of the tumor [26]. Hypoxia is regulated by the HIF-1 transcription factor in mammalian cells [27]. HIF-mediated intracellular pathways are active in the development, physiology, and pathophysiological processes. Gene products targeted by HIF-1 are divided into two distinct categories: proteins that increase O_2 efficiency and decrease O_2 consumption. In particular, the vast majority of human tumors have overexpression of these gene products [28]. Tumor cells stimulate molecular programs such as cell proliferation, cell survival, and angiogenesis in response to hypoxia. Overexpression of HIF-1 has been demonstrated by immunohistochemical analysis in prostate, lung, breast, colon, ovarian, skin, and stomach in many human malignant cancers [29]. For the first time in our study, ectopic expression of the ADAMTS2 gene in Saos-2 cells was investigated under both normal and hypoxic conditions. A chemical hypoxia mimetic agent $CoCl_2$ was used for hypoxic stimulation. $CoCl_2$ was applied to the cells at different concentrations and it was determined at what dose the optimal response occurred. In our previous study, the ADAMTS2 mRNA level was tested in different cell lines in hypoxic conditions. It has been determined that the ADAMTS2 mRNA level is increased in hypoxia in DU-145, PC-3, HT-29, MCF-7, and Saos-2 cells. The highest hypoxic response was observed in Saos-2 and MCF-7 cells [30]. ADAMTS2 is expressed in a variety of adult tissues, including heart tissue, and takes part in a large number of physiological processes. Increased expression of ADAMTS2 was observed in coronary lesion samples from patients with acute myocardial infarction. During acute myocardial infarction, cells remain oxygen-free and a hypoxic microenvironment is formed. ADAMTS2 has been shown to play a potential role in the pathogenesis of acute myocardial infarction and cardiovascular disease [21].

The hypoxic microenvironment is very important for the progression and spread of cancer in pathophysiological processes, especially in the process of cancer. In our study, the effect of overexpression of the ADAMTS2 gene, which is involved in collagen metabolism and has anti-angiogenic activity, was investigated in the formation of cells in both normal and hypoxic conditions. The ADAMTS2 gene was cloned into the expression vector and was produced ectopically in Saos-2 cells. The effect of ADAMTS2, which is overexpressed in Saos-2 cells for the first time, has been investigated in hypoxic conditions. The inhibitory effect of ADAMTS2 overexpression on cells was found.

To fully clarify the role of ADAMTS2 protein in the cancer process, hypoxic conditions also need to be taken into consideration.

5. Conclusion

As a result, ectopically overexpressed ADAMTS2 decreased the colony formation of Saos-2 cells in hypoxic conditions. We suggest that the hypoxic conditions should be examined for a more detailed understanding of the regulation of the ADAMTS2 gene.

Acknowledgment

Balikesir University Scientific Research Projects Units (BAP) projects 2015/42, was the primary sponsor of this study. The authors would like to thank Dr. Kenneth Brown, University of Cardiff, UK for the human osteogenic sarcoma cell line (Saos-2).

References

[1] Kılıç, M.Ö., Aynekin, B., Kılıç, Y., Demircan K., Bozer M., *ADAMTS Proteases in Cancer,* New Journal of Medicine, 32, 123-127, 2015.

[2] Brodsky, B., Persikov, A. V., *Molecular structure of the collagen triple helix,* Advances in Protein Chemistry, 70, 301-339, 2005.

[3] Khun, K., Mayne, R., Burgeson, R., *Structure and Function of Collagen Types*, Academic, Orlando, Florida, 1987.

[4] Robert, P.M., *The Extracellular Matrix: An Overview*, Springer, Berlin, 2011.

[5] Lodish, H., Berk, A., Kaiser, C.A., Krieger, M., Scott, M.P., Bretscher, A., Ploegh, H., Matsudaira, P., *Moleküler hücre biyolojisi*, Ahr, K., Tontonoz, M., Pantages, E.F., Rice, E., Palme Yayıncılık, Ankara, 2007.

[6] Persikov, A.V., Brodsky, B., *Unstable molecules form stable tissues*, Proceedings of the National Academy of Sciences, 99(3), 1101-1103, 2002.

[7] Rocks, N., Paulissen, G., El Hour, M., Quesada, F., Crahay, C., Gueders, M., Foidart, *ADAM-8, a metalloproteinase, drives acute allergen induced airway inflammation*, 41, 2, European Journal of Immunology, 380-391, 2011.

[8] Chou, C.W., Chen, C.C., *HDAC inhibition upregulates the expression of angiostatic ADAMTS1*, FEBS Letters, 582, 4059–4065, 2008.

[9] Colige, A., Vandenberghe, I., Thiry, M., Lambert, C. A., Van Beeumen, J., Li, S. W., *Cloning and characterization of ADAMTS-14, a novel ADAMTS displaying high homology with ADAMTS-2 and ADAMTS-3,* Journal of Biological Chemistry, 277(8), 5756-66, 2002.

[10] Dubail, J., Kesteloot, F., Deroanne, C., Motte, P., Lambert, V., Rakic, J.M., Lapiere, C., Nusgens, B., Colige, A., *Adamts-2 Functions as Anti-Angiogenic and Anti-Tumoral Molecule Independently of Its Catalytic Activity*, Cellular and Molecular Life Sciences, 67(24), 4213-4232, 2010.

[11] Malagelada, C., Xifro, X., Minano, A., Sabria, J., Alvarez, J.A., *Contribution of caspase-mediated apoptosis to the cell death caused by oxygen-glucose deprivation in cortical cell cultures*, Neurobiology of Disease, 20(1), 27-37, 2005.

[12] Ouyang, Y.B., Xu, L., Giffard, R.G., *Geldanamycin treatment reduces delayed CA I damage in mouse hippocampal organotypic cultures subjected to oxygen glucose deprivation*, Neuroscience letters, 380(3), 229-233, 2005.

[13] Semenza, G.L., *Surviving ischemia: adaptive responses mediated by hypoxia-inducible factor 1*, Journal of Clinical Investigation, 106(7), 809-812, 2000.

[14] Alper, M., Tokay, E., Kockar. F., *Amplification of GC Rich ADAMTS-2 and URG-4/URGCP Promoter Regions with Optimised Combination of PCR Enhancers*, Turkish Journal of Biology, 40(1), 196-205, 2015.

[15] Aydogan Turkoglu, S., Kockar, F., *SP1 and USF differentially regulate ADAMTS1 gene expression under normoxic and hypoxic conditions in hepatoma cells*, Gene, 575(1), 48-57, 2016.

[16] Aydogan Turkoglu, S., Okuyan, D., Kockar, F., *TGF-β downregulates CAIII expression via MAPK and PI3K signaling pathways in colon carcinoma and osteosarcoma cells,* Archives of Biological Sciences, 7(3), 393-401, 2019.

[17] Livak, K.J., Schmittgen, T.D., *Analysis of relative gene expression data using real-time quantitative PCR and the 2 (−Delta Delta C(T)) Method*, Methods 25 (4), 402–408, 2001.

[18] Daiy, H., Huangy, Y., Li, Y., Meng, G., Wang, Y., Guo, Q., *TSSC3 overexpression associates with growth inhibition, apoptosis induction and enhances chemotherapeutic effects in human osteosarcoma,* Carcinogenesis 33(1), 2012.

[19] Tota, G., Coccaro, N., Zagaria, A., Anelli, L., Casieri, P., Cellamare, A., Minervini, A., Minervini, C.F., Brunetti, C., Impera, L., Carluccio, P., Cumbo, C., Specchia, G., Albano, F., *Adamts2 Gene Dysregulation in T/Myeloid Mixed Phenotype Acute Leukemia*, BMC Cancer, 14(1), 963, 2014.

[20] Le Goff, C., Somerville, R.P., Kesteloot, F., Powell, K., Birk, D. E., Colige, A. C., Apte, S. S., *Regulation of Procollagen Amino-Propeptide Processing During Mouse Embryogenesis by Specialization of Homologous Adamts Proteases: Insights on Collagen Biosynthesis and Dermatosparaxis,* Development and Disease, 133(8), 1587-96, 2006.

[21] Wang, X., Chen, W., Zhang, J., Khan, A., Li, L., Huang, F., Qiu, Z., Wang, L., Chen, X., *Critical Role of Adamts2 (a Disintegrin and Metalloproteinase with Thrombospondin Motifs 2) in Cardiac Hypertrophy Induced by Pressure Overload,* Hypertension, 69(6), 1060-1069, 2017.

[22] Colige, A., Ruggiero, F., Vandenberghe, I., Dubail, J., Kesteloot, F., Van Beeumen, J., Beschin, A., Brys, L., Lapiere, C.M., Nusgens, B., *Domains and Maturation Processes That*

Regulate the Activity of Adamts-2, a Metalloproteinase Cleaving the Aminopropeptide of Fibrillar Procollagens Types I-Iii and V, Journal of Biological Chemistry, 280(41), 34397-34408, 2005.

[23] Alper, M., Kockar, F., *Il-6 Upregulates a Disintegrin and Metalloproteinase with Thrombospondin Motifs 2 (Adamts-2) in Human Osteosarcoma Cells Mediated by Jnk Pathway*, Molecular and Cellular Biochemistry, 393(1-2), 165-75, 2014.

[24] Alper, M., Aydemir, A.T., Kockar, F., *Induction of human ADAMTS-2 gene expression by IL-1 alpha is mediated by a multiple crosstalk of MEK/JNK and PI3K pathways in osteoblast like cells*, Gene, 573(2), 321-327, 2015.

[25] Semenza, G.L., *Oxygen Sensing, Hypoxia-Inducible Factors, and Disease Pathophysiology*, Annual Review of Pathology: Mechanisms of Disease, 9, 47-71, 2014.

[26] Rankin, E. B. Giaccia, A.J., *Hypoxic Control of Metastasis*, Science, 352, 175-180, 2016.

[27] Semenza, G.L., Nejfelt, M. K., Chi, S.M., Antonarakis, S. E., *Hypoxia Inducible Nuclear Factors Bind to an Enhancer Element Located 3' to the Human Erythropoietin Gene*, Proceeding of the National Academy of Sciences USA, 88(13), 5680- 5684, 1991.

[28] Balamurugan, K., *Hif-1 at the Crossroads of Hypoxia, Inflammation, and Cancer*, International Journal of Cancer, 138(5), 1058-1066, 2016.

[29] Brusselmans, K., Bono, F., Maxwell, P., Dor, Y., Dewerchin, M., Collen, D., Herbert, J. M., Carmeliet, P., *Hypoxia-inducible factor 2-α (HIF-2α) is involved in the apoptotic response to hypoglycemia but not to hypoxia,* Journal of Biological Chemistry, 276, 39192-39196, 2001.

[30] Aydogan Turkoglu, S., Gultekin, A. S., Kockar, F., *Variation of ADAMTS2 Gene Expression in Hypoxic Conditions in Cancer*, Afyon Kocatepe University Journal of Sciences and Engineering, 19(1), 22-33, 2019.

Adıyaman University Journal of Science
https://dergipark.org.tr/en/pub/adyujsci
DergiPark AKADEMİK
ISSN 2147-1630
e-ISSN 2146-586X

Inhibition of Colorectal Cancer Cell Survival by Paclitaxel Combined with Olaparib

Ramazan GÜNDOĞDU[1,*]

[1]*Bingol University, Vocational School of Health Services, Department of Pharmacy Services, Bingol, Turkey*
rgundogdu@bingol.edu.tr, ORCID: 0000-0001-5230-2121

Received: 14.05.2020 **Accepted:** 22.10.2020 **Published:** 30.12.2020

Abstract

Colorectal cancer is one of the main reasons for cancer-related mortality around the world and conventional chemotherapy approaches lead the clinical management of colorectal cancer treatment. Although many chemotherapeutics including paclitaxel have been effectively used to treat colorectal cancer patients, some tumour cells acquire drug resistance by increasing the regulation of various cellular mechanisms, primarily becoming addictive to some DNA repair activities. Preclinical evaluation of small-molecule inhibitors targeting various DNA damage response components is currently an active area of cancer research. This study aimed to assess the cytotoxic effect of paclitaxel combined with small-molecule PARP inhibitor olaparib in HCT116 colorectal cancer cells. We conducted clonogenic assays, showing that the paclitaxel and olaparib combination significantly inhibits the survival of colorectal cancer cells compared to paclitaxel or olaparib alone. By performing two distinct immunological methodology, Western blotting and immunofluorescence, we further demonstrated that olaparib intensifies the DNA damage accumulation induced by paclitaxel treatment. In conclusion, our preclinical study with HCT116 colorectal cancer cells suggests that olaparib may potentially serve as a combination partner to paclitaxel for effective colorectal cancer treatment.

Keywords: Colorectal cancer; Paclitaxel treatment; PARP inhibitors.

* Corresponding Author DOI: 10.37094/adyujsci.737262

HCT116 Kolorektal Kanser Hücre Sağ-kalımının Paklitaksel ve Olaparib Kombinasyon Tedavisiyle Engellenmesi

Öz

Kolorektal kanser, dünya genelinde kansere bağlı ölümün temel sebeplerinden biridir ve konvansiyonel kemoterapi yaklaşımları kolorektal kanser tedavisinin klinik yönetimine öncülük etmektedir. Paklitaksel dahil olmak üzere çoğu kemoterapötik, kolorektal kanser hastalarını tedavi etmede etkili bir şekilde kullanılmasına rağmen, bazı tümör hücreleri özellikle çeşitli DNA tamir aktivitelerine bağımlılık kazanmak suretiyle çok sayıda hücresel mekanizmaların düzenlenmesini arttırarak ilaç direnci kazanırlar. Çeşitli DNA hasar yanıtı bileşenlerini hedefleyen küçük-moleküllü inhibitörlerin klinik öncesi değerlendirmesi günümüzde kanser araştırmalarının aktif bir alanını oluşturmaktadır. Bu çalışma, HCT116 kolorektal kanser hücrelerinde paklitaksel ile kombine edilen küçük-moleküllü PARP inhibitörü olaparibin sitotoksik etkisini değerlendirmeyi amaçlamıştır. Gerçekleştirdiğimiz koloni sağ-kalım analizleri paklitaksel ve olaparib kombinasyonunun sadece paklitaksel ya da olaparib tedavisi ile kıyas edildiğinde kolorektal kanser hücrelerinin sağ kalımını önemli derecede inhibe ettiğini gösterdi. Western blot ve immünofloresan olmak üzere iki farklı immünolojik yöntem gerçekleştirilerek, olaparibin paklitaksel tedavisinin oluşturduğu DNA hasarı birikimini yoğunlaştırdığı tespit edildi. Sonuç olarak, HCT116 kolorektal kanser hücreleriyle gerçekleştirdiğimiz klinik öncesi çalışmamız, olaparib ve paklitaksel kombinasyonunun kolorektal kanser tedavisi için potansiyel bir tedavi yaklaşımı sunabileceğini göstermektedir.

Anahtar Kelimeler: Kolorektal kanser; Paklitaksel tedavisi; PARP inhibitörleri.

1. Introduction

Colorectal cancer is the third common type of malignancy worldwide, leading one of the major causes of cancer-related mortality [1]. Surgery is offered for colorectal cancer patients as the most effective treatment option and chemotherapeutical agents are mainly used to eliminate the remaining cancerous cells, repressing tumour growth and reducing recurrence of the disease [2]. Although widely-used anti-cancer agents have improved the prognosis of colorectal cancer in the clinic, their lack of selectivity and acquired resistance remain as one of the major obstacles of the treatment management [3]. Therefore, it is necessary to offer novel treatment strategies that eradicate cancer cells by targeting different cellular mechanisms at the same time.

Paclitaxel has been used as an anti-cancer agent in the treatment of various malignancies. It binds to tubulin and stabilizes polymerized microtubules, arresting cell cycle at the G2/M

checkpoint and consequently leading apoptotic cell death [4-6]. The single-agent treatment of high-dose paclitaxel is limited due to difficult-to-tolerate side effects such as peripheral neuropathy and hypersensitivity [7] and acquired paclitaxel resistance through numerous mechanisms including microtubule mutations prevents the long-term clinical success [8]. Considering these drawbacks of high-dose paclitaxel therapy, recent studies have revealed that low-dose paclitaxel application may promise better treatment approach for some malignancies owing to more tolerable toxicity and considerable reduction in drug resistance [9-13]. The cytotoxic effect of paclitaxel treatment was also evaluated in colorectal cancer cells [14, 15]. Li et al. reported that the low-dose paclitaxel treatment inhibits cell cycle at G0/G1 phase in HCT116 and LOVO cells by modulating the expression of Myc and phosphorylated-c-Myc [15]. Theoretically, low-dose paclitaxel treatment is utilized to suppress the invasive progress and metastatic activities of cancer instead of eliminating neoplastic cells through apoptotic cell death as in the conventional approach. However, contrary research argues that long-term low-dose paclitaxel single-agent therapy may provoke adverse effects such as promoting metastasis [16]. Therefore, researchers have been studying to evaluate the potential of paclitaxel at a low toxic dose combined with small-molecule inhibitors in different experimental settings [17]. Taken together, a combination of paclitaxel and novel small-molecule inhibitors may potentially offer more effective and tolerable anti-cancer responses for the treatment of colorectal cancer patients.

DNA is subjected continual insults from endogenous and exogenous sources and key proteins involved in DNA damage response (DDR) pathway are required to monitor the integrity of genetic material and to activate cell cycle checkpoints once the damage induced, including poly ADP-ribose (PAR) polymerases (PARP) [18, 19]. The PARP enzymes are classified under the group of ADP-ribosyltransferases (ARTs) and contribute to a variety of essential cellular processes including chromatin modification, cell cycle checkpoint regulation and the repair of DNA single-strand breaks (SSBs) [20, 21]. The enzymatic activity of PARPs can be silenced by PARP inhibitors, some of those have been subjected to intense preclinical and clinical investigations for the treatment of certain cancer patients with *BRCA1/2* mutations either alone or in combination with chemotherapy drugs [22]. PARP inhibitors olaparib, rucaparib and niraparib have been granted the USFDA approval for the treatment of patients with germline *BRCA*-mutant ovarian cancer [23]. Olaparib has recently been approved for germline *BRCA*-mutant metastatic breast [24] and pancreatic cancer treatments [25]. The effective use of PARP inhibitors in the management of colorectal cancer treatment has recently gained attention. Arena et al. demonstrated that PARP inhibitors have a potential to limit colorectal tumour growth and disease progression [26]. It has been also revealed that colorectal cancer cells become vulnerable to irinotecan therapy upon treatment of PARP inhibitors rucaparib [27] or niraparib [28]. Here, we

hypothesized that the combination treatment of microtubule-targeting agent paclitaxel and PARP inhibitor olaparib would synergize the cytotoxic activities of these molecules, potentially offering more solid management of colorectal cancer treatment. We found that olaparib may intensify paclitaxel cytotoxicity through increasing the overall DNA damage burden in HCT116 colorectal cancer cells.

2. Materials and Methods

2.1. Reagents

Dulbecco's modified Eagle's medium (DMEM) and fetal bovine serum (FBS) were purchased from Gibco (Thermo Fisher Scientific). Penicillin and streptomycin were purchased from Sigma Aldrich and Bioshop Canada, respectively. Dimethyl sulfoxide (DMSO) and crystal violet were purchased from Bioshop Canada and Sigma Aldrich, respectively. The primary antibodies for anti-γH2AX (Ser139) and β-Actin were bought from Cell Signaling Technology (#9718) and Santa Cruz (#sc-1616), respectively. The HRP-linked secondary antibodies against anti-rabbit and anti-goat were purchased from GE Healthcare (#GENA934) and Santa Cruz (#sc2056). The fluorescent-dye conjugated secondary antibody against anti-rabbit was bought from Stratech – Jackson (Texas Red, #711-075-152) and DAPI was from Sigma Aldrich (#32670). Olaparib, rucaparib and paclitaxel were purchased from Selleckchem (#S1060), Tocris (#6230) and Medchem Express (#HY-B0015), respectively.

2.2. Cell culture conditions

HCT116 colorectal cancer cell line was kindly provided by Dr Alexander Hergovich (UCL, London, UK) and maintained in high glucose DMEM supplemented with 10% fetal bovine serum with 1% antibiotic (pen-strep). Cells were grown in humidity-saturated cell culture incubators at 37°C with 5% CO2. Stock solutions of olaparib, rucaparib and paclitaxel were prepared in DMSO and stored at -80°C. Drug/inhibitor treatments were performed as indicated in the corresponding figure legends.

2.3. Clonogenic survival assays

Clonogenic survival assays were performed as described in [29]. Briefly, 1500 of exponential phase cells were seeded in 6-cm plates and allowed to adhere for 24 hours, before being treated with olaparib or rucaparib with/out paclitaxel for 3 days. Cell medium was refreshed every 4 days until each colony has more than 50 cells (8-10 days). Colonies were first fixed with methanol/acidic acid (3:1) solution, then stained with 0.5% crystal violet dissolved in methanol

for 15 minutes. After letting the plates air-dry overnight at room temperature, the number of colonies was counted per plate. The plating efficiencies of the corresponding controls were used to calculate the surviving fraction.

2.4. Western blotting

Protein lysates were resolved by 12% sodium dodecyl sulfate-polyacrylamide gel electrophoresis (SDS-PAGE). Samples were transferred to polyvinylidene difluoride (PVDF) membranes. Membranes were blocked with 5% skim milk prepared in TBS-T (50 mM Tris, 150 mM NaCl, 0.5% Tween-20, pH 7.5) and then incubated with the corresponding antibody overnight. The protein-antibody complex was then probed by secondary antibodies conjugated with horseradish peroxidase (HRP) and finally subjected to ECL (Amersham) substrates for chemiluminescent detection. Densitometry analysis of Western blots was conducted using the NIH ImageJ.

2.5. Immunofluorescence microscopy

Immunofluorescence experiments were conducted as defined in [30]. Briefly, cells cultured on glass coverslips were fixed in 3%-paraformaldehyde (PFA) and 2%-sucrose solution for 20 minutes at room temperature, permeabilized for 2 minutes with 0.5% (vol/vol) Triton X-100 in PBS, washed in PBS, and then incubated with anti-γH2AX primary antibody (1:100) overnight at 4°C. Following the washing step, the coverslips were incubated with blocking buffer (10% goat serum) before being incubated with anti-rabbit Texas Red secondary antibody (1:100) and DAPI (1 μg/mL) for 2 hours in the dark at room temperature, washed with PBS, and mounted using Vectashield mounting medium (Vector Lab) in a microscope slide. Finally, the corners of the cover slides were sealed with nail polish and images were obtained with an Apotome fluorescence microscope (Zeiss) and Photoshop CS5 (Adobe Systems Inc.).

2.6. Statistical analysis

GraphPad Prism software was used to acquire graphics and statistical analyses. Data are displayed as mean ± SEM. The significance of differences between the means was one-tailed unpaired Student's t-test for colony survival assays and Mann–Whitney test for immunofluorescence analyses. Differences were considered statistically significant when *p*-values were below 0.05 (*), 0.01 (**), 0.001 (***) or 0.0001 (****) for all experiments.

3. Results

3.1. Paclitaxel and Olaparib Combination Inhibits HCT116 Cancer Cell Survival

As a widely used anti-neoplastic agent in the clinic [5], paclitaxel treatment causes tubulin polymerization, dysfunctional microtubule formation and cell cycle arrest, ultimately inducing cell death [4, 6, 31]. Here, the cytotoxic effect of paclitaxel alone or in combination with small-molecule PARP inhibitors olaparib and rucaparib (Fig. 1A) were examined by *in vitro* clonogenic analysis. We employed HCT116 colorectal cancer cells characterized by microsatellite instability (MSI) [32], displaying inefficient mismatch repair and chemoresistant profile [33]. First, the cytotoxic capacity of paclitaxel single-agent treatment was evaluated in HCT116 cells. After being treated with various doses of paclitaxel (1 – 10 nM) for 3 days, cells were further cultured in the drug-free medium for another 8 to 10 days in order to assess the paclitaxel cytotoxicity. Our results demonstrated that the paclitaxel treatment of 1 nM had a minimal cytotoxic effect on the HCT116 cell survival compared to higher doses and this result prompted us to select 1 nM paclitaxel concentration as a low-dose treatment for future combination experiments. In addition, based on our preliminary studies and the literature [34, 35], we used 0.5 and 1 μM olaparib, and 0.1 and 0.5 μM rucaparib preclinical doses in our paclitaxel combination experiments with HCT116 cells.

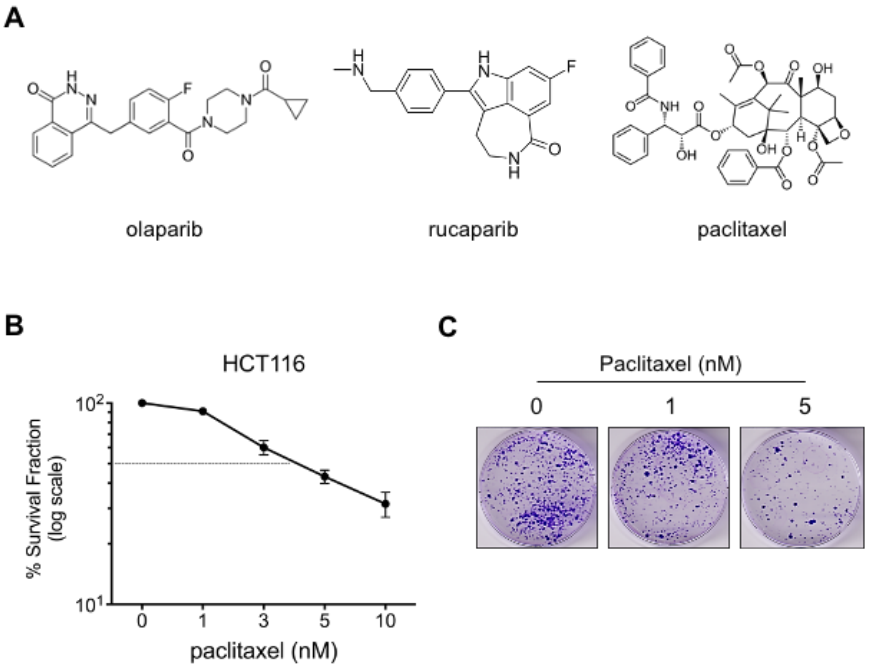

Figure 1: Cytotoxic effect of paclitaxel treatment on HCT116 colorectal cancer cells. (A) The chemical structure of olaparib, rucaparib and paclitaxel, (B) clonogenic survival of HCT116 cells treated with/out paclitaxel for 3 days. Quantifications are shown as a percentage (in log scale) of colonies formed after treatment with indicated doses (n=3). Results were corrected according to plating efficiencies of the corresponding untreated controls, (C) representative images of the clonogenic survival assays

Next, we evaluated the combined effect of paclitaxel (1 nM) and olaparib treatment on the clonogenic capacity of HCT116 cells. Cells were treated with olaparib (0.5 and 1 μM) alone or in combination with paclitaxel (1 nM) for 3 days, then further incubated with the medium without any drug. Interestingly, the paclitaxel and olaparib combination treatment had significantly repressed the survival of HCT116 colorectal cancer cells compared to the relevant single-agent treatments (Fig. 2A/B). This synergistic cytotoxicity was specific to HCT116 colorectal cancer cells since the combination treatment did not affect the clonogenic survival of U2OS osteosarcoma cells that were subjected to the same experimental procedures (Fig. 2C).

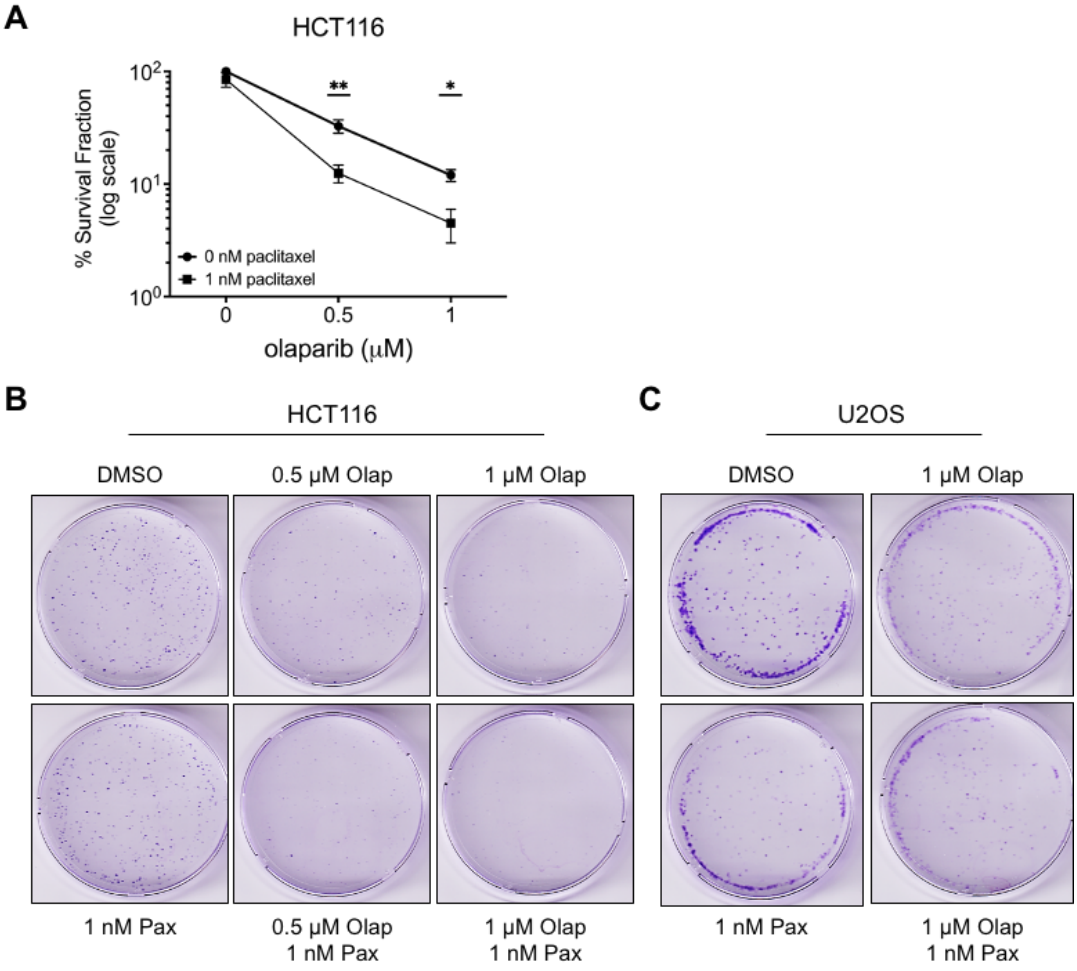

Figure 2: Olaparib enhances the cytotoxicity of paclitaxel in HCT116 cells. (A) Clonogenic survival of HCT116 cells in response to paclitaxel treatment (1 nM) with/out olaparib (0.5 and 1 μM) for 3 days. Quantifications are shown as a percentage (in log scale) of colonies formed after treatment with indicated doses (n=3). Results were corrected according to plating efficiencies of the corresponding untreated controls, (B) representative images of the clonogenic survival assays, (C) representative images of the U2OS clonogenic survival upon paclitaxel alone or in combination with olaparib for 3 days

To consolidate our findings, we further analyzed the cytotoxic activity of paclitaxel combined with rucaparib, another USFDA approved small-molecule PARP inhibitor, in HCT116

cancer cells. Cells were treated with rucaparib (0.1 and 0.5 μM) alone or in combination with paclitaxel (1 nM) for 3 days as detailed above. In line with previous results, we noticed a significant reduction in colony survival of HCT116 cells upon paclitaxel and rucaparib combination regimen compared to the relevant single-agent treatments (Fig. 3A/B). In summary, our clonogenic survival experiments revealed that HCT116 colorectal cancer cells become vulnerable to PARP inhibitor treatment when paclitaxel is included as a combination partner.

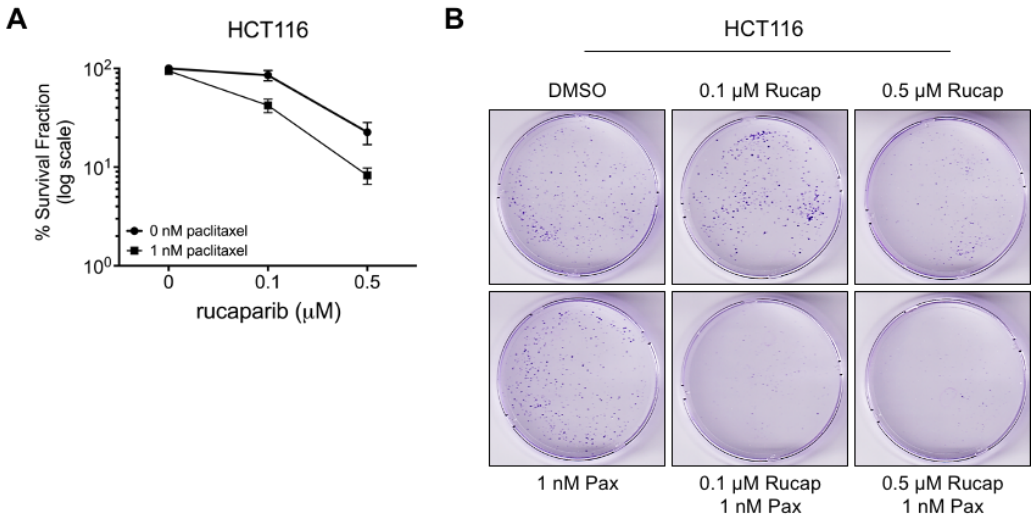

Figure 3: Rucaparib potentiates paclitaxel cytotoxicity in HCT116 cells. (A) Clonogenic survival of HCT116 cells in response to paclitaxel treatment (1 nM) with/out rucaparib (0.1 and 0.5 μM) for 3 days. Quantifications are shown as a percentage (in log scale) of colonies formed after treatment with indicated doses (n=2). Results were corrected according to plating efficiencies of the corresponding untreated controls, (B) representative images of the clonogenic survival assays

3.2. Olaparib treatment augments the Paclitaxel-induced DNA damage accumulation in HCT116 cells

After deciphering that HCT116 colorectal cancer cells have significantly impaired clonogenic capacity upon the paclitaxel and olaparib combination treatment, we further investigated the level of DNA damage induction in HCT116 cancer cell treated with paclitaxel and olaparib combined or alone. As a reliable DNA damage indicator [36], the phosphorylation status of H2AX (γH2AX-Ser139) was assessed by conducting Western blotting. HCT116 cells were treated with olaparib (1 μM) or paclitaxel (1 nM) as single agents or in combination for 24 hours. Following treatment, cells were incubated with the drug-free medium for additional 4 hours for the recovery before being subjected to Western blotting analysis (Fig. 4A). As presented in Fig. 4B/C, both olaparib and paclitaxel single-agent treatments increased the γH2AX levels (lines 3 and 4); however, the combination treatment of paclitaxel and olaparib resulted in higher and

sustained γH2AX induction (line 5), suggesting an insistent DNA damage accumulation in HCT116 colorectal cancer cells upon the combined treatment.

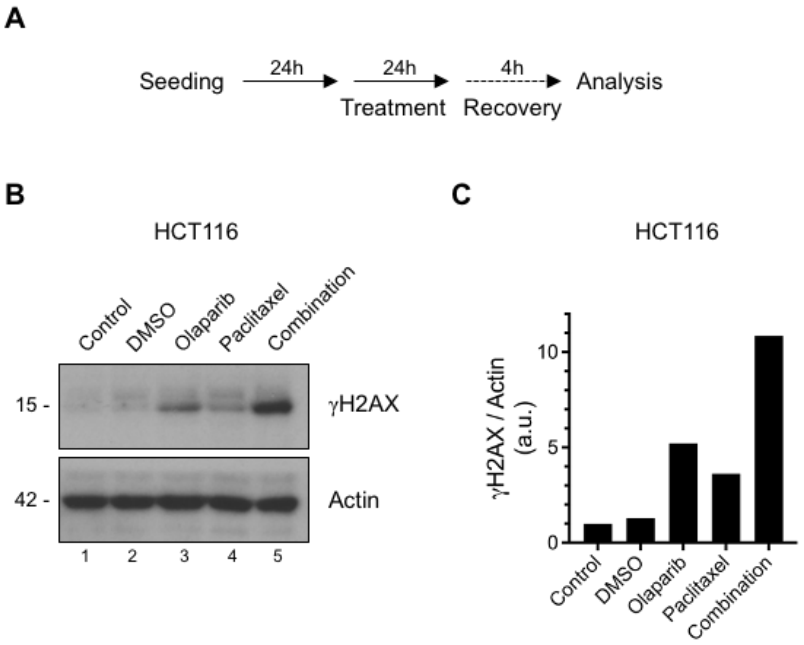

Figure 4: The olaparib-paclitaxel combination induces intensive DNA damage. (A) Schematic diagram of the experimental setting, (B) Phosphorylation of H2AX was analyzed by Western blotting. Following 24 hours of seeding, HCT116 cells were either un-treated (control) or treated with DMSO, olaparib (1 μM) and/or paclitaxel (1 nM) for 24 hours. Following treatment, cells were allowed to recover in drug-free medium for 4 hours and then processed for Western blotting, (C) histogram showing H2AX activation as judged by Ser139 phosphorylation obtained by densitometric quantification of Western blots represented in B. Arbitrary units were normalized to the expression of the corresponding β-actin

To further investigate whether the improved cytotoxic effect of the paclitaxel-olaparib combination was the consequence of increased DNA damage levels, we examined DNA damage induction by analyzing γH2AX foci formation. Cells seeded in the glass coverslips were treated with paclitaxel (1 nM) and olaparib (1 μM) alone or in combination for 24 hours before being subjected to the immunofluorescence analysis. Consistent with Western blotting analysis, we observed a significant elevation of γH2AX foci formation in HCT116 cancer cells treated with paclitaxel and rucaparib combination compared to monotherapy of each drug (Fig. 5A/B), suggesting that olaparib may intensify the cytotoxicity effect of paclitaxel through increasing the overall DNA damage accumulation in HCT116 colorectal cancer cells. Consequently, the increased DNA damage burden upon the combination treatment of paclitaxel and olaparib is the most likely cause of the reduced colony survival of HCT116 cancer cells.

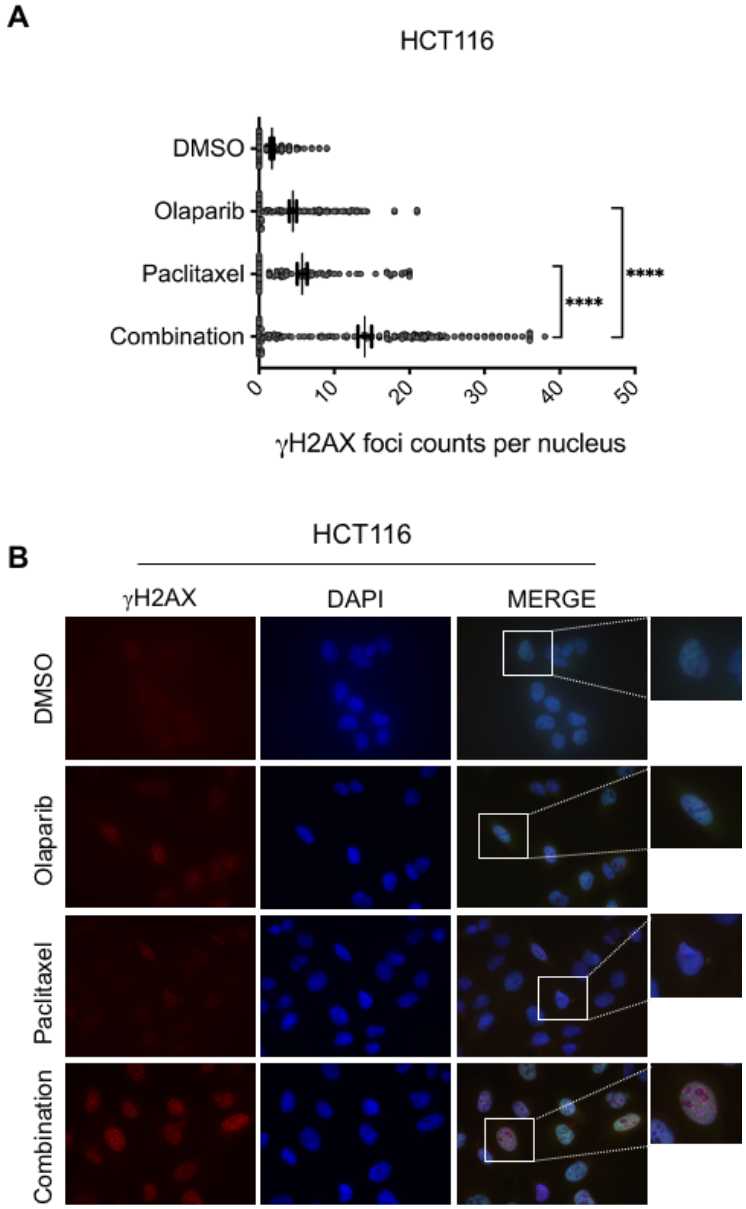

Figure 5: Paclitaxel-induced DNA damage is intensified upon olaparib treatment. (A) The dot blot graph represents quantification of nuclear γH2AX foci number in HCT116 cells treated with/out olaparib (1 μM) and/or paclitaxel (1 nM). >100 cells were scored per experiment (n=3), (B) representative images of immunodetection of γH2AX foci (red) in HCT116 cells exposed to beforementioned treatments for 24 hours. DNA is stained blue

4. Discussion

Cytotoxic chemotherapy is widely used for the management of many cancer treatments; however, *de novo* or acquired drug resistance, as well as side effects, limit the clinical success of anti-neoplastic agents. The main mechanism of action of the most chemotherapeutics is to bombard the genome with various types of DNA lesions up to a certain level that a cell decides to death [37]. This intensified DNA damaging pressure increases the genomic instability of

tumour cells, provoking them to alter the regulation of various cellular pathways to survive including DNA damage response (DDR) and repair mechanisms. Therefore, the combination of conventional drugs with smart small-molecule inhibitors targeting DDR components would potentially offer better treatment responses. Unlike directly DNA damaging cytotoxic drugs, paclitaxel interferes with the disassembly of microtubules by promoting tubulin polymerization. The formation of stable and dysfunctional microtubules causes the inhibition of cell cycle regulation and ultimately induces cell death [4-6, 31]. In this study, the combination of low-dose paclitaxel with olaparib or rucaparib was evaluated for treating colorectal cancers. The combination treatment of HCT116 cells with paclitaxel and olaparib revealed a much stronger inhibitory effect on clonogenic formation compared with paclitaxel or olaparib alone. Rucaparib treatment with paclitaxel provided similar results in the clonogenic evaluation of HCT116 cells. It has been shown that 1 nM paclitaxel treatment arrests the cell cycle at the G1 phase in HCT116 cells [12]. Considering PARP enzymes essential for the induction of G1 arrest [38], one can argue that PARP inhibition may potentially prevent the G1 arrest and therefore allow paclitaxel-treated cancer cells with dysfunctional microtubules towards the S phase, consequently causing more catastrophic DNA damage induction. Indeed, we revealed that HCT116 colorectal cancer cells acquired more DNA damage upon the combined paclitaxel and olaparib treatment compared to single-agent treatments. HCT116 colorectal cancer cells are deficient in mismatch repair and therefore characterized by microsatellite instability (MSI) [32]. Williams et al. demonstrated that the MSI status of colorectal cancer cells is dispensable for the response to PARP inhibitor niraparib, alone or in combination with DNA damaging agent irinotecan [28]. Therefore, further research is warranted to fully understand whether the genomic and proteomic profiles of HCT116 cells [32] are significant in this enhanced therapeutic response to paclitaxel and olaparib combined treatment. In addition, since paclitaxel can also cause DNA single-strand breaks (SSBs) [39-41], deficient SSB repair due to PARP inhibition may induce the accumulation of paclitaxel-induced SSBs which are eventually converted to disastrous DNA double-strand breaks (DSBs) during DNA replication [42]. Inefficient homologous recombination DSB repair mechanism owing to a possible *BRCA2* mutation in HCT116 cells [32] may also explain why the paclitaxel-olaparib treatment induces more DNA damage and less clonogenic survival of HCT116 cells. Detailed mechanisms remain to be elucidated.

5. Conclusion

The efficacy of paclitaxel and olaparib, both alone and in combination, was assessed in HCT116 colorectal cancer cells. Our results suggest that the combination of paclitaxel and

olaparib may need to be further studied to enhance the therapeutic responses of colorectal cancer patients.

Acknowledgement

The author thanks Dr. M.K. Erdogan and S. Acikgoz for critical reading of the manuscript. The author further acknowledges the funding supports of the Scientific and Technological Research Council of Turkey (TUBITAK 119S007) and the Scientific Research Projects Coordination Unit of Bingol University (BAP-SHMYO.2019.00.002).

References

[1] Bray, F., Ferlay, J., Soerjomataram, I., Siegel, R.L., Torre, L.A., Jemal, A., *Global cancer statistics 2018: GLOBOCAN estimates of incidence and mortality worldwide for 36 cancers in 185 countries*, CA: A Cancer Journal for Clinicians, 68(6), 394-424, 2018.

[2] Ades, S., *Adjuvant chemotherapy for colon cancer in the elderly: Moving from evidence to practice*, Oncology, 23(2), 162-167, 2009.

[3] Jensen, N.F., et al., *Establishment and characterization of models of chemotherapy resistance in colorectal cancer: Towards a predictive signature of chemoresistance*, Molecular Oncology, 9(6), 1169-1185, 2015.

[4] Othman, T., Goto, S., Lee, J.B., Taimura, A., Matsumoto, T., Kosaka, M., *Hyperthermic enhancement of the apoptotic and antiproliferative activities of paclitaxel*, Pharmacology, 62(4), 208-212, 2001.

[5] Barbuti, A.M., Chen, Z.S., *Paclitaxel through the ages of anticancer therapy: Exploring its role in chemoresistance and radiation therapy*, Cancers, 7(4), 2360-2371, 2015.

[6] Rowinsky, E.K., Donehower, R.C., *Paclitaxel (Taxol)*, New England Journal of Medicine, 332(15), 1004-1014, 1995.

[7] Banerji, A., Lax, T., Guyer, A., Hurwitz, S., Camargo, C.A., Long, A.A., *Management of hypersensitivity reactions to carboplatin and paclitaxel in an outpatient oncology infusion center: A 5-year review*, The Journal of Allergy and Clinical Immunology: In Practice, 2(4), 428-433, 2014.

[8] Orr, G.A., Verdier-Pinard, P., McDaid, H., Horwitz, S.B., *Mechanisms of Taxol resistance related to microtubules*, Oncogene, 22(47), 7280-7295, 2003.

[9] Lien, K., Georgsdottir, S., Sivanathan, L., Chan, K., Emmenegger, U., *Low-dose metronomic chemotherapy: A systematic literature analysis,* Eurepean Journal of Cancer, 49(16), 3387-3395, 2013.

[10] Loven, D., Hasnis, E., Bertolini, F., Shaked, Y., *Low-dose metronomic chemotherapy: From past experience to new paradigms in the treatment of cancer*, Drug Discovery Today, 18(3-4), 193-201, 2013.

[11] Gong, L.H., et al., *Piperlongumine induces apoptosis and synergizes with cisplatin or paclitaxel in human ovarian cancer cells*, *O*xidative Medicine and Cellular Longevity, 906804, 1-10, 2014.

[12] Lv, C., et al., *Low-dose paclitaxel inhibits tumor cell growth by regulating glutaminolysis in colorectal carcinoma cells*, Frontiers in Pharmacology, 8(244), 1-10, 2017.

[13] Cheng, M., et al., *Weekly dose-dense paclitaxel and triweekly low-dose cisplatin: A well-tolerated and effective chemotherapeutic regimen for first-line treatment of advanced ovarian, fallopian tube, and primary peritoneal cancer*, International Journal of Environmental Research and Public Health, 16(23), 4794, 2019.

[14] Kennedy, A.S., Harrison, G. H., Mansfield, C. M., Zhou, X. J., Xu, J. F., Balcer-Kubiczek, E. K., *Survival of colorectal cancer cell lines treated with paclitaxel, radiation, and 5-FU: Effect of TP53 or hMLH1 deficiency*, International Journal of Cancer, 90(4), 175-185, 2000.

[15] Li, H., et al., *Low-dose paclitaxel downregulates MYC proto-oncogene bHLH transcription factor expression in colorectal carcinoma cells*, Oncology Letters, 15(2), 1881-1887, 2018.

[16] Li, Q., et al., *Low doses of paclitaxel enhance liver metastasis of breast cancer cells in the mouse model,* The FEBS Journal, 283(15), 2836-2852, 2016.

[17] Shetti, D., Zhang, B., Fan, C., Mo, C., Lee, B.H., Wei, K., *Low Dose of Paclitaxel Combined with XAV939 Attenuates Metastasis, Angiogenesis and Growth in Breast Cancer by Suppressing Wnt Signaling*, Cells, 8(8), 1-22, 2019.

[18] Ciccia, A., Elledge, S.J., *The DNA Damage Response: Making It Safe to Play with Knives*, Molecular Cell, 40(2), 179-204, 2010.

[19] Goldstein, M., Kastan, M.B., *The DNA Damage Response: Implications for Tumor Responses to Radiation and Chemotherapy*, Annual Review of Medicine, 66(1), 129-143, 2015.

[20] Sonnenblick, A., de Azambuja, E., Azim, H.A., Piccart, M., *An update on PARP inhibitors-moving to the adjuvant setting*, Nature Review Clinical Oncology, 12(1), 27-41, 2015.

[21] Morales, J.C., et al., *Review of poly (ADP-ribose) polymerase (PARP) mechanisms of action and rationale for targeting in cancer and other diseases*, Critical Reviews in Eukaryotic Gene Expression., 24(1), 15-28, 2014.

[22] Dréan, A., Lord, C.J., Ashworth, A., *PARP inhibitor combination therapy*, Critical Reviews in Oncology/Hematology, 108, 73-85, 2016.

[23] Walsh, C., *Targeted therapy for ovarian cancer: The rapidly evolving landscape of PARP inhibitor use*, Minerva Ginecologica, 70(2), 150-170, 2018.

[24] The Food and Drug Administration (FDA). (2020, May 01). *FDA approves olaparib for germline BRCA-mutated metastatic breast cancer*, 2018.

[25] The Food and Drug Administration (FDA). (2020, May 01). *FDA approves olaparib for gBRCAm metastatic pancreatic adenocarcinoma,* 2019.

[26] Arena, S., et al., *A subset of colorectal cancers with cross-sensitivity to olaparib and oxaliplatin*, Clinical Cancer Research, 26(6), 1372-1384, 2020.

[27] Augustine, T., Maitra, R., Zhang, J., Nayak, J., Goel, S., *Sensitization of colorectal cancer to irinotecan therapy by PARP inhibitor rucaparib*, Investigational New Drugs, 37(5), 948-960, 2019.

[28] Genther Williams S.M., et al., *Treatment with the PARP inhibitor, niraparib, sensitizes colorectal cancer cell lines to irinotecan regardless of MSI/MSS status*, *Cancer Cell International.*, 15(1), 1-11, 2015.

[29] Gomez, V., et al., *Regulation of DNA damage responses and cell cycle progression by hMOB2*, Cellular Signalling., 27(2), 326–39, 2015.

[30] Hergovich, A., Bichsel, S.J., Hemmings, B.A., *Human NDR kinases are rapidly activated by MOB proteins through recruitment to the plasma membrane and phosphorylation*, Molecular and Cellular Biology, 25(18), 8259-8272, 2005.

[31] Weaver, B.A., *How Taxol/paclitaxel kills cancer cells, Molecular Biology of the Cell*, 25(18), 2677-2681, 2014.

[32] Berg, K.C.G., et al., *Multi-omics of 34 colorectal cancer cell lines - a resource for biomedical studies*, Molecular Cancer, 16(116), 1-16, 2017.

[33] Duldulao, M.P., et al., *Gene expression variations in microsatellite stable and unstable colon cancer cells*, Journal of Surgical Research, 174(1), 1-6, 2012.

[34] Shen, J., et al., *ARID1A Deficiency Impairs the DNA Damage Checkpoint and Sensitizes Cells to PARP Inhibitors*, Cancer Discovery, 5(7), 752-767, 2015.

[35] Wang, C., Jette, N., Moussienko, D., Gwyn Bebb, D., Lees-Miller, S.P., *ATM-Deficient Colorectal Cancer Cells Are Sensitive to the PARP Inhibitor Olaparib*, Translational. Oncology, 10(2), 190-196, 2017.

[36] Kuo, L.J., Yang, L.X., *γ-H2AX- A novel biomaker for DNA double-strand breaks*, In Vivo, 22(3), 305-309, 2008.

[37] Desai, A., Yan, Y., Gerson, S.L., *Advances in therapeutic targeting of the DNA damage response in cancer*, DNA Repair, 66(67), 24-29, 2018.

[38] Masutani, M., Nozaki, T., Wakabayashi, K., Sugimura, T., *Role of poly(ADP-ribose) polymerase in cell-cycle checkpoint mechanisms following γ-irradiation*, Biochimie, 77(6), 462-465, 1995.

[39] Ollikainen, T., et al., I*n vitro sensitivity of normal human mesothelial and malignant mesothelioma cell lines to four new chemotherapeutic agents,* Anticancer Drugs, 11(2), 93-99, 2000.

[40] Digue, L., et al., *Evaluation of the genotoxic activity of paclitaxel by the in vitro micronucleus test in combination with fluorescent in situ hybridization of a DNA centromeric probe and the alkaline single cell gel electrophoresis technique (comet assay) in human T-lymph*, Environmental and Molecular Mutagen, 34(4), 269-278, 1999.

[41] Branham, M.T., Nadin, S.B., Vargas-Roig, L.M., Ciocca, D.R., D*NA damage induced by paclitaxel and DNA repair capability of peripheral blood lymphocytes as evaluated by the alkaline comet assay*, Mutation Research/Genetic Toxicology and Environmental Mutagenesis, 560(1), 11-17, 2004.

[42] Bryant, H.E., Helleday, T., *Inhibition of poly (ADP-ribose) polymerase activates ATM which is required for subsequent homologous recombination repair*, Nucleic Acids Research, 34(6), 1685-1691, 2006.

Adıyaman University Journal of Science
https://dergipark.org.tr/en/pub/adyujsci
DergiPark AKADEMİK
ISSN 2147-1630
e-ISSN 2146-586X

Synthesis and Anticancer Activities of Water Soluble Schiff Base Metal Complexes

Burcu SAYGIDEĞER DEMİR[1,*], İlyas GÖNÜL[2], Gizem GÜMÜŞGÖZ ÇELİK[3], Seda İPEKBAYRAK[2], Yasemin SAYGIDEĞER[4]

[1]*Çukurova University, Central Research Laboratory, Adana, Turkey*
burcusaygidemir@gmail.com, ORCID: 0000-0001-5179-0522
[2]*Çukurova University, Arts and Science Faculty, Department of Chemistry, Adana, Turkey*
ilyasgonul01@gmail.com, ORCID: 0000-0002-7697-3613
seda_kzy@hotmail.com, ORCID: 0000-0001-7628-807X
[3]*Gebze Technical University, Faculty of Science, Department of Chemistry, Kocaeli, Turkey*
gizemgumusgozc@gtu.edu.tr, ORCID: 0000-0003-4816-7419
[4]*Çukurova University, Faculty of Medicine, Department of Pulmonry, Adana, Turkey*
yaseminsaygideger@gmail.com, ORCID: 0000-0003-3293-373X

Received: 18.05.2020 **Accepted:** 11.11.2020 **Published:** 30.12.2020

Abstract

In this study, we synthesized the water-soluble Schiff Base containing S, O, N heteroatoms by the condensation reaction from 4-amino-3-hydroxynaphthalene-1-sulfonic acid and 2-hydroxy-3-methoxybenzaldehyde. In addition, Cu (II), Zn (II) and Ni (II) complexes of the ligand were synthesized and characterized by elemental analysis, magnetic susceptibility and spectroscopic techniques such as FT-IR, ^{1}H-NMR and ^{13}C-NMR. The anticancer activities of ligand and its three metal complexes on A549 lung cancer cell lines were evaluated. Cell viability experiments revealed that Ligand (L) and nickel (II) complex (L-Ni) did not able to inhibit A549 cell proliferation while L-Cu and L-Zn had 12 and 80 μM of IC_{50} values respectively. These last two complexes also induced apoptosis and suppressed cell migration on A549 cells.

Keywords: Schiff base; Metal complexes; Lung cancer; Cell culture.

Suda Çözünebilir Schiff Bazı Metal Komplekslerinin Sentezi ve Antikanser Aktivitesi

Öz

* Corresponding Author DOI: 10.37094/adyujsci.738743

Bu çalışmada, 4-amino-3-hidroksinaftalin-1-sülfonik asit ve 2-hidroksi-3-metoksibenzaldehitten kondensasyon reaksiyonu ile S, O, N hetero atomları içeren suda çözünebilir bir Schiff Bazı elde edildi. Ek olarak, ligandın Cu (II), Zn (II) ve Ni (II) kompleksleri sentezlendi ve elementel analiz, manyetik duyarlılık ve FT-IR, ^{1}H-NMR ve ^{13}C-NMR gibi spektroskopik tekniklerle karakterize edildi. Ligandın ve üç metal kompleksinin A549 akciğer kanseri hücre hattında antikanser aktiviteleri değerlendirildi. L-Cu ve L-Zn olarak etiketlenmiş Bakır (II) ve Çinko (II) komplekslerinin IC_{50} değerleri sırasıyla 12 ve 80 μM olarak bulundu. L-Cu ve L-Zn komplekslerinin A549 hücrelerinde apoptozu indüklediği ve hücre göçünü inhibe ettiği görüldü. Ligand (L) ve Nikel (II) bileşiklerinin (L-Ni) A549 hücre proliferasyonu üzerinde herhangi bir etki göstermediği belirlendi.

Anahtar Kelimeler: Schiff bazı; Metal kompleksleri; Akciğer kanseri; Hücre kültürü.

1. Introduction

Due to the in vitro cytotoxic effect of metal-based compounds, the interest in these compounds is increasing day by day in cancer treatment. The electronic nature of metals, modifications in ligands and conformational changes in functional groups give rise to the discovery of drugs with different cytotoxic and pharmacokinetic properties. Schiff bases and their metal complexes are the most studied coordination compounds and their uses as anticancer agents are becoming increasingly important [1].

Schiff Bases attract the scientists because of its features containing donor atoms such as oxygen and sulfur and generation of high stability complexes with mono, di, tri and polydentate that can be coordinated to metal ions. Schiff bases are formed as a result of the condensation reaction of aldehydes and primary amines. When these ligands contain different functional groups such as sodium carboxylate and sulfonate in their structure, they acquire water-soluble properties and can be converted into structures with a wide range of chemical properties. [2, 3]. Water soluble compounds expected to have low toxicity because of their inability to bind sulfhydryl groups of proteins of kidney tubules. Therefore, water solubility provides a decrease in the adverse effects and leads improvement in cellular uptake of the drug.

In this study, the Schiff base ligand (L) was synthesized in the water-methanol medium using 4-amino-3-hydroxynaphthalene-1 sulfonic acid and 2-hydroxy-3-methoxy benzaldehyde, which is a water-soluble structure having -SO_3, -OH and -C=N hetero groups. After that, its Cu (II), Ni (II) and Zn (II) complexes were synthesized and characterized by elemental analysis and spectroscopic techniques (FT-IR, ^{1}H-NMR and ^{13}C-NMR). And also in-vitro cytotoxic, apoptotic

and anti-metastatic properties of these compounds were investigated on non-small cell lung cancer cells.

2. Materials and Methods

2.1. Materials

All solvents were commercially purchased in high purity. 4-amino-3-hydroxynaphthalene-1-sulfonic acid ($C_{10}H_9NO_4S$), 2-Hydroxy-3-methoxybenzaldehyde ($CH_3OC_6H_3$-2-(OH)CHO), sodium hydroxide (NaOH), $Zn(CH_3COO)_2.4H_2O$, $Ni(CH_3COO)_2.4H_2O$ and $Cu(CH_3COO)_2$ were purchased from Sigma-Aldrich Co.. All chemicals were analytical grade and used without further purification. Elemental analysis was carried out on LECO CHNS (model 932) instrument. FT-IR spectra of KBr discs were recorded on a Perkin-Elmer RX-1 4000-400cm^{-1} FT-IR spectrometer. ^{1}H-NMR and ^{13}C-NMR spectra were recorded a Bruker 600 MHz Ultrashield Spectrometer using TMS as an internal standard and DMSO-d_6 as a solvent. Elemental analysis was carried out by use of LECO CHNS (model 932).

A549 cells were obtained from Bingöl University, Department of Molecular Biology and Genetic and BEAS2B cells were obtained from Gaziantep University, Faculty of Medicine. MTT (Thiazolyl Blue Tetrazolium Bromide) used in the study was purchased BioFroxx. DMSO was purchased from Sigma-Aldrich Co. Biolegend APC-Annexin-V/PI apoptosis detection kit was used in the apoptosis analysis. All cell culture materials were purchased from Hyclone. The brand of the microplate reader used in the study is Biochrom EZ Read 400, and the flow cytometry analysis were performed on Beckman Coulter/CytoFLEX, (United States). Prism V 8.2.1 (GraphPad Software, Inc, CA, USA) was used for statistical analysis.

2.2. Methods

2.2.1. Synthesis of imine ligand: sodium 3-hydroxy-4 - ((2-hydroxybenzylidene amino) naphthalene-1-sulfonate (NaH_2L)

4-amino-3-hydroxynaphthalene-1-sulfonic acid (10 mmol, 2.3 g), NaOH (10 mmol, 0.4 g) and ethanol (50 ml) solution were added in a reaction flask than stirred to the soluble state were refluxed. Then 2-hydroxy-3-methoxybenzaldehyde (1.52 g, 10 mmol) was dissolved in 10 mL ethanol and added dropwise to the reaction flask [2, 4, 5]. The mixture was refluxed for 3 hours under $Ar_{(g)}$. A dark orange precipitate was obtained after cooling to room temperature, then filtered, washed several times with cold ethanol and dried in the vacuum desiccator. The structure of sodium 3-hydroxy-4-((2-hydroxy-3-methoxybenzylidene) amino) naphthalene-1-sulfonate (Ligand NaH_2L: Abbreviated as L) formed as a result of the condensation reaction is given in Fig. 1.

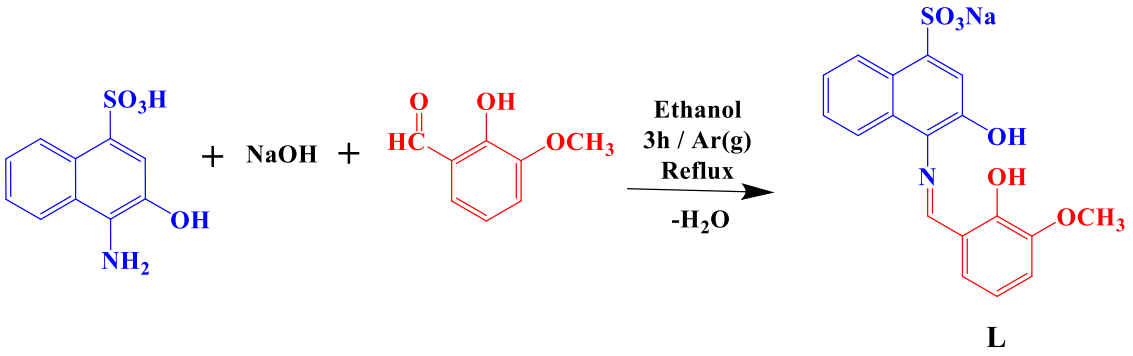

Figure 1: The structure and the reaction conditions of L

L: Yield 75% (2.96 g), m.p. >350 °C, formula wt; 395.36 g/mol. Anal. calcd. for $C_{18}H_{14}NNaO_6S$: C, 54.68; H, 3.57; N, 3.54; S, 8.11; Na, 5.8; found C, 53.92; H, 3.46; N, 3.52; S, 7.94; Na, 5.78. FT-IR (KBr pellet, cm^{-1}); 3279 ($\upsilon_{(OH)}$, m), 3076 ($\upsilon_{(OCH3)}$, v), (s), 1613 ($\upsilon_{(C=N)}$, s), 1165-1046 ($\upsilon_{(SO3)}$, s). ^{1}H-NMR (600 MHz, $DMSO_4$-d_6) σ ppm: 13.77 (s, 1H) 10.16 (s, 1H); 9.13 (s, 1H); 8.78 (d, *J*=8.40 Hz, 1H); 7.92 (s, 1H); 7.91 (d, *J*=9.00 Hz, 1H); 7.49-7.47 (m, 1H); 7.39-7.36(m, 1H); 7.27-7.25 (m, 1H); 7.17 – 7.16 (m, 1H); 6.94 (t, *J*=8.40 Hz, 1H); 3.86 (s, 3H). ^{13}C-NMR (150 MHz, $DMSO_4$-d_6) σ ppm: 168.75; 151.21; 148.44; 143.69; 143.21; 130.25; 128.53; 128.26; 126.75; 124.16; 123.45; 121.80; 119.93; 119.07; 118.47; 115.92.

2.2.2. Synthesis of metal complexes

The three mmol L was dissolved in hot 30 ml 2: 1 methanol: water mixture. Then three mmol of metal salt dissolved in 10 ml of 1: 1 methanol: water mixture was added to the medium and left under reflux for 4 hours. All metal complexes were synthesized by the same method using the appropriate amount of metal salt. Finally, half of the solvent was evaporated to leave the precipitate. The precipitate formed was filtered, washed several times with cold ethanol and allowed to dry overnight at 60 °C in a vacuum oven. The synthesized compounds were characterized by analytical and spectroscopic methods. The proposed structures for the synthesized complexes are given in Fig. 2.

$Na[CuL(H_2O)]H_2O$ (L-Cu): Yield %75 (1.05 g), dark brown, m.p. >350 °C, formula wt; 492,92 g/mol. Paramagnetic, 1.54 BM. Anal. calcd. for $NaC_{18}H_{16}NO_8SCu$: C, 43.86; H, 3.27; N, 2.84; S, 6.50; Na, 4.66; Cu, 12.89; found C, 43.91; H, 3.54; N, 2.97; S,6.81; Na, 4.74; Cu, 13.01. FT-IR (KBr pellet, cm^{-1}); 3464 ($\upsilon_{(OH)}$, m), 1600 ($\upsilon_{(C=N)}$, s), 1220-1044 ($\upsilon_{(SO3)}$, s), 550 ($\upsilon_{(M-N)}$, m), 486 ($\upsilon_{(M-O)}$, m).

Na[NiL(H_2O)]H_2O (L-Ni): Yield 65% (0.91 g), yellowish green, m.p. >350 °C, formula wt; 488.07 g/mol. Paramagnetic, 2.63 BM Anal. calcd. for $NaC_{18}H_{16}NO_8SNi$: C, 44.30; H, 3.30; N, 2.87; S, 6.57; Na, 4.71; Ni, 12.03. found C, 44.92; H, 3.41; N, 2.99; S, 6.28; Na, 4.82; Ni, 12.07. FT-IR (KBr pellet, cm^{-1}); 3223 ($\upsilon_{(OH)}$, m), 1612 ($\upsilon_{(C=N)}$, s), 1216-1042 ($\upsilon_{(SO3)}$, s), 620 ($\upsilon_{(M-N)}$, m), 496 ($\upsilon_{(M-O)}$, m).

Na[ZnL(H_2O)]H_2O (L-Zn): Yield %66 (0.94 g), dark orange, m.p. >350 °C, formula wt; 494.75 g/mol. Diamagnetic. Anal. calcd. For $NaC_{18}H_{16}NO_8SZn$: C, 43.20; H, 3.26; N, 2.83; S, 6.48; Na, 4.65; Zn, 13.21 found C, 43.36; H, 3.31; N, 2.98; S,6.54; Na, 4.73, Zn; 13.12. FT-IR (KBr pellet, cm^{-1}); 3428 ($\upsilon_{(OH)}$, m), 1610 ($\upsilon_{(C=N)}$, s), 1228-1049 ($\upsilon_{(SO3)}$, s), 530 ($\upsilon_{(M-N)}$, m), 499 ($\upsilon_{(M-O)}$, m).

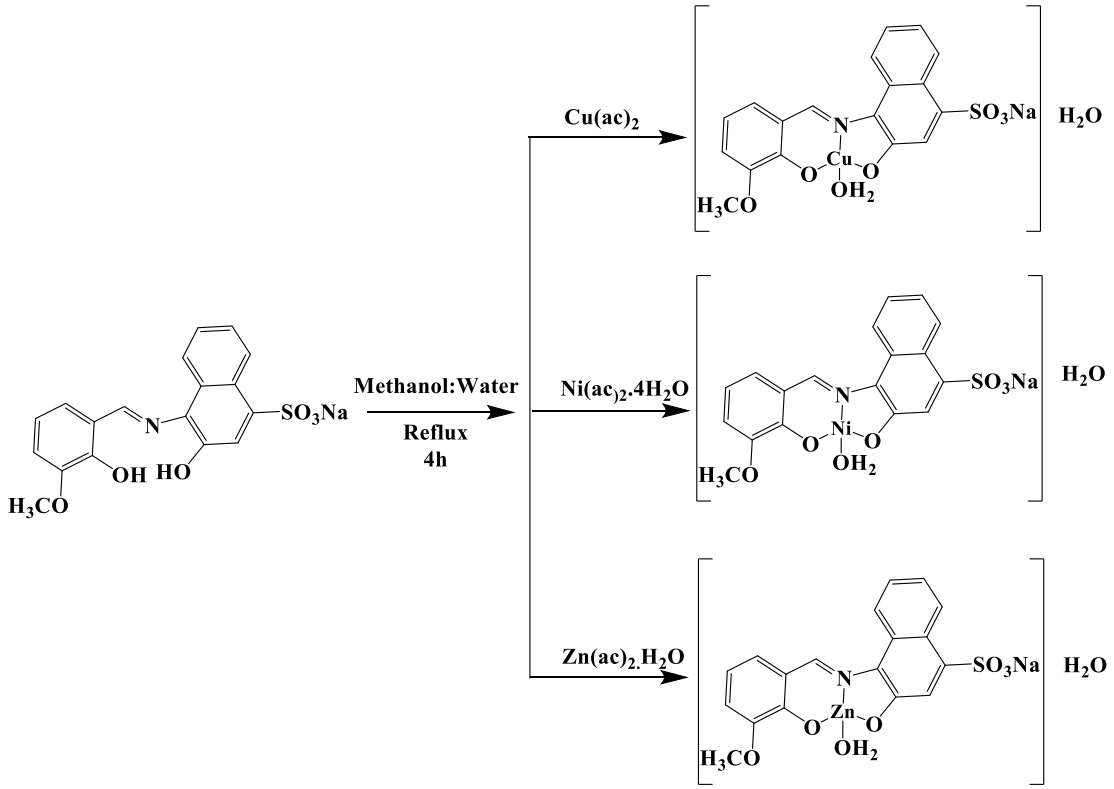

Figure 2: The proposed structures for the synthesized complexes

2.2.3. Cell visibility assay

A549 (lung cancer) cells were treated with different concentrations of the compounds to investigate the cytotoxic effect by using MTT assay according to the Mosmann's procedure [6]. Optimization experiments were performed to decide the number of cells per well to reach 80% confluency. 104 cells/well were cultured in a 96-well plate for overnight at 37 ºC, 5% CO_2 in RPMI medium containing 1% antibiotics and 10% FBS. Then, the old medium was removed and

fresh medium containing compounds at (0, 0.1, 0.3, 1, 3, 10, 30, 100) µM concentrations were added in triplicate and the cells were incubated for 24 more hours. Water was used as a vehicle control. At the end of the incubation time, MTT solution was added to the wells to reach a final concentration of 0.5 mg/mL, and the cells were incubated for 4 hrs to metabolize MTT. The medium was removed and 50 µL DMSO was added per well to dissolve the formazan crystals. Lastly, the absorbance was measured at 570 nm in a microplate reader. The same procedure was applied to the BEAS2B normal bronchial epithelial cells to check whether the compounds were selective against the lung cancer cells.

2.2.4. Flow cytometry assay

The apoptotic effects of L-Cu (20 µM) and of L-Zn (100 µM) were tested on A549 cells via flow cytometry assay. The ratio of apoptotic cells were determined according to Biolegend APC-Annexin-V/PI apoptosis detection kit protocol [7]. Briefly, 10^7 cells/mL in 6 well-plates (cell number was optimized to reach 80% confluency per well) were maintained in RPMI medium, containing either drug or vehicle and incubated in the CO_2 incubator at 37 °C for 24 hours. At the end of the incubation period, the cancer cells were harvested and incubated with APC-Annexin V and PI. The fluorescence emission of APC- Annexin-V stained cells was measured at 633 nm (Red laser) in the flow cytometer instrument. The instrument software provided the result of the analysis as living cells (APC- / PI-); early apoptotic cells (APC + / PI-); necrotic cells (APC- / PI +); and the late apoptotic cells (APC + / PI +).

2.2.5. Wound healing assay

A549 cells were plated in 6 cm plates in regular growth medium containing 10% FBS. After 24 hrs, a straight-line scratch was made on cell layers using a sterile 200 µL disposable pipette tip and washed with PBS. Then, the cells treated either with IC_{50} concentration of the compounds (12 µM L-Cu 80 µM L-Zn) and with water as a control. Images of cell migration were taken using an inverted microscope at 0 hrs and 24 hrs after the scratch. Gap lengths of the cells were measured using Image J.

2.2.6. Statistical analysis

Prism V 8.2.1 (GraphPad) was used to calculate IC50's of the compounds. The measured spectrophotometric values were first normalized, concentrations were converted to log forms and Non-linear regression (curve ft) was used to generate log (inhibitor) vs. response curves to determine IC_{50} values.

3. Results and Discussion

3.1. Synthesis and characterization of ligand and its metal complexes

Experimental percentages of the elements for all synthesized compounds were determined by using ICP-OES and elemental analysis devices. The percentages of carbon (C), hydrogen (H), sulfur (S), nitrogen (N), metal (Cu, Ni, Zn, Fe) and sodium (Na) obtained were compatible with theoretical values, which are given in the synthesis section.

3.1.1. FT-IR spectra

The data of the FT-IR spectra are listed in Table 1 and Fig. S1 in Supporting information (SI). The sharp peak observed around 1613 cm-1 in the spectrum of the ligand is the stretching vibrations of the azomethine group (Ar-C=N). This spectrum supports the successful condensation reaction. In addition, the peaks obtained at 3279 cm^{-1} and 1165-1046 cm^{-1} support the presence of Ar-OH and –SO3 groups in the molecular structure, respectively [8].

Table 1. FT-IR absorbtion bands of L and its metal complexes

Compounds	υ(OH)	υ(C=N)	υ(SO_3)	υ(M-N)	υ(M-O)
H_2L	3279	1613	1165-1046	-	-
L-Cu	3464	1600	1220-1044	550	486
L-Ni	3223	1612	1216-1042	620	496
L-Zn	3428	1610	1220-1049	530	499

In the FT-IR spectra of Cu (II), Zn (II) and Ni (II) complexes, the azomethine peak shifted from 1620 to 1600, 1612 and 1611 cm^{-1}, respectively. This shift supports the formation of the metal complex. In addition, new peaks were observed in the range of 620-486 cm^{-1} after complex formation [8, 9]. The novel peaks support the presence of M-N and M-O bonds.

3.1.2. ^{1}H-NMR and ^{13}C-NMR

^{1}H-NMR and ^{13}C-NMR spectra of NaH_2L structure recorded in DMSO-d_6 were given in Fig. 3. According to the ^{1}H-NMR spectrum the peak and its integrations of the expected structure were found to be consistent. The spectrum shows the peak of the phenolic (-OH, b) was observed at δ 13.77 ppm (s, 1H); the naphthalic hydroxy (-OH, c) at δ 10.16 ppm (s, 1H); azometine (-CH=N) at δ 9.13 (s, 1H); methoxy protons (-OCH_3, d) at δ 3.86 ppm (s, 3H); aromatic protons at δ 8.78 (d, 1H); δ 7.92 (s, 1H); δ 7.91(d, 1H); δ 7.49-7.47 (m, 1H); δ 7.39-7.36 (m, 1H); δ 7.27-7.25 (m, 1H); δ 7.17-7.16 (m, 1H); δ 6.94 (t, 1H). In accordance with ^{13}C-NMR spectrum, the observation of 18 peaks with different chemical environments as follows 168.75; 151.21; 148.44; 143.69; 143.21; 130.25; 128.53; 128.26; 126.75; 124.16; 123.45; 121.80; 119.93; 119.07; 118.47; 115.92. The ^{13}C-NMR spectrum of the NaH_2L confirms functional groups in the structure.

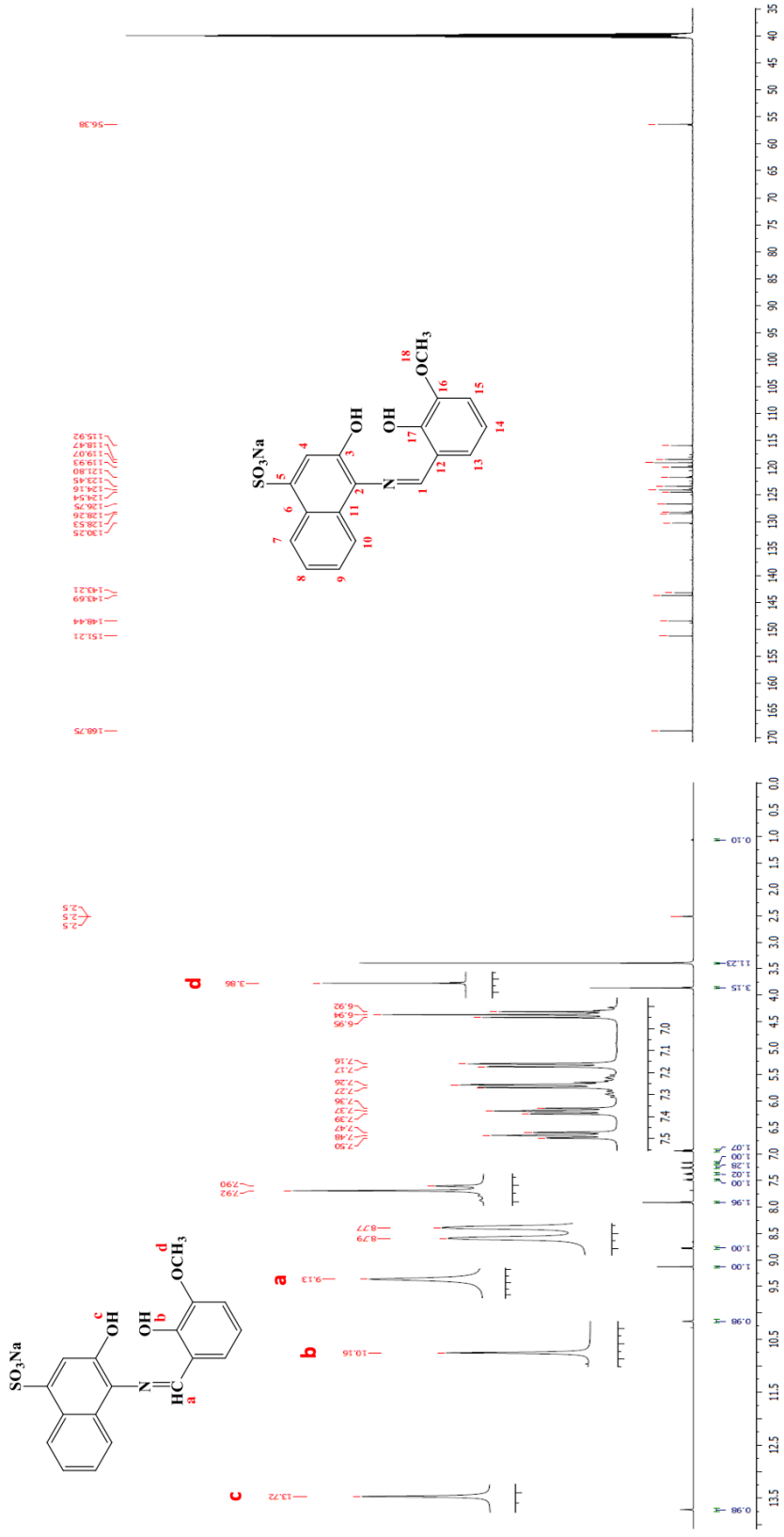

Figure 3: ^{1}H-NMR and ^{13}C-NMR spectra of L in DMSO-d$_6$

3.1.3. Magnetic susceptibility

The magnetic susceptibility results of metal complexes can give information about the structure. The values of Cu (II) and Ni (II) complexes taken from magnetic susceptibility measurements were 1.54 B.M and 2.63 B.M, respectively. Based on these data, we found that the complexes synthesized were paramagnetic as expected. As a result of the calculations, it is determined that there is one unpaired electron for Cu (II) and two for Ni (II). It is known that for the Cu (II) complex it may prefer both sp^3 or dsp^2 (tetrahedral or square plane) hybrids [10]. The presence of two unpaired electrons in the Ni (II) complex indicates that it preferred tetrahedral geometry by sp^3 hybridization [11]. In addition, the Zn (II) complex was found to have diamagnetic properties. Considering the proposed structure, it is thought that four coordinated complexes are formed and have tetrahedral geometry by sp^3 hybridization [12].

3.2. Anticancer studies

To evaluate the cytotoxic activities of the compounds in A549 cells, we incubated the cells with L, L-Ni, L-Cu and L-Zn compounds in the 0-100 μM concentration range for 24 hrs. The examined compounds are considered as not effective (IC_{50} values > 100 μM) and effective (IC_{50} < 99 μM). All experiments were independently repeated for three times. As shown in the dose-response curves (Fig. 4), L-Cu and L-Zn complexes exert an effective cytotoxic effect on A549 cells. L-Cu complex had the best cytotoxic effect on A549 cells with an average IC_{50} value of 12 μM at 24 hrs. L-Zn complex was the second best complex with an IC_{50} value of 80 μM at 24 hrs (Fig. 5). Both ligand and L-Ni complex showed no significant cytotoxic activity on A549 cells (IC_{50} > 100 μM). Cytotoxicity studies on the normal bronchial epithelial BEAS2B cell line showed that the L-Cu and L-Zn complexes had cytotoxic effects only at high concentrations that IC_{50} values could not be calculated (Fig. 5). The findings of the experiment indicated that these two compounds had a specific cytotoxic effect against the cancer cells. Further, comparing with the literature, the L-Cu complex was found slightly more potent than cisplatin, which is a current therapy agent against lung cancer, where an IC_{50} of 17.2 μM was reported for the same cell line (A549) and same treatment period [13, 14]. In addition, the water solubility of this compound might provide a great advantage in terms of toxicity.

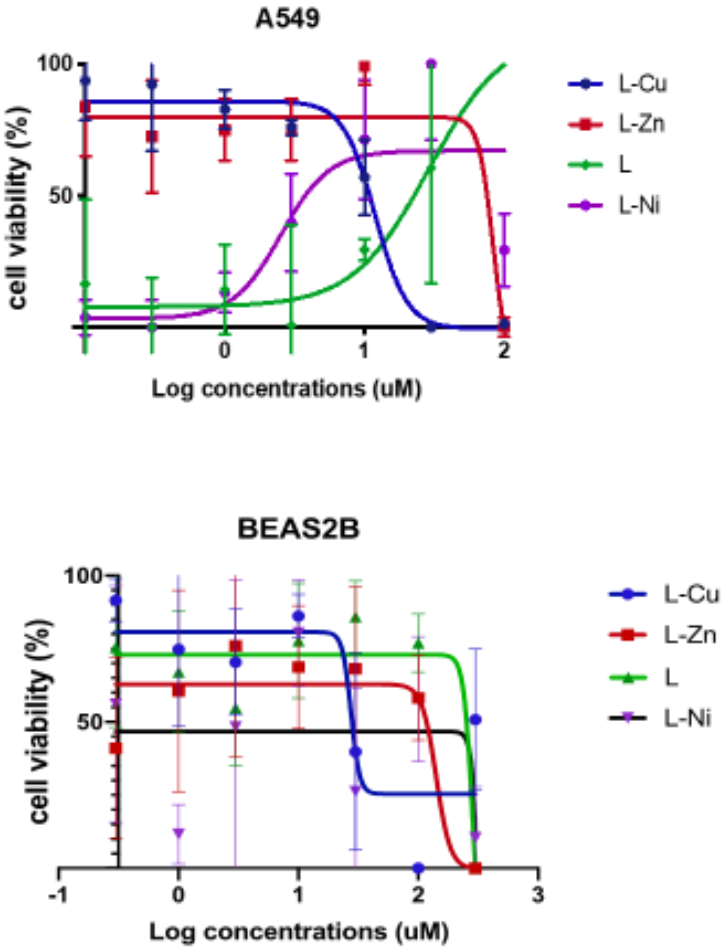

Compounds	IC_{50} values (μM)	
	A549	BEAS 2B
L-Cu	12	Very wide
L-Zn	80	Very wide
L	>100	Very wide
L-Ni	>100	Very wide

Figure 4: The **c**ells were treated with various concentrations of the compounds for 24 hrs. The cell viability assay was achieved with MTT protocol. IC_{50} values were calculated. While L-Cu and L-Zn complexes had cytotoxic effects on A549 lung cancer cells, they had no cytotoxic effect on BEAS2B normal lung cells at low concentration

Compounds may kill cells in apoptotic or toxic ways. In order to understand the cell killing mechanism of these novel compounds, we examined apoptosis induction effects for L-Cu and L-Zn complexes. After incubating the cells with the compounds at 20 μM and 80 μM concentrations respectively, we performed APC Annexin-V / PI flow cytometry analysis to determine the rate of

apoptotic cells. According to the results, the total (early and late) apoptotic cell rate of A549 cells, after normalization with water treated cells as a control, treated with L-Cu and L-Zn at 24 hours were 42.27% and 68.86% respectively, (Fig. 5). The obtained results reveal that both complexes have cytotoxic effects in an apoptotic pathway.

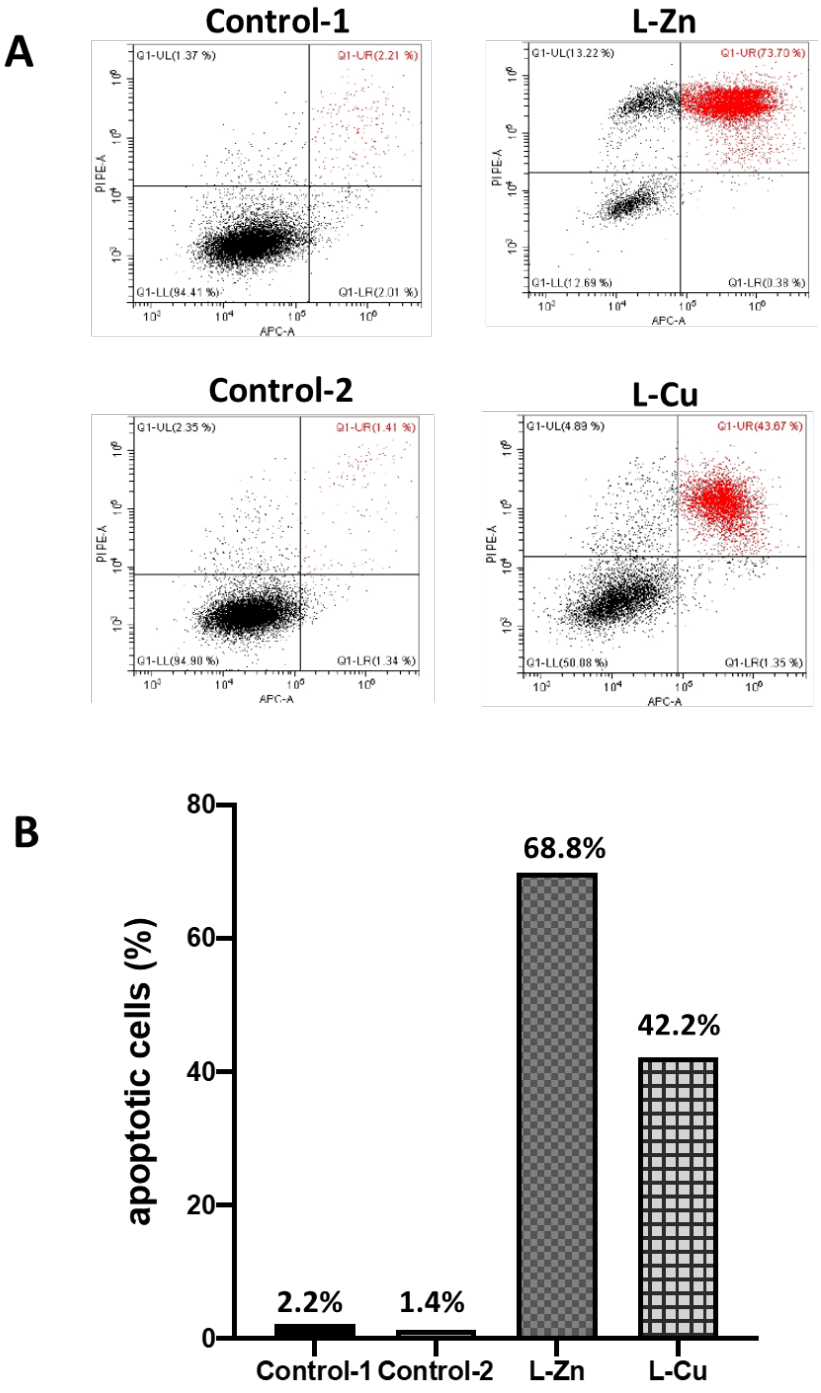

Figure 5: A549 Cells were treated with 20 μM L-Cu and 80 μM L-Zn complexes for 24 hours, cell viability was measured by flow cytometry. Upper (late) and lower (early) right quadrants show the apoptotic cells of the population (A). Apoptotic cell percentages are given in bar graphs (B)

We examined the effect of L-Cu and L-Zn on the metastasis of A549 cells. It is clearly seen in Figure 6 that the motility of the cells treated with both complexes for 24 hours is reduced. At the end of 24 hours, the gap between the cells did not close compared to the control for L-Cu (12 μM) and L-Zn (80 μM). Therefore, we concluded that these two complexes had ability to decrease the migration rate of the cells (Fig. 6).

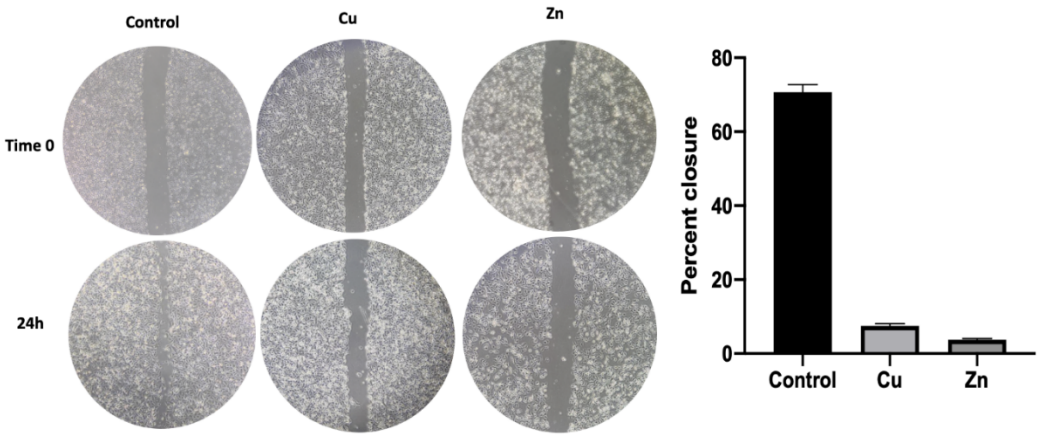

Figure 6: Representative images from the wound healing (scratch) assay using water as control are shown. L-Cu (12 μM) and L-Zn (80 μM) suppressed cell migration. Closure levels of A549 cells were analyzed after multiple measurements of the void area using image J. Statistical analysis was done using Prism V 8.2.1 and results are given in the bar graph

It is frequently seen in the literature that different metal complexes belong to the same ligand show different anticancer activity [15-17]. This may be related to the binding properties of the metal complex to DNA as well as the ligand. For example, in a study, the anticancer activity of complexes belong to the same ligand shows quite a difference according to the geometry of the complex. The activity sequence of Cu (II), Zn (II) and Ni (II) metals chelated with a ligand is given as Cu> Zn> Ni, may not be the same for another ligand [16]. Similarly, in another study, the anticancer activities of the metal complexes mentioned in the same ligand are very close to each other [17]. In this study, the activity order was determined as Cu> Zn> Ni. L-Cu, L-Zn and L-Ni complexes are tetra-coordinated. While L-Zn and L-Ni have terahedral geometry, L-Cu may have square plane geometry unlike others. The superiority of anticancer activity compared to others may be due to the difference in the geometry of the complex of covalent or non-covalent attachments with DNA. Sometimes Schiff base ligands are effective in killing cancer cells alone,

but other times accompanying with a metal may increase the anticancer activity. In a study with Schiff bases, the cytotoxic activity of most ligands in different cell lines are found to be at the level of $IC_{50} > 100$ μM [15]. In our study, while the ligand was not effective alone ($IC_{50} > 100$ μM), antitumor activity was increased when Cu (II) and Zn (II) metals were added to the structure. A number of Cu (II) chelate complexes and Zn (II) Schiff base complexes were synthesized and evaluated for their anticancer effects on various cell lines in the literature [16, 18] Comparing to those, the complexes in this study can be considered superior due to their water solubility property.

4. Conclusion

This study aimed to develop an alternative drug to non-small cell lung cancer. For this purposes a water-soluble Schiff base ligand containing S, O, N heteroatoms and its Ni (II), Cu (II), Zn (II) complexes were synthesized and characterized. The advantages of these synthesized complexes over existing anticancer agents are that they are water-soluble, easily and cheaply obtainable. Moreover, while L-Cu and L-Zn complexes had good cytotoxic effect on A549 cell line, they were not effective even in higher concentrations on healthy lung cell line BEAS2B. These compounds, which act selectively against the A549 cancer cells, have the potential to be good antitumor agents when evaluated with their other advantages.

References

[1] Boghaei, D.M., Gharagozlou, M., *Synthesis and characterization of novel water-soluble zinc (II) Schiff-base complexes derived from amino acids and salicylaldehyde-5-sulfonates*, Journal of Coordination Chemistry, 60(3), 339-346, 2007.

[2] Hosseini-Yazdi, S.A., Mirzaahmadi, A., Khandar, A.A., Eigner, V., Dušek, M., Lotfipour, F., Mahdavi, M., Soltani, S., Dehghan, G., *Synthesis, characterization and in vitro biological activities of new water-soluble copper (II), zinc (II), and nickel (II) complexes with sulfonato-substituted Schiff base ligand*, Inorganica Chimica Acta, 458, 171-180, 2017.

[3] Hosseini-Yazdi, S.A., Mirzaahmadi, A., Khandar, A.A., Eigner, V., Dušek, M., Mahdavi, M., Soltani, S., Lotfipour, F., White, J., *Reactions of copper (II), nickel (II), and zinc (II) acetates with a new water-soluble 4-phenylthiosemicarbazone Schiff base ligand: Synthesis, characterization, unexpected cyclization, antimicrobial, antioxidant, and anticancer activities*, Polyhedron, 124, 156-165, 2017.

[4] Skorokhod, L.S., Seifullina, I.I., Minin, V.V., Vlasenko, V.G., Pirog, I.V., *Synthesis and structure of Co (II), Ni (II), and Cu (II) complexes with Schiff bases, condensation products of 2-amino-4,8-naphthalenedisulfonic acid and aromatic carbinols*, Russian Journal of Inorganic Chemistry, 52(7), 1006-1012, 2007.

[5] Atahan, A., Durmus, S., *1-Amino-2-hydroxy-4-naphthalenesulfonic acid based Schiff bases or naphtho[1,2-d]oxazoles: selective synthesis and photophysical properties*, Spectrochim Acta A Mol Biomol Spectrosc, 144, 61-67, 2015.

[6] Mosmann, T., *Rapid colorimetric assay for cellular growth and survival: Application to proliferation and cytotoxicity assays*, J. Immunol. Methods, 94(1-2), 57-63, 1983.

[7] https://www.biolegend.com/nl-be/products/apc-annexin-v-apoptosis-detection-kit-with-pi-9788

[8] Erdem, E., Sari, E.Y., Kilinçarslan, R., Kabay, N., *Synthesis and characterization of azo-linked Schiff bases and their nickel (II), copper (II), and zinc (II) complexes*, Transition Metal Chemistry, 34(2), 167-174, 2008.

[9] Tunçel, M., Serin, S., *Synthesis and characterization of copper (ıı), nickel (ıı), and cobalt (ıı) chelates with tridentate schiff base ligands derived from 4-amino-5-hydroxynaphthalene-2,-7-disulfonic acid, synthesis and reactivity in ınorganic*, Metal-Organic, and Nano-Metal Chemistry, 33(6), 985-998, 2003.

[10] Al-Sha'alan, N.H., *Antimicrobial activity and spectral, magnetic and thermal studies of some transition metal complexes of a schiff base hydrazone containing a quinoline moiety*, Molecules, 12, 1080-1091, 2007.

[11] Gönül, İ., *Synthesis and structural characterization of ONO type tridentate ligands and their Co (II) and Ni (II) complexes: Investigation of electrical conductivity and antioxidant properties*, Inorg. Chim. Acta, 495, 119027 (1-8), 2019.

[12] Kalanithi, M., Kodimunthiri, D., Rajarajan, M., Tharmaraj, P., *Synthesis, characterization and biological activity of some new VO (IV), Co (II), Ni (II), Cu (II) and Zn (II) complexes of chromone based NNO Schiff base derived from 2-aminothiazole,* Spectrochimica Acta Part A: Molecular and Biomolecular Spectroscopy, 82, 290-298, 2011.

[13] Senthil, Raja, D., Ramachandran, E., Bhuvanesh, N.S.P., Natarajan, K., *Synthesis, structure and in vitro pharmacological evaluation of a novel 2-oxo-1, 2-dihydroquinoline-3-carbaldehyde (2'-methylbenzoyl) hydrazone bridged copper (II) coordination polymer*. European Journal of Medicinal Chemistry, 64, 148-159, 2013.

[14] Huang, K.B., Chen, Z.F., Liu, Y.C., Wang, M., Wei, J.H., Xie, X.L., Zhang, J.L., Hu K., Liang, H., *Copper (II/I) complexes of 5-pyridin-2-yl-[1,3]dioxolo[4,5-g]isoquinoline: synthesis, crystal structure, antitumor activity and DNA interaction*, European Journal of Medicinal Chemistry, 70, 640-648, 2013.

[15] Hejchman, E., Kruszewska, H., Maciejewska, D., Sowirka-Taciak, B., Tomczyk M., Sztoksz-Ignasiak A., Jankowski, J., Młynarczuk-Biały, I., *Design, synthesis, and biological activity of Schiff bases bearing salicyl and 7-hydroxycoumarinyl moieties*, Monatshefte für Chemie - Chemical Monthly, 155, 255-266, 2019.

[16] Barone, G., Terenzi, A., Lauria, A., Almerico, A.M., Leal, J.M., Busto, N., García, B., *DNA-binding of nickel (II), copper (II) and zinc (II) complexes: Structure–affinity relationships*, Coordination Chemistry Review, 257(19-20), 2848-2862, 2013.

[17] Mokhles, M.A., Ammar, A.L., Hanan, A.M, Samia, A.M., Mamdouh, M.A., Ahmed, A.R., *Synthesis, anticancer activity and molecular docking study of Schiff base complexes containing thiazole moiety*, Beni-Suef University Journal of Basic and Applied Sciences, 5, 85-96, 2016.

[18] Tripathi, L.P., Kumar, Singhai, A.K., *Role of chelates in treatment of cancer*, Indian Journal of Cancer, 44(2), 62, 2007.

Adıyaman University Journal of Science
https://dergipark.org.tr/en/pub/adyujsci
DergiPark AKADEMİK
ISSN 2147-1630
e-ISSN 2146-586X

Synthesis of 2-Methacryloyloxyethyl Phosphorylcholine (MPC) Based P(2-hydroxyethyl methacrylate) P(HEMA) Cryogel Membranes

Erdoğan ÖZGÜR[1,*]

[1]*Hacettepe of University, Advanced Technologies Application and Research Center, Ankara, Turkey*
erdoganozg@gmail.com, ORCID: 0000-0003-2494-4244

Received: 04.06.2020 **Accepted:** 11.11.2020 **Published:** 30.12.2020

Abstract

Synthesis of artificial/natural polymeric biomaterials having resistance to nonspecific protein adsorption, blood coagulation, and bacterial adhesion has attracted great attention, so nonspecific adsorption of proteins and biomolecules causes unfavorable biological responses inluding blood clotting, inflammation, cell adhesion, cell differentiation, and biofilm formation. A zwitterionic phosphorylcholine (PC) group of 2-methacryloyloxyethyl phosphorylcholine (MPC) is employed for biologically inert functions, especially in resistance to protein adsorption. So, it is aimed to develop bio-inspired, efficient and environmentally friendly MPC containing cryogel membranes for polymeric scaffolds for promoting cell-biomaterial. Cryogel membranes were synthesized in a semi-frozen medium by free radical polymerization in an ice bath and characterized by SEM/EDX, micro-CT, and swelling ratio measurements. In vitro biocompatibility was assessed from cell viability studies performed using cultured fibroblast cells.

Keywords: 2-Methacryloyloxyethyl Phosphorylcholine; 2-Hydroxyethyl Methacrylate; Cryogel.

* Corresponding Author DOI: 10.37094/adyujsci.747927

2-Metakriloiloksietil Fosforilkolin (MPC) Temelli P(2-Hidroksietil metakrilat) P(HEMA) Kriyojel Membranların Sentezi

Öz

Spesifik olmayan protein adsorpsiyonu, kan pıhtılaşması ve bakteriyel yapışmaya dirençli yapay / doğal polimerik biyomalzemelerin sentezi büyük ilgi görmektedir, çünkü proteinlerin ve biyomoleküllerin spesifik olmayan adsorpsiyonu, kan pıhtılaşması, enflamasyon, biyofilm oluşumu, hücre yapışması ve hücre farklılaşması gibi olumsuz biyolojik tepkilere yol açmaktadır. 2-metakriloksietil fosforilkolindeki (MPC) zwitter iyonik grup olan fosforilkolin (PC) biyolojik inert fonksiyonlardan sorumludur, özellikle de özellikle protein adsorpsiyonuna direnç göstermektedir. Böylelikle, hücre-biyomateryal etkileşimlerini teşvik etmek için polimerik yapı iskeleleri olarak biyo-esinlenilmiş, verimli ve çevre dostu MPC içeren kriyojel membranların geliştirilmesi amaçlanmıştır. Kriyojel membranlar, bir buz banyosunda serbest radikal polimerizasyonu ile yarı dondurulmuş ortamda sentezlendi ve SEM/EDX, mikro-CT ve şişme oranı ölçümleri ile karakterize edilmiştir. In vitro biyouyumluluk, kültür edilmiş fibroblast hücreleri kullanılarak yapılan hücre yaşayabilirlik çalışmalarıyla değerlendirilmiştir.

Anahtar Kelimeler: 2-Metakriloksietil fosforilkolin; 2-Hidroksietil Metakrilat; Kriyojel.

1. Introduction

Cryogels with unique physical properties such as swelling ratio, pore size, pore interconnectivity, mechanical behavior can be tuned as polymeric scaffolds for promoting cell-biomaterial [1-3]. Cryogels which are a subclass of hydrogels are synthesized via cryogelation technique at subzero temperatures (typically between -5 and -20ºC) yielding highly interconnected polymeric network [4]. Cryogels respond to external stimuli such as electrical [5], thermal [6], magnetic [7], and pH [8] etc. are promising materials for drug delivery and tissue enginering. Cryogels (can also have ionic, nonionic, amphoteric, or zwitterionic characters) are synthesized using synthetic and/or naturally derived polymers, and a polymer matrix incorporating materials such as nano, micro-, or macroparticles [9-14]. The extracellular matrix components can be also used to form biomimetic cryogels that exhibit improved biological and cell-adhesive features for tissue engineering applications.

Biomimicry of structural and biorecognition features of cellular components/sub-components provides to design novel synthetic biomaterials [15-17] which can be used in various biomedical applications such as diverse as tissue engineering [18], drug delivery [19], therapeutics [20], diagnostics [21], etc. Grafting or incorporation of zwitterionic

phosphorylcholine (PC) group containing moieties, a polar phospholipid presents in cell membranes, is one of the promising options to realize the biomimicry strategy [22-25]. A synthetic biomimetic molecule, 2-methacryloyloxyethyl phosphorylcholine (MPC) based polymeric materials have been widely used for tissue engineering and drug delivery systems to improve blood compatibility, resist protein adsorption, denaturation and cell adhesion, and prevent bacterial adherence [26]. The electrically neutral feature and formation of hydration shell surrounding the PC group provide these characteristics to MPC molecules [27-29]. Due to the reactivity of the methacrylate group, MPC can be easily copolymerized via various methods to develop numerous materials, having various applications in biomedical fields [22].

Herein, the present study on the influence of MPC on the in-vitro biocompatibility of poly(2-hydroxyethyl methacrylate) P(HEMA) cryogel membranes. P(HEMA) membranes cryogel membranes containing 0, 10, 20, and 30 mg of MPC were synthesized in a semi-frozen medium by free radical polymerization in an ice bath and characterized by SEM/EDX, micro-CT, and swelling ratio measurements. In vitro biocompatibility was assessed from cell viability studies performed using cultured fibroblast cells. So, it is aimed to develop bio-inspired, efficient and environmentally friendly MPC containing cryogel membranes which can be applied as polymeric scaffolds.

2. Materials and Methods

2.1. Materials

2-Methacryloyloxyethyl phosphorylcholine (MPC), N, N′-methylene-bis(acrylamide) (MBAAm), 2-hydroxyethyl methacrylate (HEMA), and ammonium persulfate (APS) were supplied by Sigma (St Louis, MO, USA). N, N, N′, N′-Tetramethylene diamine (TEMED) was supplied from Fluka A.G. (Buchs, Switzerland). L929 fibroblast cell line was obtained from ŞAP Institute (Ankara, Turkey). Dulbecco's modified eagle medium (DMEM), fetal bovine serum (FBS), and trypsin-EDTA were purchased from Biological Industries (Cromwell-US). 3-(4,5-Dimethylthiazol-2-yl)-2,5-diphenyltetrazolium bromide (MTT) was purchased from Serva (Heidelberg, Germany).

2.2. Synthesis of p(HEMA) cryogel membranes

Briefly, HEMA (2.475 ml) and MPC (10, 20, and 30 mg separately) were dissolved in deionized water (2.525 mL). MBAAm (0.54 g) was dissolved in deionized water (DI) (10 mL). The two aqueous solutions were mixed and degassed. Total concentration of monomers was 20% (w/v). PHEMA cryogel membranes were synthesized between two glass plates at -16°C for 24 h

via free radical polymerization initiated by TEMED (30.0 µL) and APS (30.0 mg). After adding APS, the solution was cooled for 2 min. TEMED was added and the reaction mixture was stirred for 30 s. Right after, the four polymerization solutions containing 0, 10, 20, and 30 mg separately were poured between two glass plates (four different glass couples) separated with 2.0 mm thick spacer and were kept at -16°C for 24 h and following thawed at 25°C. After extensively washing with an excess of DI and pure ethanol until obtaining a clear washing solution, the cryogels were cut into circular membranes (0.5 cm in diameter). The cryogel membranes were stored in buffer at 4 °C.

2.3. Characterization of PHEMA cryogel membranes

Cryogel membranes were dried to constant weight (Wdry) in the oven at 50°C and soaked in DI in an isothermal water bath (25 ± 0.5 ºC) for 2h. The swollen cryogel membrane was taken out from the aqueous medium and weighed ($W_{swollen,}$ g) after carefully removing of water adsorbed on the surface. The swelling degree was calculated as:

$$SD\% = (W_{swollen}-W_{dry}) / W_{dry}$$

The morphology and chemical characterization of a cross-section of the cryogel membranes was analyzed by scanning electron microscope with energy-dispersive X-ray spectroscopy (SEM–EDX) (Gaia 3, Tescan, Czech Republic).

The internal structure of cryogel membranes in a non-destructive manner was investigated by micro-computed tomography (micro-CT) (Bruker, Skyscanner 1272). The cryogel membranes were scanned with a voxel size of 8.0 µm at a voltage of 30 kV and a current of 45 µA.

2.3. MTT cell proliferation assay

The reduction reaction of tetrazolium salts is a reliable option to evaluate cell proliferation. The tetrazolium MTT is reduced by metabolically active cells (by mitochondrial enzymes related to metabolic activity) to form reducing agents such as nicotinamide adenine dinucleotide (NADH) and nicotinamide adenine dinucleotide phosphate (NADPH). The resulting intracellular purple formazan can be quantified at 570 nm spectrophotometrically. The MTT cell proliferation assay measures the cell proliferation rate and inversely when metabolic events lead to apoptosis or necrosis, the reduction in cell viability. The tetrazolium ring in the solutions is broken down by dehydrogenase enzymes in mitochondria and forms purple colored formazan crystals. The color change observed in living cells gives the absorbance values using Elisa Plate Reader.

L929 fibroblast cells were cultured in 25 cm^2 culture flasks containing Dulbecco's Modified Eagle Medium (DMEM, Invitrogen) supplemented with 10% fetal bovine serum (FBS), at 37ºC with 5% CO_2. At 95% confluence, the cells were trypsinized and subsequently, resuspended in complete medium. L929 cells (10x104 cell/mL) were seeded in 96-well plates and incubated overnight.

Cryogel membrane extracts were prepared for the determination of cryogel membranes cytotoxicity. According to the ISO 10993-5 standard, the concentration of 0.2 g/mL cryogel membranes were incubated into the cell culture medium at 37ºC under 5% CO_2 stream for 72h. After the incubation, membrane extracts were pipetted onto the cell. Plates were incubatted for 24 h at 37ºC under 5% CO_2 stream. Fresh medium containing MTT (5.0 mg/mL) was pipetted to each well. Later 2 h of incubation at 37ºC, 100 mL of MTT solvent (isopropanol-HCl) was added to the wells and absorbance was read at 570 nm in an ELISA plate reader. The measurements were studied in 8 replicates. Only the medium was used as the control group. The percent cell viability was calculated as below formula based on control groups.

Viab. % = 100 X OD_{570e} / OD_{570b}

OD_{570e}: Optical density of samples

OD_{570b}: Optical density of negative control groups

3. Results and Discussion

3.1. Characterization of PHEMA cryogel membranes

Scanning electron microscopy images of the highly and interconnected porous structure of the PHEMA and P(HEMA-MPC) cryogel membranes with nonporous bead like walls were given in Fig. 1. The pore size of the cryogel membranes depends on the amount of MPC incorporated to polymeric structure. The degree of porosity became smaller with increasing MPC amounts. MPC was incorporated at a varying amount of 10, 20, and 30 mg. SEM-EDX results also showed that the percentage of MPC in polymeric structures is proportional to these ratios if the atomic percentage of the phosphorus atom due to the existence of MPC in the polymeric structure was discussed Fig. 1.

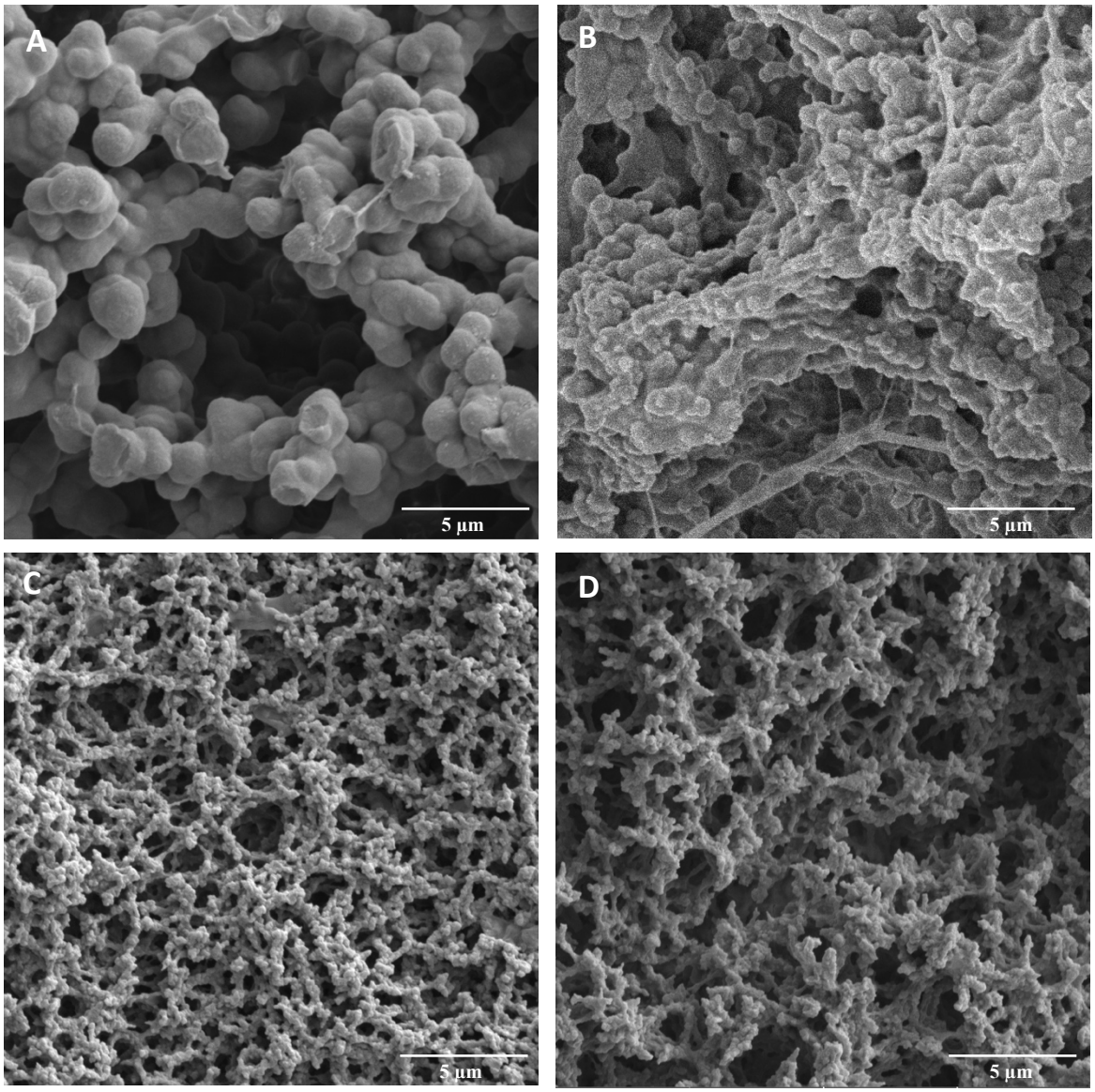

Figure 1: SEM images of PHEMA cryogel membranes containing MPC A) 0 mg, B) 10 mg, C) 20 mg, and D) 30 mg

The pore size ranged between 8.001-424.0034 µm, 8.001-296.0024 µm, 8.001-168.0015 µm, and 9.3001-46.5004 µm for PHEMA, PHEMA incorporated 10 mg of MPC, PHEMA incorporated 20 mg of MPC, and PHEMA incorporated 30 mg of MPC, respectively (at the voxel resolution of 8.0 µm). The range of pore size decreased with an increasing amount of MPC which indicated that the porosity feature of cryogel membranes shifted from super-macroporous to macroporous structure (Fig. 2).

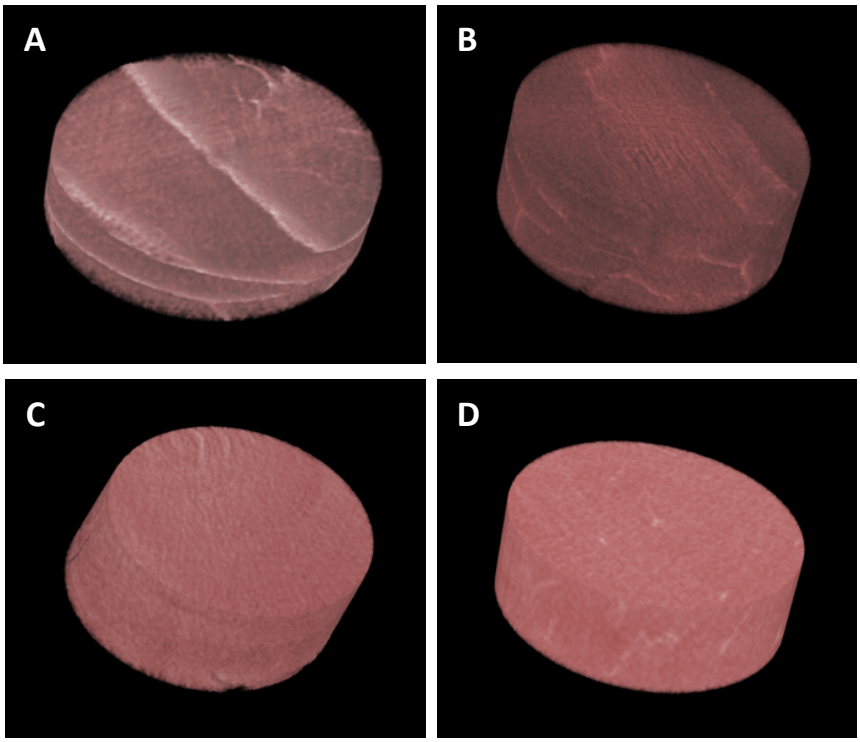

Figure 2: Micro-CT analysis reveals 3D reconstruction of PHEMA cryogel membranes containing MPC A) 0 mg, B) 10 mg, C) 20 mg, and D) 30 mg

The equilibrium swelling degrees of the bare PHEMA cryogel membrane and croslinked P(HEMA-MPC) cryogel membrane containing 30 mg of MPC were 4.76 g H_2O/g cryogel and 6.71 g H_2O/g cryogel. The swelling degree of crosslinked P(HEMA-MPC) cryogel membrane was higher than the bare PHEMA cryogel membrane due to the high hydrating ability (derived from the electrostatic interactions as well as hydrogen bonds) of poly(MPC) chain inside the polymeric structure. Besides, a smaller porous structure reduced interconnected flow- channel while increasing specific polymeric surface. All types of cryogel membranes are opaque, sponge like squeezable and highly elastic. Water accumulated inside the pores of the cryogel membrane can be easly removed through compressing by hand.

The cryogel membranes with cells were washed with PBS buffer and fixed with 2.5% glutaraldehyde in PBS buffer for 1 h and immersed to sequential dehydration in graded ethanol (35, 50, 70, 80, 90, 100%) and were dehydrated with hexamethyldisilazane (HDMS). After drying, the samples were coated with gold/palladium mixture for SEM examination.

To the investigation of the cell adhesion on the cryogel membranes, L929 cells were cultured on the cryogel membranes as mentioned before. After 5 days of incubation periods, SEM images of cryogel membranes were taken (Fig. 3). According to the images, L929 cells adhered to the surface of the cryogel membranes containing 10, 20, and 30 mg of MPC (Fig. 3B, C, and

D). There was not seen a cell on the cryogel membrane A few cells were seen on the cryogel membrane B. A large number of cells adhered to the surface of the cryogel membranes containing 20.0 mg and 30.0 mg of MPC (Fig. 3C and D). Cellular extensions of outgrown cells were clearly seen as shown in Fig. 3C and D. The results indicate that increasing the MPC amount in the polymeric structure increased L929 cells outgrow on the cryogel membranes.

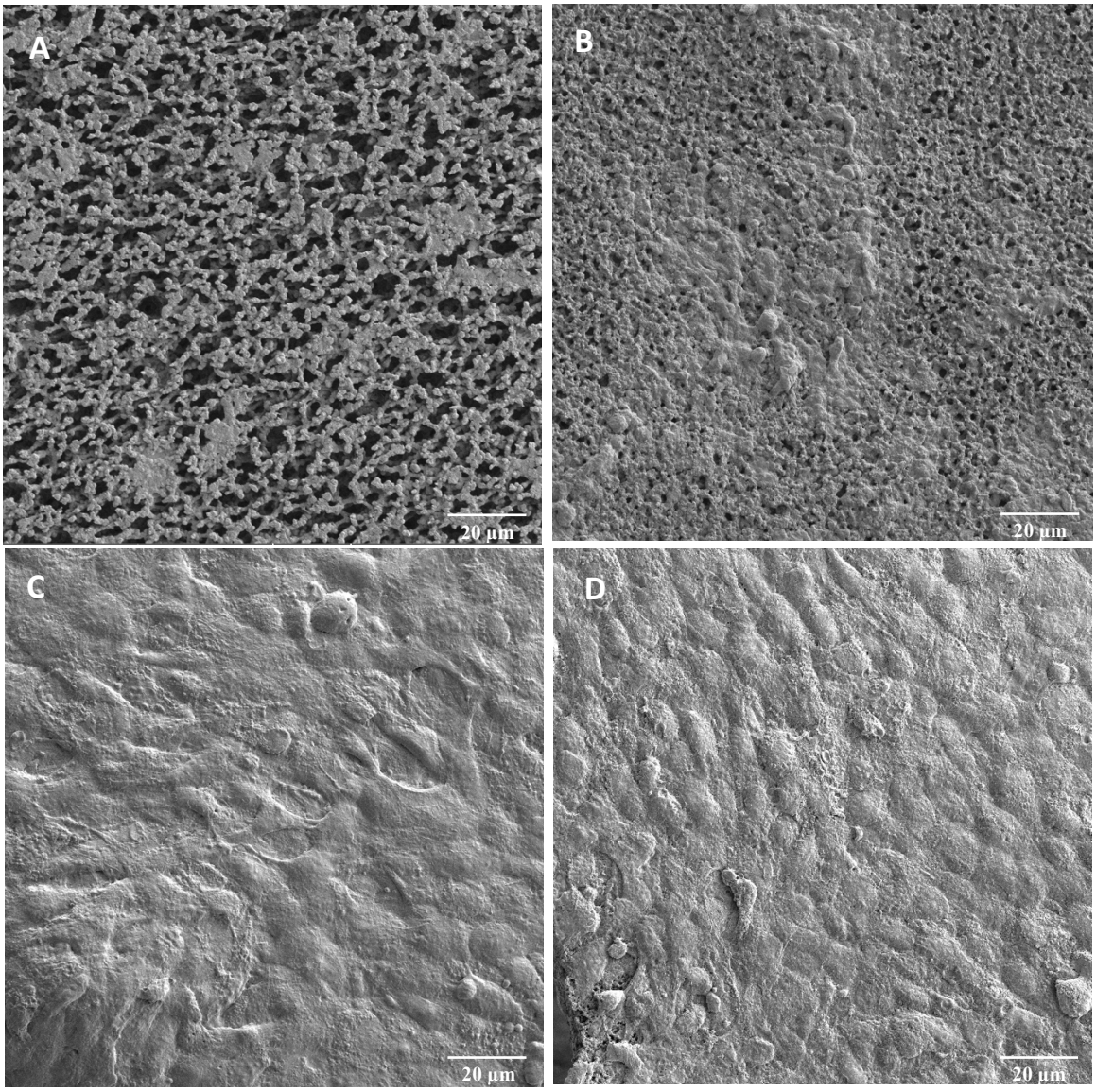

Figure 3: SEM images of L929 cells cultured on the PHEMA cryogel membranes containing MPC A) 0 mg, B) 10 mg, C) 20 mg, and D) 30 mg

The viability percentage of the L929 cells cultured on PHEMA cryogel membrane containing 0 mg of MPC was found 51.5% ± 2.81%. The viability percentages of the L929 cell line cultured on PHEMA cryogel membranes containing 10, 20, and 30 mg of MPC were found 53.83% ± 1.43%, 72. 92% ± 1.94%, and 93.85% ± 2.22%, respectively. There was a statistically

significant difference in cell viability of PHEMA cryogel membrane containing 10 mg and 20 mg MPC compared with the negative control group ($P<0.05$). There was no significant difference in cell viability between PHEMA cryogel membrane containing 30 mg MPC with the negative control group ($P>0.05$). As a result of the cell viability studies, the copolymerization of MPC residue with HEMA increases the biocompatibility of the PHEMA cryogel membranes ($P<0.05$). When PHEMA cryogel membranes containing MPC were compared among themselves, the viability percentage of the L929 cell line increased with the increasing amount of MPC ($P<0.05$) (Fig. 4).

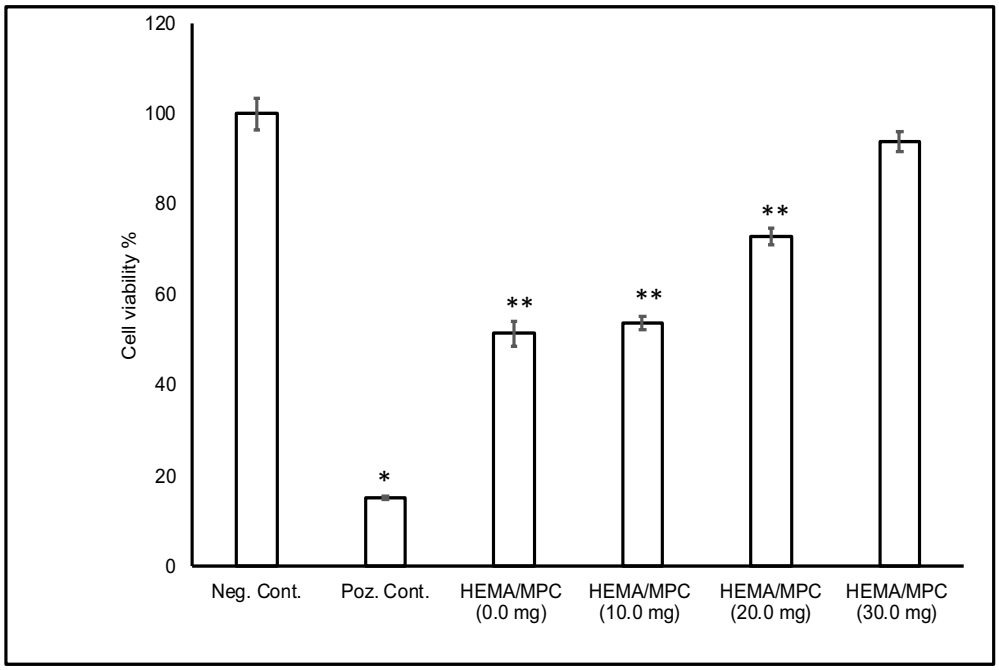

Figure 4: Indirect cytotoxicity of PHEMA membranes with different MPC amount with L929 cells (** $P < 0.05$)

4. Conclusion

Phospholipid based biomimicry has been applied to obtain improved in vitro biocompatibility of P(HEMA) cryogel membranes through the copolymerization of MPC and HEMA in a semi-frozen medium by free radical polymerization. P(HEMA) cryogel membranes containing 20.0 mg and 30.0 mg of MPC exhibit the significant characteristics for increased L929 cells outgrow ($P<0.05$). A large number of cells adhered to the surface of the cryogel membranes containing 20.0 mg and 30.0 mg of MPC. The viability percentages of the L929 cell line cultured on PHEMA cryogel membranes were found as 72. 92% ± 1.94% and 93.85% ± 2.22%, respectively. According to the SEM/EDX, micro-CT, swelling ratio measurements, and cell viability studies, it was developed bio-inspired, efficient, and environmentally friendly cryogel membranes which can be applied as polymeric scaffolds.

Acknowledgement

The author would like to thank Dr. Murat Demirbilek for cell viability studies.

References

[1] Eggermont, L.J., Rogers, Z.J., Colombani, T., Memic, A., Bencherif, A.S., *Injectable cryogels for biomedical applications*, Trends in Biotechnology, 2019.

[2] Offeddu, G.S., Mela, I., Jeggle, P., Henderson, R.M., Smoukov, S.K., Oyen, M.L., *Cartilage-like electrostatic stiffening of responsive cryogel scaffolds*, Scientific Reports, 7, 42948, 2017.

[3] Hixon, K.R., Lu, T., Sell, S.A., *A comprehensive review of cryogels and their roles in tissue engineering applications*, Acta Biomaterialia, 62, 29-41, 2017.

[4] Henderson, T.M.A., Ladewig, K., Haylock, D.N., McLean, K.M., O'Connor, A.J., *Cryogels for biomedical applications,* Journal of Materials Chemistry B, 1(21), 2682-2695, 2013.

[5] Kennedy, S., Bencherif, S., Norton, D., Weinstock, L., Mehta, M., Mooney, D., *Rapid and extensive collapse from electrically responsive macroporous hydrogels*, Advanced Healthcare Materials, 3 500-507, 2014.

[6] Zhang, X., Yang, X., Chen, X., Zhang, M., Luo, L., Peng, M., Yao, S., *Novel magnetic bovine serum albumin imprinted polymers with a matrix of carbon nanotubes, and their application to protein separation*, Analytical and Bioanalytical Chemistry, 401(9), 2855-2863, 2011.

[7] Zhang, F., Wu, W., Zhang, X., Meng, X., Tong, G., Deng, Y., *Temperature-sensitive poly-NIPAm modified cellulose nanofibril cryogel microspheres for controlled drug release*, Cellulose, 23, 415-425, 2016.

[8] Dragan, E.S., Cocarta, A.I., *Smart macroporous IPN hydrogels responsive to pH, temperature, and ionic strength: synthesis, characterization, and evaluation of controlled release of drugs*, ACS Applied Materials & Interfaces, 8, 12018-12030, 2016.

[9] Kirsebom, H., Topgaard, D., Galaev, I., Mattiasson, B., *Modulating the porosity of cryogels by influencing the nonfrozen liquid phase through the addition of inert solutes*, Langmuir, 26, 16129-16133, 2010.

[10] Jayaramudu, T., Ko, H.U., Kim, H.C., Kim, J.W., Muthoka, R.M., Kim, J., *Electroactive hydrogels made with polyvinyl alcohol/cellulose nanocrystals*, Materials, 11, 1615, 2018.

[11] Memic, A., Colombani, T., Eggermont, L.J., Rezaeeyazdi, M., Steingold, J., Rogers, Z.J., Navare, K.J., Mohammed, H.S., Bencherif, S.A., *Latest advances in cryogel technology for biomedical applications*, Advances in Therapy, 2, 1800114, 2019.

[12] Bereli, N., Andaç, M., Baydemir, G., Say, R., Galaev, I.Y., Denizli, A., *Protein recognition via ion-coordinated molecularly imprinted supermacroporous cryogels*, Journal of Chromatography A, 1190(1-2), 18-26, 2008.

[13] Bereli, N., Şener, G., Altıntaş, E.B., Yavuz, H., Denizli, A., *Poly(glycidyl methacrylate) beads embedded cryogels for pseudo-specific affinity depletion of albumin and immunoglobulin G*, Materials Science and Engineering C, 30(2), 323-329, 2010.

[14] Andaç, M., Galaev, I.Y., Denizli, A., *Affinity based and molecularly imprinted cryogels: Applications in biomacromolecule purification*, Journal of Chromatography B, 1021, 69-80, 2016.

[15] Abraham, S., Brahim, S., Ishihara, K., Guiseppi-Elie, A., *Molecularly engineered p(HEMA)-based hydrogels for implant biochip biocompatibility*, Biomaterials, 26(23), 4767-4778, 2005.

[16] Özgür, E., Parlak, O., Beni, V., Turner, A.P.F., Uzun, L., *Bioinspired design of a polymer-based biohybrid sensor interface*, Sensors and Actuators B, 251, 674-682, 2017.

[17] Whitesides, G.M., *Bioinspiration: something for everyone*, Interface Focus, 5, 1-10, 2015.

[18] Zoulalian, V., Zürcher, S., Tosatti, S., Textor, M., Monge, S., Robin, J.-J., *Self-assembly of poly(ethylene glycol)−poly(alkyl phosphonate) terpolymers on titanium oxide surfaces: synthesis, interface characterization, investigation of nonfouling properties*, *and long-term stability*, Langmuir, 26 (1), 74-82, 2010.

[19] Licciardi, M., Tang, Y., Billingham, N.C., Armes, S. P., Lewis, A. L., *Synthesis of novel folic acid-functionalized biocompatible block copolymers by atom transfer radical polymerization for gene delivery and encapsulation of hydrophobic drugs*, Biomacromolecules, 6(2), 1085–1096, 2005.

[20] Gagner, J.E., Kim, W., Chaikof, E.L., *Designing Protein-Based Biomaterials for Medical Applications,* Acta Biomaterials, 10(4), 1542-1557, 2014.

[21] Goda, T., Kjall, P., Ishihara, K., Richter-Dahlfors, A., Miyahara, Y., *Biomimetic interfaces reveal activation dynamics of C-reactive protein in local microenvironments*, Advanced Healthcare Materials, 3(11), 1733-1738, 2014.

[22] Goda, T., Ishihara, K., Miyahara, Y., *Critical update on 2-methacryloyloxyethyl phosphorylcholine (MPC) polymer science*, Journal of Applied Polymer Science, 132, 41766, 2015.

[23] Ishihara, K., Mu, M., Konno, T., Inoue, Y., Fukazawa, K., *The unique hydration state of poly(2-methacryloyloxyethyl phosphorylcholine)*, Journal of Biomaterials Science, Polymer Edition, 10–12, 884–899, 2017.

[24] Yuan, B., Chen, Q., Ding, W.-Q., Liu, P.-S., Wu, S.-S., Lin, S.-C., Shen, J., Gai, Y., *Copolymer coatings consisting of 2-methacryloyloxyethyl phosphorylcholine and 3-methacryloxypropyl trimethoxysilane via ATRP to improve cellulose biocompatibility*, ACS Applied Materials & Interfaces, 4, 4031-4039, 2012.

[25] Barthélémy, B., Maheux, S., Devillers, S., Kanoufi, F., Combellas, C., Delhalle, J., Mekhalif, Z., *Synergistic effect on corrosion resistance of phynox substrates grafted with surface-initiated ATRP (Co)polymerization of 2-Methacryloyloxyethyl Phosphorylcholine (MPC) and 2-Hydroxyethyl Methacrylate (HEMA)*, ACS Applied Materials & Interfaces, 6, 10060-10071, 2014.

[26] Monge, S., Canniccioni, B., Graillot, A., Robin, J.-J., *Phosphorus-containing polymers: a great opportunity for the biomedical field*, Biomacromolecules, 12, 1973-1982, 2011.

[27] Berkowitz, M.L., Vacha, R., *Aqueous solutions at the interface with phospholipid bilayers,* Accounts of Chemical Research, 45, 74-82, 2012.

[28] Krylov, N.A., Pentkovsky, V.M., Efremov, R.G., *Nontrivial behavior of water in the vicinity and inside lipid bilayers as probed by molecular dynamics simulations*, ACS Nano, 7, 9428-9442, 2013.

[29] Schlenoff, J.B., *Zwitteration: coating surfaces with zwitterionic functionality to reduce nonspecific adsorption*, Langmuir, 30, 9625-9636, 2014.

Adıyaman University Journal of Science
https://dergipark.org.tr/en/pub/adyujsci
DergiPark AKADEMİK
ISSN 2147-1630
e-ISSN 2146-586X

Rapid and Specific Purification of RNA by PolyUracil Membranes

Canan ARMUTCU[1,*]

[1]*Hacettepe University, Faculty of Science, Department of Chemistry, TR-06800 Ankara, Turkey*
cananarmutcu@hacettepe.edu.tr, ORCID: 0000-0002-0920-2843

Received: 13.08.2020 **Accepted:** 10.12.2020 **Published:** 30.12.2020

Abstract

Ribonucleic acid (RNA) plays a critically important role in cellular defense, deoxyribonucleic acid (DNA) replication, transcription, and gene expression for living organisms as well as, a lot of diseases such as cancer, immunodeficiency, tumors has been associated with RNA's disruption. For this purpose, supermacropores membranes were designed to purify RNA using nucleotide-based ligand. In this study, polymerizable uracil monomer as uracil methacrylate (UraM) was synthesized, and 2-hydroxyethyl methacrylate (HEMA)-based membranes [poly(HEMA-UraM)] were prepared by bulk polymerization under partially frozen conditions by copolymerization of monomers, UraM, and HEMA. These membranes were characterized via swelling studies, Fourier transform infrared spectroscopy (FTIR), and scanning electron microscopy (SEM). To optimize separation conditions, effects of pH, initial RNA concentration, time, and temperature on RNA adsorption capacity were examined. Maximum adsorption of RNA on poly(HEMA-UraM) membrane was found to be 15.52 mg/g for 0.5 mg/mL RNA initial concentration at 25.0°C with an optimum pH of 7.0. After ten repetitive adsorption-desorption cycles, the RNA adsorption capacity decreased only 3.68%.

Keywords: Membrane; Uracil methacrylate; Nucleotide; Ribonucleic acid; Purification.

* Corresponding Author DOI: 10.37094/adyujsci.780049

PoliUrasil Membranlar ile Hızlı ve Spesifik RNA Saflaştırılması

Öz

Ribonükleik asit (RNA), hücresel savunma, deoksiribonükleik asit (DNA) replikasyonu, transkripsiyon, canlı organizmalar için gen ekspresyonununda önemli bir rol oynar, bunun yanı sıra kanser, immün yetmezlik, tümör gibi birçok hastalık RNA'nın bozulmasıyla ilişkililendirilmiştir. Bu amaçla, RNA saflaştırmak için nükleotid bazlı ligand kullanılarak gözenekli membranlar tasarlanmıştır. Bu çalışmada, polimerize edilebilir urasil monomeri urasil metakrilat (UraM) olarak sentezlenmiş, 2-hidroksietil metakrilat (HEMA) bazlı membranlar [poli(HEMA-UraM)] UraM ve HEMA monomerlerinin kopolimerizasyonu ile kısmen dondurulmuş koşullar altında yığın polimerizasyonu ile hazırlanmıştır. Bu membranlar şişme çalışması, Fourier dönüşümlü kızılötesi spektroskopisi (FTIR) ve taramalı elektron mikroskobu (SEM) ile karakterize edilmiştir. Ayırma koşullarını optimize etmek için, pH, başlangıç RNA konsantrasyonu, süre ve sıcaklığın RNA adsorpsiyon kapasitesi üzerindeki etkileri incelenmiştir. Poli(HEMA-UraM) membranın maksimum RNA adsorpsiyonu 25.0 °C, pH 7.0, 0.5 mg/mL RNA başlangıç derişiminde 15.52 mg/g olduğu bulunmuştur. On tekrarlı adsorpsiyon-desorpsiyon döngüsünden sonra, RNA adsorpsiyon kapasitesi yalnızca %3.68 oranında azaldığı gözlenmiştir.

Anahtar Kelimeler: Membran; Urasil metakrilat; Nükleotid; Ribonükleik asit; Saflaştırma.

1. Introduction

Ribonucleic acid (RNA) plays important roles in heredity and essentially biological processes [1, 2]. There are also some remarkable roles for RNA in biology according to the report from the studies in the last 20 years [3]. The discovery of the RNA features, therapeutic strategy, and the importance of diagnosis lead to purification of RNA with different methods [4-6]. To provide reliable results, RNA purification methods should be highly pure, durable, and provide the production of stable RNA chains.

Many chromatographic techniques have recently been reported for the separation and purifications of biomolecules [7-13]. The traditional techniques still show several disadvantages including the requirement of organic solvents, difficult to scale up, time-consuming, and expensive material [14, 15]. Affinity chromatographic techniques based on the recognition of target molecules using affinity ligand have been developed to overcome these challenges, especially for protein and nucleic acid separation and purification [16, 17]. Affinity chromatography provides using various affinity matrices as solid support can be used to isolate

many kinds of molecules with high selectivity and stability [18, 19]. Thus, this technique eliminates sequential separation steps from a crude medium in one step.

Membranes are three-dimensional polymeric system of interconnected networks of macropores with a size of 10-100 [20, 21]. The large pores and superior flow properties of membranes have allowed these materials to be used in different applications [22]. Membranes also provide easy, fast, and effective elution through their porous structure [23]. Affinity ligands derived from amino acids for using as a functional monomer is an intelligent bio-inspired approach to create a direct biofunctional polymeric network [24]. Herein, nucleotide-based affinity ligands incorporated membrane column was successfully synthesized for the bioseparation of RNA. The presence of membranes composed of nucleotide derivative affinity ligand provides enough specific binding sites and reversible interactions between membranes and RNA.

In the present study, a new approach was developed to investigate rapid and efficient RNA separation in a single step. Firstly, a nucleotide-based functional monomer, the uracil methacrylate (UraM) was synthesized in the presence of methacryloyl chloride and uracil. Secondly, the poly(HEMA-UraM) membranes containing different UraM amounts were obtained by bulk polymerization under partially frozen conditions. Then, Fourier transform infrared (FTIR) spectroscopy, scanning electron microscopy (SEM), and swelling studies were carried out for the characterization of membranes. As finally, the effects of various factors including pH, ligand density, RNA concentration, temperature, and time were investigated to identify the adsorption performance of the adsorbent.

2. Experimental

2.1. Materials

RNA (R6625-25G, Type VI, Torula Yeast), 2-Hydroxyethyl methacrylate (HEMA), ethylene glycol dimethacrylate (EDMA), and sodium dodecyl sulfate (SDS) were obtained from Sigma (St. Louis, MO, USA). Ammonium persulfate (APS), and N,N,N′,N′-tetramethylene diamine (TEMED) were obtained from Merck AG (Darmstadt, Germany). All other chemicals of reagent grade were purchased from Merck AG (Darmstadt, Germany).

2.2. Methods

2.2.1. Synthesis of UraM

The UraM monomer was synthesized according to the literature [24]. Briefly, the uracil (0.01 mol) was dissolved in sodium hydroxide (NaOH) solution (1.0 M). Benzotriazole methacrylate (0.01 mol) and triethylamine (TEA) (0.011 mol) were dissolved in toluene and then this solution was cooled to 0-5ºC. The uracil solution was slowly poured into this solution. This mixture was incubated at room temperature and terminated after 5h. After that, the remaining unreacted TEA and H-benzotriazole were removed out with a vacuum evaporator and functional monomer (uracil methacrylate, UraM) was acquired as an oil-like yellowish solid.

2.2.2. The Synthesis of membranes

Membranes were prepared by bulk polymerization of UraM and 2-hydroxyethyl methacrylate (HEMA) under partially frozen-conditions. Phase I solution contained of HEMA (2.45 mL) and UraM with different amounts (50, 75, or 100 mg UraM) were dissolved in deionized water (2.55 mL). Phase II solution consisted of SDS (0.50 g), and EGDMA (0.6 mL) was dissolved in deionized water (9.40 mL) as an organic phase. Then, both liquid phases were mixed in a magnetic stirrer and then cooled for 20 min. APS (10 mg) and TEMED (50 µL) were mixed into this solution to initiate polymerization. The polymerization was carried out between two glass plates at −12.0ºC for 24 h. After the polymerization was terminated, the poly(HEMA-UraM) membranes thawed at room temperature and were cut with a perforator (6.0 mm in diameter). Afterward, the obtained membranes were washed with deionized water and ethanol until no remaining monomers. Then, membranes were stored in a buffer containing sodium azide (0.1% by weight) to prevent bacterial growth until use. The plain membrane was synthesized via the same polymerization process in the absence UraM monomer as a control.

2.2.3. Characterization of membranes

The water uptake ratios of the membranes were determined by using deionized water [21]. The membranes were lyophilized at -60.0°C using Christ Alpha, 1–2 LD Plus; M Christ GmbH, Germany to get dry weight (w_{dry}). Then, the membranes put into deionized water at ambient temperature for 2 h until they reached a stable wet weight. The membranes were removed from the water, wiped out with filter paper, and reweighed ($w_{swollen}$). The sample weight (dried and wet) were recorded to calculate the membranes water content by means of the below equation:

$$\text{Water uptake ratio } \% = \left[\left(W_{swollen} - W_{dry}\right)/W_{dry}\right]x100 \quad (1)$$

W_{dry} and $W_{swollen}$ are the respective sample weights (g) of membrane before and after water uptake.

The macropores of the membranes was calculated by below equation:

$$\text{Macroporosity } \% = \left[\left(m_{swollen} - m_{squeezed}\right)/m_{swollen}\right] \times 100 \quad (2)$$

Wherein $m_{swollen}$ and $m_{squeezed}$ are the weights (g) of squeezed (after removing free water within macropores) and swollen (after reaching complete swollen state) membranes, respectively.

The poly(HEMA-UraM) membranes were analyzed by FTIR spectrophotometer (Perkin Elmer, Spectrum One, USA) to characterize the functional group. The finely ground membrane samples (2 mg) were dispersed in KBr (98 mg), and turned into a disc form. The FTIR spectrum was recorded over the range of 900- 4000 cm^{-1} wavelengths.

In order to assess the morphology of the membranes, SEM instrument (Tescan, GAIA3, Czech Republic) was utilized from Hacettepe University, Advanced Technologies Application and Research Center (HUNITEK, Ankara, Turkey). The dried membranes were coated with gold and scanned by SEM equipment with different magnifications at high vacuum.

2.2.4. Adsorption/Desorption studies

RNA adsorption experiments were carried out using a batch system in aqueous solution whereas poly(HEMA-UraM) membrane and poly(HEMA) membranes were incubated with appropriate buffer solutions containing RNA solution (1.5 mL) and then incubated for 2 h on a rotator at 100 rpm. The adsorbed RNA amount onto membrane was determined by the measuring UV absorbance of initial and final RNA concentration at 260 nm that was given in the following equation:

$$Q = [(C_i - C_f) \times V]/m \quad (3)$$

where Q, C_i and C_f are adsorbed amount of RNA (mg/g), the initial and final concentrations (mg/mL) of RNA, respectively; V and m are the volume of the aqueous phase (mL), and the mass of the membrane used (g), respectively. The effect of initial RNA concentration (0.025-2.0 mg/mL), pH (4.0-10.0), ligand density (50, 75 and, 100 mg), temperature (4-45 °C), and time (5-120 min) on the binding capacity of the membranes was investigated to determine the optimum RNA adsorption conditions. All experiments were carried out in triplicate within 95% confidence level for all data.

RNA desorption was performed in a batch adsorption process for all membranes. After each adsorption step, adsorbed RNA was eluted using HCl acid solution (0.1 M, 5 mL) at 25°C for 1 h. The successive adsorption-desorption cycle carried out ten times. Finally, the membranes were washed with NaOH solution (50 mM, 5 mL) and deionized water (5 mL) to ready for the next adsorption cycle.

3. Results and Discussion

3.1. Characterization studies

The water uptake capability and mechanical properties of membranes are affiliated to the swelling behavior in an aqueous solution of membrane. Equilibrium swelling degree of poly(HEMA-UraM)-100 membrane was observed to be 5.08 g water/g membrane. Moreover, the equilibrium swelling ratios and macroporosity of membrane was 408% and 77%, respectively. It is demonstrated that the addition of UraM into the polymer structure probably increased the water uptake in aqueous solutions.

FTIR analyses were applied to observe the chemical properties of poly(HEMA-UraM)-100 and poly(HEMA) membranes for evaluating the functional groups (Fig. 1). As seen in FTIR spectra, characteristic bands at 3444 cm^{-1}, and 1716 cm^{-1} were assigned for –OH and -CO stretching, respectively. Additionally, amide I–II bands observed at 1541 cm^{-1} and 1650 cm^{-1} were characteristic bands for UraM which was demonstrated to participate functional monomer successfully in the membrane structure [25].

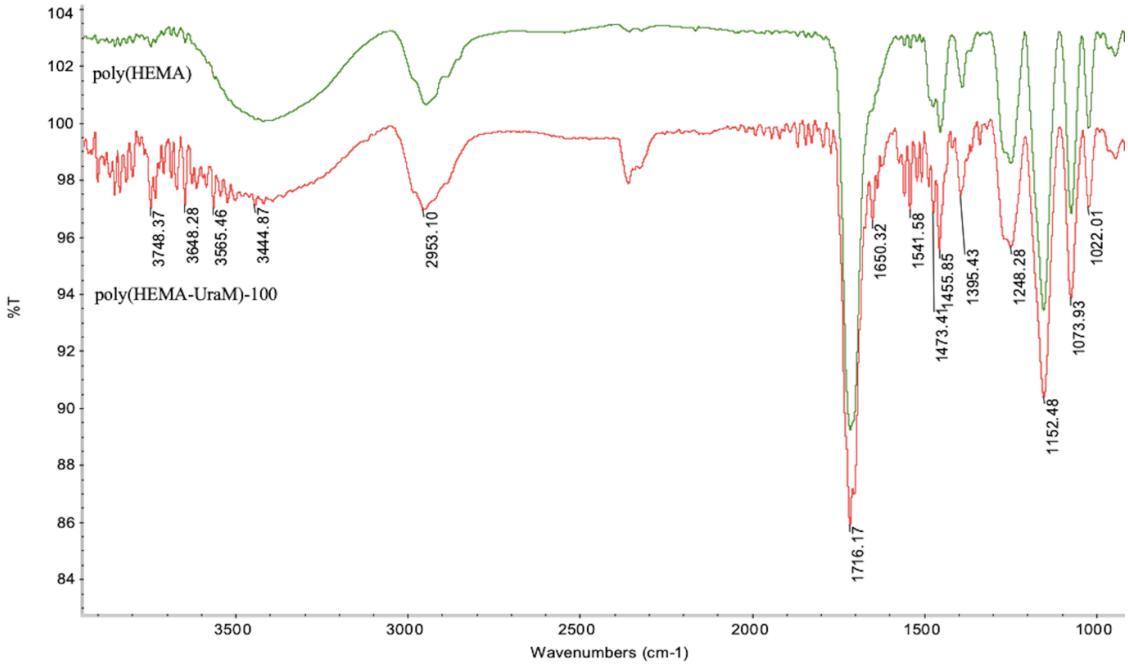

Figure 1: FTIR spectrum of poly(HEMA) and poly(HEMA-UraM)-100 membranes

The SEM images for all membranes were given in Fig. 2. The interconnected macropores, rough surface of the membranes, and also small bead formations are clearly seen in Fig. 2. The different morphological structure of these membranes from the traditional membrane was further verified by SEM images due to the presence of sodium dodecyl sulfate as a surfactant [26]. As

seen in Fig. 2., the synthesized membranes have a unique combination of properties such as interconnected pores of 2– 5 µm size.

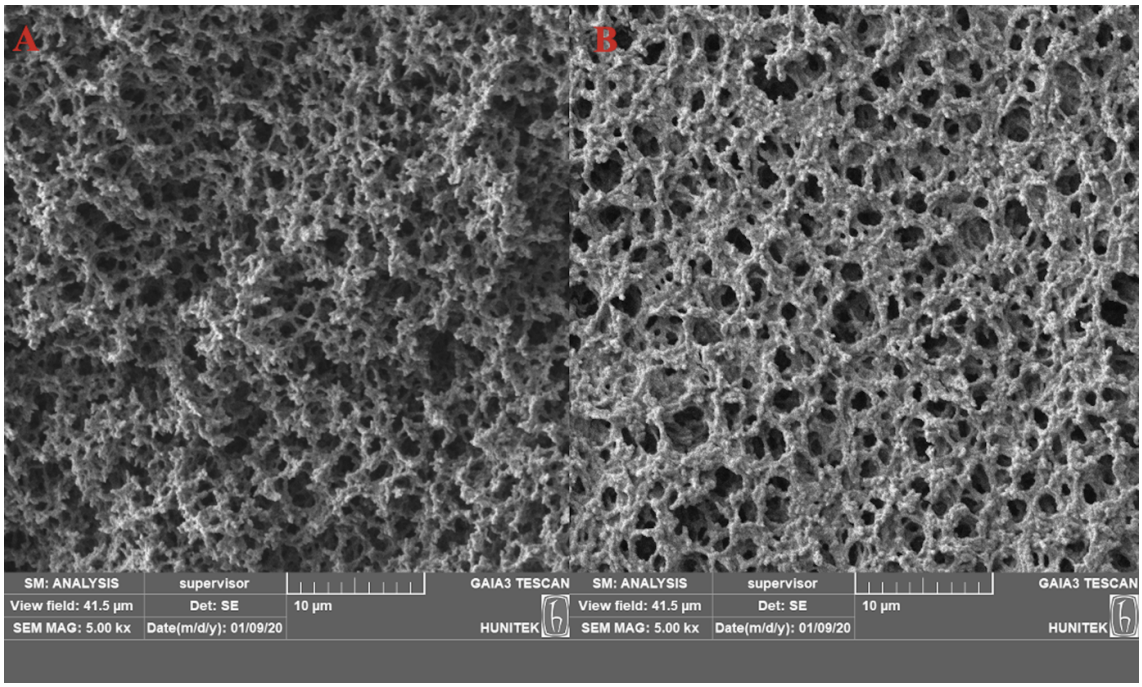

Figure 2: The SEM image of (A) poly(HEMA) and (B) poly(HEMA-UraM)-100 membranes

3.2. RNA Adsorption from aqueous solutions

3.2.1. Effect of pH

The pH effects on RNA adsorption capacity were examined at room temperature for 120 min. RNA adsorption studies were performed at different buffer solutions using acetate (4–5), phosphate (6–8), and carbonate (9-10) buffer systems (Fig. 3). As illustrated in Fig. 3, the maximum RNA binding capacity on poly(HEMA-UraM)-100 membrane was found as 1.91 mg/g at the 0.10 mg/mL initial concentration of RNA in PBS at pH 7.0. At this pH, there are strong hydrogen bonds between the uracil on the polymeric backbone and the adenine in the RNA chain. This effective binding can be explained by the pKa1 (10.01) value of the N3 atom in the uracil and the pka1 (3.88) value of the N1 atom in adenine. At the average of these values (pH: 7.0), they have an optimal charge for H-bonding [26]. Adsorption capacities were reduced at higher and lower this pH value because of the broken of hydrogen bonds between the affinity ligand and RNA chains [27].

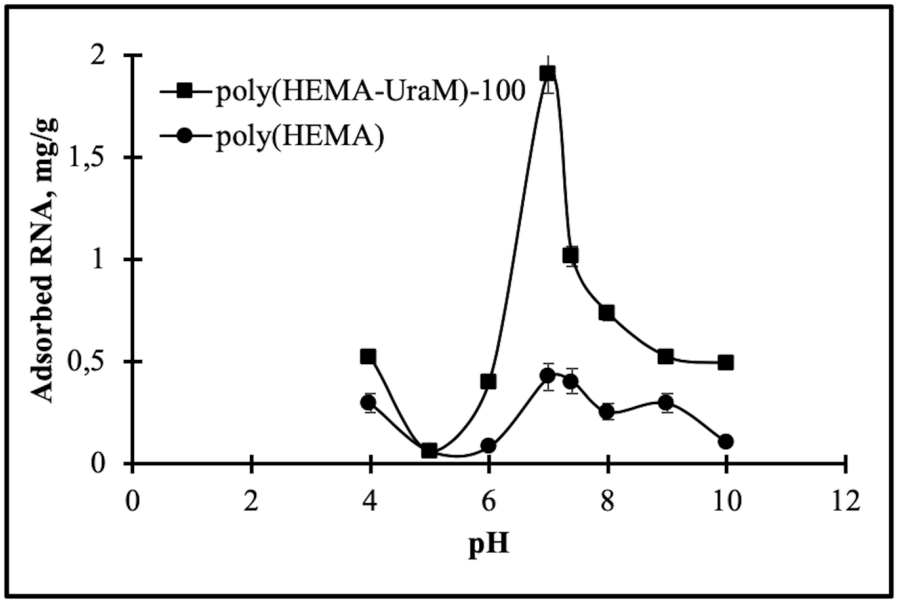

Figure 3: The effect of pH. C_{RNA}: 0.1 mg/mL; time: 120 min; temperature: 25°C

3.2.2. Effect of initial RNA concentration and ligand density

The initial RNA concentration on the adsorption of RNA was investigated at pH 7.0 for 120 min at room temperature. As illustrated in Fig. 4A, the adsorbed RNA amount was increased with an increasing RNA concentration up to 0.75 mg/mL, then remained almost constant. At higher initial concentrations effective active binding sites of membranes were surrounded by RNA and thus, RNA adsorption was reached an equilibrium state.

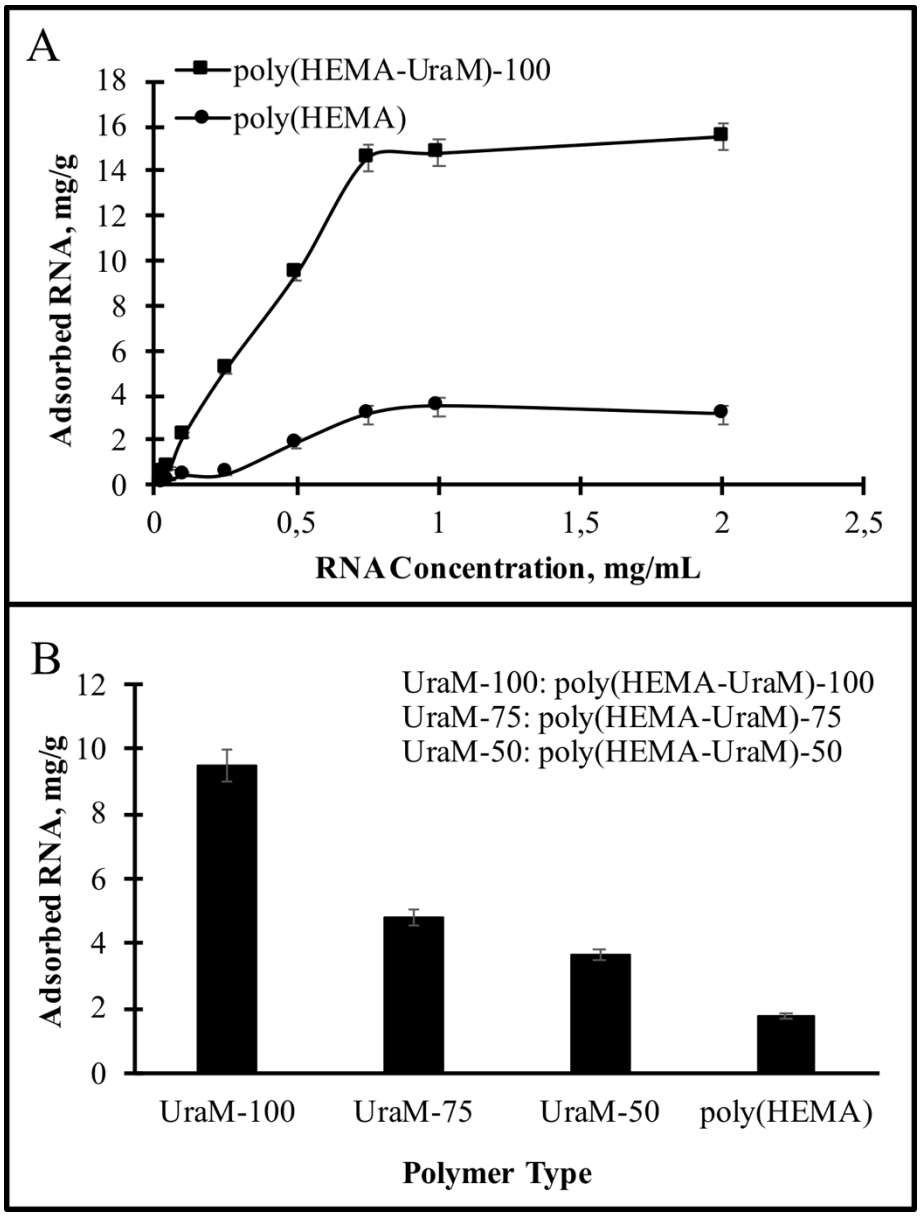

Figure 4: The effect of (A) initial RNA concentration; (B) comparison of RNA adsorption capacities in respect to the amount of functional ligand. pH: 7.0; time: 120 min; temperature: 25°C

The effect of UraM amount was also investigated on the membranes on RNA adsorption. The different UraM amount (50/75/100 mg) in the membranes was analyzed to choose optimal monomer ratio (Fig. 4B). The maximum binding capacities for poly(HEMA-UraM)-50/75/100 membranes were found as 3.66, 4.79, and 9.49 mg/g membrane, respectively. Sufficient number of functional groups play a fundamental role in the recognition of the target molecule and its high adsorption capacity. The results showed that the increasing monomer ratio provided an increase in the adsorption capacity. A negligible amount of RNA adsorption onto the plain poly(HEMA) cryogel was determined. The reason for this negligible binding is that the diffusion of the target molecules into the pores and non-specific interaction [26, 28].

3.2.3. Effect of time

The interaction time on RNA adsorption was investigated by the poly(HEMA) and poly(HEMA-UraM)-100 membranes in the interval of 5–120 min (Fig. 5). The RNA solution can rapidly enter into the large and interconnected porous structures of the membranes. Thus, the adsorption of RNA occurred quite quickly in the first 30 minutes, and then adsorption equilibrium (i.e. plateaus values) were reached within 60 min; that is, the effective binding sites on the membranes were fully occupied and data indicating no significant increase of RNA adsorption. These results confirmed that the poly(HEMA-UraM) membrane showed higher binding capacity for RNA than poly(HEMA) membrane because of the high affinity between ligand and target molecules. These results also supported by occurring of hydrogen bonds between affinity ligand and the target molecule.

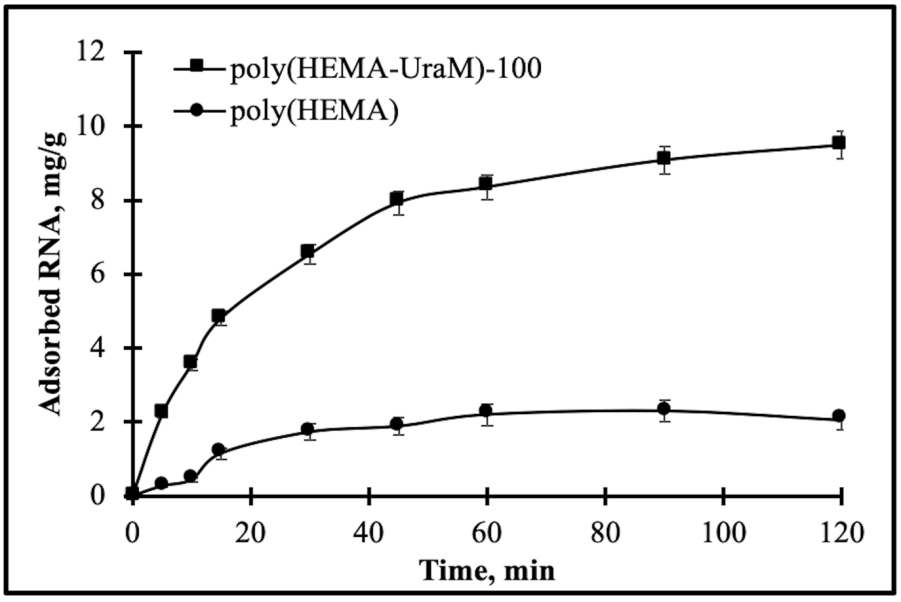

Figure 5: The effect of time. pH: 7.0; C_{RNA}: 0.5 mg/mL; temperature: 25 °C

3.2.4. Effect of temperature

The temperature behavior on the adsorption capacity was performed at different temperatures (4-45°C). As illustrated in Fig. 6, the adsorbed RNA amount was decreased with increasing temperature from 4°C to 45°C. Adsorbed RNA amount reduced from 9.59 mg/g to 8.74 mg/g for poly(HEMA-UraM)-100 membrane by the increasing temperature. The relationship between temperature and RNA adsorption provides important data to determine the basic interactions in the adsorption process. The amount of hydrogen bonds between RNA molecule and UraM monomer may weaken by the increasing temperature. The results also showed that this

strong binding between RNA and poly(HEMA-UraM)-100 membranes mainly rely on hydrogen bonding.

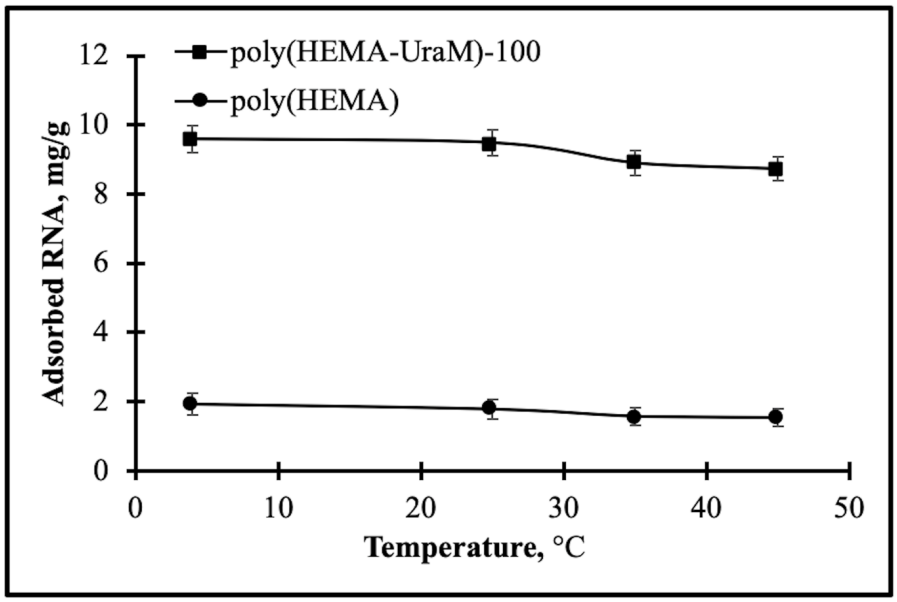

Figure 6: The effect of temperature. pH: 7.0; C_{RNA}: 0.5 mg/mL; time: 120 min

3.3. Adsorption isotherms and kinetic models

Several mathematical isotherm and kinetic models were calculated on the adsorption equilibrium data to describe the RNA adsorption process and surface coverage of adsorbent. Langmuir and Freundlich are frequently investigated methods to define equilibrium adsorption. Flory–Huggins model was also used for the thermodynamic behavior of polymers. The pseudo-first-order, pseudo-second-order, Weber–Morris, and film diffusion models also were examined to kinetic interpretations. In addition, the initial adsorption rate and half adsorption time were calculated. Linearized forms of the equations were given as follows [29-33]:

Adsorption Isotherms at Equilibrium State:

Langmuir $$\frac{1}{Q_{eq}} = \frac{1}{Q_m} + \left(\frac{1}{b.Q_m}\right).\left(\frac{1}{C_{eq}}\right) \quad (4)$$

Freundlich $$\ln Q_{eq} = \ln K_F + \frac{1}{n} \ln C_{eq} \quad (5)$$

Flory-Huggins $$\log\left(\frac{\theta}{C_o}\right) = \log K_{FH} + n_{FH} \log[1-\theta] \quad (6)$$

Where, C_o, C_{eq}, Q_{eq} and Q_m are the concentration of RNA at initial and equilibrium (mg/mL), the amount of RNA adsorbed at equilibrium, and theoretical (mg/g), respectively; θ is

the degree of surface coverage; b, 1/n, K_F, K_{FH}, and n_{FH} are constants of adsorption isotherms, respectively. 1/n shows surface heterogeneity whereas K_{FH} is used to determine Gibbs free energy.

Adsorption Kinetic Modelling:

First order $$\log\left(Q_{eq}-Q_t\right)=\log Q_{eq}-\frac{k_1}{2.303}.t \quad (7)$$

Second order $$\frac{t}{Q_t}=\frac{1}{k_2 Q_{eq}^2}+\frac{t}{Q_{eq}} \quad (8)$$

Weber-Morris (intra-particle diffusion) $$Q_t=k_d t^{0.5}+C_{WM} \quad (9)$$

Initial adsorption rate $$h=k_2 Q_{eq}^2 \quad (10)$$

Half adsorption time $$t_{1/2}=\frac{1}{k_2 Q_{eq}} \quad (11)$$

Film diffusion $$\ln(1-F)=-k_{fd}.t \quad (\text{whereas } F=Q_t/Q_{eq}) \quad (12)$$

Here, k_1 is first order kinetic constant (1/min); k_2 is second order kinetic constant [g/(mg.min)]; k_d is intraparticle diffusion rate constant [g/(mg.min$^{0.5}$)]; Q_{eq} and Q_t are the adsorbed amounts (mg/g) of RNA at t=0 and t=t, respectively [29]. C_{WM} is Weber-Morris constant (mg/g); K_{fd} is the film diffusion constant (1/min).

Table 1: The parameters calculated from adsorption isotherm and kinetic models

Isotherms			Kinetics			
Langmuir			First order			Initial adsorption rate
Q_{max} (mg/g)	b (mL/mg)	R^2	Q_{eq} (mg/g)	k_1 (1/min)	R^2	h (mg/g.min)
29.76	1.307	0.9953	6.57	0.023	0.8023	0.550
Equation: y = 0.0257x + 0.0336			Equation: y = -0.01x + 0.8176			
Freundlich			Second order			Half adsorption rate
K_F	1/n	R^2	Q_{eq} (mg/g)	k_2 (g/mg.min)	R^2	$t_{1/2}$ (min)
17.47	0.8024	0.9339	11.123	$4.49x10^{-3}$	0.9994	20.21
Equation: y = 0.8024x + 2.8603			Equation: y = 0.0899x + 1.8167			
Flory-Huggins			Weber-Morris			Fim diffusion coefficient
K_{FH}	n_{FH}	R^2	k_{id} (g/mg.min$^{0.5}$)	C_{WM}	R^2	k_{fd} (1/min)
158.82	-0,5605	0.7668	0.8396	1.2807	0.8823	0.0343
Equation: y = -0.5605x + 2.2009			Equation: y = 0.8396x + 1.2807			

RNA adsorption isotherms and kinetic data for poly(HEMA-UraM)-100 membrane were given in Table 1. As summarized in Table 1, R^2 value for Langmuir (0.9953) was much higher than Freundlich isotherm (0.9339), and also 1/n value of Freundlich isotherm was calculated as 0.8024 which was also confirming the monolayer adsorption process. According to values of 1/n and R^2, Langmuir isotherm was well-fitted to the adsorption system, as well as, the functional groups (UraM) distribution of the adsorbent surface was energetically homogenous and the adsorption was realized without any diffusion problem and lateral interaction. In addition, Flory–Huggins model was used again to describe the spontaneous nature of adsorption procedure. Gibbs free energy was found as -7.087 kJ/mol using Flory–Huggins equilibrium constant K_{FH} and Gibbs free energy equation ($\Delta G=-RTlnK_{FH}$). As a result, the RNA adsorption was occurred spontaneously due to the required lower energy for the adsorption process [34].

Table 1 displays that calculated R^2 for second-order (0.9994) is higher than first-order kinetic model (0.8023). When the linear correlation coefficients of these models were compared, data was fixed with second-order kinetic model indicating chemical interactions between specific sites of membranes and RNA molecules without any diffusional problems. Furthermore, initial adsorption rate (h), half adsorption rate ($t_{1/2}$),and film diffusion coefficient (k_{fd}) were calculated as 0.550 mg/(g min), 20.21 min, and 0.0343 1/min, respectively. Weber-Morris model is frequently treated as a check whether the intraparticle diffusion and film diffusion are the rate-limiting steps. As illustrated in Table 1, the linear correlation coefficients of Weber-Morris model are lower than the other models. The results show that adsorption process occurred without any diffusion restrictions. This result demonstrated the interconnected macropores structure of membranes having superior flow properties during the adsorption process.

3.4. Desorption and reusability

The development of reusable adsorbent materials is very important in terms of cost-friendly and high stability. For this purpose, the reusability and retained adsorption capacity were investigated using the same membranes. Poly(HEMA-UraM) membrane was used ten times in consequent adsorption-desorption cycles in a batch system using optimal condition, desorbing agent (0.1 M HCl), alkaline solution (5 mM NaOH), and PBS pH 7.0. After the tenth cycle, the adsorbed amount of RNA was found as 9.14 mg/g and maintains 96.32 % of its RNA adsorption capacity (Fig. 7). According to these results, 0.1 M HCl was proved as an appropriate desorption agent. It was demonstrated that RNA could be used many times without no significant decrease for RNA adsorption capacity of the membrane.

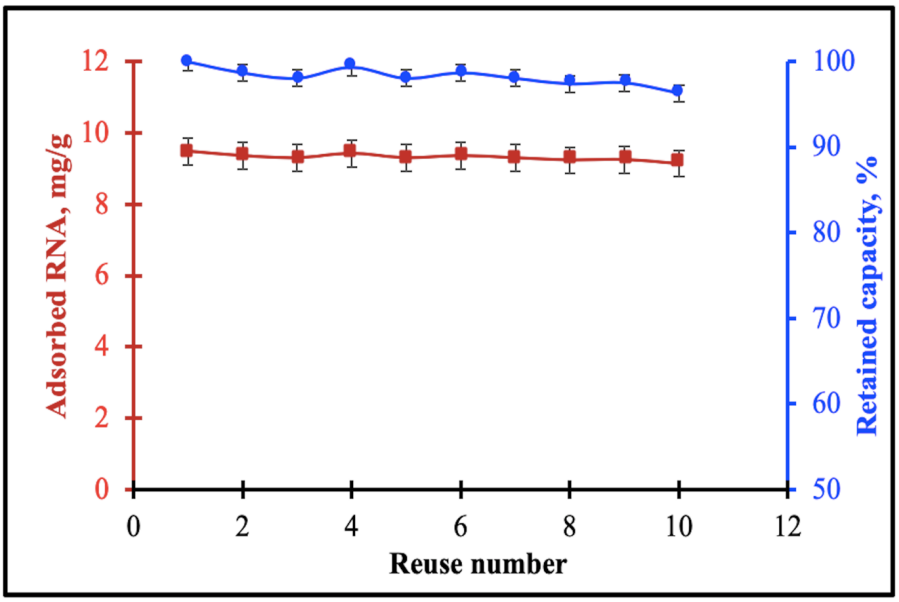

Figure 7: The reusability and retained adsorption capacity. pH: 7.0; C_{RNA}: 0.5 mg/mL; time: 120 min; temperature: 25°C; desorbing agent: 0.1 M HCl

4. Conclusion

The desired feature in affinity chromatography studies is to provide high efficiency RNA adsorption in a short time. Since RNA molecules are hydrolyzed in a short time and also extremely sensitive, there is a growing demand for specific, fast, and efficient RNA separation system. In this context, developed poly(HEMA-UraM) membranes can be classified as a suitable adsorbent due to incorporating a nucleotide into the membrane structure. Herein, polymerizable uracil nucleotide in the polymeric structure ensured to mimic natural Uracil-Adenine interactions which provided high affinity between ligand and target molecules. Moreover, advantages of the bioinspired functional nucleotide with membrane were combined to develop an alternative adsorbent from the structural stability, flow dynamics, and osmotic features of membranes. It was demonstrated that these membranes showed a high reusability performance without significant loss in RNA adsorption capacity. The equilibrium adsorption isotherms fitted well to Langmuir isotherms (R^2 = 0.9953) and the value of adsorption capability (Q_{max}) and equilibrium constant (b) were estimated to be 29.76 mg/g and 1.307 mg/mL for the poly(HEMA-UraM) membrane, respectively. The kinetics of adsorption fitted best to pseudo-second order (R^2 = 0.8023). Finally, the developed membranes promising as a good alternative as supports having high affinity, reusability, and cost-friendly adsorbent.

Acknowledgement

C. Armutcu thanks Sena Piskin, Mirac Tuysuz and Dr. E. Ozgur for their valuable help during the study.

Declaration of conflict of interest

The author has declared no conflict of interest.

References

[1] Sharp, P.A., *The centrality of RNA*, Cell, 136, 577-580, 2009.

[2] Perçin, I., İdil, N., Denizli, A., *RNA purification from Escherichia coli cells using boronated nanoparticles*, Colloids and Surfaces B: Biointerfaces, 162, 146-153, 2018.

[3] Martins, R., Queiroz, J., Sousa, F., *Ribonucleic acid purification*, Journal of Chromatography A, 1355, 1-14, 2014.

[4] Cooper, T.A., Wan, L., Dreyfuss, G., *RNA and disease*, Cell, 136, 777-793, 2009.

[5] Köse, K., Denizli, A., P*oly (hydroxyethyl methacrylate) based magnetic nanoparticles for lysozyme purification from chicken egg white*, Artificial cells, nanomedicine, and biotechnology, 41, 13-20, 2013.

[6] Yang, G., Lu, X., Yuan, L., *LncRNA: a link between RNA and cancer*, Biochimica et Biophysica Acta (BBA)-Gene Regulatory Mechanisms, 1839, 1097-1109, 2014.

[7] Kim, I., Mckenna, S.A., Puglisi, E.V., Puglisi, J.D., *Rapid purification of RNAs using fast performance liquid chromatography (FPLC)*, RNA, 13, 289-294, 2007.

[8] Martins, R., Queiroz, J.A., Sousa, F., *Histidine affinity chromatography-based methodology for the simultaneous isolation of Escherichia coli small and ribosomal RNA*, Biomedical Chromatography, 26, 781-788, 2012.

[9] McGinnis, A.C., Chen, B., Bartlett, M.G., *Chromatographic methods for the determination of therapeutic oligonucleotides*, Journal of Chromatography B, 883, 76-94, 2012.

[10] Romanovskaya, A., Sarin, L.P., Bamford, D.H., Poranen, M.M., *High-throughput purification of double-stranded RNA molecules using convective interaction media monolithic anion exchange columns*, Journal of Chromatography A, 1278, 54-60, 2013.

[11] Vomelova, I., Vaníčková, Z., Šedo, A., *Technical note methods of RNA purification. All ways (should) lead to Rome*, Folia Biologica (Praha), 55, 243-251, 2009.

[12] Warren, W.J., Vella, G., *Principles and methods for the analysis and purification of synthetic deoxyribonucleotides by high-performance liquid chromatography*, Molecular Biotechnology, 4, 179, 1995.

[13] Srivastava, A., Shakya, A.K., Kumar, A., *Boronate affinity chromatography of cells and biomacromolecules using cryogel matrices*, Enzyme and Microbial Technology, 51, 373-381, 2012.

[14] Uhlenbeck, O., *Keeping RNA happy*, RNA, 1, 4, 1995.

[15] Edwards, A.L., Garst, A.D., Batey, R.T., *Determining structures of RNA aptamers and riboswitches by X-ray crystallography, Nucleic Acid and Peptide Aptamers*, Springer2009, pp. 135-163.

[16] Garcia, F., Pires, E., *Recovery processes for biological materials*, Chromatography, Wiley, London, UK, 415-451, 1993.

[17] Scouten, W.H., *Affinity chromatography; bioselective adsorption on inert matrices*, Wiley, NewYork, 1981.

[18] Ayyar, B.V., Arora, S., Murphy, C., O'Kennedy, R., *Affinity chromatography as a tool for antibody purification*, Methods, 56, 116-129, 2012.

[19] Roque, A.C., Silva, C.S., Taipa, M.Â., *Affinity-based methodologies and ligands for antibody purification: advances and perspectives*, Journal of Chromatography A, 1160, 44-55, 2007.

[20] Andaç, M., Tamahkar, E., Denizli, A., *Molecularly imprinted smart cryogels for selective nickel recognition in aqueous solutions*, Journal of Applied Polymer Science, 49746.

[21] Emin Çorman, M., Bereli, N., Özkara, S., Uzun, L., Denizli, A., *Hydrophobic cryogels for DNA adsorption: Effect of embedding of monosize microbeads into cryogel network on their adsorptive performances*, Biomedical Chromatography, 27, 1524-1531, 2013.

[22] Bereli, N., Yavuz, H., Denizli, A., *Protein chromatography by molecular imprinted cryogels*, Journal of Liquid Chromatography & Related Technologies, 1-14, 2020.

[23] Öncel, P., Çetin, K., Topçu, A.A., Yavuz, H., Denizli, A., *Molecularly imprinted cryogel membranes for mitomycin C delivery*, Journal of Biomaterials Science Polymer Edition, 28, 519-531, 2017.

[24] Hur, D., Ekti, S.F., Say, R., *N-Acylbenzotriazole mediated synthesis of some methacrylamido amino acids*, Letters in Organic Chemistry, 4, 585-587, 2007.

[25] Armutcu, C., Çorman, M.E., Bayram, E., Uzun, L., *Purification of Fab and Fc using papain immobilized cryogel bioreactor separator system*, Journal of Chromatography B, 122396, 2020.

[26] Köse, K., Erol, K., Uzun, L., Denizli, A., *PolyAdenine cryogels for fast and effective RNA purification*, Colloids and Surfaces B: Biointerfaces, 146, 678-686, 2016.

[27] Köse, K., Uzun, L., *PolyGuanine methacrylate cryogels for ribonucleic acid purification*, Journal of Separation Science, 39, 1998-2005, 2016.

[28] Çorman, M.E., *Poly-l-lysine modified cryogels for efficient bilirubin removal from human plasma*, Colloids and Surfaces B: Biointerfaces, 167, 291-298, 2018.

[29] Daoud-Attieh, M., Chaib, H., Armutcu, C., Uzun, L., Elkak, A., Denizli, A., *Immunoglobulin G purification from bovine serum with pseudo-specific supermacroporous cryogels*, Separation and Purification Technology, 118, 816-822, 2013.

[30] Foo, K.Y., Hameed, B.H., *Insights into the modeling of adsorption isotherm systems*, Chemical engineering journal, 156, 2-10, 2010.

[31] Sarı, M.M., Armutcu, C., Bereli, N., Uzun, L., Denizli, A., *Monosize microbeads for pseudo-affinity adsorption of human insulin*, Colloids and Surfaces B: Biointerfaces, 84, 140-147, 2011.

[32] Erol, B., Erol, K., Gökmeşe, E., *The effect of the chelator characteristics on insulin adsorption in immobilized metal affinity chromatography*, Process Biochemistry, 83, 104-113, 2019.

[33] Ohale, P.E., Onu, C.E., Ohale, N.J., Obah, S.N., *Adsorptive kinetics, isotherm and thermodynamic analysis of fishpond effluent coagulation using chitin derived coagulant from waste Brachyura shell*, Chemical Engineering Journal Advances, 100036, 2020.

[34] Javadian, H., Ruiz, M., Taghvai, M., Sastre, A.M., *Novel magnetic nanocomposite of calcium alginate carrying poly (pyrimidine-thiophene-amide) as a novel green synthesized polyamide for adsorption study of neodymium, terbium, and dysprosium rare-earth ions*, Colloids and Surfaces A: Physicochemical and Engineering Aspects, 603, 125252, 2020.

Adıyaman University Journal of Science
https://dergipark.org.tr/en/pub/adyujsci
DergiPark AKADEMİK
ISSN 2147-1630
e-ISSN 2146-586X

Increasing the Efficiency of Percentile Parameter Estimation Method for Weibull Distribution

Ülkü ERİŞOĞLU[1], Murat ERİŞOĞLU[2], Tayfun SERVİ[3,*]

[1]*Necmettin Erbakan University, Faculty of Science, Department of Statistics, Konya, Turkey*
ugokal@erbakan.edu.tr, ORCID: 0000-0002-9826-3460
[2]*Necmettin Erbakan University, Faculty of Science, Department of Statistics, Konya, Turkey*
merisoglu@erbakan.edu.tr, ORCID: 0000-0002-4589-1383
[3]*Adıyaman University, Faculty of Economics and Administrative Science of Science, Department of Economics, Adıyaman, Turkey*
tservi@adiyaman.edu.tr, ORCID: 0000-0002-3173-327X

Received: 25.06.2020 **Accepted:** 10.08.2020 **Published:** 30.12.2020

Abstract

The Weibull distribution is one of the most widely used probability distributions in statistical applications. The percentile parameter estimation method is commonly used in parameter estimation of the two-parameter Weibull distribution in terms of easy computability and efficiency. The effectiveness of the percentile method depends on the selected percentile points and chosen empirical distribution function. In this study, the appropriate empirical distribution function and percentile points were determined to increase the efficiency of the percentile method for two-parameter Weibull distribution by simulation study.

***Keywords*:** Weibull distribution; Percentile estimation; Empirical distribution function.

Weibull Dağılımı için Persentil Parametre Tahmin Yönteminin Etkinliğinin Artırılması

Öz

* Corresponding Author DOI: 10.37094/adyujsci.757642

Weibull dağılımı istatistiksel uygulamalarda en yaygın kullanılan olasılık dağılımlarından biridir. Persentil parametre tahmin yöntemi kolay hesaplanama ve etkinlik açısından iki parametreli Weibull dağılımının parametre tahmininde yaygın olarak kullanılır. Persentil yönteminin etkinliği seçilen persentil noktalara ve seçilen ampirik dağılım fonksiyonuna bağlıdır. Bu çalışmada, simülasyon çalışması ile iki parametreli Weibull dağılımı için persentil yönteminin etkinliğini artırmak amacıyla uygun ampirik dağılım fonksiyonu ve persentil noktaları belirlenmiştir.

***Anahtar Kelimeler*:** Weibull dağılımı; Persentil tahmin; Ampirik dağılım fonksiyonu.

1. Introduction

The Weibull distribution is one of the widely used probability distributions which has many different applications and used for solving a variety of problems from many different disciplines. The Weibull distribution has many useful properties because its form is flexible to model different shapes. Weibull distribution has increasing, decreasing or stable failure rates depending on the values of the shape parameter. This feature has provided widespread use of the Weibull distribution. Because of its importance, many different estimation methods have been proposed for estimating parameters of Weibull distribution.

Percentile method is one of the commonly used methods for estimating the parameters of Weibull distribution and has some advantages unlike the other estimation methods in terms of ease compute and efficiency in parameter estimation [1].

The percentile method may be applied via two different approaches. The approach 1 is based on percentiles and is structurally similar to the traditional method of moments. The approach 2 is mainly obtained by minimizing the squared Euclidean distance between the sample percentile and population percentile [2].

The effectiveness of the percentile estimators depends on the selected percentile points and chosen empirical distribution function.

Dubey [3] proposed 17th and 97th percentiles for shape parameter and 40th and 82th percentiles for scale parameter. Seki and Yokoyama [4] suggested 31st and 63rd percentiles to estimate shape and scale parameters. Wang and Keats [5] proposed 15th and 63rd percentiles for parameter estimation of the Weibull distributions. Marks [6] stated that the best results were obtained with 10th and 90th percentiles for the shape and scale parameters.

In this study, we aimed to determine the appropriate empirical distribution and the percentile points to increase the effectiveness of the percentile estimators for the Weibull distribution. We used mean squared error (MSE) and mean total error (MTE) as performance criteria in the simulation study.

2. Weibull Distribution

The two-parameter Weibull distribution is specified by the probability density function (pdf)

$$f(x;\alpha,\beta)=\frac{\alpha}{\beta}\left(\frac{x}{\beta}\right)^{\alpha-1}e^{-\left(\frac{x}{\beta}\right)^{\alpha}}, \tag{1}$$

where $\alpha>0$ and $\beta>0$ are the shape and scale parameters, respectively. The corresponding cumulative distribution function (cdf) and survival function (sf) are given as bellow:

$$F(x;\alpha,\beta)=1-e^{-\left(\frac{x}{\beta}\right)^{\alpha}}, \tag{2}$$

$$S(x;\alpha,\beta)=e^{-\left(\frac{x}{\beta}\right)^{\alpha}}. \tag{3}$$

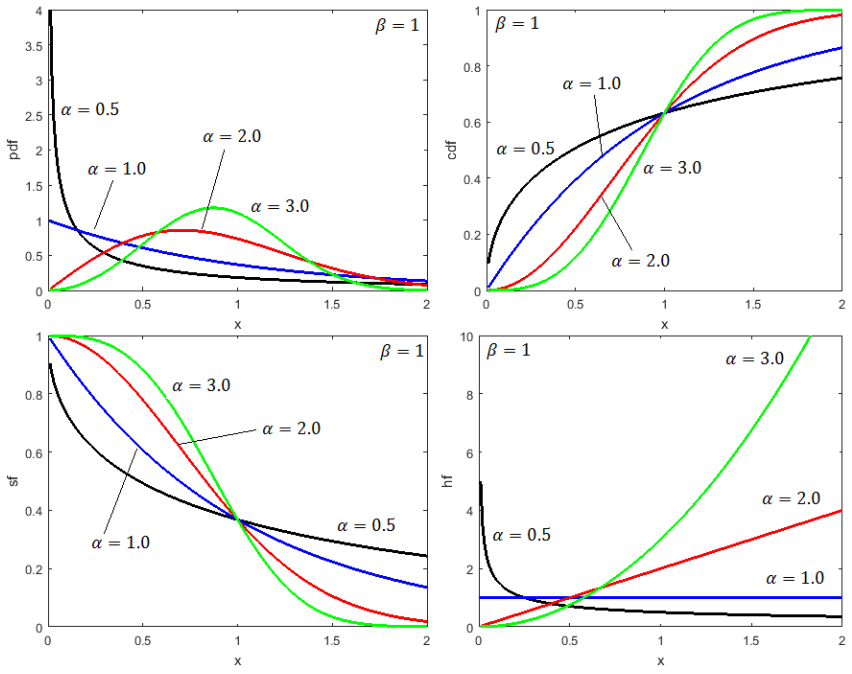

Figure 1: The curves of the pdf, cdf, sf and hf of Weibull distribution for selected parameter values

The hazard function (hf) is given

$$h(x;\alpha,\beta)=\alpha\beta^{-\alpha}x^{\alpha-1}, \tag{4}$$

which can be increase, decrease or constant depending on , $\alpha > 1$, $\alpha < 1$ or $\alpha = 1$, respectively.

The curves of the pdf, cdf, sf and hf of Weibull distribution are shown in Fig. 1 for selected parameter values.

3. Percentile Method (PM)

The quantile function corresponding to Eqn. (1) is

$$x_p = \beta[-ln(1-p)]^{1/\alpha}. \tag{5}$$

Percentile estimations of the Weibull distribution are calculated based on the obtained equations from selected two percentile points in the quantile function. The percentile estimators of the shape and scale parameters for Weibull distribution are respectively given by

$$\hat{\alpha} = \frac{ln[-ln(1-p_1)]-ln[-ln(1-p_2)]}{ln(x_{p_1})-ln(x_{p_2})}, \tag{6}$$

$$\hat{\beta} = \frac{x_{p_1}}{(-ln(1-p_1))^{1/\hat{\alpha}}}, \tag{7}$$

where p_1 and p_2 are selected two percentile points and x_{p_1} and x_{p_2} are observation values corresponding to p_1 and p_2 , respectively. There are many approaches for selection of the p_1 and p_2. For example, we can obtain an estimate for scale parameter by using one of these approaches like setting $p_1 = 1 - exp(-1) \cong 0.632$ (63.2th percentile point) into Eqn. (7). In this approach, the percentile estimators for Weibull distribution are given

$$\hat{\beta} = x_{1-exp\,(-1)}, \tag{8}$$

$$\hat{\alpha} = \left(\frac{ln[-ln(1-p_2)]}{ln(x_{p_2})-ln(\hat{\beta})}\right), \tag{9}$$

where $0 < x_{p_2} < x_{0.632}$ [7]. There are some suggestions for the optimum value of p_2. Wang and Keats [5] showed by simulation that 0.15 would be the correct choice for p_2. Seki and Yokoyama [8] suggested $p_2 = 0.31$.

The percentile based estimators for α and β of Weibull distribution according to approach 2 can be obtained by minimizing

$$\sum_{i=1}^{n}\left\{lnx_{(i)} - ln\beta - \frac{1}{\alpha}ln\left(-ln\,(1-\hat{F}_{(i)})\right)\right\}^2, \tag{10}$$

with respect to α and β. The percentile estimators for α and β of the Weibull distribution are given by

$$\hat{\alpha} = \frac{A^2 - nB}{AC - nD}, \tag{11}$$

$$\hat{\beta} = exp\left(\frac{1}{n}\left(C - \frac{A}{\hat{\alpha}}\right)\right), \tag{12}$$

where $A = \sum_{i=1}^{n} ln\left(-ln\left(1-\hat{F}_{(i)}\right)\right)$, $B = \sum_{i=1}^{n}\left\{ln\left(-ln\left(1-\hat{F}_{(i)}\right)\right)\right\}^2$, $C = \sum_{i=1}^{n} lnx_i$ and $D = \sum_{i=1}^{n} lnx_i ln\left(-ln\left(1-\hat{F}_{(i)}\right)\right)$.

4. Simulation Study

In this study, we designed a simulation according to different sample size and different parameter values with the following purposes:

- To determine the best empirical distribution function respect to MSE for approach 1 in the percentile method.

- To choose the best selected second percentile point p_2 when setting $p_1 = 1 - exp(-1) \cong 0.632$ for approach 1.

- To determine the best percentile pair among from several selected percentile pairs for approach 1 in the percentile estimation.

- To determine the best empirical distribution function for the best successful estimation according to MTE in the percentile estimation by approach 2.

Table 1: The selected empirical distribution functions

Kaplan-Meir	$\hat{F}_1(x_{(i)}) = \frac{i}{n}$
Herd-Johnson (Mean rank)	$\hat{F}_2(x_{(i)}) = \frac{i}{n+1}$
Median (Symmetrical)	$\hat{F}_3(x_{(i)}) = \frac{i-0.5}{n}$
Median rank	$\hat{F}_4(x_{(i)}) = \frac{i-0.3}{n+0.4}$
Approximate Normal	$\hat{F}_5(x_{(i)}) = \frac{i-\frac{3}{8}}{n+\frac{1}{4}}$

Firstly, we examined fitness between empirical distribution functions and actual cumulative distribution function values of the Weibull distribution for approach 1 in the percentile estimation method. The selected EDFs are given in Table 1.

We used mean squared error (MSE) in the comparison of the fitness between empirical distribution functions and actual cumulative distribution function values of Weibull distribution for the different parameter values and sample sizes.

$$MSE_m = \frac{1}{100000}\sum_{r=1}^{100000}\sum_{i=1}^{n}\frac{\left[F(x_{(i)};\alpha,\beta)-\hat{F}_m(x_{(i)})\right]^2}{n} \tag{13}$$

In the simulation study, 100000 random samples of sizes 10, 30, 50 and 100 were generated from Weibull distributions having $\alpha = 0.5, 1, 1.5, 2, 3.4, 5$ and $\beta = 1, 10$. The comparisons of the empirical distribution functions respect to MSE are given in Table 2.

In accordance with Table 2, the empirical distribution function that best matches the actual cumulative distribution function values of the Weibull distribution is Hard-Johnson's empirical distribution function for all the cases. Hard-Johnson's function will be used as empirical distribution function in the determination of the best percentile pairs for the percentile estimations according to approach 1.

At this stage of the study, we will try to determine the best percentile point for the $p_1 = 1 - exp\,(-1) \cong 0.632$ in the approach 1. For this, the $MSE(\hat{\alpha})$ values for all candidate points were determined with 0.01 increases from 0 to 0.63.

$$MSE(\hat{\alpha}) = \frac{1}{10000}\sum_{r=1}^{10000}(\alpha - \hat{\alpha}_r)^2 \tag{14}$$

In the simulated study for the different parameter values and sample sizes, the percentile point with the smallest $MSE(\hat{\alpha})$ was determined, and the results are given in Table 3.

Table 2: The comparison of the EDFs according to MSE for different sample sizes and parameter values

α	n	$\beta = 1$					$\beta = 10$				
		$\hat{F}_1$	$\hat{F}_2$	$\hat{F}_3$	$\hat{F}_4$	$\hat{F}_5$	$\hat{F}_1$	$\hat{F}_2$	$\hat{F}_3$	$\hat{F}_4$	$\hat{F}_5$
0.5	10	0.01825	**0.01503**	0.01567	0.01523	0.01537	0.01830	**0.01522**	0.01588	0.01544	0.01557
	30	0.00583	**0.00548**	0.00556	0.00551	0.00552	0.00573	**0.00537**	0.00546	0.00540	0.00542
	50	0.00342	**0.00328**	0.00332	0.00330	0.00330	0.00342	**0.00328**	0.00331	0.00329	0.00330
	100	0.00167	**0.00163**	0.00164	0.00164	0.00164	0.00168	**0.00165**	0.00166	0.00166	0.00166
1	10	0.01851	**0.01534**	0.01604	0.01558	0.01572	0.01842	**0.01530**	0.01595	0.01551	0.01564
	30	0.00578	**0.00539**	0.00549	0.00543	0.00545	0.00574	**0.00537**	0.00545	0.00540	0.00542
	50	0.00340	**0.00326**	0.00329	0.00327	0.00328	0.00342	**0.00329**	0.00332	0.00330	0.00330
	100	0.00169	**0.00166**	0.00167	0.00167	0.00167	0.00168	**0.00165**	0.00165	0.00165	0.00165
1.5	10	0.01798	**0.01479**	0.01545	0.01500	0.01514	0.01837	**0.01522**	0.01595	0.01547	0.01562
	30	0.00574	**0.00534**	0.00544	0.00538	0.00540	0.00571	**0.00532**	0.00542	0.00536	0.00538
	50	0.00339	**0.00325**	0.00328	0.00326	0.00326	0.00346	**0.00332**	0.00335	0.00333	0.00334
	100	0.00166	**0.00162**	0.00163	0.00163	0.00163	0.00168	**0.00165**	0.00166	0.00165	0.00166

2	10	0.01822	**0.01512**	0.01577	0.01533	0.01546	0.01829	**0.01508**	0.01573	0.01529	0.01542
	30	0.00577	**0.00543**	0.00551	0.00546	0.00547	0.00564	**0.00530**	0.00539	0.00533	0.00535
	50	0.00337	**0.00324**	0.00327	0.00325	0.00326	0.00342	**0.00331**	0.00334	0.00332	0.00333
	100	0.00167	**0.00164**	0.00165	0.00165	0.00165	0.00169	**0.00166**	0.00166	0.00166	0.00166
3.4	10	0.01833	**0.01530**	0.01598	0.01553	0.01567	0.01829	**0.01502**	0.01573	0.01526	0.01541
	30	0.00578	**0.00540**	0.00549	0.00543	0.00545	0.00578	**0.00541**	0.00549	0.00543	0.00545
	50	0.00344	**0.00331**	0.00335	0.00333	0.00333	0.00340	**0.00327**	0.00330	0.00328	0.00329
	100	0.00167	**0.00164**	0.00164	0.00164	0.00164	0.00167	**0.00163**	0.00164	0.00163	0.00163
5	10	0.01833	**0.01520**	0.01589	0.01543	0.01557	0.01859	**0.01529**	0.01599	0.01553	0.01567
	30	0.00570	**0.00536**	0.00545	0.00539	0.00541	0.00573	**0.00535**	0.00544	0.00538	0.00540
	50	0.00346	**0.00332**	0.00335	0.00333	0.00334	0.00340	**0.00327**	0.00330	0.00328	0.00329
	100	0.00168	**0.00165**	0.00166	0.00165	0.00165	0.00170	**0.00167**	0.00168	0.00167	0.00167

Table 3: The percentile points values which have the smallest MSE($\hat{\alpha}$) for different sample sizes and parameter values

Sample Size	$\boldsymbol{\beta = 1}$						$\boldsymbol{\beta = 10}$					
	$\boldsymbol{\alpha}$						$\boldsymbol{\alpha}$					
$\boldsymbol{n}$	**0.5**	**1**	**1.5**	**2**	**3.4**	**5**	**0.5**	**1**	**1.5**	**2**	**3.4**	**5**
10	0.13	0.13	0.13	0.13	0.13	0.13	0.13	0.13	0.13	0.13	0.13	0.13
30	0.11	0.14	0.14	0.14	0.14	0.14	0.14	0.14	0.14	0.14	0.14	0.14
50	0.12	0.12	0.12	0.14	0.10	0.12	0.12	0.10	0.12	0.14	0.10	0.14
100	0.11	0.12	0.11	0.12	0.12	0.13	0.14	0.13	0.12	0.13	0.13	0.12

According to Table 3, the most suitable percentile points is found ranges 0.10 to 0.14 for the $p_1 \cong 0.632$ in the approach 1. The best percentile point was 0.13 with respect to $MSE(\hat{\alpha})$ in the shape parameter estimation of the Weibull distribution by this approach when the small sample size is $n = 10$.

Here, the best percentile pair will be determined from the selected percentile pairs in the percentile estimation by approach 1 of the Weibull distribution parameters. The comparison is based on MTE criterion defined by

$$MTE = \frac{1}{10000}\sum_{r=1}^{10000}\left(\left(\frac{\hat{\alpha}_r-\alpha}{\alpha}\right)^2 + \left(\frac{\hat{\beta}_r-\beta}{\beta}\right)^2\right). \quad (15)$$

In this study, the selected percentile pairs are denoted in Table 4.

Table 4: The selected pairs of percentage point

$A: P\left(\frac{1}{n+1}, \frac{n}{n+1}\right)$	$B: P(0.25, 0.75)$	$C: P\left(0.25, \frac{n}{n+1}\right)$	$D: P\left(\frac{1}{n+1}, 0.75\right)$
$E: P\left(0.5, \frac{n}{n+1}\right)$	$F: P\left(\frac{1}{n+1}, 0.5\right)$	$G: P(0.632, 0.30)$	$H: P(0.05, 0.95)$
$I: P(0.10, 0.90)$	$J: P(0.17, 0.97)$	$K: P(0.24, 0.93)$	$L: P(0.632, 0.12)$

In the simulation study, the obtained MTE values for different parameter values and sample sizes are given in Table 5.

According to Table 5, in case of the scale parameter is equal 1, J and K percentile pairs point are more successful than other percentile pairs for ≥ 1 . The B percentile pair is more successful than other pairs for $\alpha < 1$ and $\beta = 1$. In case of the scale parameter is set as $\beta = 10$, B percentile pair is more successful than other percentile pairs for $\alpha \leq 1$. The K percentile pair is more successful than other pairs for $\alpha = 2$ and $\beta = 10$. In addition, J percentile pair showed more performance than other pairs for $\alpha = 5$ and $\beta = 10$.

Finally, we performed a simulation study to investigate the performance of empirical distribution functions in the percentile estimates for parameters of the Weibull distribution by approach 2. The comparison results of the empirical distribution functions according to MTE for different sample sizes and parameter values in the approach 2 are given in Table 6.

Table 5: The comparison results of the selected percentage points according to MTE

β	α	n	A	B	C	D	E	F	G	H	I	J	K	L
1	0.5	10	1.725	1.201	1.376	**1.126**	1.405	3.677	1.617	1.725	1.725	1.538	1.376	1.679
		30	0.899	**0.265**	0.418	0.288	0.320	1.478	0.394	0.457	0.348	0.544	0.328	0.408
		50	0.689	**0.150**	0.262	0.178	0.182	0.530	0.176	0.260	0.186	0.226	0.165	0.177
		100	0.553	**0.070**	0.148	0.104	0.091	0.308	0.090	0.131	0.086	0.108	0.078	0.094
	1	10	0.341	0.462	0.315	0.336	0.540	0.640	0.428	0.341	0.341	**0.312**	0.315	0.552
		30	0.201	0.109	0.104	0.132	0.106	0.280	0.132	0.124	0.103	0.119	**0.092**	0.160
		50	0.167	0.064	0.068	0.093	0.066	0.155	0.075	0.077	0.061	0.062	**0.054**	0.075
		100	0.143	0.031	0.040	0.065	0.036	0.107	0.038	0.042	0.030	0.032	**0.027**	0.046
	1.5	10	0.264	0.523	0.271	0.332	0.620	0.586	0.424	0.264	0.264	**0.250**	0.271	0.610
		30	0.143	0.111	0.077	0.139	0.098	0.237	0.126	0.096	0.084	0.081	**0.073**	0.168
		50	0.117	0.065	0.050	0.101	0.062	0.146	0.075	0.059	0.051	0.046	**0.045**	0.076
		100	0.098	0.030	0.029	0.076	0.034	0.107	0.037	0.033	0.025	0.024	**0.023**	0.049
	2	10	0.279	0.647	0.304	0.391	0.773	0.685	0.503	0.279	0.279	**0.270**	0.304	0.752
		30	0.142	0.131	0.079	0.167	0.112	0.266	0.147	0.099	0.090	0.079	**0.078**	0.203
		50	0.113	0.076	0.050	0.123	0.071	0.170	0.088	0.061	0.055	**0.047**	0.049	0.089
		100	0.093	0.035	0.029	0.094	0.039	0.127	0.043	0.034	0.028	**0.024**	**0.024**	0.059
	3.4	10	0.405	1.052	0.464	0.615	1.262	1.079	0.798	0.405	0.405	**0.401**	0.464	1.220
		30	0.191	0.207	0.112	0.264	0.172	0.408	0.230	0.141	0.131	**0.107**	0.113	0.324
		50	0.149	0.120	0.070	0.196	0.110	0.267	0.138	0.087	0.080	**0.065**	0.072	0.140
		100	0.118	0.055	0.040	0.152	0.061	0.201	0.067	0.047	0.041	**0.033**	0.036	0.094
	5	10	0.576	1.534	0.668	0.891	1.843	1.566	1.159	0.576	0.576	**0.575**	0.668	1.780
		30	0.268	0.300	0.158	0.384	0.249	0.590	0.333	0.200	0.188	**0.150**	0.161	0.472
		50	0.208	0.174	0.099	0.285	0.159	0.387	0.201	0.123	0.114	**0.092**	0.102	0.203
		100	0.163	0.080	0.056	0.222	0.088	0.292	0.097	0.067	0.058	**0.046**	0.051	0.137
10	0.5	10	17.08	**10.58**	13.31	10.63	11.52	34.29	14.61	17.08	17.08	14.93	13.31	14.45
		30	8.534	**2.384**	4.152	2.538	2.950	13.81	3.678	4.403	3.298	5.195	3.177	3.661
		50	6.913	**1.280**	2.456	1.468	1.617	4.867	1.534	2.410	1.679	2.083	1.498	1.525
		100	5.311	**0.602**	1.454	0.796	0.804	2.826	0.779	1.204	0.781	1.018	0.707	0.775

1	10	2.365	1.891	1.938	**1.779**	2.033	3.527	2.508	2.365	2.365	2.076	1.938	2.173
	30	1.519	**0.549**	0.764	0.621	0.617	1.753	0.765	0.878	0.692	0.906	0.641	0.732
	50	1.321	**0.315**	0.491	0.401	0.368	0.847	0.393	0.540	0.390	0.442	0.343	0.376
	100	1.115	**0.156**	0.305	0.243	0.194	0.537	0.202	0.288	0.193	0.233	0.173	0.194
1.5	10	1.091	1.139	**0.911**	0.934	1.245	1.679	1.630	1.091	1.091	0.949	**0.911**	1.128
	30	0.717	**0.305**	0.351	0.354	0.315	0.785	0.426	0.422	0.339	0.404	0.307	0.377
	50	0.629	0.174	0.227	0.240	0.192	0.423	0.234	0.263	0.195	0.208	**0.171**	0,208
	100	0.538	**0.086**	0.140	0.156	0.102	0.279	0.117	0.140	0.097	0.111	0.087	0.105
2	10	0.738	1.021	**0.648**	0.731	1.138	1.297	1.567	0.738	0.738	0.649	**0.648**	0.898
	30	0.467	0.244	0.230	0.286	0.233	0.549	0.353	0.283	0.234	0.257	**0.208**	0.287
	50	0.407	0.137	0.148	0.202	0.145	0.319	0.198	0.176	0.136	0.137	**0.120**	0.164
	100	0.347	0.067	0.090	0.138	0.077	0.217	0.097	0.094	0.067	0.073	**0.060**	0.081
3.4	10	0.562	1.264	0.573	0.748	1.443	1.368	2.099	0.562	0.562	**0.526**	0.573	0.961
	30	0.305	0.257	0.165	0.301	0.217	0.487	0.395	0.207	0.183	0.170	**0.160**	0.283
	50	0.255	0.141	0.105	0.224	0.138	0.315	0.225	0.128	0.109	**0.096**	0.098	0.167
	100	0.209	0.068	0.060	0.164	0.074	0.226	0.107	0.067	0.054	0.050	**0.048**	0.080
5	10	0.645	1.740	0.712	0.973	1.999	1.810	2.945	0.645	0.645	**0.628**	0.712	1.271
	30	0.318	0.338	0.187	0.395	0.274	0.610	0.529	0.233	0.215	**0.184**	0.186	0.364
	50	0.256	0.183	0.117	0.299	0.176	0.409	0.302	0.143	0.128	**0.107**	0.117	0.217
	100	0.204	0.088	0.065	0.223	0.093	0.142	0.074	0.063	0.063	**0.055**	0.057	0.103

Table 6: The comparison results of the empirical distribution functions according to MTE for different sample sizes and parameter values in the approach 2

α	n	$\beta = 1$					$\beta = 10$				
		$\widehat{F}_1$	$\widehat{F}_2$	$\widehat{F}_3$	$\widehat{F}_4$	$\widehat{F}_5$	$\widehat{F}_1$	$\widehat{F}_2$	$\widehat{F}_3$	$\widehat{F}_4$	$\widehat{F}_5$
0.5	10	**0.6209**	1.2054	0.8843	0.8976	0.9490	**5.6093**	11.584	8.2614	7.0162	8.9809
	30	**0.1872**	0.2579	0.2137	0.2210	0.2236	**1.6950**	2.4080	1.9811	1.8365	2.0847
	50	**0.1157**	0.1439	0.1238	0.1278	0.1284	**1.0498**	1.3319	1.1438	1.0858	1.1906
	100	**0.0563**	0.0647	0.0579	0.0595	0.0594	**0.5066**	0.5902	0.5293	0.5127	0.5445
1	10	0.2533	0.2632	0.2600	**0.2384**	0.2500	1.3328	1.6937	1.4358	**1.1833**	1.4813
	30	0.0791	0.0840	0.0755	**0.0751**	0.0757	0.4369	0.4981	0.4433	**0.4030**	0.4545
	50	0.0485	0.0511	**0.0457**	0.0461	0.0461	0.2704	0.2972	0.2696	**0.2523**	0.2753
	100	0.0247	0.0258	**0.0232**	0.0236	0.0235	0.1341	0.1440	0.1332	**0.1277**	0.1354
1.5	10	0.2562	0.2186	0.2479	**0.2147**	0.2254	0.7622	0.7778	0.7332	**0.6168**	0.7262
	30	0.0770	0.0762	0.0696	**0.0683**	0.0684	0.2385	0.2494	0.2277	**0.2120**	0.2300
	50	0.0468	0.0473	0.0421	0.0422	**0.0420**	0.1458	0.1518	0.1391	**0.1330**	0.1407
	100	0.0242	0.0247	**0.0218**	0.0222	0.0220	0.0728	0.0758	0.0700	**0.0683**	0.0709
2	10	0.2998	**0.2418**	0.2884	0.2444	0.2567	0.5974	0.5413	0.5556	**0.4810**	0.5305
	30	0.0889	0.0864	0.0791	0.0773	**0.0772**	0.1810	0.1815	0.1671	**0.1610**	0.1668
	50	0.0540	0.0540	0.0477	0.0479	**0.0474**	0.1099	0.1117	0.1018	**0.1004**	0.1023
	100	0.0281	0.0285	**0.0249**	0.0254	0.0251	0.0555	0.0569	**0.0519**	**0.0519**	0.0524
3.4	10	0.4657	**0.3656**	0.4500	0.3761	0.3950	0.5763	0.4645	0.5415	**0.4838**	0.4879
	30	0.1374	0.1326	0.1212	0.1182	**0.1177**	0.1700	0.1646	0.1514	0.1538	**0.1483**
	50	0.0834	0.0831	0.0730	0.0732	**0.0724**	0.1030	0.1026	0.0916	0.0949	**0.0911**

	100	0.0436	0.0442	**0.0383**	0.0391	0.0385	0.0531	0.0539	**0.0476**	0.0497	0.0479
5	10	0.6727	**0.5264**	0.6515	0.5433	0.5705	0.7258	**0.5715**	0.6938	0.6165	0.6133
	30	0.1984	0.1913	0.1749	0.1705	**0.1697**	0.2137	0.2060	0.1888	0.1932	**0.1838**
	50	0.1205	0.1200	0.1053	0.1056	**0.1043**	0.1296	0.1289	0.1138	0.1189	**0.1129**
	100	0.0631	0.0639	**0.0552**	0.0565	0.0556	0.0675	0.0683	**0.0595**	0.0627	0.0599

In the large sample sizes ($n = 50$ and 100), the difference between MTE values of the empirical distribution functions was not significant according to Table 6. In case of the shape parameter is set as $\alpha = 0.5$, Kaplan-Meir's empirical distribution function has lower MTE value than other empirical distribution functions for $\beta = 1$ and 10.

5. Conclusion

In this paper, we aimed at improving the effectiveness of the percentile method for two parameter Weibull distribution. Based on simulation study, the empirical distribution function that best fits the actual Weibull cumulative distribution function is the empirical distribution function of Hard Johnson according to MSE. In conclusion, the most suitable percentage points ranged from 0.10 to 0.14 when p_1 value was nearly set as 0.632 in the percentile method by approach 1. In general, (0.17, 0.97) and (0.24, 0.93) percentile pairs were the best successful percentile pairs for $\alpha \geq 1$. In case of the $\alpha < 1$, (0.25, 0.75) percentile pair was more successful than other percentile pairs. Also, median (symmetrical) empirical distribution function has been more successful in case of large sample size ($n = 100$) for percentile method by approach 2.

References

[1] Castillo, E., Hadi, A.S., *A method for estimating parameters and quantiles of distributions of continuous random variables,* Computational Statistics & Data Analysis, 20(4), 421-439, 1995.

[2] Erisoğlu, U., Erisoğlu, M., *Percentile estimators for two-component mixture distribution models*, Iranian Journal of Science and Technology, Transactions A: Science, 43(2), 601-619, 2019.

[3] Dubey, S.D., *Some percentile estimators for Weibull parameters*, Technometrics, 9(1), 119-129, 1967.

[4] Seki, T., Yokoyama, S., *Simple and robust estimation of the Weibull parameters*, Microelectronics Reliability, 33(1), 45-52, 1993.

[5] Wang, F.K., Keats, J.B., *Improved percentile estimation for the two-parameter Weibull distribution,* Microelectronics Reliability, 35(6), 883-892, 1995.

[6] Marks, N.B., *Estimation of Weibull parameters from common percentiles*, Journal of Applied Statistics, 32(1), 17-24, 2005.

[7] Teimouri, M., Hoseini, S.M., Nadarajah, S., *Comparison of estimation methods for the Weibull distribution*, Statistics, 47(1), 93-109, 2013.

[8] Seki, T., Yokoyama, S., *Robust parameter-estimation using the bootstrap method for the 2-parameter Weibull distribution*, IEEE Transactions on Reliability, 45(1), 34-41, 1996.

Adıyaman University Journal of Science
https://dergipark.org.tr/en/pub/adyujsci
DergiPark AKADEMİK
ISSN 2147-1630
e-ISSN 2146-586X

Conformally Flat Minimal C-totally Real Submanifolds of (κ,μ)-Nullity Space Forms

Ahmet YILDIZ[1,*]

[1]*İnönü University, Education Faculty, Department of Mathematics, Malatya, Turkey*
a.yildiz@inonu.edu.tr, ORCID: 0000-0002-9799-1781

Received: 28.05.2020 **Accepted:** 08.10.2020 **Published:** 30.12.2020

Abstract

In this paper we study conformally flat minimal C-totally real submanifolds of (κ,μ)-nullity space forms.

***Keywords*:** Contact metric manifold; (κ,μ)-space form; Conformally flat manifold; Second fundamental form; Totally geodesic.

(κ,μ)-Nullity Uzay Formlarının Konformal Flat Minimal C-total Reel Altmanifoldları

Özet

Bu çalışmada (κ,μ)-nullity uzay formlarının konformal flat minimal C-total reel altmanifoldlarını çalıştık.

Anahtar Kelimeler: Değme metrik manifold; (κ,μ)-uzay formu; Konformal flat manifold; İkinci temel form; Total jeodezik.

1. Introduction

Let M^m be a minimal C-totally real submanifold of dimension m, having constant $\breve{\varphi}$-sectional curvature c in a $(2m+1)$-dimensional Sasakian space form $\breve{M}$ of constant $\breve{\varphi}$-sectional

* Corresponding Author DOI: 10.37094/adyujsci.743557

curvature $\check{c}$. B.Y. Chen and K. Ogiue [1] studied totally real submanifolds and proved that if a such a submanifold is totally geodesic, then it is of constant curvature $c = \frac{1}{4}\check{c}$. Then D. Blair [2] showed that such a submanifold is totally geodesic if and only if it is of constant curvature $c = \frac{1}{4}(\check{c} + 3)$. Also S. Yamaguchi, M. Kon and T. Ikawa [3] stated that if such a submanifold is compact and has constant scalar curvature, then it is totally geodesic and has constant sectional curvature c satifying $c = \frac{1}{4}(\check{c} + 3)$ or $c \leq 0$. Later D. E. Blair and K. Ogiue [4] proved that if M is compact and $c > \frac{m-2}{4(2m-1)}(\check{c} + 3)$, then M is totally geodesic. Also P. Verheyen and L. Verstraelen [5] obtained that if M^m $(m \geq 4)$ is a compact conformally flat submanifold admitting constant scalar curvature $scal > \frac{(m-1)^3(m+2)}{4(m^2+m-4)}(\check{c} + 3)$ and $\breve{\varphi}$-sectional curvature c satisfying $c > \frac{(m-1)^2}{4m(m^2+m-4)}(\check{c} + 3)$, then it is totally geodesic.

In the present paper, we study the results indicated above for a conformally flat minimal C-totally real submanifold M in a (κ, μ)-nullity space form $\breve{M}^{2m+1}$ with constant $\breve{\varphi}$-sectional curvature $\check{c}$. We prove the followings:

Theorem 1. Let $\breve{M}^{2m+1}$ be a (κ, μ)-nullity space form of constant $\breve{\varphi}$-sectional curvature $\check{c}$ and M^m be an $m \geq 4$-dimensional compact conformally flat minimal C-totally real submanifold of a $\breve{M}^{2m+1}$. Then

$$scal > \frac{(m-1)^3(m+2)}{4(m^2+m-4)}(\check{c} + 3) + \frac{2(m-1)[m(m^2-2)\lambda(\lambda+2)+(m-2)\lambda]}{4(m^2+m-4)},$$

implies that M^m is totally geodesic, where $\lambda = \sqrt{1-\kappa}$.

Theorem 2. Let M^m be a minimal C-totally real submanifold of a (κ, μ)-nullity space form $\breve{M}^{2m+1}$. If M^m has constant curvature c, then either

$$c = \frac{1}{4}[(\check{c} + 3) + 2\lambda^2 + 8\lambda],$$

in which case M^m is totally geodesic, or $c \leq 0$.

2. Preliminiaries

Let $\breve{M}^{2m+1}$ be a contact metric manifold with the $(\breve{\varphi}, \xi, \breve{\eta}, \breve{g})$ satisfying

$$\breve{\varphi}^2 = -I + \breve{\eta} \otimes \xi,$$

$$\breve{\eta}(\xi) = 1, \breve{\varphi}\xi = 0, \breve{\eta}(U) = \breve{g}(U, \xi), \tag{1}$$

$$\breve{g}(\breve{\varphi}U,\breve{\varphi}V) = \breve{g}(U,V) - \breve{\eta}(U)\breve{\eta}(V), \quad \breve{g}(\breve{\varphi}U,V) = d\breve{\eta}(U,V),$$

for vector fields U and V on $\breve{M}$. The operator h defined by $h = -\frac{1}{2}L_{\xi}\breve{\varphi}$, vanishes iff ξ is Killing. Also we have

$$\breve{\varphi}h + h\breve{\varphi} = 0,\ h\xi = 0,\ \breve{\eta}oh = 0,\ tr\ h = tr\ \breve{\varphi}h = 0. \tag{2}$$

Due to anti-commuting h with $\breve{\varphi}$, if U is an eigenvector of h with the eigenvalue λ then $\breve{\varphi}U$ is also an eigenvector of h with the eigenvalue $-\lambda$ [6]. Moreover, for the Riemannian connection $\breve{\nabla}$ of $\breve{g}$, we have

$$\breve{\nabla}_U\xi = -\breve{\varphi}U - \breve{\varphi}hU. \tag{3}$$

If ξ is Killing then contact metric manifold $\breve{M}$ is said to be a *K-contact Riemannian manifold*. On a K-contact Riemannian manifold, we have

$$\breve{R}(U,\xi)\xi = U - \breve{\eta}(U)\xi.$$

A Sasakian manifold is known as a normal contact metric manifold. A contact metric manifold to be Sasakian if and only if $\breve{R}(U,V)\xi = \breve{\eta}(V)U - \breve{\eta}(U)V$, where $\breve{R}$ is the curvature tensor on $\breve{M}$. Moreover, *every Sasakian manifold is a K-contact manifold* [2].

The (κ,μ)-*nullity distribution* for a contact metric manifold $\breve{M}$ is a distribution

$$Null(\kappa,\mu): p \longrightarrow Null_p(\kappa,\mu) = \begin{Bmatrix} W \in T_pM | \breve{R}(U,V)W = \kappa[\breve{g}(V,W)U - \breve{g}(U,W)V] \\ +\mu[\breve{g}(V,W)hU - \breve{g}(U,W)hV] \end{Bmatrix},$$

for any $U, V \in T_p(\breve{M})$, where $\kappa, \mu \in \mathbb{R}$ and $\kappa \leq 1$. We consider that $\breve{M}$ is a contact metric manifold with ξ concerning to the (κ,μ)-nullity distribution, i.e.,

$$R(U,V)\xi = \kappa[\breve{\eta}(V)U - \breve{\eta}(U)V] + \mu[\breve{\eta}(V)hU - \breve{\eta}(U)hV]. \tag{4}$$

The necessary and sufficient condition for the manifold $\breve{M}$ to be a Sasakian manifold is that $\kappa = 1$ and $\mu = 0$ [7]. Also, for more details, one can see [8] and [9]. For $\kappa < 1$, (κ,μ)-contact metric manifolds have constant scalar curvature. Also, the sectional curvature $\breve{K}(U,\breve{\varphi}U)$ according to a $\breve{\varphi}$-section determined by a vector U is called a $\breve{\varphi}$-*sectional curvature*. A (κ,μ)-contact metric manifold with constant $\breve{\varphi}$-sectional curvature $\breve{c}$ is a (κ,μ)-*nullity space form*. The *curvature tensor* of a (κ,μ)-nullity space form $\breve{M}$ is given by [10]

$$\breve{R}(U,V)W = \frac{1}{4}(\breve{c}+3)\{g(V,W)U - g(U,W)V\}$$

$$
\begin{aligned}
&+\frac{\breve{c}+3-4\kappa}{4}\begin{Bmatrix}\breve{\eta}(U)\breve{\eta}(W)V-\breve{\eta}(V)\breve{\eta}(W)U\\+g(U,W)\breve{\eta}(V)\xi-g(V,W)\breve{\eta}(U)\xi\end{Bmatrix}\\
&+\frac{\breve{c}-1}{4}\begin{Bmatrix}2g(U,\breve{\varphi}V)\breve{\varphi}W+g(U,\breve{\varphi}W)\breve{\varphi}V\\-g(V,\breve{\varphi}W)\breve{\varphi}U\end{Bmatrix}\\
&+\frac{1}{2}\begin{Bmatrix}g(hV,W)hU-g(hU,W)hV\\+g(\breve{\varphi}hU,W)\breve{\varphi}hV-g(\breve{\varphi}hV,W)\breve{\varphi}hU\\+g(\breve{\varphi}V,\breve{\varphi}W)hU-g(\breve{\varphi}U,\breve{\varphi}W)hV\\+g(hU,W)\breve{\varphi}^2V-g(hV,W)\breve{\varphi}^2U\end{Bmatrix}\\
&+\frac{1}{2}\begin{Bmatrix}g(hV,W)hU-g(hU,W)hV\\+g(\breve{\varphi}hU,W)\breve{\varphi}hV-g(\breve{\varphi}hV,W)\breve{\varphi}hU\\+g(\breve{\varphi}V,\breve{\varphi}W)hU-g(\breve{\varphi}U,\breve{\varphi}W)hV\\+g(hU,W)\breve{\varphi}^2V-g(hV,W)\breve{\varphi}^2U\end{Bmatrix}\\
&+\mu\begin{Bmatrix}\breve{\eta}(V)\breve{\eta}(W)hU-\breve{\eta}(U)\breve{\eta}(W)hV\\+g(hV,W)\breve{\eta}(U)\xi-g(hU,W)\breve{\eta}(V)\xi\end{Bmatrix},
\end{aligned}
\tag{5}
$$

where $\breve{c}$ is constant $\breve{\varphi}$-sectional curvature.

3. *C*-totally Real Submanifolds

Let M be an m-dimensional submanifold in a $(2m+1)$-dimensional manifold $\breve{M}$ equipped with a Riemannian metric g. We denote by ∇ (resp. $\breve{\nabla}$) the covariant derivation with respect to g (resp.$\breve{g}$). Then the *second fundamental form* B is given by

$$B(U,V)=\breve{\nabla}_UV-\nabla_UV. \tag{6}$$

For a normal vector field ξ on M, we write $\breve{\nabla}_U\xi=-A_\xi U+D_U\xi$, where $-A_\xi U$ (resp. $D_U\xi$) denotes the tangential (resp. normal) component of $\breve{\nabla}_U\xi$. Then, we have

$$\breve{g}(B(U,V),\xi)=g(A_\xi U,V). \tag{7}$$

A normal vector field ξ on M is said to be *parallel* if $D_U\xi=0$ for any tangent vector U. For any orthonormal basis $\{w_1,\dots,w_m\}$ of the tangent space T_pM, the *mean curvature vector* $H(p)$ is given by

$$H(p)=\frac{1}{m}\sum_{i=1}^{m}B(w_i,w_i). \tag{8}$$

The submanifold M is *totally geodesic* in $\breve{M}$ if $B = 0$, and *minimal* if $H = 0$. If $B(U,V) = g(U,V)H$ for all $U,V \in TM$, then M is *totally umbilical*. For the second fundamental form B, with respect to the covariant derivation $\overline{\nabla}$ is defined by

$$(\overline{\nabla}_U B)(V,W) = D_U(B(V,W)) - B(\nabla_U V, W) - B(V, \nabla_U W), \tag{9}$$

for all U,V and W on M [11], where $\overline{\nabla}$ is the covariant differentiation operator of *van der Waerden-Bortolotti*.

Also the equations of *Gauss, Codazzi* and *Ricci* are given by

$$g(R(U,V)W,T) = g(\breve{R}(U,V)W,T) \tag{10}$$

$$+g(B(U,W),B(V,T)) - g(B(V,W),B(U,T)),$$

$$(\breve{R}(U,V)W)^{\perp} = (\overline{\nabla}_U B)(V,W) - (\overline{\nabla}_V B)(U,W), \tag{11}$$

$$g(\breve{R}(U,V)W,N) = g(R^{\perp}(U,V)W,N) + g([A_N, A_W]U,V), \tag{12}$$

where R and $\breve{R}$ are the Riemannian curvature tensor of M and $\breve{M}$ and $(\breve{R}(U,V)W)^{\perp}$ denotes the normal component of $\breve{R}(U,V)W$ [11]. The second covariant derivative $\overline{\nabla}^2 B$ of B is defined by

$$(\overline{\nabla}^2 B)(W,T,U,V) = (\overline{\nabla}_U \overline{\nabla}_V B)(W,T)$$

$$= \nabla^{\perp}_U((\overline{\nabla}_V B)(W,T)) - (\overline{\nabla}_V B)(\nabla_U W, T) \tag{13}$$

$$-(\overline{\nabla}_U B)(W, \nabla_V T) - (\overline{\nabla}_{\nabla_U V} B)(W,T).$$

Then, we have

$$(\overline{\nabla}_U \overline{\nabla}_V B)(W,T) - (\overline{\nabla}_V \overline{\nabla}_U B)(W,T) = (\bar{R}(U,V)B)(W,T)$$

$$= R^{\perp}(U,V)B(W,T) - B(R(U,V)W,T) - B(W, R(U,V)T), \tag{14}$$

where $\bar{R}$ is the curvature tensor belonging to the connection $\overline{\nabla}$. The *Laplacian of the square of the lenght of the second fundamental form* is defined

$$\frac{1}{2}\Delta\|B\|^2 = g(\overline{\nabla}^2 B, B) + \left\|\overline{\nabla}B\right\|^2, \tag{15}$$

where $\|B\|$ is the length of the second fundemental form B, so that

$$\|B\|^2 = \sum_{i,j} g(B(w_i, w_j), B(w_i, w_j)), \tag{16}$$

and using (3.8), we can write

$$\left\|\overline{\nabla}B\right\|^2 = \sum_{i,j,k} g((\overline{\nabla}_{w_i}\overline{\nabla}_{w_i}B)(w_j, w_k), (\overline{\nabla}_{w_i}\overline{\nabla}_{w_i}B)(w_j, w_k)), \tag{17}$$

and

$$g(\overline{\nabla}^2 B, B) = \sum_{i,j,k} g((\overline{\nabla}_{w_i}\overline{\nabla}_{w_i}B)(w_j, w_k), B(w_j, w_k)). \tag{18}$$

A submanifold M in a contact metric manifold is called a C-*totally real submanifold* [12] if every tangent vector of M belongs to the contact distribution. Hence, a submanifold M in a contact metric manifold is a C-*totally real submanifold* if ξ is normal to M. A submanifold M in an almost contact metric manifold is called a C-*totally real submanifold* if $\breve{\varphi}(TM) \subset T^{\perp}(M)$ [13].

4. Conformally Flat Minimal C-totally Real Submanifolds of (κ, μ)-Nullity Space Forms

Let M^m be a C-totally real submanifold of a (κ, μ)-nullity space form $\breve{M}^{2m+1}$ with $\breve{\varphi}$-sectional curvature $\breve{c}$ and structure tensors $(\breve{\varphi}, \xi, \breve{\eta}, \breve{g})$, with ξ normal to M. The *conformal curvature tensor field* of M^m is defined by

$$C(U,V)W = R(U,V)W + \frac{1}{m-2}\begin{bmatrix} Ric(U,W)V - Ric(V,W)U \\ +g(U,W)QV - g(V,W)QU \end{bmatrix}$$

$$-\frac{scal}{(m-1)(m-2)}[g(U,W)V - g(V,W)U], \tag{19}$$

for all vector fields U, V, and W, where Q denotes the *Ricci operator* defined by $g(QU,V) = Ric(U,V)$. For $m \geq 4$, the manifold M is *conformally flat manifold* if and only if $C = 0$ [11].

Lemma 3. Let M be an m-dimensional C-totally real submanifold on (κ, μ)-contact metric manifold $\breve{M}^{2m+1}$. Then, we have

$i)\ A_{\breve{\varphi}w_i}w_j = A_{\breve{\varphi}w_j}w_i,$

$ii)\ tr(\sum_i A_i^2)^2 = \sum_{i,j} (trA_iA_j)^2.$

Lemma 4. A C-totally real submanifold M of dimension $m \geq 4$ *in a* (κ, μ)-nullity space form $\breve{M}^{2m+1}$ conformally flat if and only if

$$(m-1)(m-2)\begin{Bmatrix}\sum\limits_{\alpha}\{g(A_\alpha w_j,w_k)g(A_\alpha w_i,w_l)\\ -g(A_\alpha w_i,w_k)g(A_\alpha w_j,w_l)\}\end{Bmatrix}$$

$$+\left\{\sum_{\alpha}(tr(A_\alpha)^2-\|B\|^2\right\}\{g(w_j,w_k)g(w_i,w_l)-g(w_i,w_k)g(w_j,w_l)\} \tag{20}$$

$$+(m-1)\begin{Bmatrix}\sum\limits_{\alpha} tr(A_\alpha)\{g(A_\alpha w_i,w_k)g(w_j,w_l)-g(A_\alpha w_j,w_k)g(w_i,w_l)\\ +g(A_\alpha w_j,w_l)g(w_i,w_k)-g(A_\alpha w_i,w_l)g(w_j,w_k)\}\end{Bmatrix}$$

$$-(m-1)\begin{Bmatrix}\sum\limits_{\alpha,t}\{g(A_\alpha w_i,w_t)g(A_\alpha w_k,w_t)g(w_j,w_l)\\ -g(A_\alpha w_j,w_t)g(A_\alpha w_k,w_t)g(w_i,w_l)\\ +g(A_\alpha w_j,w_t)g(A_\alpha w_l,w_t)g(w_i,w_k)\\ -g(A_\alpha w_i,w_t)g(A_\alpha w_l,w_t)g(w_j,w_k)\}\end{Bmatrix}=0,$$

where

$$\|B\|^2=\sum_{\alpha,i,j}g(A_\alpha w_i,w_j)^2=trA^*, \tag{21}$$

and

$$A^*=\sum_{\alpha}(A_\alpha)^2. \tag{22}$$

Proof. Let M be a conformally flat manifold. Then, from Eqn. (5) and Eqn. (19), we have

$$(m-1)(m-2)g(R(w_i,w_j)w_k,w_l)$$

$$+(m-1)\begin{Bmatrix}Ric(w_i,w_k)g(w_j,w_l)-Ric(w_j,w_k)g(w_i,w_l)\\ +Ric(w_j,w_l)g(w_i,w_k)-Ric(w_i,w_l)g(w_j,w_k)\end{Bmatrix} \tag{23}$$

$$-scal\{g(w_i,w_k)g(w_j,w_l)-g(w_j,w_k)g(w_i,w_l)\}=0.$$

Using Eqn. (10) in Eqn. (23), we get

$$(m-1)(m-2)\sum_{\alpha}\{g(A_\alpha w_j,w_k)g(A_\alpha w_i,w_l)-g(A_\alpha w_i,w_k)g(A_\alpha w_j,w_l)\}$$

$$+\tfrac{(m-1)(m-2)}{4}\{(c+3)+2\lambda^2+8\lambda\}+scal\}\begin{Bmatrix}g(w_j,w_k)g(w_i,w_l)\\ -g(w_i,w_k)g(w_j,w_l)\end{Bmatrix} \tag{24}$$

$$+(m-1)\begin{Bmatrix}Ric(w_i,w_k)g(w_j,w_l)-Ric(w_j,w_k)g(w_i,w_l)\\ +Ric(w_j,w_l)g(w_i,w_k)-Ric(w_i,w_l)g(w_j,w_k)\end{Bmatrix}=0,$$

where Ric and $scal$, respectively, the Ricci tensor and scalar curvature of M, defined by

$$Ric(w_j, w_k) = \frac{(m-1)}{4}\{(c+3) + 2\lambda^2 + 8\lambda\}g(w_j, w_k) \tag{25}$$

$$+\sum_{\alpha} tr(A_\alpha)g(A_\alpha w_j, w_k) - g(A_\alpha w_j, A_\alpha w_k),$$

and

$$scal = \frac{m(m-1)}{4}\{(c+3) + 2\lambda^2 + 8\lambda\} + \sum_{\alpha} (tr(A_\alpha))^2 - \|B\|^2. \tag{26}$$

From Eqn. (24)-Eqn. (26), we have Eqn. (20).

Lemma 5. Let M be an m-dimensional C-totally real submanifold on (κ, μ)-contact metric manifold $\breve{M}^{2m+1}$. If M is minimal, then Eqn. (20) becomes

$$\begin{aligned}&(m-1)(m-2)g([A_i, A_j]w_k, w_l)\\ &-\|B\|^2\{g(w_j, w_k)g(w_i, w_l) - g(w_i, w_k)g(w_j, w_l)\}\\ &-(m-1)\{g(w_j, w_l)tr(A_iA_k) - g(w_i, w_l)tr(A_jA_k)\\ &+g(w_i, w_k)tr(A_jA_l) - g(w_j, w_k)tr(A_iA_l)\} = 0.\end{aligned} \tag{27}$$

Lemma 6. Let M be a conformally flat minimal C-totally real submanifold of dimension $m \geq 4$ in a (κ, μ)-nullity space form $\breve{M}^{2m+1}$, then

$$(m-1)(m-2)\sum_{i,j} tr(A_iA_j)^2 = \|B\|^4 + (m-1)(m-4)tr(A^*)^2. \tag{28}$$

Also we have the following:

Lemma 7. In any (κ, μ)-contact metric manifold, we have

$$i)\left\|\overline{\nabla}B\right\|^2 \geq \|B\|^2, \tag{29}$$

$$ii)\ tr(A^*)^2 \leq \|B\|^4. \tag{30}$$

Now using Lemma 7, we get the following:

Lemma 8. Let $\breve{M}^{2m+1}$ be a (κ, μ)-nullity space form of constant $\breve{\varphi}$-sectional curvature $\breve{c}$ and M be an $m \geq 4$-dimensional minimal C-totally real submanifold of $\breve{M}$. The Laplacian of the square of the length of the second fundamental form B of M

$$\frac{1}{2}\Delta\|B\|^2 = \left\|\overline{\nabla}B\right\|^2 + \left(\frac{(\check{c}-1)+m(\check{c}+3)}{4} + \frac{\lambda}{2}(m(\lambda+4)-\lambda)\right)\|B\|^2$$

$$+2\sum_{\alpha,\beta} tr(A_\alpha A_\beta)^2 - 3tr(A^*)^2, \tag{31}$$

where $\lambda = \sqrt{1-\kappa}$.

Proof. If M is minimal then, from [11], we have

$$(\overline{\nabla}^2 B)(U,V) = \sum_i (R(w_i,U)B)(w_i,V). \tag{32}$$

For an orthonormal base w_i, from Eqn. (12), we have

$$(R(w_k,w_i)B)(w_k,w_j) = R^\perp(w_k,w_i)B(w_k,w_j) - B(R(w_k,w_i)w_k,w_j) \tag{33}$$

$$-B(w_k,R(w_k,w_i)w_j).$$

Using Eqn. (10) in Eqn. (33), we get

$$g((R(w_k,w_i)B)(w_k,w_j),B(w_i,w_j)) = g(R^\perp(w_k,w_i)B(w_k,w_j),B(w_i,w_j))$$

$$-g(B(\bar{R}(w_k,w_i)w_k,w_j),B(w_i,w_j)) - \sum_{\alpha,\beta} g(A_\beta A_\alpha w_k, A_\beta A_\alpha w_k) \tag{34}$$

$$+\sum_{\alpha,\beta} tr(A_\alpha)tr(A_\beta^2 A_\alpha) - g(B(w_k,\bar{R}(w_k,w_i)w_j),B(w_i,w_j))$$

$$-\sum_{\alpha,\beta}(tr(A_\alpha A_\beta))^2 + \sum_{\alpha,\beta} tr(A_\beta A_\alpha)^2.$$

Again using Eqn. (11) in Eqn. (34), we have

$$g((R(w_k,w_i)B)(w_k,w_j),B(w_i,w_j)) = g(\bar{R}(w_k,w_i)B(w_k,w_j),B(w_i,w_j))$$

$$-g(B(\bar{R}(w_k,w_i)w_k,w_j),B(w_i,w_j)) - g(B(w_k,\bar{R}(w_k,w_i)w_j),B(w_i,w_j))$$

$$+\sum_{\alpha,\beta}\begin{bmatrix} tr(A_\alpha A_\beta - A_\beta A_\alpha)^2 - (tr(A_\beta A_\alpha))^2 \\ tr(A_\alpha)trA_\beta^2 A_\alpha) \end{bmatrix}. \tag{35}$$

After some calculations, we have

$$g(\bar{R}(w_k,w_i)B(w_k,w_j),B(w_i,w_j)) = \left(\frac{\check{c}-1}{4} - \frac{\lambda^2}{2}\right)\|B\|^2, \tag{36}$$

$$g(B(\bar{R}(w_k,w_i)w_k,w_j),B(w_i,w_j)) = \frac{(1-m)((\check{c}+3)+2\lambda(\lambda+4))}{4}\|B\|^2, \tag{37}$$

$$g(B(w_k,\bar{R}(w_k,w_i)w_j),B(w_i,w_j)) = \left(\frac{-(\check{c}+3)-2\lambda(\lambda+4))}{4}\right)\|B\|^2, \tag{38}$$

$$\sum_{\alpha,\beta}\left[tr(A_\alpha A_\beta - A_\beta A_\alpha)^2 - (tr(A_\beta A_\alpha))^2\right] = \sum_{\alpha,\beta} 2tr(A_\beta A_\alpha) - 3tr(A^*)^2. \tag{39}$$

Thus, using Eqn. (36)-(39) in Eqn. (35), we get Eqn. (31).

5. Proofs of the Main Results

For a conformally flat submanifold M of dimension $m \geq 4$ we use equation Eqn. (28) to replace $\sum_{\alpha,\beta} tr(A_\alpha A_\beta)^2$ in Eqn. (31), we have

$$\begin{aligned}\frac{1}{2}(m-1)(m-2)\Delta\|B\|^2 &= (m-1)(m-2)\left\|\overline{\nabla}B\right\|^2 \\ &+(m-1)(m-2)\left(\frac{(\check{c}-1)+m(\check{c}+3)}{4}+\frac{\lambda}{2}(m(\lambda+4)-\lambda)\right)\|B\|^2 \\ &-(m-1)(m+2)tr(A^*)^2+2\|B\|^4.\end{aligned} \tag{40}$$

So from Lemma 7, we get

$$\begin{aligned}&\frac{1}{2}(m-1)(m-2)\Delta\|B\|^2 \\ &\geq (m-1)(m-2)\|B\|^2+2\|B\|^4-(m-1)(m+2)\|B\|^4 \\ &+\frac{1}{4}(m-1)(m-2)[(\check{c}-1)+m(\check{c}+3)+2\lambda(m(\lambda+4)-\lambda)]\|B\|^2 \\ &=\|B\|^2\begin{bmatrix}\frac{(m-1)(m-2)(m+1)(\check{c}+3)}{4}+(m-1)(m-2)\frac{\lambda(m(\lambda+4)-\lambda)}{2}\\ -(m^2+m-4)\|B\|^2\end{bmatrix},\end{aligned} \tag{41}$$

If $\check{c} > -3$, then

$$\|B\|^2 \leq \frac{(m^2-1)(m-2)(\check{c}+3)}{4(m^2+m-4)}+(m-1)(m-2)\frac{\lambda(m(\lambda+4)-\lambda)}{2(m^2+m-4)}, \tag{42}$$

which implies that $\Delta\|B\|^2 \geq 0$. For a compact submanifold M, Hopf's lemma states that $\Delta\|B\|^2 = 0$ and from Eqn. (41) and Eqn. (42), we conclude that $\|B\|^2 = 0$. Hence, we have

$$scal = \frac{m(m-1)}{4}\{(\check{c}+3)+2\lambda^2+8\lambda\}-\|B\|^2, \tag{43}$$

for every compact minimal C-totally real submanifold in a (κ,μ)-nullity space form $\breve{M}$. Thus, the proof of Theorem 1 is completed.

On the other hand, since M^m has constant curvature c and $scal = m(m-1)\tilde{c}$, from Eqn. (26), we have

$$\|B\|^2 = m(m-1)\left(\frac{(\check{c}+3)+2\lambda^2+8\lambda}{4} - c\right),$$

and

$$c \leq \frac{(\check{c}+3)+2\lambda^2+8\lambda}{4}.$$

Also, Eqn. (10) becomes

$$\left(c - \frac{1}{4}\{(\check{c}+3)+2\lambda^2+8\lambda\}\right)\{g(w_j,w_k)g(w_i,w_l) - g(w_i,w_k)g(w_j,w_l)\}$$
$$= g([A_i,A_j]w_k,w_l). \tag{44}$$

Multiplying this equation by $\sum_N g(A_N w_l, w_i)g(A_N w_j, w_k)$, we obtain

$$\left(c - \frac{1}{4}\{(\check{c}+3)+2\lambda^2+8\lambda\}\right)\|B\|^2 = \sum_{i,j} tr(A_iA_j)^2 - \sum_{i,j}(tr(A_iA_j))^2. \tag{45}$$

Since $Ric = \frac{scal}{m}g$, from Eqn. (25) and Lemma 3, we have

$$tr(A_jA_l) = g(A_\alpha w_j, A_\alpha w_l) = \frac{scal}{m}g(w_j,w_l) = \frac{\|B\|^2}{m}g(w_j,w_l),$$

and

$$tr(A_iA_j)^2 = \left(c - \frac{1}{4}\{(\check{c}+3)+2\lambda^2+8\lambda\}\right)\|B\|^2 + \frac{\|B\|^4}{m}.$$

Substituting the last equation into Eqn. (31), we obtain

$$\left\|\overline{\nabla}B\right\|^2 = \left[\frac{(m+1)}{m(m-1)}\|B\|^2 - \frac{m(\check{c}+3)+(\check{c}-1)}{4} + \frac{\lambda(m(\lambda+4)-\lambda}{2}\right]\|B\|^2.$$

Now using

$$\|B\|^2 = m(m-1)\{\frac{1}{4}\{(\check{c}+3)+2\lambda^2+8\lambda\}\},$$

and Lemma 7, we get

$$\left\|\overline{\nabla}B\right\|^2 = m(m^2-1)\left(c - \left\{\frac{(\check{c}+3)+2\lambda^2+8\lambda}{4}\right\}\right)\left(c - \frac{1}{m+1}\right)$$

$$\geq m(m-1)\left\{\frac{(\check{c}+3)+2\lambda^2+8\lambda}{4}-c\right\}.$$

Thus, the proof of Theorem 2 is completed.

Acknowledgement

The authors are thankful to the referees for their valuable comments and suggestions towards the improvement of the paper.

References

[1] Chen B.Y., Ogiue K., *On totally real submanifolds*, Transactions of the American Mathematical Society, 193, 257-266, 1974.

[2] Blair D.E., *Contact manifolds in Riemannian geometry*, Lectures Notes in Mathematics 509, Springer-Verlag, Berlin, 146p, 1976.

[3] Yamaguchi S., Kon M., Ikawa T., *C-totally real submanifolds*, Journal of Differential Geometry, 11, 59-64, 1976.

[4] Blair D.E., Ogiue K., *Geometry of ıntegral submanifolds of a contact distribution*, Illinois Journal of Mathematics, 19, 269-275, 1975.

[5] Verheyen P., Verstraelen L., *Conformally flat C-totally real submanifolds of Sasakian space forms*, Geometriae Dedicata, 12, 163-169, 1982.

[6] Tanno S., *Ricci Curvatures of Contact Riemannian manifolds*, Tôhoku Mathematical Journal, 40, 441-448, 1988.

[7] Blair D.E., Ogiue K., *Positively curved ıntegral submanifolds of a contact distribution*, Illinois Journal of Mathematics, 19, 628-631, 1975.

[8] Blair D.E., Koufogiorgos T., Papantoniou, B.J., *Contact metric manifolds satisfying a nullity condition*, Israel Journal of Mathematics, 91,189-214, 1995.

[9] Verstraelen L., Vrancken L., *Pinching Theorems for C-Totally Real Submanifolds of Sasakian Space Forms*, Journal of Geometry, 33, 172-184, 1988.

[10] Koufogiorgos T., *Contact Riemannian manifolds with constant φ -sectional curvature*, Geometry and Topology of Submanifolds VIII, World Scientific, 1996, ISBN 981-02-2776-0.

[11] Yano K., Kon M., *Structures on manifolds*, World Scientific, 508p, 1984.

[12] Yano K., Kon M., *Anti-invariant submanifolds of a Sasakian Space Forms*, Tôhoku Mathematical Journal, 29, 9-23, 1976.

[13] Yano K., Kon M., *Anti-Invariant submanifolds*, Marcel Dekker, New York. 185p, 1978.

Adıyaman University Journal of Science
https://dergipark.org.tr/en/pub/adyujsci
DergiPark AKADEMİK
ISSN 2147-1630
e-ISSN 2146-586X

Soft Quasilinear Spaces and Soft Normed Quasilinear Spaces

Hacer BOZKURT[1,*]

[1]*Batman University, Faculty of Science and Letters, Department of Mathematics, Batman, Turkey*
hacer.bozkurt@batman.edu.tr ORCID: 0000-0002-2216-2516

Received: 29.04.2020 **Accepted:** 09.11.2020 **Published:** 30.12.2020

Abstract

In this study, a recent concepts of soft quasilinear spaces and soft proper quasilinear spaces are presented. Further, soft quasi vectors in soft quasilinear spaces are investigated, and several related properties are examined such as quasilinear dependent and quasilinear independent. Also, the concept of soft quasi norm of soft quasilinear spaces is given. Lastly, soft quasilinear operators on soft normed quasilinear spaces are defined, and some results about the bounded soft quasilinear operators and continuous soft quasilinear operators are obtained.

***Keywords*:** Soft quasilinear space; Soft quasi vector; Soft normed quasilinear space; Soft quasilinear operator.

Esnek Quasilineer Uzaylar ve Esnek Normlu Quasilineer Uzaylar

Öz

Bu çalışmada, yeni bir kavram olan esnek quasilineer uzay ve esnek proper quasilineer uzay kavramları sunulmuştur. Ayrıca esnek quasilineer uzayda bir esnek quasi vektör tanımı verilmiş ve bu yeni kavram ile ilgili quasilineer bağımlılık-bağımsızlık özellikleri ele alınmıştır. Esnek quasilineer uzaylarda esnek quasi norm kavramı tanıtılmıştır. Son olarak bir esnek normlu quasilineer uzayda esnek quasilineer operatör tanımı verilmiş ve sınırlı esnek quasilineer operatör ile sürekli esnek quasilineer operatörlerle ilgili bazı sonuçlar elde edilmiştir.

* Corresponding Author DOI: 10.37094/adyujsci.728934

***Anahtar Kelimeler*:** Esnek quasilineer uzay; Esnek quasi vektör; Esnek normlu quasilineer uzay; Esnek quasilineer operatör.

1. Introduction

In [1], Molodtsov introduced the notion of soft sets which is an unexplored mathematical tool for dealing with ambiguities. After, many papers regarding soft sets were published. In the paper [2] and [3], the authors preferred the notion of soft element by handling a function and they investigated soft real number by using soft element, respectively. After then, in [2], soft vector space was presented by handling the notion of soft element and in [4, 5] they worked on soft normed spaces and soft linear operators and their fundamental properties.

On the other hand, in the paper [6], Aseev offered the notions of quasilinear spaces and normed quasilinear spaces. Owing to these new definitions, he obtained some results consistent with linear spaces. In [7], they presented the idea of topological quasilinear spaces. In [8], they worked on proper quasilinear spaces and explored quasilinear dependence-independence. In [9], they worked on inner product quasilinear spaces. After, in [10, 11], the authors studied on some properties of quasilinear spaces.

Actually, in the existing paper, we define the concepts of soft quasilinear spaces, soft normed quasilinear spaces and soft quasilinear operators. In section two, we give some preliminaries about the soft sets and quasilinear spaces. In section three, we give the soft quasilinear spaces as a new concept and search some of its properties with examples. Further, we study soft proper quasilinear spaces. In section four, we define the soft norm in soft quasilinear spaces and present soft quasilnear operators and its various properties.

2. Preliminaries

Firstly, we remember some notions in soft set theory and some basic concepts such as quasilinear spaces and normed quasilinear spaces.

Let V be an universe and F be a set of all probable parameters. Let $P(V)$ indicate the power set of V and B be a non-empty subset of F.

Definition 1. [1] A pair (G, B) is called a soft set over V, where G is a mapping defined by $G: B \to P(V)$.

Definition 2. [12] A soft set (G, B) over V is said to be a null soft set represented by Φ, if for every $b \in B$, $G(b) = \emptyset$.

Definition 3. [13] For a soft set (G,B) over V, the set $Supp(G,B) = \{b \in B: G(b) \neq \emptyset\}$ is called support of the soft set (G,B). The null soft set is a soft set with an empty support. A soft set (G,B) is non-null if $Supp(G,B) \neq \emptyset$.

Definition 4. [12] A soft set (G,B) over V is said to be an absolute soft set represented by $\tilde{V}$, if for every $b \in B$, $G(b) = V$.

Definition 5. [3] Let $V \neq \emptyset$ and B be a nonempty parameter set. Then a function $\varepsilon: B \to V$ is said to be soft element of V.

Definition 6. [14, 15] A soft set (G,B) over V is said to be a soft point if there is certainly a $b \in B$, such that $G(b) = \{v\}$ for some $v \in V$ and $G(b') = \emptyset$, for every $b' \in V/\{b\}$. It will be indicated by $\tilde{v}_b$.

Definition 7. [6] A quasilinear space over a field $\mathbb{R}$ is a set Q with a partial order relation $\preccurlyeq$, with the operations of addition $Q \times Q \to Q$ and scalar multiplication $\mathbb{R} \times Q \to Q$ satisfying the following conditions:

$(Q1)$ $q \preccurlyeq q$,

$(Q2)$ $q \preccurlyeq z$, if $q \preccurlyeq w$ and $w \preccurlyeq z$,

$(Q3)$ $q = w$, if $q \preccurlyeq w$ and $w \preccurlyeq q$,

$(Q4)$ $q + w = w + q$,

$(Q5)$ $q + (w + z) = (q + w) + z$,

$(Q6)$ there exists an element $\theta \in Q$ such that $q + \theta = q$,

$(Q7)$ $\alpha \cdot (\beta \cdot q) = (\alpha \cdot \beta) \cdot q$,

$(Q8)$ $\alpha \cdot (q + w) = \alpha \cdot q + \alpha \cdot w$,

$(Q9)$ $1 \cdot q = q$,

$(Q10)$ $0 \cdot q = \theta$,

$(Q11)$ $(\alpha + \beta) \cdot q \preccurlyeq \alpha \cdot q + \beta \cdot q$,

$(Q12)$ $q + z \preccurlyeq w + v$, if $q \preccurlyeq w$ and $z \preccurlyeq v$,

$(Q13)$ $\alpha \cdot q \preccurlyeq \alpha \cdot w$, if $q \preccurlyeq w$,

for every $q, w, z, v \in Q$ and every $\alpha, \beta \in \mathbb{R}$.

If an element q has an inverse, then it is called *regular*. If an element q has no inverse, then it is called *singular*. Also, Q_r express for the set of all regular elements in Q and Q_s imply the sets of all singular elements in Q. Besides, Q_r, Q_d and $Q_s \cup \{0\}$ are subspaces of Q, where Q_r regular subspace of Q, Q_d symmetric subspace of Q and $Q_s \cup \{0\}$ singular subspace of Q. Further, let Q be a quasilinear space, $W \subseteq Q$ and $q \in W$. The set

$$F_q^W = \{m \in W_r : m \preccurlyeq q\},$$

is called *floor in W of q*. In the case of $W = Q$ it is called only *floor of q* and written briefly F_q instead of F_q^Q [8].

Definition 8. [8] Let Q be a quasilinear space, $W \subseteq Q$ and $q, w \in W$. W is called proper set if the following cases hold:

$(PQ1)$ $F_q^W \neq \emptyset$ for every $q \in W$,

$(PQ2)$ $F_q^W \neq F_w^W$ for all pair of points q, w such that $q \neq w$.

Definition 9. [6] Let Q be a quasilinear space. A function $\|.\|_Q : Q \to \mathbb{R}$ is named a norm if the following circumstances hold:

$(NQ1)$ $\|q\|_Q > 0$ if $q \neq 0$,

$(NQ2)$ $\|q + w\|_Q \leq \|q\|_Q + \|w\|_Q$,

$(NQ3)$ $\|\alpha \cdot q\|_Q = |\alpha| \cdot \|q\|_Q$,

$(NQ4)$ if $q \preccurlyeq w$, then $\|q\|_Q \leq \|w\|_Q$,

$(NQ5)$ if for any $\varepsilon > 0$ there exists an element $q_\varepsilon \in Q$ such that, $q \preccurlyeq w + q_\varepsilon$ and $\|q_\varepsilon\|_Q \leq \varepsilon$ then $q \preccurlyeq w$ for any elements $q, w \in Q$ and any real number $\alpha \in \mathbb{R}$.

A quasilinear space Q is called normed quasilinear space with a norm defined on it. Let Q be a normed quasilinear space. Then, Hausdorff or norm metric on Q is defined by

$$h_Q(q, w) = \inf\{r \geq 0 : q \preccurlyeq w + a_1^r, w \preccurlyeq q + a_2^r, \|a_i^r\| \leq r\}.$$

Definition 10. [6] Let Q and W be quasilinear spaces. Then a quasilinear operator $\lambda : Q \to W$ is a function satisfying:

$(QO1)$ $\lambda(\alpha \cdot q) = \alpha \cdot \lambda(q)$,

$(QO2)$ $\lambda(q + w) \preccurlyeq \lambda(q) + \lambda(w)$,

$(QO3)$ $\lambda(q) \preccurlyeq \lambda(w)$, if $q \preccurlyeq w$ for any $q, w \in Q$ and $\alpha \in \mathbb{R}$.

3. Soft Quasilinear Spaces

In this part, we present the definitions of soft quasilinear space and soft proper quasilinear space which are given the first time.

Let Q be a quasilinear space over $\mathbb{R}$ and B be a parameter set. If we define a function $G: B \to P(Q)$ such that $G(b) = P(y) \in Q$ for every $b \in B$, then (G, B) is called a soft set over Q.

Definition 11. Let (G, B) be a non-null soft set over a quasilinear space Q. Then (G, B) is called a soft quasilinear space over Q if $G(b)$ is a subquasilinear space of Q for every $b \in Supp(G, B)$.

Example 12. Let $Q = \Omega_C(\mathbb{R})$ be the quasilinear space and $\left(G, \left(\Omega_C(\mathbb{R})\right)_r\right)$ be a soft set over Q and $G: \left(\Omega_C(\mathbb{R})\right)_r \to P(Q)$ is a function described by

$$G(X) = \left\{[-X, X]: X \in \left(\Omega_C(\mathbb{R})\right)_r\right\}.$$

Since $G(X)$ is a subquasilinear space of $\Omega_C(\mathbb{R})$ for every $X \in Supp\left(G, \left(\Omega_C(\mathbb{R})\right)_r\right)$, $\left(G, \left(\Omega_C(\mathbb{R})\right)_r\right)$ is called a soft quasilinear space over $\Omega_C(\mathbb{R})$.

Example 13. Consider the intervals quasilinear space $I\mathbb{R}^2$ over $\mathbb{R}$ and (G, B) be a soft set over $I\mathbb{R}^2$, where $B = I\mathbb{R}$ and $G: I\mathbb{R} \to P(I\mathbb{R}^2)$ be defined as follows:

$$G(X) = \{(X \cdot r, 0): r \in \mathbb{R}\},$$

for every $X \in I\mathbb{R}$. Then $G(X)$ is a subquasilinear space of $I\mathbb{R}^2$ for every $X \in Supp(G, I\mathbb{R})$. Then $(G, I\mathbb{R})$ is a soft quasilinear space of $I\mathbb{R}^2$. If we define another function $F: I\mathbb{R} \to I\mathbb{R}^2$ such that

$$F(X) = \{(X \cdot r, 1): r \in \mathbb{R}\},$$

for every $(X) \in I\mathbb{R}$. Then F is a not soft quasilinear space of $I\mathbb{R}^2$.

If every element in soft quasilinear space (G, B) has an reverse element in (G, B) then notion of soft quasilinear space coincides with the soft linear space.

Definition 14. Assume that (G,B) is a soft quasilinear space of Q over $\mathbb{R}$ and $(F,B) \subseteq (G,B)$ is a soft set over (G,B). Then (F,B) is called a soft subquasilinear space of (G,B) whenever (F,B) is quasilinear space with identical partial ordering and identical operations on Q.

Theorem 15. A soft subset (F,B) of a soft quasilinear space (G,B) is a soft subquasilinear space of a soft quasilinear space (G,B) if and only if $\alpha \cdot F + \beta \cdot F \subset F$ for every $\alpha, \beta \in \mathbb{R}$.

Proof. Let (F,B) be a soft subquasilinear space of a soft quasilinear space (G,B) of Q over $\mathbb{R}$ and $b \in B$. Then

$$(\alpha \cdot F + \beta \cdot F)(b) \subset F(b),$$

since $F(b)$ is a subquasilinear space and $\alpha \cdot M + \beta \cdot N \in F(b)$ for every $M, N \in F(b)$ and $\alpha, \beta \in \mathbb{R}$.

Let $\alpha \cdot F + \beta \cdot F \subset F$ for all scalars $\alpha, \beta \in \mathbb{R}$. Then

$$(\alpha \cdot F + \beta \cdot F)(b) = \{\alpha \cdot M + \beta \cdot N : M, N \in F(b)\} \subset F(b),$$

for every $\alpha, \beta \in \mathbb{R}$ and for all $b \in B$. From here, we get $\alpha \cdot M + \beta \cdot N \in F(b)$ for all $M, N \in F(b)$ and $\alpha, \beta \in \mathbb{R}$. Hence, $F(b)$ is a subquasilinear space of Q over $\mathbb{R}$ for all $b \in B$. Since (F,B) is a soft subset of (G,B), $F(b) \subset G(b)$ for every $b \in B$. Thus, (F,B) is a soft subquasilinear space of (G,B).

Definition 16. Let (G,B) be a soft quasilinear space over Q and (F,C) be a soft quasilinear space over P. The product of soft quasilinear spaces (G,B) and (F,C) is described as $(G,B) \times (F,C) = (V, B \times C)$, where $V(b,c) = G(b) \times F(c)$ for every $(b,c) \in B \times C$.

Theorem 17. Let (G,B) be a soft quasilinear space over Q and (F,C) be a soft quasilinear space over P. If it is non-null, then $(G,B) \times (F,C)$ is a soft quasilinear space over $Q \times P$.

Proof. Proof is similar to soft linear spaces.

Definition 18. Let (G,B) and (F,C) be two soft quasilinear spaces over Q. The algebraic sum operation of soft quasilinear spaces (G,B) and (F,C) is defined as $(G,B) + (F,C) = (E, B \times C)$, where

$$E(b,c) = G(b) + F(c),$$

for every $(b,c) \in B \times C$.

Theorem 19. Let (G,B) and (F,C) be two soft quasilinear spaces over Q. If it is non-null, then $(G,B)+(F,C)$ and $\alpha\cdot(G,B)$ are soft quasilinear spaces over Q.

Proof. Proof is similar to soft linear spaces.

Example 20. Let $Q=M_2\big(\Omega_C(\mathbb{R})\big)$ be the quasilinear space over $\mathbb{R}$, $B=2\cdot\Omega_C(\mathbb{R})$, $C=4\cdot\Omega_C(\mathbb{R})$. Consider the set-valued interval functions defined by

$$G\colon B\to P(Q)$$

$$G(X)=\left\{\begin{bmatrix}0 & k\cdot X\\ 0 & k\cdot X\end{bmatrix}\colon k\in\mathbb{R}\right\},$$

for every $X\in 2\cdot\Omega_C(\mathbb{R})$ and

$$F\colon C\to P(Q)$$

$$F(X)=\left\{\begin{bmatrix}0 & k\cdot X\\ 0 & 0\end{bmatrix}\colon k\in\mathbb{R}\right\},$$

for every $X\in 4\cdot\Omega_C(\mathbb{R})$. For every $X\in 4\cdot\Omega_C(\mathbb{R})$, $F(X)$ is a subquasilinear space of $G(X)$. So, $\big(F,4\cdot\Omega_C(\mathbb{R})\big)$ is a soft subquasilinear space of $\big(G,2\cdot\Omega_C(\mathbb{R})\big)$. Further, let (F,D) be an another soft set over $Q=M_2\big(\Omega_C(\mathbb{R})\big)$, where $D=2\cdot\Omega_C(\mathbb{R})$ and

$$F\colon D\to P(Q)$$

$$F(X)=\left\{\begin{bmatrix}0 & 0\\ 0 & k\cdot X\end{bmatrix}\colon k\in\mathbb{R}\right\},$$

for every $X\in 2\cdot\Omega_C(\mathbb{R})$. Let $(F,C)+(F,D)=(E,C\times D)$, where $E(X,Y)=F(X)+F(Y)$ for every $(X,Y)\in C\times D$. Then

$$E(X,Y)=\left\{\begin{bmatrix}0 & k\cdot X\\ 0 & k\cdot X\end{bmatrix}\colon k\in\mathbb{R}\right\}$$

is a subquasilinear space of $M_2\big(\Omega_C(\mathbb{R})\big)$ for every $(X,Y)\in C\times D$. From here, we get $(E,C\times D)$ is a soft quasilinear space over $M_2\big(\Omega_C(\mathbb{R})\big)$.

Definition 21. Let (G,B) be a non-null soft quasilinear spaces over a quasilinear space Q. (G,B) is called proper soft set if the following cases hold:

a) $F_b^{(G,B)}\neq\emptyset$ for all $b\in Supp(G,B)$,

b) $F_{b_1}^{(G,B)} \neq F_{b_2}^{(G,B)}$ for every $b_1, b_2 \in Supp(G,B)$ with $b_1 \neq b_2$.

Otherwise, (G,B) is called improper soft set. If (G,B) is proper soft set then (G,B) is called proper soft quasilinear space.

Clearly, every soft linear space is a proper soft quasilinear space with "=".

Example 22. Let us consider the quasilinear space $\Omega_C(\mathbb{R})$. Let (G,B) be a soft set over $\Omega_C(\mathbb{R})$, where $B = \left(\Omega_C(\mathbb{R})\right)_r$ and $G: \left(\Omega_C(\mathbb{R})\right)_r \to P\left(\Omega_C(\mathbb{R})\right)$ is described by $G(b) = [-b, b]$ for every $b \in \left(\Omega_C(\mathbb{R})\right)_r$. Clearly, $\left(G, \left(\Omega_C(\mathbb{R})\right)_r\right) = \left(\Omega_C(\mathbb{R})\right)_d$. From here, $\left(G, \left(\Omega_C(\mathbb{R})\right)_r\right)$ is a soft quasilinear space since $\left(\Omega_C(\mathbb{R})\right)_d$ is a subquasilinear space of $\Omega_C(\mathbb{R})$. Further, $\left(G, \left(\Omega_C(\mathbb{R})\right)_r\right)$ is an improper soft quasilinear space since $\left(\Omega_C(\mathbb{R})\right)_d$ is an imroper.

Example 23. Let $Q = \Omega_C(\mathbb{R})$ be quasilinear space over $\mathbb{R}$ and (G,B) be a soft set over Q, where $B = \Omega_C(\mathbb{R})$ and $G: \Omega_C(\mathbb{R}) \to P(Q)$ is defined by $G(X) = \{X \cdot k : k \in \mathbb{R}\}$ for every $X \in \Omega_C(\mathbb{R})$. $\left(G, \Omega_C(\mathbb{R})\right)$ is a soft quasilinear space since $G(X)$ is a subquasilinear space of $\Omega_C(\mathbb{R})$. Also, $\left(G, \Omega_C(\mathbb{R})\right)$ is a proper soft quasilinear space since $\Omega_C(\mathbb{R})$ is a proper quasilinear space . If $B = \left(\Omega_C(\mathbb{R})\right)_s$ and $G: \left(\Omega_C(\mathbb{R})\right)_s \to P(Q)$ is defined by $G(X) = \{X \cdot k : k \in \mathbb{R}\}$ for every $X \in Q$. $\left(G, \left(\Omega_C(\mathbb{R})\right)_s\right)$ is a soft quasilinear space since $G(X)$ is a subquasilinear space of $\Omega_C(\mathbb{R})$. But, $\left(G, \left(\Omega_C(\mathbb{R})\right)_s\right)$ is an improper soft quasilinear space since $\left(\Omega_C(\mathbb{R})\right)_s$ is an improper quasilinear space.

Example 24. Let $\Omega_C(\mathbb{R}^2)$ be the quasilinear space over $\mathbb{R}$ and (G,B) be a soft set over $\Omega_C(\mathbb{R}^2)$, where $B = \left\{\{(m,k)\} : m = 0,\ k \in \mathbb{R}\right\}$ and $G: B \to P\left(\Omega_C(\mathbb{R}^2)\right)$ is a function defined by

$$G(X) = \left\{Z \in \left(\Omega_C(\mathbb{R}^2)\right)_s \cup B : X \subseteq Z \text{ for a } X \in B\right\}.$$

Since $G(X)$ is a subquasilinear space of $\Omega_C(\mathbb{R}^2)$ for every $X \in Supp(G,B)$, (G,B) is a soft quasilinear space over $\Omega_C(\mathbb{R}^2)$. Further, if we take two different element in $Supp(G,B)$ such as

$$X_1 = \left\{\{(m,k)\} : m = 0,\ \ 1 \leq k \leq 2\right\},$$

$$X_2 = \left\{\{(m,k)\} : 0 \leq m \leq 1,\ \ 1 \leq k \leq 2\right\},$$

we get

$$F_{X_1}^{(G,B)} = F_{X_2}^{(G,B)} = \{\{(m,k)\}: m = 0,\ \ 1 \leq k \leq 2\}.$$

Thus, (G,B) is an improper soft quasilinear subspace of proper quasilinear space $\Omega_C(\mathbb{R}^2)$.

4. Soft Quasi Vectors and Soft Normed Quasilinear Spaces

In this section, we will give the notion of soft normed quasilinear space which is one of the fundamental purposes of the study. Firstly, we will give the notion of soft normed quasilinear space and soft quasi vector and some results related this notions. Later, we present the definition of soft quasilinear operator.

Definition 25. Let (G,B) is a soft quasilinear space of Q. A soft element of Q is said to be a soft quasi vector of (G,B). A soft element of the soft set $(\mathbb{R},B)$ is said to be a soft scalar.

Example 26. Let us consider the Example 12 and the soft quasilinear space $\left(G,\left(\Omega_C(\mathbb{R})\right)_r\right)$. Let $\tilde{q}$ is a soft element of $\Omega_C(\mathbb{R})$ as the following;

$$\tilde{q}\,(r) = [-r,r] \in \Omega_C(\mathbb{R}).$$

Then $\tilde{q}$ is a soft quasi vectors of $\left(G,\left(\Omega_C(\mathbb{R})\right)_r\right)$.

A soft quasi vector $\tilde{q}$ in a soft quasilinear space (G,B) is said to be null soft quasi vector if $\tilde{q}\,(b) = \theta$ for every $b \in B$. The zero element of quasilinear space Q will be denoted by Θ.

Let $\tilde{q}$ and $\tilde{w}$ be soft quasi vectors of (G,B) and $\tilde{k}$ be a soft scalar. Then a partial order relation $\tilde{q} \preccurlyeq \tilde{w}$, the sum $\tilde{q} + \tilde{w}$ of $\tilde{q}\,, \tilde{w}$, and scalar multiplication $\tilde{k} \cdot \tilde{q}$ are defined by

$$q \preccurlyeq \tilde{w} \Leftrightarrow \tilde{q}\,\tilde{(}b) \preccurlyeq \tilde{w}\,(b),$$

$$(\tilde{q} + \tilde{w})(b) = \tilde{q}\,(b) + \tilde{w}\,(b),$$

$$\left(\tilde{k} \cdot \tilde{q}\right)(b) = \tilde{k}\,(b) \cdot \tilde{q}\,(b), \text{ for all } b \in B.$$

From here, we have $\tilde{q} + \tilde{w}$ and $\tilde{k} \cdot \tilde{q}$ are soft quasi vectors of (G,B).

Proposition 27. Let (G,B) be a soft quasilinear space over Q. Then

a) $\overline{0} \cdot \tilde{q} = \Theta$, for all $\tilde{q} \in (G,B)$,

b) $\tilde{k} \cdot \Theta = \Theta$, for all soft scalar $\tilde{k}$,

c) $\left(-\tilde{1}\right)\cdot\tilde{q}=-\tilde{q}$, for all $\tilde{q}\in(G,B)$.

Proof. The proof is similar to soft linear spaces.

Definition 28. Let (G,B) be a soft quasilinear space of quasilinear space Q. Let $\tilde{q}_1,\tilde{q}_2,\ldots,\tilde{q}_n\in(G,B)$ and $\tilde{\alpha}_1,\tilde{\alpha}_2,\ldots,\tilde{\alpha}_n\in(\mathbb{R},B)$. The element

$$\tilde{\alpha}_1\cdot\tilde{q}_1+\tilde{\alpha}_2\cdot\tilde{q}_2+\cdots+\tilde{\alpha}_n\cdot\tilde{q}_n=\sum_{k=1}^{n}\tilde{\alpha}_k\cdot\tilde{q}_k,$$

of (G,B) is said to be quasilinear combination of the soft quasi vectors $\tilde{q}_1,\tilde{q}_2,\ldots,\tilde{q}_n$.

Example 29. Let us consider the soft quasilinear space $\left(G,\left(\Omega_C(\mathbb{R})\right)_r\right)$ as Example 12. Let $\tilde{q}_n=[-n,n]\in\Omega_C(\mathbb{R})$ for $n=1,2,3$. Then $\tilde{q}_1+\overline{2}\cdot\tilde{q}_2$, $\overline{3}\cdot\tilde{q}_1+\tilde{q}_2+\tilde{q}_3$ are some quasilinear combinations of $\tilde{q}_1,\tilde{q}_2,\tilde{q}_3$.

Definition 30. Let (G,B) be a soft quasilinear space of quasilinear space Q. $\left(\tilde{q}_k\right)_{k=1}^{n}\subset(G,B)$ and $(\tilde{\alpha}_k)_{k=1}^{n}\subset(\mathbb{R},B)$. If

$$\Theta\preccurlyeq\tilde{\alpha}_1\cdot\tilde{q}_1+\tilde{\alpha}_2\cdot\tilde{q}_2+\cdots+\tilde{\alpha}_n\cdot\tilde{q}_n,$$

implies $\tilde{\alpha}_1=\tilde{\alpha}_2=\cdots=\tilde{\alpha}_n=\overline{0}$, then $\left(\tilde{q}_k\right)_{k=1}^{n}$ is said to be quasilinear independent, otherwise $\left(\tilde{q}_k\right)_{k=1}^{n}$ is said to be quasilinear dependent.

Example 31. Let us consider again the soft quasilinear space $\left(G,\left(\Omega_C(\mathbb{R})\right)_r\right)$ as Example 12 and $Z=\left\{\tilde{q}_n=[-n,n]:n=1,2,3\right\}\subset(G,B)$ and $(\tilde{\alpha}_k)_{k=1}^{3}\subset(\mathbb{R},B)$. Then

$$\Theta\preccurlyeq\tilde{\alpha}_1\cdot\tilde{q}_1+\tilde{\alpha}_2\cdot\tilde{q}_2+\tilde{\alpha}_3\cdot\tilde{q}_3,$$

is satisfied every $(\tilde{\alpha}_k)_{k=1}^{3}\subset(\mathbb{R},B)$. So, Z is quasilinear dependent in $\left(G,\left(\Omega_C(\mathbb{R})\right)_r\right)$.

Example 32. Let $I\mathbb{R}^2$ be the quasilinear space over $\mathbb{R}$, $(G,I\mathbb{R})$ be a soft set over $I\mathbb{R}^2$ and $G:I\mathbb{R}\to P(I\mathbb{R}^2)$ is function defined by

$$G(X)=\{(0,X\cdot m):m\in\mathbb{R}\},$$

for all $(X)\in I\mathbb{R}$. Since $(G,I\mathbb{R})$ is subquasilinear space of $I\mathbb{R}^2$, $(G,I\mathbb{R})$ is a soft quasilinear space over $I\mathbb{R}^2$. The subset $\left\{\tilde{q}_n=(0,[n,n+1]):n=1,2,3\right\}\subset(G,B)$ is quasilinear independent in (G,B) because of

$$\Theta \preccurlyeq \tilde{\alpha}_1 \cdot (0,[1,2]) + \tilde{\alpha}_2 \cdot (0,[2,3]) + \tilde{\alpha}_3 \cdot (0,[3,4]),$$

is satisfied if and only if $\tilde{\alpha}_1 = \tilde{\alpha}_2 = \tilde{\alpha}_3 = \overline{0}$.

The set of all soft quasi vectors over $\tilde{Q}$ will be denoted by $SQV(\tilde{Q})$.

Theorem 33. The set $SQV(\tilde{Q})$ is a quasilinear space with the relation "$\tilde{\preccurlyeq}$"

$$\tilde{q}_{e_1} \tilde{\preccurlyeq} \tilde{w}_{e_2} \Leftrightarrow \tilde{q} \preccurlyeq \tilde{w} \text{ and } e_1 \leq e_2,$$

the sum operation

$$\tilde{q}_{e_1} + \tilde{w}_{e_2} = (\widetilde{q+w})_{e_1+e_2},$$

and the soft real-scalar multiplication

$$\tilde{\alpha} \cdot \tilde{q}_{e_1} = (\widetilde{\alpha \cdot q})_{\alpha e_1},$$

for every $\tilde{q}_{e_1}, \tilde{w}_{e_2} \in SQV(\tilde{Q})$ and for every soft real numbers $\tilde{\alpha}$.

Proof. Clearly, $\tilde{q}_{e_1} \tilde{\preccurlyeq} \tilde{q}_{e_1}$ for every $\tilde{q}_{e_1} \in SQV(\tilde{Q})$. Let $\tilde{q}_{e_1} \tilde{\preccurlyeq} \tilde{w}_{e_2}$ and $\tilde{w}_{e_2} \tilde{\preccurlyeq} \tilde{z}_{e_3}$ for every $\tilde{q}_{e_1}, \tilde{w}_{e_2}, \tilde{z}_{e_3} \in SQV(\tilde{Q})$. Since $\tilde{Q}$ is an absolute soft quasilinear space, we obtain $\tilde{q}_{e_1} \preccurlyeq \tilde{z}_{e_3}$.

$$\tilde{q}_{e_1} + \tilde{w}_{e_2} = (\widetilde{q+w})_{e_1+e_2} = (\widetilde{w+q})_{e_2+e_1} = \tilde{w}_{e_2} + \tilde{q}_{e_1}.$$

$$\tilde{q}_{e_1} + (\tilde{w}_{e_2} + \tilde{z}_{e_3}) = \tilde{q}_{e_1} + (\widetilde{w+z})_{e_2+e_3} = (q + \widetilde{w+z})_{e_1+e_2+e_3} = (\tilde{q}_{e_1} + \tilde{w}_{e_2}) + \tilde{z}_{e_3}.$$

If $\theta \in Q$ is zero vector then $\tilde{q}_{e_1} + \theta_0 = (\widetilde{q+\theta})_{e_1+0} = \tilde{q}_{e_1}$. So, θ_0 is zero vector in $SQV(\tilde{Q})$.

$$\tilde{\alpha} \cdot (\tilde{\beta} \cdot \tilde{q}_{e_1}) = \tilde{\alpha} \cdot \left(\widetilde{\beta \cdot q}\right)_{\beta e_1} = (\tilde{\alpha}\,\tilde{\beta}) \cdot \tilde{q}_{e_1}.$$

$$\tilde{\alpha} \cdot \left(\tilde{q}_{e_1} + \tilde{w}_{e_2}\right) = \tilde{\alpha} \cdot (\widetilde{q+w})_{e_1+e_2} = (\alpha \cdot \widetilde{q+\alpha} \cdot w)_{\alpha e_1+\alpha e_2} = \tilde{\alpha} \cdot (\tilde{q})_{e_1} + \tilde{\alpha} \cdot \tilde{w}_{e_2}.$$

$$\tilde{1} \cdot \tilde{q}_{e_1} = \left(\widetilde{1 \cdot q}\right)_{e_1} = \tilde{q}_{e_1}.$$

$$\theta_0 \cdot \tilde{q}_{e_1} = \left(\widetilde{\theta \cdot q}\right)_{0.e_1} = \theta_0.$$

$$\left(\tilde{\alpha} + \tilde{\beta}\right) \cdot \tilde{q}_{e_1} = \left((\widetilde{\alpha+\beta}) \cdot q\right)_{(\alpha+\beta)e_1} \preccurlyeq \left(\alpha \cdot \widetilde{q+\beta} \cdot q\right)_{\alpha e_1+\beta e_1}$$

$$= (\widetilde{\alpha \cdot q})_{\alpha e_1} + \left(\widetilde{\beta \cdot q}\right)_{\beta e_1} = \tilde{\alpha} \cdot \tilde{q}_{e_1} + \tilde{\beta} \cdot \tilde{q}_{e_1}.$$

If $\tilde{q}_{e_1} \tilde{\preccurlyeq} \tilde{w}_{e_2}$ and $\tilde{z}_{e_3} \tilde{\preccurlyeq} \tilde{v}_{e_4}$, then $\tilde{q} \preccurlyeq \tilde{w}$ and $e_1 \leq e_2$ and $\tilde{z} \preccurlyeq \tilde{v}$ and $e_3 \leq e_4$. From here, we get $\tilde{q} + \tilde{z} \preccurlyeq \tilde{w} + \tilde{v}$ and $e_1 + e_3 \leq e_2 + e_4$. This gives $\tilde{q}_{e_1} + \tilde{z}_{e_3} \tilde{\preccurlyeq} \tilde{w}_{e_2} + \tilde{v}_{e_4}$.

If $\tilde{q}_{e_1} \tilde{\preccurlyeq} \tilde{w}_{e_2}$, then $\tilde{q} \preccurlyeq \tilde{w}$ and $e_1 \leq e_2$. Thus, we obtain $\tilde{\alpha} \cdot \tilde{q}_{e_1} \tilde{\preccurlyeq} \tilde{\alpha} \cdot \tilde{w}_{e_2}$ since $\tilde{\alpha} \cdot \tilde{q} \preccurlyeq \tilde{\alpha} \cdot \tilde{w}$ and $\alpha e_1 \leq \alpha e_2$ for every $\tilde{q}_{e_1}, \tilde{w}_{e_2}, \tilde{z}_{e_3}, \tilde{v}_{e_4} \in SQV(\tilde{Q})$ and for every soft real numbers $\tilde{\alpha}, \tilde{\beta}$.

Definition 34. Let $SQV(\tilde{Q})$ be a soft quasilinear space and $\tilde{N} \subset SQV(\tilde{Q})$ be a subset. If $\tilde{N}$ is a soft quasilinear space, then $\tilde{N}$ is said to be a soft quasilinear subspace of $SQV(\tilde{Q})$ and stated by $SQV(\tilde{N}) \subset SQV(\tilde{Q})$.

Definition 35. Let $SQV(\tilde{Q})$ be a soft quasilinear space. Then a mapping $\|.\|: SQV(\tilde{Q}) \to \mathbb{R}^+(\mathbb{R})$ is said to be a soft norm on the soft quasilinear space $SQV(\tilde{Q})$, if $\|.\|$ satisfies the following conditions:

(SNQ1) $\|\tilde{q}_e\| \tilde{\succ} \tilde{0}$ if $\tilde{q}_e \neq \tilde{\theta}_0$ for all $\tilde{q}_e \in SQV(\tilde{Q})$,

(SNQ2) $\|\tilde{q}_{e_1} + \tilde{w}_{e_2}\| \tilde{\leq} \|\tilde{q}_{e_1}\| + \|\tilde{w}_{e_2}\|$ for all $\tilde{q}_{e_1}, \tilde{w}_{e_2} \in SQV(\tilde{Q})$,

(SNQ3) $\|\tilde{\alpha} \cdot \tilde{q}_{e_1}\| = |\tilde{\alpha}| \|\tilde{q}_{e_1}\|$ for every $\tilde{q}_{e_1} \in SQV(\tilde{Q})$ and for every soft scalar $\tilde{\alpha}$,

(SNQ4) if $\tilde{q}_{e_1} \tilde{\preccurlyeq} \tilde{w}_{e_2}$, then $\|\tilde{q}_{e_1}\| \tilde{\leq} \|\tilde{w}_{e_2}\|$ for all $\tilde{q}_{e_1}, \tilde{w}_{e_2} \in SQV(\tilde{Q})$,

(SNQ5) if for any $\tilde{\epsilon} \tilde{\succ} \tilde{0}$ there exists an element $\tilde{z}_\epsilon$ $SQV(\tilde{Q})$ such that $\tilde{q}_{e_1} \tilde{\preccurlyeq} \tilde{w}_{e_2} + \tilde{z}_\epsilon$ and $\|\tilde{z}_\epsilon\| \tilde{\leq} \tilde{\epsilon}$ then $\tilde{q}_{e_1} \tilde{\preccurlyeq} \tilde{w}_{e_2}$.

The soft quasilinear space $SQV(\tilde{Q})$ with a soft norm $\|.\|$ on $\tilde{Q}$ is said to be a soft normed quasilinear space and is indicated by $(\tilde{Q}, \|.\|)$.

Example 36. Let Q be a normed quasilinear space. We define $\|.\|: SQV(\tilde{Q}) \to \mathbb{R}^+(\mathbb{R})$ by $\|\tilde{q}_e\| = |e| + \|q\|_Q$. Then $\|.\|$ satisfied first three norms axioms same as . We only show the other axioms. For every $\tilde{q}_{e_1}, \tilde{w}_{e_2} \in SQV(\tilde{Q})$ and for every soft real scalar $\tilde{\epsilon}$.

Let $\tilde{q}_{e_1} \tilde{\preccurlyeq} \tilde{w}_{e_2}$. We find $q \preccurlyeq_Q w$ and $e_1 \leq e_2$ by Theorem 33. Since Q is normed quasilinear space, we get $\|q\|_Q \leq \|w\|_Q$. Then $\|\tilde{q}_{e_1}\| \tilde{\leq} \|\tilde{w}_{e_2}\|$.

Let for any $\tilde{\epsilon} \tilde{>} \tilde{0}$ there exists an element $\tilde{q}_{\epsilon}\ SQV(\tilde{Q})$ such that $\tilde{q}_{e_1} \tilde{\preccurlyeq} \tilde{w}_{e_2} + \tilde{z}_{\epsilon}$ and $\|\tilde{z}_{\epsilon}\| \tilde{\leq} \tilde{\epsilon}$. From Theorem 33, we have $q \preccurlyeq_Q w + z$ and $e_1 \leq e_2 + \epsilon$. On the other hand, we get $|\epsilon| + \|z\|_Q \leq \epsilon$ since $\|\tilde{z}_{\epsilon}\| \tilde{\leq} \tilde{\epsilon}$. This gives $q \preccurlyeq_Q w$. Also, $e_1 \leq e_2$. Thus, we obtain $\tilde{q}_{e_1} \tilde{\preccurlyeq} \tilde{w}_{e_2}$.

Definition 37. Let $(\tilde{Q}, \|.\|)$ be a soft normed quasilinear space. Soft Hausdorff metric or soft norm metric on $\tilde{Q}$ is defined by equality

$$h_{\tilde{Q}}(\tilde{q}_{e_1}, \tilde{w}_{e_2}) = \inf\left\{\tilde{r} \geq \tilde{0} : \tilde{q}_{e_1} \tilde{\preccurlyeq} \tilde{w}_{e_2} + \tilde{a_1^r}, \tilde{w}_{e_2} \tilde{\preccurlyeq} \tilde{q}_{e_1} + \tilde{a_2^r}, \|\tilde{a_i^r}\| \tilde{\leq} \tilde{r}\right\}.$$

Same as the definition of Hausdorff metric on normed quasilinear space, we obtain $\tilde{q}_{e_1} \tilde{\preccurlyeq} \tilde{w}_{e_2} + \left(\tilde{q}_{e_1} - \tilde{w}_{e_2}\right)$ and $\tilde{w}_{e_2} \tilde{\preccurlyeq} \tilde{q}_{e_1} + \left(\tilde{w}_{e_2} - \tilde{q}_{e_1}\right)$ for every $\tilde{q}_{e_1}, \tilde{w}_{e_2} \in SQV(\tilde{Q})$. So,

$$h_{\tilde{Q}}(\tilde{q}_{e_1}, \tilde{w}_{e_2}) \tilde{\leq} \left\|\tilde{q}_{e_1} - \tilde{w}_{e_2}\right\|.$$

Here, we should note that $h_{\tilde{Q}}(\tilde{q}_{e_1}, \tilde{w}_{e_2})$ may not equal to $\left\|\tilde{q}_{e_1} - \tilde{w}_{e_2}\right\|$ since $\tilde{Q}$ is a soft quasilinear space.

Proposition 38. Let $(\tilde{Q}, \|.\|)$ be a soft normed quasilinear space. The function $h_{\tilde{Q}}(\tilde{q}_{e_1}, \tilde{w}_{e_2})$ satisfies all of the soft metric axioms for all $\tilde{x}_{e_1}, \tilde{y}_{e_2} \in \tilde{Q}$.

Proof. We get, $h_{\tilde{Q}}(\tilde{q}_{e_1}, \tilde{w}_{e_2}) \tilde{\geq} \tilde{0}$ from definition of soft Hausdorff metric for all $\tilde{q}_{e_1}, \tilde{w}_{e_2} \in \tilde{Q}$. If $h_{\tilde{Q}}(\tilde{q}_{e_1}, \tilde{w}_{e_2}) = \tilde{0}$, then $\tilde{q}_{e_1} \tilde{\preccurlyeq} \tilde{w}_{e_2}$ and $\tilde{w}_{e_2} \tilde{\preccurlyeq} \tilde{q}_{e_1}$ since $\tilde{Q}$ is soft normed quasilinear space. Thus, we get $\tilde{q}_{e_1} = \tilde{w}_{e_2}$ for all $\tilde{q}_{e_1}, \tilde{w}_{e_2} \in \tilde{Q}$. Conversely, if $\tilde{q}_{e_1} = \tilde{w}_{e_2}$, then $\tilde{q}_{e_1} \tilde{\preccurlyeq} \tilde{w}_{e_2}$ and $\tilde{w}_{e_2} \tilde{\preccurlyeq} \tilde{q}_{e_1}$. Hence, we find $h_{\tilde{Q}}(\tilde{q}_{e_1}, \tilde{w}_{e_2}) = \tilde{0}$. Clearly, $h_{\tilde{Q}}(\tilde{q}_{e_1}, \tilde{w}_{e_2}) = h_{\tilde{Q}}(\tilde{w}_{e_2}, \tilde{q}_{e_1})$. From (SNQ2) and definition of soft Hausdorff metric, we have $h_{\tilde{Q}}(\tilde{q}_{e_1}, \tilde{z}_{e_3}) \tilde{\leq} h_{\tilde{Q}}(\tilde{q}_{e_1}, \tilde{w}_{e_2}) + h_{\tilde{Q}}(\tilde{w}_{e_2}, \tilde{z}_{e_3})$.

On a soft normed quasilinear space the following conditions always true (here, soft Hausdorff metric $h_{\tilde{Q}}$ induced by soft norm):

$$h_{\tilde{Q}}\left(\tilde{\alpha} \cdot \tilde{q}_{e_1}, \tilde{\alpha} \cdot \tilde{w}_{e_2}\right) = \tilde{\alpha} \cdot h_{\tilde{Q}}\left(\tilde{q}_{e_1}, \tilde{w}_{e_2}\right),$$

for all soft scalar $\tilde{\alpha}$,

$$h_{\tilde{Q}}\left(\tilde{q}_{e_1} + \tilde{w}_{e_2}, \tilde{z}_{e_3} + \tilde{v}_{e_4}\right) \tilde{\leq} h_{\tilde{Q}}\left(\tilde{q}_{e_1}, \tilde{z}_{e_3}\right) + h_{\tilde{Q}}(\tilde{w}_{e_2}, \tilde{v}_{e_4}),$$

$$\left\|\tilde{q}_{e_1}\right\| = h_{\tilde{Q}}(\tilde{q}_{e_1}, \tilde{\theta}).$$

Definition 39. A sequence of soft elements $\left\{\tilde{q}_{e_n}^n\right\}$ in a soft normed quasilinear space $\left(\tilde{Q}, \|.\|\right)$ is said to be converges to a soft element $\tilde{q}_{e_0}^0$ if $h_{\tilde{Q}}(\tilde{q}_{e_n}^n, \tilde{q}_{e_0}^0) \to \tilde{0}$ as $n \to \infty$.

Definition 40. A sequence of soft elements $\left\{\tilde{q}_{e_n}^n\right\}$ in a soft normed quasilinear space $\left(\tilde{Q}, \|.\|\right)$ is said to be a Cauchy sequence if corresponding to every $\tilde{\epsilon} \tilde{>} \tilde{0}, \exists m \in \mathbb{N}$ such that $h_{\tilde{Q}}(\tilde{q}_{e_i}^i, \tilde{q}_{e_j}^j) \tilde{\leq} \tilde{\epsilon}$ for all $i, j > m$ i.e. $h_{\tilde{Q}}(\tilde{q}_{e_i}^i, \tilde{q}_{e_j}^j) \to \tilde{0}$ as $i, j \to \infty$.

Theorem 41. The operation of algebraic sum and the operation of multiplication by soft real scalars are continuous according to the soft Hausdorff metric.

Proof. Let $\left\{\tilde{q}_{e_n}^n\right\} \to \tilde{q}_{e_0}^0$ and $\left\{\tilde{w}_{e_n}^n\right\} \to \tilde{w}_{e_0}^0$ in a soft normed quasilinear space $\left(\tilde{Q}, \|.\|\right)$ as $n \to \infty$. Then there is at least one $n_0, n_0' \in \mathbb{N}$ such that

$$\tilde{q}_{e_n}^n \tilde{\leqslant} \tilde{q}_{e_0}^0 + \tilde{a_1^r}, \ \tilde{q}_{e_0}^0 \tilde{\leqslant} \tilde{q}_{e_n}^n + \tilde{a_2^r}, \ \left\|\tilde{a_i^r}\right\| \tilde{\leq} \frac{\tilde{r}}{2}$$

and

$$\tilde{w}_{e_n}^n \tilde{\leqslant} \tilde{w}_{e_0}^0 + \tilde{b_1^r}, \ \tilde{w}_{e_0}^0 \tilde{\leqslant} \tilde{w}_{e_n}^n + \tilde{b_2^r}, \ \left\|\tilde{b_i^r}\right\| \tilde{\leq} \frac{\tilde{r}}{2},$$

for every $n \geq n_0$ and for every $n \geq n_0'$, respectively. Since $\tilde{Q}$ is soft normed quasilinear space, we obtain

$$\tilde{q}_{e_n}^n + \tilde{w}_{e_n}^n \tilde{\leqslant} \tilde{q}_{e_0}^0 + \tilde{w}_{e_0}^0 + \tilde{a_1^r} + \tilde{b_1^r}, \ \tilde{q}_{e_0}^0 + \tilde{w}_{e_0}^0 \tilde{\leqslant} \tilde{q}_{e_n}^n + \tilde{w}_{e_n}^n + \tilde{a_2^r} + \tilde{b_2^r},$$

for every $n \geq n_0, n_0'$. From (NQ3), we get $\left\|\tilde{a_i^r} + \tilde{b_i^r}\right\| \leq \left\|\tilde{a_i^r}\right\| + \left\|\tilde{b_i^r}\right\| \tilde{\leq} \tilde{r}$. So, $\tilde{q}_{e_n}^n + \tilde{w}_{e_n}^n \to \tilde{q}_{e_0}^0 + \tilde{w}_{e_0}^0$.

Let $\left\{\tilde{q}_{e_n}^n\right\} \to \tilde{q}_{e_0}^0$ in a soft normed quasilinear space $\left(\tilde{Q}, \|.\|\right)$ as $n \to \infty$ and $\tilde{\alpha}$ is a soft scalars. Again, there is at least one $n_0 \in \mathbb{N}$ such that

$$\tilde{q}_{e_n}^n \tilde{\leqslant} \tilde{q}_{e_0}^0 + \tilde{a_1^r}, \ \tilde{q}_{e_0}^0 \tilde{\leqslant} \tilde{q}_{e_n}^n + \tilde{a_2^r}, \ \left\|\tilde{a_i^r}\right\| \tilde{\leq} \frac{\tilde{r}}{|\tilde{\alpha}|},$$

for every $n \geq n_0$. Since $\tilde{Q}$ is soft normed quasilinear space, we find

$$\tilde{\alpha} \cdot \tilde{q}_{e_n}^n \tilde{\leqslant} \tilde{\alpha} \cdot \tilde{q}_{e_0}^0 + \tilde{\alpha} \cdot \tilde{a_1^r}, \ \tilde{\alpha} \cdot \tilde{q}_{e_0}^0 \tilde{\leqslant} \tilde{q}_{e_n}^n \cdot \tilde{\alpha} + \tilde{a_2^r} \cdot \tilde{\alpha},$$

for every $n \geq n_0$. Now, $\left\|\tilde{\alpha} \cdot \tilde{a_i^r}\right\| = |\tilde{\alpha}|\left\|\tilde{a_i^r}\right\| \leq \tilde{r}$. Thus, we obtain $\tilde{\alpha} \cdot \tilde{q}_{e_n}^n \to \tilde{\alpha} \cdot \tilde{q}_{e_0}^0$.

Theorem 42. If $\left\{\tilde{q}_{e_n}^n\right\}$ and $\left\{\tilde{w}_{e_n}^n\right\}$ are Cauchy sequences in a soft normed quasilinear space $\left(\tilde{Q}, \|.\|\right)$ then $\left\{\tilde{q}_{e_n}^n + \tilde{w}_{e_n}^n\right\}$ is Cauchy sequence in a soft normed quasilinear space $\left(\tilde{Q}, \|.\|\right)$.

Proof. Let $\left\{\tilde{q}_{e_n}^n\right\}$ and $\left\{\tilde{w}_{e_n}^n\right\}$ are Cauchy sequences in a soft normed quasilinear space $\left(\tilde{Q}, \|.\|\right)$. Then for every $\tilde{r} \tilde{>} \tilde{0}$, $\exists K_1, K_2 \in \mathbb{N}$ such that

$$\tilde{q}_{e_n}^n \tilde{\lessapprox} \tilde{q}_{e_m}^m + \tilde{a_1^r}, \ \tilde{q}_{e_m}^m \tilde{\lessapprox} \tilde{q}_{e_n}^n + \tilde{a_2^r}, \ \left\|\tilde{a_i^r}\right\| \tilde{\leqq} \frac{\tilde{r}}{2}$$

and

$$\tilde{w}_{e_n}^n \tilde{\lessapprox} \tilde{w}_{e_m}^m + \tilde{b_1^r}, \ \tilde{w}_{e_m}^m \tilde{\lessapprox} \tilde{w}_{e_n}^n + \tilde{b_2^r}, \ \left\|\tilde{b_i^r}\right\| \tilde{\leqq} \frac{\tilde{r}}{2},$$

for all $m, n > K_1$ and for all $m, n > K_2$, respectively. Since $\left(\tilde{Q}, \|.\|\right)$ is a soft normed quasilinear space, we obtain

$$\tilde{q}_{e_n}^n + \tilde{w}_{e_n}^n \tilde{\lessapprox} \tilde{q}_{e_m}^m + \tilde{w}_{e_m}^m + \tilde{a_1^r} + \tilde{b_1^r}, \ \tilde{q}_{e_m}^m + \tilde{w}_{e_m}^m \tilde{\lessapprox} \tilde{q}_{e_n}^n + \tilde{w}_{e_n}^n + \tilde{a_2^r} + \tilde{b_2^r}.$$

Now, $\left\|\tilde{a_i^r} + \tilde{b_i^r}\right\| \tilde{\leqq} \left\|\tilde{a_i^r}\right\| + \left\|\tilde{b_i^r}\right\| \tilde{\leqq} \tilde{r}$. Otherwise, if we take $K = \max\{K_1, K_2\}$ then

$$\tilde{q}_{e_n}^n + \tilde{w}_{e_n}^n \tilde{\lessapprox} \tilde{q}_{e_m}^m + \tilde{w}_{e_m}^m + \tilde{a_1^r} + \tilde{b_1^r},$$

$$\tilde{q}_{e_m}^m + \tilde{w}_{e_m}^m \tilde{\lessapprox} \tilde{q}_{e_n}^n + \tilde{w}_{e_n}^n + \tilde{a_2^r} + \tilde{b_2^r}, \ \left\|\tilde{a_i^r} + \tilde{b_i^r}\right\| \tilde{\leqq} \tilde{r},$$

for all $m, n > K$. Hence, $\left\{\tilde{q}_{e_n}^n + \tilde{w}_{e_n}^n\right\}$ is Cauchy sequence in $\tilde{Q}$.

Definition 43. Let $\lambda: SQV\left(\tilde{Q}\right) \to SQV(\tilde{W})$ be a soft mapping. Then λ is said to be a soft quasilinear operator if

(SQO1) $\lambda\left(\tilde{q}_e + \tilde{w}_{e'}\right) \tilde{\lessapprox} \lambda\left(\tilde{q}_e\right) + \lambda(\tilde{w}_{e'})$,

(SQO2) $\lambda\left(\tilde{\alpha} \cdot \tilde{q}_e\right) = \tilde{\alpha} \cdot \lambda\left(\tilde{q}_e\right)$,

(SQO3) $\tilde{q}_e \tilde{\lessapprox} \tilde{w}_{e'} \Rightarrow \lambda\left(\tilde{q}_e\right) \tilde{\lessapprox} \lambda(\tilde{w}_{e'})$

for every $\tilde{q}_e, \tilde{w}_{e'} \in SQV\left(\tilde{Q}\right)$ and for all soft scalar $\tilde{\alpha}$.

Example 44. Let us consider the absolute soft set generated by $\Omega_C(\mathbb{R})$ and let us show it by $\Omega_C\tilde{(}\mathbb{R})$, i.e., $\left(\Omega_C\tilde{(}\mathbb{R})\right)(e) = \Omega_C(\mathbb{R})$ for every $e \in B \subseteq \Omega_C(\mathbb{R})$. Then $\Omega_C\tilde{(}\mathbb{R})$ is absolute soft quasilinear space. For a $\tilde{X} \in \Omega_C\tilde{(}\mathbb{R})$ let us define $\left\|\tilde{X}\right\|(e) = \left\|\tilde{X}_e\right\|_{\Omega_C(\mathbb{R})} = \sup_{b\in\tilde{X}_e}|b|$ for all $e \in B$. Then $\Omega_C\tilde{(}\mathbb{R})$ is a soft normed quasilinear space with $\left\|\tilde{X}\right\|(e) = \sup_{b\in\tilde{X}_e}|b|$. For $\tilde{X} \in \Omega_C\tilde{(}\mathbb{R})$, let us define

$$\lambda(\tilde{X})(e) = \tilde{2} \cdot \tilde{X}_e.$$

Clearly, for every $\tilde{X} \in \Omega_C\tilde{(}\mathbb{R})$, $\lambda(\tilde{X})(e) \in \Omega_C\tilde{(}\mathbb{R})$ for every $e \in B$. Further,

$$\lambda(\tilde{X} + \tilde{Y})(e + e') = \tilde{2} \cdot (\tilde{X} + \tilde{Y})_{e+e'} = \lambda(\tilde{X})(e) + \lambda(\tilde{Y})(e'),$$

for every $\tilde{X}, \tilde{Y} \in \Omega_C\tilde{(}\mathbb{R})$.

$$\lambda(\tilde{\alpha} \cdot \tilde{X})(e) = \tilde{2} \cdot \tilde{\alpha} \cdot \tilde{X}_e = \tilde{\alpha} \cdot \lambda(\tilde{X}_e),$$

for every $\tilde{X}, \tilde{Y} \in \Omega_C\tilde{(}\mathbb{R})$ and for every soft scalar $\tilde{\alpha}$. Let $\tilde{X}_e \tilde{\leqslant} \tilde{Y}_{e'}$ for every $\tilde{X}, \tilde{Y} \in \Omega_C\tilde{(}\mathbb{R})$. Clearly, $\lambda(\tilde{X}_e) \tilde{\leqslant} \lambda(\tilde{Y}_{e'})$. So, we obtain λ is soft quasilinear operator to $\Omega_C\tilde{(}\mathbb{R})$ from $\Omega_C\tilde{(}\mathbb{R})$.

Definition 45. The soft quasilinear operator $\lambda: SQV\left(\tilde{Q}\right) \to SQV(\tilde{W})$ is said to be soft continuous at $\tilde{q}^0_{e_0} \in SQV\left(\tilde{Q}\right)$, if for every sequence $\tilde{q}^n_{e_n}$ of soft quasi vectors of $SQV\left(\tilde{Q}\right)$ with $\tilde{q}^n_{e_n} \to \tilde{q}^0_{e_0}$ as $n \to \infty$, we get $\lambda\left(\tilde{q}^n_{e_n}\right) \to \lambda\left(\tilde{q}^0_{e_0}\right)$ as $n \to \infty$.

Definition 46. The soft quasilinear operator $\lambda: SQV\left(\tilde{Q}\right) \to SQV(\tilde{W})$ is said to be soft bounded, if there exists a soft real numbers $\tilde{k}$ such that

$$\left\|\lambda\left(\tilde{q}_e\right)\right\| \tilde{\leq} \tilde{k}\left\|\tilde{q}_e\right\|,$$

for all $\tilde{q}_e \in SQV\left(\tilde{Q}\right)$.

Theorem 47. Let $\lambda: SQV\left(\tilde{Q}\right) \to SQV(\tilde{W})$ be a soft quasilinear operator. Then λ is said to be soft bounded if and only if it is soft continuous.

Proof. Assume that $\lambda: SQV\left(\tilde{Q}\right) \to SQV(\tilde{W})$ is soft bounded. Let the sequence $\left\{\tilde{x}^n_{e_n}\right\}$ is convergent to the $\left\{\tilde{x}^0_{e_0}\right\}$. From Definition 39, we have there is at least one $n_0 \in \mathbb{N}$ such that

$$\tilde{q}^n_{e_n} \tilde{\leqslant} \tilde{q}^0_{e_0} + \tilde{a_1^r},\ \tilde{q}^0_{e_0} \tilde{\leqslant} \tilde{q}^n_{e_n} + \tilde{a_2^r},\ \left\|\tilde{a_i^r}\right\| \tilde{\leq} \frac{\tilde{r}}{\tilde{k}},$$

for every $n \geq n_0$. Since λ is soft quasilinear operator, we obtain

$$\lambda\left(\tilde{q}_{e_n}^{n}\right) \tilde{\lesssim} \lambda\left(\tilde{q}_{e_0}^{0}\right) + \lambda(\tilde{a_1^r})$$

and

$$\lambda\left(\tilde{q}_{e_0}^{0}\right) \tilde{\lesssim} \lambda\left(\tilde{q}_{e_n}^{n}\right) + \lambda(\tilde{a_2^r}).$$

On the other hand, because of λ is soft bounded, we write

$$\left\|\lambda(\tilde{a_1^r})\right\| \tilde{\leq} \tilde{k}\left\|\tilde{a_1^r}\right\| \tilde{\leq} \tilde{r} \text{ and } \left\|\lambda(\tilde{a_2^r})\right\| \tilde{\leq} \tilde{k}\left\|\tilde{a_2^r}\right\| \tilde{\leq} \tilde{r}.$$

So, above three inequality give us the soft bounded quasilinear operator λ is continuous.

The other side of the proof is similar to soft linear counterpart.

5. Conclusion

In this work, the notion of soft quasilinear space is defined. After, the concept of soft quasi vectors in soft quasilinear spaces is presented as a new structure. Also, some consistent results related with this concept are obtained and supported by new examples. Further, the definitions of soft normed quasilinear space and soft proper quasilinear space are introduced. Continuity and boundedness of soft quasilinear operators have been given and proved some related theorems.

References

[1] Molodtsov, D., *Soft set-theory first results*, Computational and Applied Mathematics, 37, 19-31, 1999.

[2] Das, S., Samanta, S.K., *On soft metric spaces*, Journal of Fuzzy Mathematics, 21, 707-734, 2013.

[3] Das, S., Samanta, S.K., *Soft real sets, soft real numbers and their properties*, Journal of Fuzzy Mathematics, 20 (3), 551-576, 2012.

[4] Das, S., Majumdar, P., Samanta, K., *On soft linear spaces and soft normed linear spaces*, Annals of Fuzzy Mathematics and Informatics, 9(1), 91-109, 2015.

[5] Das, S., Samanta, S.K., *Soft linear operators in soft normed linear spaces*, Annals of Fuzzy Mathematics and Informatics, 6(2), 295-314, 2013.

[6] Aseev, S.M., *Quasilinear operators and their application in the theory of multivalued mappings*, Proceedings of the Steklov Institute of Mathematics, 2, 23-52, 1986.

[7] Yılmaz, Y., Çakan, S., Aytekin, Ş., *Topological quasilinear spaces*, Abstract and Applied Analysis, (2012), 951374, 2012.

[8] Çakan, S., Yılmaz, Y., *Normed proper quasilinear spaces*, Journal of Nonlinear Sciences and Applications, 8, 816-836, 2015.

[9] Yılmaz, Y., Bozkurt, H., Çakan, S., *On orthonormal sets in inner product quasilinear spaces*, Creative Mathematics and Informatics, 25(2), 237-247, 2016.

[10] Levent, H., Yilmaz, Y., *Hahn- Banach extension theorem for interval-valued functions and existence of quasilinear functionals*, New Trends in Mathematical Sciences, 6(2), 19-28, 2018.

[11] Levent, H., Yilmaz, Y., *Translation, modulation and dilation systems set-valued signal processing*, Carpathian Mathematical Publications, 10(1), 143-164, 2018.

[12] Maji, P.K., Biswas, R., Roy, A.R., *Soft set theory*, Computational and Applied Mathematics, 45, 555-562, 2003.

[13] Feng, F., Jun, Y. B., Zhao, X., *Soft semiring*, Computational and Applied Mathematics, 56, 2621-2628, 2008.

[14] Das, S., Samanta, S.K., *Soft metric*, Annals of Fuzzy Mathematics and Informatics, 6(1), 77-94, 2013.

[15] Bayramov, S., Gündüz (Aras), C., *Soft locally compact and soft paracompact spaces*, Journal of Mathematics and System Science, 3, 122-130, 2013.

[16] Yazar, M.İ., Bilgin, T., Bayramov, S., Gündüz, Ç., *A new view on soft normed spaces*, International Mathematical Forum, 9(24), 1149-1159, 2014.

Adıyaman University Journal of Science
https://dergipark.org.tr/en/pub/adyujsci
DergiPark AKADEMİK
ISSN 2147-1630
e-ISSN 2146-586X

A Different Interpretation on Magnetic Surfaces Generated by Special Magnetic Curve in $\mathbf{Q^2 \subset E_1^3}$

Fatma ALMAZ[1,*], Mihriban ALYAMAÇ KÜLAHCI[2]

[1]*Fırat University, Science of Faculty, Mathematics of Department, 23119, Elazığ, Turkey*
fb_fat_almaz@hotmail.com, ORCID: 0000-0002-1060-7813
[2]*Fırat University, Science of Faculty, Mathematics of Department, 23119, Elazığ, Turkey*
mihribankulahci@gmail.com, ORCID: 0000-0002-8621-5779

Received: 02.04.2020 **Accepted:** 10.11.2020 **Published:** 30.12.2020

Abstract

By thinking the magnetic flow connected by the Killing magnetic field, the magnetic field on the setting out particle orbit is investigated in $\mathbf{Q^2 \subset E_1^3}$. Clearly, dealing with the Killing magnetic field of α -magnetic curve, the rotational surface generated by α -magnetic is expressed in $\mathbf{Q^2 \subset E_1^3}$, and the variant kinds of axes of rotation in lightlike cone $\mathbf{Q^2 \subset E_1^3}$ is given. Furthermore, the specific kinetic energy, specific angular momentum and conditions being geodesic on rotational surface generated by α -magnetic curve are expressed with the help of Clairaut's theorem.

***Keywords*:** Magnetic curve; Null cone; Killing vector field; Specific kinetic energy; Specific angular momentum.

* Corresponding Author DOI: 10.37094/adyujsci.713156

$\mathbf{Q^2} \subset \boldsymbol{E_1^3}$'de Özel Manyetik Eğri Tarafından Oluşturulan Manyetik Yüzeyler Üzerine Farklı Bir Yorum

Öz

Killing manyetik alanı ile bağlantılı manyetik akış düşünülerek, parçacık yörüngesindeki manyetik alan $\mathbf{Q}^2 \subset E_1^3$ uzayında incelendi. Açıkçası, $\mathbf{Q}^2 \subset E_1^3$ Lightlike cone uzayında farklı tipten dönme ekseni verilerek α -manyetik eğrinin Killing manyetik alanı kullanılıp α -manyetik dönel yüzey $\mathbf{Q}^2 \subset E_1^3$ uzayında ifade edildi. Ayrıca, elde edilen manyetik yüzey üzerinde spesifik kinetik enerji, spesifik açısal momentum ve dönel yüzey üzerinde α -manyetik eğrilerin jeodezik olma koşulları Clairaut's teoremi yardımı ile ifade edildi.

***Anahtar Kelimeler*:** Manyetik eğri; Null koni; Killing vektör alanı; Spesifik kinetik enerji; Spesifik açısal momentum.

1. Introduction

The geodesics have been commonly studied in Riemannian geometry, metric geometry and general relativity by a lot of mathematicians. More definitely, a curve on a surface is called to be geodesic if its geodesic curvature is zero. The geodesic equations are given by constant of motion due to energy, many approaches that reflect serious use of energy idea are introduced in many books according to concerned topics. However, it seems attractive to use the relativistic energy in describing the central force problem. Furthermore, the equation of action including the energy and angular momentum are a natural topic using by many applications. Though we consider about the submanifolds of the pseudo-Riemannian space forms, also we can obtain less studying on submanifolds of the pseudo-Riemannian lightlike cone than we think.

In [1], different magnetic curves were found in the $2-$dimensional lightlike cone using the Killing magnetic field of magnetic curves by the authors. Also, some characterizations and definitions and examples of these curves with their shapes were given. Studying on the degenerate submanifolds of Lorentzian manifolds with degenerate metric was studied by a lot of mathematicians finding out significant connection between null submanifolds and spacetime [2]. In [3, 4], the authors gave some knowledge about magnetic curves corresponding to a Killing magnetic fields. The magnetic curves on a Riemannian manifold (M, d) were defined orbits of charged particles setting out on M under the motion of a magnetic field F. Namely, each trajectory δ is obtained by solving the Lorentz equation $\nabla_{\delta'}\delta' = \psi(\delta')$, where ψ is the Lorentz force as to F and ∇ is the Levi Civita connection of d, [4]. A magnetic field F on M is a closed $2-$form on

(M, d) and it is related to F with a $(1,1)$-tensor field ψ, is said to be the Lorentz force. They are associated as to $d(\psi(X), Y) = F(X, Y)$, for any vector fields X, Y on M, [5]. In [6], the magnetic flow combination by the Killing magnetic field was examined by Bozkurt et al. in a three-dimensional orientated Riemannian manifold (M^3, d). For the study of the magnetic curves associated to magnetic fields on arbitrary dimensional spaces, we also refer the reader to [7-9]. References [10-13] contain detailed information about surfaces and curves. In [14], the authors expressed a precise classification of the magnetic curves of the resembling magnetic field for an discretionary 3-dimensional normal paracontact metric structure equipped by a Killing characteristic vector field. In [15], magnetic curves as to the Killing magnetic field W in the $\mathbb{R}_1^3$ were examined by the authors. In [16, 17], the authors expressed some characterizations about curves in 3-Dimensional null cone. In [18], the expressions of the cone curvature function and cone curves were investigated by the author. In [19], the functions of the cone curves that was defined and the formulas of the curves were also given by the author in $\mathbf{Q}^2$ and $\mathbf{Q}^3$.

The physical properties as energy and momentum are replaced by the specific quantities found by partitioning out the mass, and the term of the motion is very considerable in terms of its specific energy and specific angular momentum. In an evident sense, it is considered that use of relativistic energy is required and considerable.

Hence, we can say that the specific energy of the particle is constant because of the point of view of its motion in space as the physical approach according to references [20, 21], it is only accelerated perpendicular to the surface. If a force is accountable for this acceleration, that is to say the normal force which supplies the particle on the surface, since it is perpendicular to the velocity of the particle. Therefore, we can say that its energy and specific energy E must be constant. Resembling the speed must be constant along a geodesic according to this cause.

In this study, the specific energy and specific angular momentum on rotated surface generated by α −magnetic curve are tried to express in Galilean space and that the speed is constant along a geodesic is shown using Clairaut's theorem. Furthermore, using some parameters geodesic formulas are given.

2. Preliminaries

Let E_1^3 be the 3 −dimensional pseudo-Euclidean space as follows

$$d(X, Y) = \langle X, Y \rangle = x_1 y_1 + x_2 y_2 - x_3 y_3,$$

for all $X = (x_1, x_2, x_3)$, $Y = (y_1, y_2, y_3) \in E_1^3$. E_1^3 is a smooth pseudo-Riemannian manifold pointing out by $(2,1)$.

Let M be a submanifold of E_1^3. If the pseudo-Riemannian metric d of E_1^3 is reduced a pseudo-Riemannian metric $\tilde{d}$ (in turn in order, a Riemannian metric, a degenerate quadratic form) on M, then M is named a timelike (in turn in order, spacelike, lightlike) submanifold of E_1^3.

The lightlike cone is given by

$$\mathbf{Q}^2 = \{\delta \in E_1^3 : d(\delta, \delta) = 0\}.$$

A vector $X \neq 0$ in E_1^3 is called spacelike, timelike, null, if $\langle X, X\rangle > 0, \langle X, X\rangle < 0, \langle X, X\rangle = 0$, in turn in order. A frame field $\{\delta, \alpha, y\}$ on E_1^3 is called an asymptotic orthonormal frame field, if following equals hold

$$\langle \delta, \delta\rangle = \langle y, y\rangle = \langle \delta, \alpha\rangle = \langle y, \alpha\rangle = 0, \ \langle \delta, y\rangle = \langle \alpha, \alpha\rangle = 1.$$

Let the curve $\delta: I \to \mathbf{Q}^2 \subset E_1^3$ be a regular curve in $\mathbf{Q}^2$ for $\xi \in I$ and for $\delta'(\xi) = \alpha(\xi)$, using an asymptotic orthonormal frame along the curve $\delta(\xi)$ and the cone Frenet formulas of $\delta(\xi)$ are written as follows

$$\begin{aligned} \delta'(\xi) &= \alpha(\xi) \\ \alpha'(\xi) &= \kappa(\xi)\delta(\xi) - y(\xi) \\ y'(\xi) &= -\kappa(\xi)\alpha(\xi), \end{aligned} \tag{1}$$

where cone curvature function of the curve $\delta(\xi)$ is expressed by the function $\kappa(\xi)$, [18].

Let $\delta: I \to \mathbf{Q}^2 \subset E_1^3$ be a spacelike curve in $\mathbf{Q}^2$ with arc length parameter s. Then the curve $\delta = \delta(s) = (\delta_1, \delta_2, \delta_3)$ can be taken down by

$$\delta(s) = \frac{g_s^{-1}}{2}(g^2 - 1, 2g, g^2 + 1),$$

for some non constant function $g(s)$ and $g_s = g'$, [19].

The Lorentzian cross-product $\times: E_1^3 \times E_1^3 \to E_1^3$ is expressed with following formula

$$\beta \times \varsigma = \begin{bmatrix} i & j & -k \\ \beta_1 & \beta_2 & \beta_3 \\ \varsigma_1 & \varsigma_2 & \varsigma_3 \end{bmatrix},$$

where $\beta = (\beta_1, \beta_2, \beta_3)$, $\varsigma = (\varsigma_1, \varsigma_2, \varsigma_3) \in E_1^3$. Here i, j, k indices are used as common meaning. We can express that this product has resembling algebra properties as the cross product in E^3. Thus, it is antisymetric and $\beta \times \varsigma$ is ortogonal on both β and ς.

The Lorentz force ψ of a magnetic field F on $\mathbf{Q}^2$ is defined to be a skew-symmetric operator given by

$$d(\psi(X), Y) = F(X, Y),$$

for all $X, Y \in \mathbf{Q}^2$, [5].

The α −magnetic trajectories of F are δ on $\mathbf{Q}^2$ that satisfy the Lorentzian equation [5]

$$\nabla_{\delta'}\delta' = \psi(\delta').$$

In addition, the mixed product of the vector fields $X, Y, Z \in \mathbf{Q}^2$ is defined by

$$d(X \times Y, Z) = dv_d(X, Y, Z),$$

where a volume on $\mathbf{Q}^2$ is denoted by dv_d and if W is a Killing vector in $\mathbf{Q}^2$ and let $F_W = \iota_W vol_d$ be the Killing magnetic field and the inner product is expressed by ι. Thus, the equation Lorentz force of F_W is given by

$$\psi(X) = W \times X, \forall X \in \mathbf{Q}^2.$$

Clearly, the Lorentz equation is expressed as [5]

$$\nabla_{\delta'}\delta' = \psi(\delta') = W \times \delta'.$$

In E_1^3, to think over the Killing vector field $W = a\partial_\delta + b\partial_\alpha + c\partial_y$, $a, b, c \in \mathbb{R}_0$, solutions of the Lorentz equation given by

$$\delta'' = W \times \delta',$$

are the magnetic trajectories $\delta: I \to \mathbf{Q}^2 \subset E_1^3$ determined by W, [5].

Definition 1. Let γ be a curve given by

$$\gamma(s) = \big(x(w(s), v(s)), y(w(s), v(s)), z(w(s), v(s))\big)$$

which is an arc-length parametrized geodesic on a surface of revolution. We need the differential equations satisfied by $(w(s), v(s))$. Denote the differentiation with respect to s by an overdot. From the Lagrangian

$$L = \dot{w}^2 + \rho^2 \dot{v}^2, \tag{2}$$

we obtain the Euler-Langrange equations

$$\frac{\partial}{\partial s}\left(\frac{\partial L}{\frac{\partial w}{\partial s}}\right) = \frac{\partial L}{\partial w}; \frac{\partial}{\partial s}\left(\frac{\partial L}{\frac{\partial v}{\partial s}}\right) = \frac{\partial L}{\partial v} \; or \; \ddot{u} = \rho\rho' \dot{v}^2; \frac{d}{ds}(\rho \dot{v}^2) = 0, \tag{3}$$

so that is a constant of the motion [5, 15].

Theorem 1. (Clairaut's Theorem) Let γ be a geodesic on a surface of revolution S, let ρ be the distance function of a point of S from the axis of rotation, and let θ be the angle between γ and the meridians of S. The $\rho sin\theta$ is constant along γ. On the contrary, if $\rho sin\theta$ is constant along some curve γ on the surface, and if no part of γ is part of some parallel of S, then γ is a geodesic [5].

Definition 2. A one-parameter group of diffeomorphisms of a manifold M is a smooth map $\psi: M \times \mathbb{R} \to M$, such that $\varphi_t(x) = \varphi(x, t)$, where

1. $\varphi_t: M \to M$ is a diffeomorphism,
2. $\varphi_0 = id.$
3. $\varphi_{s+t} = \varphi_s o \varphi_t.$

This group is associated with a vector field W given by $\frac{d}{dt}\varphi_t(x) = W(x)$, and the group of diffeomorphisms is called the flow of W [22].

If a one-parameter group of isometries is generated by a vector field W, then this vector field is called a Killing vector field [22].

3. The Expression of α −Magnetic Curves in $\mathbf{Q^2} \subset \boldsymbol{E_1^3}$

In this section, a new kind of a magnetic curve called α −magnetic curves in $\mathbf{Q}^2 \subset E_1^3$ and some theorems are given.

Definition 3. Let $\delta: I \to \boldsymbol{Q}^2 \subset E_1^3$ be a spacelike curve in $\boldsymbol{Q}^2$ and F_W be a magnetic field on $\boldsymbol{Q}^2 \subset E_1^3$, the curve δ is called as α −magnetic curve if its W_α vector field satisfies the Lorentz force equation [1]

$$\nabla_\alpha \alpha = \psi^\alpha(\alpha) = W_\alpha \times \alpha.$$

Theorem 2. Let $\delta(s)$ be a spacelike α −magnetic curve in the $\boldsymbol{Q}^2 \subset E_1^3$ with the asymptotic orthonormal frame $\{\delta, \alpha, y\}$. Hence, the Lorentz force is expressed by

$$\psi^\alpha = \begin{bmatrix} w_1 & 1 & 0 \\ \kappa & 0 & -1 \\ 0 & -\kappa & -w_1 \end{bmatrix}, \tag{4}$$

where w_1 is a function defined by $w_1 = d(\psi^\alpha(\delta), y)$ [1].

Theorem 3. Let δ be a spacelike curve in the $\boldsymbol{Q}^2 \subset E_1^3$. The curve δ is an α −magnetic trajectory of α −magnetic field W_α if and only if the vector field W_α is written by

$$W_\alpha = \mp w_1 \vec{\alpha}\,, \tag{5}$$

and δ is a geodesic curve, where $w_1 = d(\psi^\alpha(\delta), y)$, the cone curvature function $\kappa(\xi) = -1$ [1].

Theorem 4. Let δ be an α −magnetic trajectory generated by the Killing vector field $W_\alpha = \mp w_1 \vec{\alpha}$ in $\boldsymbol{Q}^2 \subset E_1^3$. Then the curve δ is written by

$$\delta_\alpha(\xi) = \delta(0) + c\xi, \tag{6}$$

where $c = \mp \frac{1}{w_1} \in \mathbb{R}_0$. Remark that, *if* $W_\alpha = \mp w_1 \vec{\alpha}$ holds, the magnetic curve δ is a straight line in the direction of W_α [1].

4. The Surface of Rotation Formed by α −magnetic Curve in $\mathbf{Q}^2 \subset \boldsymbol{E_1^3}$

In this section, using α −magnetic trajectory, a new kind of a magnetic surface of rotated by α −magnetic curve is defined, and some characterizations are given in $\mathbf{Q}^2 \subset E_1^3$.

Theorem 5. Let δ be an α −magnetic trajectory as to the killing vector field W_α in $\boldsymbol{Q}^2 \subset E_1^3$. Then

i) The rotational surface $\Lambda^\alpha(\xi, t)$ formed by the ψ^α is given by

$$\Lambda^{\alpha}(\xi,t)=\begin{pmatrix}\left(\begin{pmatrix}\frac{2\kappa\sinh(w_1\xi)}{w_1^3}+\frac{2\kappa\cosh(w_1\xi)}{w_1}\\ -1-\frac{\xi}{w_1^2}-\frac{\xi^2}{2!}+w_1e^{w_1\xi}+(\frac{4\kappa^2\xi^5}{5!}+\dots)\end{pmatrix}\right)(at+b),\\ (\cosh(\sqrt{2\kappa}\xi)+\frac{2\kappa w_1^2\xi^4}{4!}+\dots)(at+b),\\ (\frac{\kappa e^{w_1\xi}}{w_1}-2\kappa^2\sinh(\sqrt{2\kappa}\xi)+(\frac{-4(\kappa w_1)^2\xi^5}{5!}+\dots))(at+b)\end{pmatrix}.$$

ii) The Gaussian and mean curvatures of the rotated surface Λ_1^{α} generated by $\delta_{\alpha}(t)$ are given by

$$K=\frac{-\left(\left(\frac{\kappa'+\kappa w_1}{w_1}+\frac{\sqrt{2}\kappa^2\kappa'}{\sqrt{\kappa}}\right)\left(\frac{2}{w_1^2}\right)\right)^2}{b\zeta_1},$$

$$H=\frac{-a}{2\xi_1}\begin{pmatrix}\left(\frac{\kappa'+\kappa w_1}{w_1}+\frac{\sqrt{2}\kappa^2\kappa'}{\sqrt{\kappa}}\right)\\ \begin{pmatrix}\frac{4\kappa'}{w_1^2}+\frac{2\kappa''+2\kappa w_1^2}{w_1}\\ -1+w_1^3\\ -\kappa'\left(\frac{2\kappa}{w_1}-1+w_1\right)\end{pmatrix}\\ +\frac{\kappa'\kappa}{w_1}\left(\frac{2\kappa-1}{w_1^2}+\frac{2\kappa'}{w_1}\right)\end{pmatrix}\begin{pmatrix}\begin{pmatrix}\frac{2\kappa}{w_1}\\ -1\\ +w_1\end{pmatrix}^2+\\ 1-\left(\frac{\kappa}{w_1}\right)^2\end{pmatrix}$$

$$+\frac{2a}{w_1^2\xi_1}\begin{pmatrix}\frac{\kappa'+\kappa w_1}{w_1}\\ +\frac{\sqrt{2}\kappa^2\kappa'}{\sqrt{\kappa}}\end{pmatrix}\begin{pmatrix}\left(\frac{2\kappa-1}{w_1^2}+\frac{2\kappa'}{w_1}\right)\\ \left(\frac{2\kappa}{w_1}-1+w_1\right)\\ \frac{-\kappa}{w_1}\begin{pmatrix}\frac{\kappa'+\kappa w_1}{w_1}\\ +\frac{\sqrt{2}\kappa^2\kappa'}{\sqrt{\kappa}}\end{pmatrix}\end{pmatrix},$$

where the previous equations are consisted without loss of generality for $\xi,t=0$.

iii) If κ =constant, the Gaussian and mean curvatures of the rotated surface Λ_1^{α} generated by $\delta_{\alpha}(t)$ are given by

$$K=\frac{\xi_3}{\zeta_2},\qquad H=\frac{-\xi_4}{2\zeta_2},$$

where

$$\xi_2 = \begin{pmatrix} b^2\left(\left(\frac{2\kappa-1}{w_1^2}+w_1^2\right)^2-\kappa^2(1-2\kappa\sqrt{2\kappa})^2\right)\left((\frac{2\kappa-1}{w_1^2}+w_1^2)(\frac{2\kappa}{w_1}-1+w_1)-\frac{\kappa^2}{w_1}\right) \\ -\left((\frac{2\kappa-1}{w_1^2}+w_1^2)(\frac{2\kappa}{w_1}-1+w_1)-\frac{\kappa^2}{w_1}(1-2\kappa\sqrt{2\kappa})b\right)^2 \end{pmatrix},$$

$$\xi_3 = -8b^2\kappa^5\left(\frac{2\kappa-1}{w_1^2}+w_1^2\right)^2,$$

$$\xi_4 = \begin{pmatrix} b^2\kappa\left(2\kappa w_1-1+w_1^3\right)\left(1-2\kappa\sqrt{2\kappa}\right) \\ +2\kappa^2b^2\begin{pmatrix}\frac{1}{w_1}\left(\frac{2\kappa-1}{w_1^2}+w_1^2\right) \\ -\left(1-2\kappa\sqrt{2\kappa}\right)\left(\frac{2\kappa}{w_1}+w_1-1\right)\end{pmatrix} \\ -\kappa b^2w_1(\frac{2\kappa-1}{w_1^2}+w_1^2)) \end{pmatrix}\left((\frac{2\kappa}{w_1}+w_1-1)^2+1-\left(\frac{\kappa}{w_1}\right)^2\right)$$

$$-2\left((\frac{2\kappa-1}{w_1^2}+w_1^2)(\frac{2\kappa}{w_1}-1+w_1)-\frac{\kappa^2}{w_1}(1-2\kappa\sqrt{2\kappa})b\right)\left(2b\kappa^2\sqrt{2\kappa}(\frac{2\kappa-1}{w_1^2}+w_1^2)\right),$$

where the curvature of the curve δ is κ and $\delta_\alpha(t) = (0, at+b, 0),\ a \neq 1,\ b \in \mathbb{R}_0$.

Proof. We will research one parameter group of Lorentz of transformation which is unchangeable all points on the α −axis. It necessitates the Killing vector field to supply $W_\alpha(\xi) = w_1\overrightarrow{\alpha(\xi)}$. Hence, we can use 3×3 matrix ψ^α, and we can write the one parameter group of homomorphism $\varphi_\xi(\delta,\alpha,y)$ expressed as $\varphi'_\xi(\delta) = \psi^\alpha\varphi_\xi(\delta)$. Therefore, we find $\varphi_\xi = e^{\xi\psi_\xi}$ and calculating the matrix exponential, we have

$$\Pi^{\alpha}(\xi)=\begin{bmatrix} w_1\sinh(\sqrt{2\kappa}\xi) & \frac{2\kappa\sinh(w_1\xi)}{{w_1}^3} & \frac{\cosh(\sqrt{w_1}\xi)}{w_1} \\ -1 & +\frac{2\kappa\cosh(w_1\xi)}{w_1} & +\frac{2\kappa\xi^4}{4!} \\ +\cosh(\sqrt{2\kappa}\xi) & +w_1e^{w_1\xi} & +\dots \\ -w_1e^{w_1\xi} & +(\frac{4\kappa^2\xi^5}{5!} & \\ +(\frac{4\kappa w_1\xi^5}{5!} & +\dots) & \\ +\dots) & -1-\frac{\xi}{w_1^2} & \\ & -\frac{\xi^2}{2!} & \\ \frac{\kappa(\cosh(w_1\xi)}{w_1} & \cosh(\sqrt{2\kappa}\xi) & \frac{\sinh(w_1\xi)-}{w_1} \\ \frac{+\cosh(\sqrt{w_1}\xi))}{w_1} & +\frac{2\kappa w_1^2\xi^4}{4!} & \frac{\cosh(w_1\xi)}{w_1} \\ +2\kappa^2(\frac{\xi^3}{3!}+\dots) & +\dots & +\frac{2\kappa w_1\xi^4}{4!} \\ +(\frac{2w_1\kappa^2\xi^4}{4!}+\dots) & & +\dots \\ \frac{\kappa^2\cos(w_1\xi)}{w_1} & \frac{\kappa e^{w_1\xi}}{w_1} & \kappa\cosh(\sqrt{2\kappa}\xi) \\ +\frac{2\kappa^3\xi^4}{4!} & -2\kappa^2\sinh(\sqrt{2\kappa}\xi) & e^{-w_1\xi} \\ +\dots & +(\frac{-4(\kappa w_1)^2\xi^5}{5!} & -\frac{\xi\sinh(\sqrt{2\kappa}\xi)}{\sqrt{2\kappa}} \\ & +\dots) & +(\frac{4\kappa w_1^3\xi^5}{5!} \\ & & +\dots) \end{bmatrix}, \quad (7)$$

where $-\infty<\xi<\infty$. Here, we deal with the Lorentz force ψ^{α} rotation for α −magnetic curve. Also, we say rotating a curve taking the rotation matrix $\Pi^{\alpha}(\xi)$, and here the axis of rotation is written as $W_{\alpha}(\xi)=w_1\overrightarrow{\alpha(\xi)}$. Barely, we can carry any point in $\mathbf{Q}^2$ to the α −axis using some expressions, we can suppose that the curve δ_{α} lies on α −axis. Therefore, we can give one of its parametrizations as follows

$$\delta_{\alpha}(t)=(0,at+b,0), a\neq 1, b\in\mathbb{R}_0.$$

Namely, the rotated surface $\Lambda^{\alpha}_{W_{\alpha}}$ around W_{α} can be parametrized by

$$\Lambda^{\alpha}(\xi,t)=\Pi^{\alpha}(\xi)\times\begin{bmatrix}0\\ at+b\\ 0\end{bmatrix}$$

$$=((\frac{2\kappa\sinh(w_1\xi)}{w_1^3}+\frac{2\kappa\cosh(w_1\xi)}{w_1}-1-\frac{\xi}{w_1^2}-\frac{\xi^2}{2!}+w_1e^{w_1\xi}+(\frac{4\kappa^2\xi^5}{5!}+\dots))(at+b),$$

$$(\cosh(\sqrt{2\kappa}\xi)+\frac{2\kappa w_1^2\xi^4}{4!}+\dots)(at+b),$$

$$(\frac{\kappa e^{w_1\xi}}{w_1}-2\kappa^2\sinh(\sqrt{2\kappa}\xi)+(\frac{-4(\kappa w_1)^2\xi^5}{5!}+\dots))(at+b)); \quad -\infty<\xi<\infty, t\in I.$$

Hence, we have researched the rotated surface Λ^{α} without loss of generality we suppose that $\xi, t = 0$. Then, we get the first and second fundamental forms as follows

$$E = b^2\left(\left(\frac{2\kappa-1}{w_1^2}+\frac{2\kappa'}{w_1}\right)^2-\left(\frac{\kappa'+\kappa w_1}{w_1}+\frac{\sqrt{2}\kappa^2\kappa'}{\sqrt{\kappa}}\right)^2\right),$$

$$F = ab\left(\left(\frac{2\kappa-1}{w_1^2}+\frac{2\kappa'}{w_1}\right)\left(\frac{2\kappa}{w_1}-1+w_1\right)-\frac{\kappa}{w_1}\left(\frac{\kappa'+\kappa w_1}{w_1}+\frac{\sqrt{2}\kappa^2\kappa'}{\sqrt{\kappa}}\right)\right),$$

$$G = a^2\left(\left(\frac{2\kappa}{w_1}-1+w_1\right)^2+1-\left(\frac{\kappa}{w_1}\right)^2\right),$$

$$L = ab^2\left(\begin{array}{l}\left(\frac{\kappa'+\kappa w_1}{w_1}+\frac{\sqrt{2}\kappa^2\kappa'}{\sqrt{\kappa}}\right).\left(\frac{4\kappa'}{w_1^2}+\frac{2\kappa''+2\kappa w_1^2}{w_1}-1+w_1^3-\kappa'\left(\frac{2\kappa}{w_1}-1+w_1\right)\right)\\ +\frac{\kappa'\kappa}{w_1}\left(\frac{2\kappa-1}{w_1^2}+\frac{2\kappa'}{w_1}\right)\end{array}\right),$$

$$M = ba^2\left(\left(\frac{\kappa'+\kappa w_1}{w_1}+\frac{\sqrt{2}\kappa^2\kappa'}{\sqrt{\kappa}}\right)\left(\frac{2}{w_1^2}\right)\right),\ \ N = 0;$$

$$n_{\Lambda_1^{\alpha}} = ab\left(\begin{array}{l}\left(\frac{\kappa'+\kappa w_1}{w_1}+\frac{\sqrt{2}\kappa^2\kappa'}{\sqrt{\kappa}}\right),\\ \left(\frac{\kappa}{w_1}\left(\frac{2\kappa-1}{w_1^2}+\frac{2\kappa'}{w_1}\right)-\left(\frac{2\kappa}{w_1}-1+w_1\right)\left(\frac{\kappa'+\kappa w_1}{w_1}+\frac{\sqrt{2}\kappa^2\kappa'}{\sqrt{\kappa}}\right)\right),\\ \left(\frac{2\kappa-1}{w_1^2}+\frac{2\kappa'}{w_1}\right)\end{array}\right). \tag{8}$$

Hence, these results in the first and second fundamental form are given by

$$I_{\Lambda_1^{\alpha}} = a^2b^2\left(\begin{array}{l}\left(\left(\frac{2\kappa-1}{w_1^2}+\frac{2\kappa'}{w_1}\right)^2-\left(\frac{\kappa'+\kappa w_1}{w_1}+\frac{\sqrt{2}\kappa^2\kappa'}{\sqrt{\kappa}}\right)^2\right).\left(\left(\frac{2\kappa}{w_1}-1+w_1\right)^2+1-\left(\frac{\kappa}{w_1}\right)^2\right)\\ -\left(\left(\frac{2\kappa-1}{w_1^2}+\frac{2\kappa'}{w_1}\right)\left(\frac{2\kappa}{w_1}-1+w_1\right)-\frac{\kappa}{w_1}\left(\frac{\kappa'+\kappa w_1}{w_1}+\frac{\sqrt{2}\kappa^2\kappa'}{\sqrt{\kappa}}\right)\right)^2\end{array}\right) = a^2b^2\zeta_1$$

$$II_{\Lambda_1^{\alpha}} = -b^2a^4\left(\left(\frac{\kappa'+\kappa w_1}{w_1}+\frac{\sqrt{2}\kappa^2\kappa'}{\sqrt{\kappa}}\right)\left(\frac{2}{w_1^2}\right)\right)^2.$$

So, by using formulas, we obtain the Gaussian and the mean curvatures as follows

$$K = \frac{-\left(\left(\frac{\kappa'+\kappa w_1}{w_1}+\frac{\sqrt{2}\kappa^2\kappa'}{\sqrt{\kappa}}\right)\left(\frac{2}{w_1^2}\right)\right)^2}{b\zeta_1};$$

.

$$H=\frac{-a}{2\xi_1}\begin{pmatrix}\left(\frac{\kappa^{'}+\kappa w_1}{w_1}+\frac{\sqrt{2}\kappa^2\kappa^{'}}{\sqrt{\kappa}}\right)\\ \left(\frac{4\kappa^{'}}{w_1^2}+\frac{2\kappa^{''}+2\kappa w_1^2}{w_1}-1+w_1^3-\kappa^{'}\left(\frac{2\kappa}{w_1}-1\right)\right)\\ +\frac{\kappa^{'}\kappa}{w_1}\left(\frac{2\kappa-1}{w_1^2}+\frac{2\kappa^{'}}{w_{_1}}\right)\end{pmatrix}\left(\left(\frac{2\kappa}{w_1}-1+w_1\right)^2+1-\left(\frac{\kappa}{w_{_1}}\right)^2\right)$$

$$+\frac{4a}{w_1^2\xi_1}\left(\frac{\kappa'+\kappa w_1}{w_1}+\frac{\sqrt{2}\kappa^2\kappa'}{\sqrt{\kappa}}\right)\left(\left(\frac{2\kappa-1}{w_1^2}+\frac{2\kappa'}{w_{_1}}\right)\left(\frac{2\kappa}{w_1}-1+w_1\right)-\frac{\kappa}{w_{_1}}\left(\frac{\kappa'+\kappa w_1}{w_1}+\frac{\sqrt{2}\kappa^2\kappa'}{\sqrt{\kappa}}\right)\right).$$

If κ =constant, we can give the following equations for K and H,

$$E=b^2\left(\left(\frac{2\kappa-1}{w_1^2}+w_{_1}^2\right)^2-\kappa^2(1-2\kappa\sqrt{2\kappa})^2\right),$$

$$F=\left(\frac{2\kappa-1}{w_1^2}+w_{_1}^2\right)\left(\frac{2\kappa}{w_{_1}}-1+w_{_1}\right)-\frac{\kappa^2}{w_1}(1-2\kappa\sqrt{2\kappa})b,$$

$$G=\left(\frac{2\kappa}{w_{_1}}+w_{_1}-1\right)^2+1-\left(\frac{\kappa}{w_{_1}}\right)^2,$$

$$L=b^2\kappa(2\kappa w_{_1}-1+w_{_1}^3)(1-2\kappa\sqrt{2\kappa})$$

$$+2\kappa^2b^2\left(\frac{1}{w_1}\left(\frac{2\kappa-1}{w_1^2}+w_{_1}^2\right)-(1-2\kappa\sqrt{2\kappa})\left(\frac{2\kappa}{w_{_1}}+w_{_1}-1\right)\right)$$

$$-\kappa b^2w_1\left(\frac{2\kappa-1}{w_1^2}+w_{_1}^2\right));\ M=2b\kappa^2\sqrt{2\kappa}\left(\frac{2\kappa-1}{w_1^2}+w_{_1}^2\right);\quad N=0;$$

$$n_{\Lambda_2^\alpha}=b\begin{pmatrix}\kappa(1-2\kappa\sqrt{2\kappa}),\\ \kappa\left(\frac{1}{w_1}\left(\frac{2\kappa-1}{w_1^2}+w_{_1}^2\right)-(1-2\kappa\sqrt{2\kappa})\left(\frac{2\kappa}{w_{_1}}+w_{_1}-1\right)\right),\\ \left(\frac{2\kappa-1}{w_1^2}+w_{_1}^2\right)\end{pmatrix}.$$

And, these results in the first and the second fundamental form are given by

$$I_{\Lambda_2^\alpha}=\begin{pmatrix}b^2\left(\left(\frac{2\kappa-1}{w_1^2}+w_{_1}^2\right)^2-\kappa^2(1-2\kappa\sqrt{2\kappa})^2\right).\left(\left(\frac{2\kappa-1}{w_1^2}+w_{_1}^2\right)\left(\frac{2\kappa}{w_{_1}}-1+w_{_1}\right)-\frac{\kappa^2}{w_1}\right)\\ -\left(\left(\frac{2\kappa-1}{w_1^2}+w_{_1}^2\right)\left(\frac{2\kappa}{w_{_1}}-1+w_{_1}\right)-\frac{\kappa^2}{w_1}(1-2\kappa\sqrt{2\kappa})b\right)^2\end{pmatrix}=\zeta_2$$

$$II_{\Lambda_2^\alpha}=-8b^2\kappa^5\left(\frac{2\kappa-1}{w_1^2}+w_{_1}^2\right)^2=\xi_3.$$

By using formulas $K = \frac{LN-M^2}{EG-F^2}$, $H = -\frac{1}{2}\frac{LG-2MF+NE}{EG-F^2}$, we have the Gaussian and mean curvatures as follows

$$K = \frac{\xi_3}{\zeta_2},$$

$$H = \frac{-1}{2\zeta_2}\begin{pmatrix} \begin{pmatrix} b^2\kappa(2\kappa w_1 - 1 + w_1^3)(1-2\kappa\sqrt{2\kappa}) \\ +2\kappa^2 b^2 \begin{pmatrix} \frac{1}{w_1}(\frac{2\kappa-1}{w_1^2} + w_1^2) \\ -(1-2\kappa\sqrt{2\kappa})(\frac{2\kappa}{w_1} + w_1 - 1) \end{pmatrix} \\ -\kappa b^2 w_1(\frac{2\kappa-1}{w_1^2} + w_1^2)) \end{pmatrix}. \\ \left((\frac{2\kappa}{w_1} + w_1 - 1)^2 + 1 - \left(\frac{\kappa}{w_1}\right)^2\right) \\ -2\begin{pmatrix} \left(\frac{2\kappa-1}{w_1^2} + w_1^2\right)\left(\frac{2\kappa}{w_1} - 1 + w_1\right) \\ -\frac{\kappa^2}{w_1}(1-2\kappa\sqrt{2\kappa})b \end{pmatrix}. \\ \left(2b\kappa^2\sqrt{2\kappa}(\frac{2\kappa-1}{w_1^2} + w_1^2)\right) \end{pmatrix} = \frac{-\xi_4}{2\zeta_2}.$$

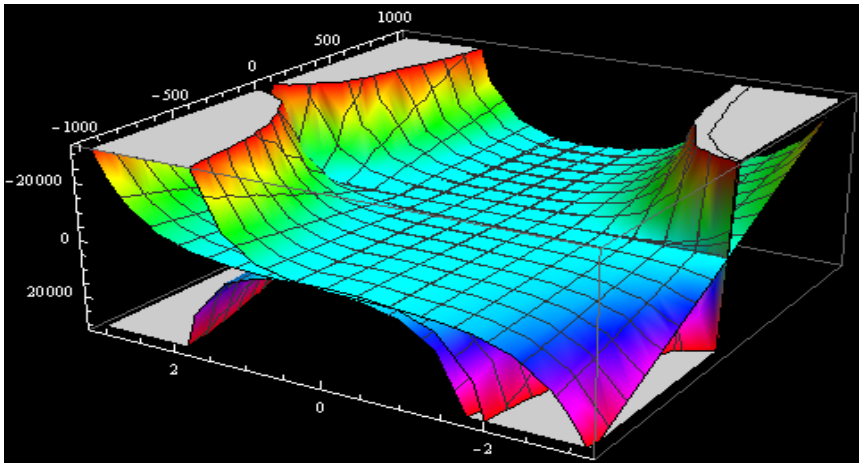

Figure 1: The α − magnetic surface formed by the W_α trajectory

4.1. The Clairaut's Theorem on magnetic surface generated by α −magnetic curve in $\mathbf{Q^2} \subset \boldsymbol{E_1^3}$

In this section, Clairaut's theorem is given on magnetic surface generated by α −magnetic curve in $\mathbf{Q}^2 \subset E_1^3$. Also, the general equations of geodesics on surface formed by an α −magnetic curve in $\mathbf{Q}^2$ are expressed.

Theorem 6. Let $\Lambda^\alpha(\xi, t)$ be the α −magnetic surface generated by α −magnetic curve and let $\delta_\alpha(t): I \subset \mathbb{R} \to \boldsymbol{Q}^2$ be a regular curve in $\boldsymbol{Q}^2$. Then the following statements are held

1. For $h(\xi)$ =constant, the following equation supplies

$$0 = \begin{pmatrix} \frac{4}{w_1^3}(\sinh^2(w_1\xi) + \cosh^2(w_1\xi)) - 2(\frac{f'}{w_1^3} + f)\sinh(w_1\xi) \\ -2\cosh(w_1\xi)(\frac{f'}{w_1} + \frac{f}{w_1^2}) + \frac{\sqrt{2}}{2}\sin(2\sqrt{2}\xi) + g'\cos(\sqrt{2}\xi) \\ -\sqrt{2}g\sin(\sqrt{2}\xi) + 2(\frac{1}{w_1^5} + \frac{1}{w_1})\sinh(2w_1\xi) + ff' + gg' \end{pmatrix}.$$

Hence, the Lagrange equation on the magnetic surface $\Lambda^\alpha(\xi, t)$ is given by

$$E(\xi, t)\dot{\xi}^2 + G(\xi)\dot{t}^2 = L.$$

2. The curve $\delta(s) = \Lambda^\alpha(\xi(s), t(s))$ is a geodesic on the surface $\Lambda^\alpha(\xi, t)$ if and only if the following equations satisfy

$$\xi = \int \frac{\cos\theta}{at+b} ds + c_8 \left(\text{or } \xi = \int \frac{\cos\theta}{at+b} ds\right),\ 2\int E(\xi, t)d\xi = c_5 s + c_6,$$

$$0 = 2G(\xi)\dot{t} - \left\{\int \frac{\partial E(\xi,t)}{\partial t}\dot{\xi} ds + c_4\right\},$$

or

$$t = \int \sin\theta ds (\text{or } t = \int \sin\theta ds + c_3),\ t = \frac{c_1 s}{2G(\xi)} + c_2,$$

$$2E(\xi, t)\ddot{\xi} = G_\xi \dot{t}^2 - E_\xi \dot{\xi}^2,$$

where $c_i \in \mathbb{R}_0$.

Proof. Let $\Lambda^\alpha(\xi, t)$ be the magnetic surface generated by α −magnetic curve and let $\delta_\alpha(t): I \subset \mathbb{R} \to \mathbf{Q}^2$ be a regular curve in $\mathbf{Q}^2$ are parametrized by

$$\Lambda^\alpha(\xi, t) = \begin{pmatrix} (\frac{2\kappa sinh(w_1\xi)}{w_1^3} + \frac{2\kappa cosh(w_1\xi)}{w_1} + f(\xi))(at + b), \\ (cosh(\sqrt{2\kappa}\xi) + g(\xi))(at + b), \\ (\frac{\kappa e^{w_1\xi}}{w_1} - 2\kappa^2 sinh(\sqrt{2\kappa}\xi) + h(\xi))(at + b)); \end{pmatrix},$$

where

$$f(\xi) = -1 - \frac{\xi}{w_1^2} - \frac{\xi^2}{2!} + w_1 e^{w_1\xi} + \frac{4\kappa^2\xi^5}{5!} + \cdots, \tag{9}$$

$$g(\xi) = \frac{2\kappa w_1^2 \xi^4}{4!} + \ldots; h(\xi) = \frac{-4(\kappa w_1)^2 \xi^5}{5!} + \ldots$$

Also,

$$\Lambda_{\xi}^{\alpha}=\left\{\begin{array}{l}\left(\begin{array}{l}\left(\frac{2\kappa'}{w_1^3}+2\kappa\right)\sinh(w_1\xi)\\+\left(\frac{2\kappa}{w_1^2}+\frac{2\kappa'}{w_1}\right)\cosh(w_1\xi)+f'(\xi)\end{array}\right)(at+b),\\\left(\left(\sqrt{2\kappa}+\frac{\sqrt{2}\kappa'}{2\sqrt{\kappa}}\xi\right)\sinh(\sqrt{2\kappa}\xi)+g'(\xi)\right)(at+b),\\\left(\begin{array}{l}-4\kappa\kappa'\sinh(\sqrt{2\kappa}\xi)\\-2\kappa'\left(\sqrt{2\kappa}+\frac{\sqrt{2}\kappa'}{2\sqrt{\kappa}}\xi\right)\cosh(\sqrt{2\kappa}\xi)+h'(\xi)\end{array}\right)(at+b)\end{array}\right\}=(at+b)N_{\xi},$$

$$\Lambda_{t}^{\alpha}=\left(\begin{array}{l}(\frac{2\kappa\sinh(w_1\xi)}{w_1^3}+\frac{2\kappa\cosh(w_1\xi)}{w_1}+f(\xi))a,\\(\cosh(\sqrt{2\kappa}\xi)+g(\xi))a,\\(\frac{\kappa e^{w_1\xi}}{w_1}-2\kappa^2\sinh(\sqrt{2\kappa}\xi)+h(\xi))a;\end{array}\right)=N_t.$$

Hence, we have

$$E(\xi,t)=(at+b)^2\left(\begin{array}{l}A^2\sinh^2(w_1\xi)+2A\sinh(w_1\xi)\big(B\cosh(w_1\xi)+f'(\xi)\big)\\+B^2\cosh^2(w_1\xi)+2B\cosh(w_1\xi)f'(\xi)+f'^2(\xi)\\+(C^2-16\kappa^2\kappa')\sinh^2\big(\sqrt{2\kappa}\xi\big)+2C\sinh\big(\sqrt{2\kappa}\xi\big)g'(\xi)\\+g'^2(\xi)+8\kappa\kappa'\sinh\big(\sqrt{2\kappa}\xi\big)\Big(h'(\xi)-2\kappa'C\cosh\big(\sqrt{2\kappa}\xi\big)\Big)\\-h'^2(\xi)+4\kappa'C\cosh\big(\sqrt{2\kappa}\xi\big)-4\kappa'^2C^2\cosh^2\big(\sqrt{2\kappa}\xi\big)\end{array}\right),$$

$$E(\xi,t)=P(t)N(\xi),$$

where $A=\frac{2\kappa'}{w_1^3}+2\kappa, B=\frac{2\kappa}{w_1^2}+\frac{2\kappa'}{w_1}, C=\sqrt{2\kappa}+\frac{\sqrt{2}\kappa'}{2\sqrt{\kappa}}\xi.$

$$G(\xi)=a\left(\begin{array}{l}\frac{4\kappa^2}{w_1^6}\sinh^2(w_1\xi)+\frac{2\kappa}{w_1^3}\sinh(w_1\xi)\left(\frac{2\kappa}{w_1}\cosh(w_1\xi)+f(\xi)\right)\\+\frac{4\kappa^2}{w_1^2}\cosh^2(w_1\xi)+\frac{4\kappa}{w_1}f(\xi)\cosh(w_1\xi)+f^2(\xi)\\+\cosh^2(\sqrt{2\kappa}\xi)+2g(\xi)\cosh(\sqrt{2\kappa}\xi)+g^2(\xi)\\-4\kappa^4\sinh^2(\sqrt{2\kappa}\xi)+4\kappa^2\sinh(\sqrt{2\kappa}\xi)h(\xi)-h^2(\xi)\end{array}\right),\tag{10}$$

for the following equation

$$h(\xi)=\text{constant},$$

$$0=\left(\begin{array}{l}\frac{4}{w_1^3}(\sinh^2(w_1\xi)+\cosh^2(w_1\xi))\\-2\left(\frac{f'}{w_1^3}+f\right)\sinh(w_1\xi)-2\cosh(w_1\xi)\left(\frac{f'}{w_1}+\frac{f}{w_1^2}\right)\\+\frac{\sqrt{2}}{2}\sin\big(2\sqrt{2}\xi\big)+g'\cos\big(\sqrt{2}\xi\big)-\sqrt{2}g\sin\big(\sqrt{2}\xi\big)\\+2\left(\frac{1}{w_1^5}+\frac{1}{w_1}\right)\sinh(2w_1\xi)+ff'+gg'\end{array}\right),\tag{11}$$

where for the α −magnetic curve, we have $\kappa = -1, \frac{1}{w_1} = c$, we obtain $F(\xi) = 0$. Thus, the first fundamental form is given by

$$I = \begin{pmatrix} E(\xi,t) & 0 \\ 0 & G(\xi) \end{pmatrix}. \tag{12}$$

Moreover, it is important to note that, the coordinates of parametrization are orthogonal, since the first fundamental form is diagonal. So, from the first fundamental form, we have the Lagrangian equation given by

$$E(\xi,t)d^2\xi + G(\xi)d^2t = L \text{ or } E(\xi,t)\dot{\xi}^2 + G(\xi)\dot{t}^2 = L, \tag{13}$$

and a geodesic on the surface $\Lambda^\alpha(\xi,t)$ is given by the Euler-Lagrangian equations,

$$\frac{\partial}{\partial s}\left(\frac{\partial L}{\frac{\partial \xi}{\partial s}}\right) = \frac{\partial L}{\partial \xi}; \frac{\partial}{\partial s}\left(\frac{\partial L}{\frac{\partial t}{\partial s}}\right) = \frac{\partial L}{\partial t}.$$

i) For the equation

$$2E(\xi,t)\ddot{\xi} = G_\xi \dot{t}^2 - E_\xi \dot{\xi}^2, \tag{14}$$

and from the equation $\frac{\partial}{\partial s}\left(\frac{\partial L}{\frac{\partial t}{\partial s}}\right) = \frac{\partial L}{\partial t} = 0$, we obtain $\frac{\partial}{\partial s}\left(2G(\xi)\dot{t}\right) = 0$, which means $2G(\xi)\dot{t}$ is constant along the geodesic and we have

$$t = \frac{c_1 s}{2G(\xi)} + c_2. \tag{15}$$

Let δ_α be a geodesic on the surface $\Lambda^\alpha(\xi,t)$, so the curve is written as $(\xi(s), t(s))$, also let θ be the angle between $\dot{\delta}_\alpha$ and a meridian and N_ξ is the vector pointing along meridians of Λ^α and N_t is the vector pointing along meridians of Λ^α. We can say that $\{N_\xi, N_t\}$ orthonormal basis and hence a unit vector $\dot{\delta}$ tangent to $\Lambda^\alpha(\xi,t)$ can be written by

$$\dot{\delta} = \dot{\xi}\Lambda^\alpha_\xi + \dot{t}\Lambda^\alpha_t = N_\xi \cos\theta + N_t \sin\theta = \dot{\xi}(at+b)N_\xi + \dot{t}N_t.$$

We see that $\dot{t} = \sin\theta$, hence we write

$$2G(\xi)\dot{t} = 2G(\xi)\sin\theta \tag{16}$$

being a constant along δ_α. On the contrary, let δ be $\alpha-$magnetic curve with $2G(\xi)\dot{t} = 2G(\xi)\sin\theta$ is a constant. Hence, the second Euler-Lagrange equation is satisfied, differentiating L and substituting this into the first equation yields the first Euler-Lagrange equation. Furthermore, we can also write

$$t = \int \sin\theta ds \text{ or } t = \int \sin\theta ds + c_3. \tag{17}$$

ii) For the equation

$$2G(\xi)\dot{t} - \left\{\int \frac{\partial E(\xi,t)}{\partial t}\dot{\xi}ds + c_4\right\} = 0, \tag{18}$$

from the equation $\frac{\partial}{\partial s}\left(\frac{\partial L}{\frac{\partial w}{\partial s}}\right) = \frac{\partial L}{\partial w} = 0$, we obtain $\frac{\partial L}{\frac{\partial w}{\partial s}} = 2E(\xi,t)\dot{\xi}$ is constant and which means

$$2\int E(\xi,t)d\xi = c_5 s + c_6,$$

which has a constant along the geodesic. We see that $(at+b)\dot{\xi} = \cos\theta$, hence we write

$$2E(\xi,t)\dot{\xi} = \frac{2E(\xi,t)}{at+b}\cos\theta, \tag{19}$$

being a constant along δ_α. On the contrary, δ_α is a curve with $2E(\xi,t)\dot{\xi} = \frac{2E(\xi,t)}{at+b}\cos\theta$ that it is a constant. Hence, the first Euler-Lagrange equation is satisfied, differentiating L and substituting this into the second equation yields the second Euler-Lagrange equation. Furthermore, we can write equation as follows

$$\xi = \int \frac{\cos\theta}{at+b}ds \text{ or } \xi = \int \frac{\cos\theta}{at+b}ds + c_8. \tag{20}$$

Theorem 7. The general equations of geodesics on the surface generated by an $\alpha-$magnetic curve in $\boldsymbol{Q}^2$ are given by

i) For the parameter $\xi = \int \frac{cos\theta}{at+b}ds + c_8$ (or $\xi = \int \frac{cos\theta}{at+b}ds$) and the equations $2\int E(\xi,t)d\xi = c_5 s + c_6$, $2G(\xi)\dot{t} - \left\{\int \frac{\partial E(\xi,t)}{\partial t}\dot{\xi}ds + c_4\right\} = 0$, *the following equation holds*

$$\frac{dt}{d\xi} = c_{11}\sqrt{\frac{E(\xi,t)}{G(\xi)}}\sqrt{LE(\xi,t) - c_{10}} = \frac{at+b}{\sqrt{G(\xi)}\cos\theta}\sqrt{L - \frac{E(\xi,t)\cos^2\theta}{at+b}}.$$

ii) For the parameters $t = \int sin\theta ds$ $(or\ t = \int sin\theta ds + c_3)$ or $t = \frac{c_1 s}{2G(\xi)} + c_2$ and the equation $2E(\xi,t)\ddot{\xi} = G_\xi \dot{t}^2 - E_\xi \dot{\xi}^2$, the following equation holds

$$\frac{d\xi}{dt} = c_1 G(\xi)\sqrt{\frac{G(\xi)\varepsilon - c_2}{E(\xi,t)G(\xi)}} = \frac{1}{sin\theta}\sqrt{\frac{\varepsilon - G(\xi)sin^2\theta}{E(\xi,t)}},$$

where $c_i \in \mathbb{R}_0, i \in I$.

Proof. In order to obtain the general equation of geodesics, we should use the Euler Lagrange equations,

i) For the parameters $\xi = \int \frac{\cos\theta}{at+b} ds + c_8$ (or $\xi = \int \frac{\cos\theta}{at+b} ds$) and the equations $2\int E(\xi,t)d\xi = c_5 s + c_6$,

$$2G(\xi)\dot{t} - \left\{\int \frac{\partial E(\xi,t)}{\partial t}\dot{\xi} ds + c_4\right\} = 0,$$

we have $\frac{\partial}{\partial s}\left(\frac{\partial L}{\frac{\partial t}{\partial s}}\right) = \frac{\partial L}{\partial t} \neq 0$ and $\frac{\partial}{\partial s}\left(\frac{\partial L}{\frac{\partial \xi}{\partial s}}\right) = \frac{\partial L}{\partial \xi} = 0$. From the solving of the second Lagrangian equation, we get $\frac{\partial}{\partial s}\left(2E(\xi,t)\dot{\xi}\right) = 0$, which means $\frac{d\xi}{ds} = \frac{c_5}{2E(\xi,t)}$.

If we put the value of $\dot{\xi}$ at $E(\xi,t)\dot{\xi}^2 + G(\xi)\dot{t}^2 = L$,

$$E(\xi,t)\left(\frac{d\xi}{ds}\right)^2 + G(\xi)\left(\frac{dt}{d\xi}\frac{d\xi}{ds}\right)^2 = L, \tag{21}$$

we obtain the general equation of geodesics on $\Lambda^\alpha(\xi,t)$ as follow

$$\frac{dt}{d\xi} = c_{11}\sqrt{\frac{E(\xi,t)}{G(\xi)}}\sqrt{LE(\xi,t) - c_{10}} \quad or \quad \frac{dt}{d\xi} = \frac{at+b}{\sqrt{G(\xi)}\cos\theta}\sqrt{L - \frac{E(\xi,t)\cos^2\theta}{at+b}}. \tag{22}$$

ii) For the parameters $t = \int \sin\theta ds$ (or $t = \int \sin\theta ds + c_7$) or $t = \frac{c_5 s}{2G(\xi)} + c_6$ and the equation

$$2E(\xi,t)\ddot{\xi} = G_\xi \dot{t}^2 - E_\xi \dot{\xi}^2, \tag{23}$$

since $\frac{\partial}{\partial s}\left(\frac{\partial L}{\frac{\partial \xi}{\partial s}}\right) = \frac{\partial L}{\partial \xi} \neq 0$ and from the solving of the differential equations in $\frac{\partial}{\partial s}\left(\frac{\partial L}{\frac{\partial t}{\partial s}}\right) = \frac{\partial L}{\partial t} = 0$,

$$\dot{t} = \sin\theta \text{ or } \dot{t} = \frac{c_1}{2G(\xi)},$$

using equations $\frac{\partial}{\partial s}\left(\frac{\partial L}{\frac{\partial t}{\partial s}}\right) = \frac{\partial L}{\partial t}$, we have $\frac{\partial}{\partial s}\left(2G(\xi)\dot{t}\right) = 0$, which means

$$\frac{dt}{ds} = \frac{c_1}{2G(\xi)}. \tag{24}$$

If we put the value of $\dot{t}$ at $E(\xi,t)\dot{\xi}^2 + G(\xi)\dot{t}^2 = L$,

$$E(\xi,t)\left(\frac{d\xi}{dt}\frac{dt}{ds}\right)^2 + G(\xi)\left(\frac{dt}{ds}\right)^2 = L, \tag{25}$$

we can obtain the general equation of geodesics on $\Lambda^\alpha(\xi,t)$ as follow

$$\frac{d\xi}{dt} = c_1 G(\xi)\sqrt{\frac{G(\xi)L - c_2}{E(\xi,t)G(\xi)}} \quad or \quad \frac{d\xi}{dt} = \frac{1}{\sin\theta}\sqrt{\frac{L - G(\xi)\sin^2\theta}{E(\xi,t)}}. \tag{26}$$

5. The Physical Approach on α −magnetic Surface in $\mathbf{Q^2} \subset \boldsymbol{E_1^3}$

In this section, we try to express as the point of view of a physicist to imagine tracing out a geodesic by determining the affine parameter s with the time, thinking that the picture is now of a point particle that is moving on the surface, tracing out a path called the orbit of the particle.

Let $\Lambda^\alpha(\xi(s),t(s))$ be a parametrized curve on surface as

$$\Lambda^\alpha(\xi(s),t(s)) = \begin{pmatrix} (\frac{2\kappa\sinh(w_1\xi)}{w_1^3} + \frac{2\kappa\cosh(w_1\xi)}{w_1} + f(\xi))(at+b), \\ (\cosh(\sqrt{2\kappa}\xi) + g(\xi))(at+b), \\ (\frac{\kappa e^{w_1\xi}}{w_1} - 2\kappa^2\sinh(\sqrt{2\kappa}\xi) + h(\xi))(at+b)) \end{pmatrix}.$$

Also, the Lagrange equation on $\Lambda^\alpha(\xi,t)$ the magnetic surface is given as follows

$$E(\xi,t)\dot{\xi}^2 + G(\xi)\dot{t}^2 = L.$$

Furthermore, the tangent vector to this curve can be obtained using the chain rule as follow

$$\dot{\delta} = \frac{d\Lambda^\alpha(\xi(s),t(s))}{ds} = \frac{d\xi(s)}{ds}\Lambda^\alpha_\xi + \frac{dt(s)}{ds}\Lambda^\alpha_t = N_\xi\cos\theta + N_t\sin\theta$$

$$= \dot{\xi}\Lambda^\alpha_\xi + \dot{t}\Lambda^\alpha_t = \dot{\xi}(at+b)N_\xi + \dot{t}N_t. \tag{27}$$

Hence, we can write the tangent vector of the geodesic curve as follows

$$\vec{Y} = \frac{d\Lambda^\alpha(\xi(s),t(s))}{ds} = Y^\xi\Lambda^\alpha_\xi + Y^t\Lambda^\alpha_t \tag{28}$$

and we can also write with two component vector notation for components according to the basis vectors $\Lambda^\alpha_t, \Lambda^\alpha_\xi$ and its norm $Y = \langle\vec{Y},\vec{Y}\rangle^{1/2} = \sqrt{g_{ij}\frac{dz^i}{ds}\frac{dz^j}{ds}}$ is the speed, which is just the time rate

of change of the arc length along the curve δ. Think that $Y^{\xi^*} = \sqrt{E(\xi,t)}Y^{\xi} = Y\cos\theta$ is just the radial velocity while Y^{ξ} is the horizontal angular velocity and $Y^{t^*} = \sqrt{G(\xi)}Y^{t} = Y\sin\theta$ is the vertical component of the velocity vector. Hence, we can give the velocity in terms of polar coordinates in the tangent plane to explain its magnitude and slope angle according to the radial direction on the surface.

The role of the radial variable on this velocity plane is played by the speed, here we can say that the direction of the velocity according to the direction $\Lambda^{\alpha}_{t^*}$ on this plane is given by the angle θ. Also, we can say that the speed is constant along the geodesic. In [20, 21], to find out the system of two second order geodesic equations it is expressed that a standard physics technique of partially can be used integrating them by anyone and so lessen them to two first order equations by taking two constants of the movement that it comes out from the two independent symmetries of the equations of movement. Those physical properties as energy and momentum are replaced by the specificquantities found by partitioning out the mass. Therefore, we can write the specific kinetic energy as follows

$$E = \frac{1}{2}Y^2 = \frac{1}{2}E(\xi,t)\left(\frac{d\xi}{ds}\right)^2 + \frac{1}{2}G(\xi)\left(\frac{dt}{ds}\right)^2 = \frac{1}{2}(Y^2\cos^2\theta + Y^2\sin^2\theta), \tag{29}$$

using the right side of the previous equations we can say that both the specific energy and speed have to be constant along geodesic.

In the point of view of the physics, the specific kinetic energy of the particle is constant because of its motion in space, and only accelerates perpendicular to the surface. If a force is accountable for this acceleration, that is to say that the normal force that it supplies the particle on the surface, because of perpendicular to the velocity of the particle it wouldn't study on the particle. Therefore, the specific energy E has to be constant. Resembling, we say that the speed $Y = \sqrt{2E}$ is constant along a geodesic in respect of this cause.

Theorem 8. Let $\Lambda^{\alpha}(\xi,t)$ be the magnetic surface generated by α −magnetic curve. Then the specific kinetic energy of the particle on the α −magnetic surface $\Lambda^{\alpha}(\xi,t)$ is constant under evident conditions and the following statements are held:

1. For the parameter $t = \int sin\theta ds$ $\left(\text{or } t = \frac{c_1 s}{2G(\xi)} + c_2\right)$ and the equation $2E(\xi,t)\ddot{\xi} = G_{\xi}\dot{t}^2 - E_{\xi}\dot{\xi}^2$, the specific angular momentum ℓ_1 and specific kinetic energy E^1 are constants along a geodesic, and are given as following equations

$$\ell_1 = \sqrt{G(\xi)}Y\sin\theta;\ E^1 = \frac{1}{2}\left(E(\xi,t)\left(\frac{d\xi}{ds}\right)^2 + \frac{\ell_1^2}{G(\xi)}\right). \tag{30}$$

2. For the parameter $\xi = \int \frac{cos\theta}{at+b}ds$ and the equations $2\int E(\xi,t)d\xi = c_5 s + c_6$, $2G(\xi)\dot{t} - \left\{\int \frac{\partial E(\xi,t)}{\partial t}\dot{\xi}ds + c_4\right\} = 0$, the specific angular momentum ℓ_2 and specific kinetic energy E^2 are constant along a geodesic, and are given as follows

$$\ell_2 = -\sqrt{E(\xi,t)}Ycos\theta;\ E^2 = \frac{1}{2}\left(\frac{\ell_2^2}{E(\xi,t)} + G(\xi)\left(\frac{dt}{ds}\right)^2\right), \tag{31}$$

where $c_i \in \mathbb{R}_0$, and Y is the tangent vector of the geodesic curve.

Proof. 1) For the equation $\mathrm{t} = \int \sin\theta \mathrm{ds}\left(\text{or } \mathrm{t} = \frac{\mathrm{c_1 s}}{2\mathrm{G}(\xi)} + \mathrm{c_2}\right)$ and the equation $2\mathrm{E}(\xi,\mathrm{t})\ddot{\xi} = \mathrm{G_\xi}\dot{\mathrm{t}}^2 - \mathrm{E_\xi}\dot{\xi}^2$, we write $2\mathrm{G}(\xi)\dot{\mathrm{t}} = 2\mathrm{G}(\xi)\sin\theta$ being a constant along δ and by using this situation we explain in this physics language. Also, we can explain as to circular motion around an axis with radius $\left\|\overrightarrow{R_1}\right\| = \sqrt{\mathrm{G}(\xi)}$ or $\overrightarrow{R_1} = \sqrt{\mathrm{G}(\xi)}\overrightarrow{e_1}$, namely the velocity $\mathrm{Y^{t^*}} = \sqrt{\mathrm{G}(\xi)}\mathrm{Y^t} = \mathrm{Y}\sin\theta = \sqrt{\mathrm{G}(\xi)}\frac{\mathrm{dt}}{\mathrm{ds}}$ in the angular direction multiplied by the radius $\sqrt{\mathrm{G}(\xi)}$ of the circle. Physically, the specific angular momentum ℓ_1 can be written as following equation

$$\ell_1 = \overrightarrow{e_3}.\left(\overrightarrow{R_1} \times_{G_3} \vec{\mathrm{Y}}\right) = \sqrt{G(\xi)}Y\sin\theta, \tag{32}$$

since $Y^{t^*} = Y\sin\theta = \sqrt{G(\xi)}\frac{dt}{ds}$, we can write $\sqrt{G(\xi)}Y\sin\theta = G(\xi)\frac{dt}{ds}$ being a constant along $\delta(\xi)$, and we say that the specific angular momentum ℓ_1 is constant along a geodesic and we get

$$\ell_1 = G(\xi)\frac{dt}{ds} \Rightarrow \frac{dt}{ds} = \frac{\ell_1}{G(\xi)}. \tag{33}$$

This expression can be rewritten the changeable angular velocity dt/ds in the specific energy formula according to the constant angular momentum, the specific energy E^1 is given as

$$E^1 = \frac{1}{2}(E(\xi,t)\left(\frac{d\xi}{ds}\right)^2 + \frac{\ell_1^2}{G(\xi)}). \tag{34}$$

2) For the parameter $\xi = \int \frac{\cos\theta}{at+b}ds$ and the equations $2\int E(\xi,t)d\xi = c_5 s + c_6$, $2G(\xi)\dot{t} - \left\{\int \frac{\partial E(\xi,t)}{\partial t}\dot{\xi}ds + c_4\right\} = 0$, we write $2E(\xi,t)\dot{\xi} = 2E(\xi,t)\cos\theta$ being a constant along $\delta(\xi)$ and by using this situation we explain in this physics language. Also, we can express as in the case of circular movement round an axis with radius $\left\|\overrightarrow{R_2}\right\| = \sqrt{E(\xi,t)}$ or $\overrightarrow{R_2} = \sqrt{E(\xi,t)}\overrightarrow{e_2}$, that is to say the velocity $Y^{\xi^*} = \sqrt{E(\xi,t)}Y^\xi = Y\cos\theta = \sqrt{E(\xi,t)}\frac{d\xi}{ds}$ in the angular direction

multiplied by the radius $\sqrt{E(\xi,t)}$ of the circle. The first geodesic equation is told that the specific angular momentum is constant along a geodesic, and the specific angular momentum ℓ_2 can be taken down as following equation

$$\ell_2 = \overrightarrow{e_3}.\left(\overrightarrow{R_2} \times_{G_3} \vec{Y}\right) = -\sqrt{E(\xi,t)}Y\cos\theta, \tag{35}$$

since $\sqrt{E(\xi,t)}\frac{d\xi}{ds} = Y\cos\theta$, we can write $-E(\xi,t)\frac{d\xi}{ds} = -\sqrt{E(\xi,t)}Y\cos\theta$, and we say that the specific angular momentum is constant along a geodesic. So, we have

$$\ell_2 = -E(\xi,t)\frac{d\xi}{ds} \Rightarrow \frac{d\xi}{ds} = \frac{-\ell_2}{E(\xi,t)}. \tag{36}$$

Hence, this statement can be rewritten the changeable angular velocity $d\xi/ds$ in the specific energy formula according to the constant angular momentum specific energy E^2 is given by

$$E^2 = \frac{1}{2}\left(\frac{\ell_2^2}{E(\xi,t)} + G(\xi)\left(\frac{dt}{ds}\right)^2\right). \tag{37}$$

6. Conclusion

In this study, the α −magnetic surfaces constituted by using the α −magnetic curves to be geodesics on the surface are expressed. The α −magnetic surfaces generated by the α −magnetic curves are examined, and some certain results of describing the geodesics are given on the surfaces. Our results show that the specific energy and specific angular momentum obtained on the α −magnetic surfaces can be expressed in $\mathbf{Q}^2$. The physical meanings of specific energy and specific angular momentum are of course related with the physical meaning itself. First of all, the conditions of being geodesic of the curves selected as magnetic curves are examined, and these geodesic conditions allows us to express the specific energy. We are working on the properties of these surfaces with a view to devising suitable metric in $\mathbf{Q}^2$. It is hoped that researches will benefit from this study about the rotated surface.

Acknowledgement

The authors wish to express their thanks to the authors of literatures for the supplied scientific aspects and idea for this study. Furthermore, we request to explain great thanks to reviewers for the constructive comments and inputs given to improve the quality of our work.

References

[1] Almaz, F., Kulahci, M.A., *A survey on magnetic curves in 2-dimensional lightlike cone*, Malaya Journal of Matematik, 7(3), 477-485, 2019.

[2] Asperti, A., Dajezer, M., *Conformally Flat Riemannian Manifolds as Hypersurface of the Light Cone*, Canadian Mathematical Bulletin, 32, 281-285, 1989.

[3] Barros, M., Cabrerizo, M.F., Romero, A., *Magnetic Vortex Filament Flows*, Journal of Mathematical Physics, 48, 1-27, 2007.

[4] Barros, M., Romero, A., *Magnetic Vortices*, Europhysics Letters, 77, 1-5, 2007.

[5] Sunada, T., *Magnetic Flows on a Riemannian Surface*, In Proceedings of KAIST Mathematics Workshop, 93-108, 1993.

[6] Bozkurt, Z., Gök, İ., Yaylı, Y., Ekmekci, F.N., *A new approach for magnetic curves in Riemannian 3D-manifolds*, Journal of Mathematical Physics, 55, 1-12, 2014.

[7] Bejan, C.L., Druta-Romaniuc, S.L., *Walker manifolds and Killing magnetic curves*, Differential Geometry and its Applications, 35, 106-116, 2014.

[8] Kruiver, P.P., Dekkers, M.J., Heslop, D., *Quantification of magnetic coercivity componets by the analysis of acquisition*, Earth and Planetary Science Letters, 189(3-4), 269-276, 2001.

[9] Munteanu, M.I., Nistor, A.I., *A note magnetic curves on* S^{2n+1}, Comptes Rendus de l'Académie des Sciences - Series I, 352, 447-449, 2014.

[10] Brinkmann, W.H., *On Riemannian spaces conformal to Euclidean space*, Proceedings of the National Academy of Sciences of the United States of America, 9, 1-3, 1923.

[11] Kuhnel, W., *Differential geometry curves- surfaces and manifolds*, American Mathematical Society, Second Edition, United States of America, 2005.

[12] Kulkarni, D.N., Pinkall, U., *Conformal geometry,* A Publication of the Max-Planck-Institut für Mathematik, Bonn, Aspects of Mathematics, 12, 1988.

[13] Pressley, A., *Elementary differential geometry*, Springer Undergraduate Mathematics Series, Second Edition, Springer-Verlag London, 2010.

[14] Calvaruso, G., Munteanu, M.I., Perrone, A., *Killing magnetic curves in three-dimensional almost paracontact manifolds*, Journal of Mathematical Analysis and Applications, 426, 423-439, 2015.

[15] Druta-Romaniuc, S.L., Munteanu, M.I., *Killing magnetic curves in a Minkowski 3-space*, Nonlinear Analysis Real World Applications, 14, 383-396, 2013.

[16] Kulahci, M., Bektas, M., Ergüt, M., *Curves of AW(k)-type in 3-dimensional null cone*, Physics Letters A, 371, 275-277, 2007.

[17] Kulahci, M., Almaz, F., *Some characterizations of osculating in the lightlike cone*, Boletim da Sociedade Paranaense de Matematica, 35(2), 39-48, 2017.

[18] Liu, H., *Curves in the lightlike cone*, Contributions to Algebra and Geometry, 45(1), 291-303, 2004.

[19] Liu, H., Meng, Q., *Representation formulas of curves in a two- and three-dimensional lightlike cone*, Results in Mathematics, 59, 437-451, 2011.

[20] Walecka, J.D., *Introduction to general relativity*, World Scientific, Singapore, 2007.

[21] Walecka, J.D., *Topics in modern physics: theoretical foundations*, World Scientific, 2013.

[22] Lerner, D., *Lie derivatives, ısometries, and Killing vectors,* Department of Mathematics, University of Kansas, Lawrence, Kansas, 66045-7594, 2010.

Adıyaman University Journal of Science
https://dergipark.org.tr/en/pub/adyujsci
DergiPark AKADEMİK
ISSN 2147-1630
e-ISSN 2146-586X

Some Commutativity Theorems on Lie Ideals of Semiprime Rings

Zeliha BEDİR[1,*], Öznur GÖLBAŞI[2]

[1]*Cumhuriyet University, Faculty of Science, Department of Mathematics, 58140 Sivas, Turkey*
zelihabedir@cumhuriyet.edu.tr, ORCID: 0000-0002-4346-2331
[2]*Cumhuriyet University, Faculty of Science, Department of Mathematics, 58140 Sivas, Turkey*
ogolbasi@cumhuriyet.edu.tr, ORCID: 0000-0002-9338-6170

Received: 25.10.2019 **Accepted:** 02.12.2020 **Published:** 30.12.2020

Abstract

In this paper, we show that any U noncentral square closed Lie ideal of a $2-$torsion free semiprime ring R contains a nonzero ideal. With this result, some theorems will be extended on the multiplicative generalized derivations of Lie ideals of semiprime rings.

***Keywords*:** Semiprime ring; Lie ideal; Multiplicative generalized derivation.

Yarıasal Halkaların Lie İdealleri Üzerinde Bazı Değişmelilik Teoremleri

Öz

Bu çalışmada, $2-$torsion free bir R yarıasal halkasının kare kapalı merkezi olmayan bir U Lie idealinin, halkanın sıfırdan farklı bir idealini kapsadığı gösterilecektir. Ayrıca bu sonuçla, yarı asal halkaların Lie ideallerinin çarpımsal genelleştirilmiş türevleri üzerine bazı teoremler genelleştirilecektir.

***Anahtar Kelimeler*:** Yarıasal halka; Lie ideal; Çarpımsal genelleştirilmiş türev.

* Corresponding Author DOI: 10.37094/adyujsci.638265

1. Introduction

Let R be an assosiative ring with center $Z(R)$. Recall that R is prime if for $a, b \in R$,$aRb = \{0\}$ implies either $a = 0$ and $b = 0$. R is said to be semiprime if for $a \in R$, $aRa = \{0\}$ implies $a = 0$. Let R be a prime ring. For any pair of elements implies either $x, y \in R$, we shall write $[x, y]$ (resp.xoy) for the commutator $xy - yx$ (resp., for the Jordan product $xy + yx$). An additive subgroup L of R is called a Lie ideal of R if $[u, r] \in L$ for all $u \in L$ and $r \in R$. It is clear that if characteristic of R is 2, then Lie ideals of R coincide. Lie ideal U of R is said to be square closed if $u^2 \in U$ for all $u \in U$.

An additive map $d: R \to R$ is called a derivation if $d(xy) = d(x)y + xd(y)$ holds, for all $x, y \in R$. In [1], Bresar introduced the generalized derivation: An additive mapping $F: R \to R$ is called a generalized derivation if there exists a derivation (an associated derivation of F) such that for all $x, y \in R$. The notion a generalized derivation covers both the notions of a derivation and of a left multiplier (i.e., an additive mapping $f: R \to R$ satisfying $f(xy) = f(x)y$, for all $x, y \in R$). R is said to be 2 −torsion-free, if $2x = 0$, $x \in R$ implies $x = 0$.

In the present paper, our main object is to investigate commutativity of semiprime ring satisfying certain differential identities on a nonzero Lie ideal. Let us first recall that the study of commutativity of rings using differential identities goes back to the wellknown Posner's Theorems [2] in which he researched that the presence of a nonzero centralizing derivation d on a prime ring R forces the ring R to be commutative. This result is known by Posner's Second Theorem. Also motivated by this theorem, several authors have introduced new kind of differential identities.

It is important to mention that the study of identities on square closed Lie ideals. Indeed, it is clear that every ideal is a square closed Lie ideal. By [3] Theorem 1.1, every nonzero Jordan ideal of 2-torsion free semiprime rings contains a nonzero ideal. In this paper, we give a similar result for square closed Lie ideals. Then, only the case of ideals could be of interest. Recall the background of study about multiplicative (generalized)-derivations. Firstly, the concept of multiplicative derivation was considered by Daif motivated by Martindale in [4], in the year 1991. Following [5], $d: R \to R$ is called a multiplicative derivation if $d(xy) = xd(y) + d(x)y$ holds for all pairs $x, y \in R$. These maps are not additive. Later, this mapping were completely described in [6]. Inspired by the definition of multiplicative derivation, Daif and Tammam-El-Sayiad defined the notion of multiplicative generalized derivations. Further, the concept of multiplicative derivations was extended to multiplicative generalized derivations for rings by they in [7] as follows: A mapping $F: R \to R$ is called a multiplicative generalized derivation if there exists a

derivation d such that $F(xy) = F(x)y + xd(y)$ holds, for all $x, y \in R$. For completeness of notation, in the present paper, a multiplicative generalized derivation will be denoted by (F, d). A slight generalization of this concept was made by Dhara and Ali [8] by taking d as a mapping (d isn't necessarily a derivation). Therefore, one may find that the definition of multiplicative generalized derivation covers the notion of multiplicative derivation as well as multiplicative left centralizers. The examples of this concepts can be found in [9]. Obviously, any generalized derivation is a multiplicative generalized derivation,but the converse is not true in general (see [8]). So, it should be interesting to extend some results concerning derivations and generalized derivations to multiplicative generalized derivations. However, there are only few papers about this subject (see [2, 6, 10-13]), for a partial bibliography). The main objective of the present paper is to explore the cases when a multiplicative generalized derivation (F, d) satisfies the identities:

i) $F([u_1, u_2]) = \pm u_1, d(u_2)]$,

ii) $F(u_1 o u_2) = \pm(u_1 o d(u_2))$,

iii) $F([u_1, u_2]) = \pm(F(u_2)u_1)$,

iv) $F(u_1 o u_2) = \pm(F(u_2)u_1)$,

for all u_1, u_2 in some appropriate subsets of R. These results investigated by Huang [14]. In this study, these identities are proved without assuming $d(U) \subseteq U$.

In this paper, we will make a lot of calculations with Lie product and Jordan product and mostly use the following identities:

$[u_1u_2, u_3] = u_1[u_2, u_3] + [u_1, u_3]u_2$ and $[u_1, u_2u_3] = u_2[u_1, u_3] + [u_1, u_2]u_3$,

$u_1 o(u_2u_3) = (u_1 o u_2)u_3 - u_2[u_1, u_3] = u_2(u_1 o u_3) + [u_1, u_2]u_3$,

$(u_1u_2)o u_3 = u_1(u_2 o u_3) - [u_1, u_3]u_2 = (u_1 o u_3)u_2 + u_1[u_2, u_3]$.

2. Results

The following Lemmas are required for the proof of our main results.

Lemma 1. [7, Lemma 1.3] Let R be a ring with no non-zero nilpotent ideals in which $2x = 0$ implies $x = 0$. Suppose that $U \neq (0)$ is both a Lie ideal and a subring of R. Then either $U \subseteq Z$, the center of R, or U contains a non-zero ideal of R.

Lemma 2. [15, Lemma 2.1] Let R be a semiprime ring, I be a nonzero two-sided ideal of R and $a \in R$ such that $axa = 0$, for all $x \in I$, then $a = 0$.

Theorem 3. Let R be a 2 −torsion free semiprime ring and U be a noncentral square-closed Lie ideal of R. Then U contains a nonzero ideal of R.

Proof. By the hypothesis, we have $u^2 \in U$, for all $u \in U$. Using this, we obtain that

$$uv + vu = (u + v)^2 - u^2 - v^2 \in U,$$

for all $u, v \in U$. That is,

$$uv + vu \in U, \text{ for all } u, v \in U. \tag{1}$$

On the other hand, using the fact U a Lie ideal of R, then

$$uv - vu \in U, \text{ for all } u, v \in U. \tag{2}$$

Combining Eqn. (1) and Eqn. (2), we arrive at $2uv \in U$, for all $u, v \in U$.

Let define $2U = \{u + u | u \in U\}$. We prove that $2U$ set is subring and Lie ideal of R. Indeed, for all $2u, 2v \in 2U$, we have

$$2u - 2v = 2(u - v) \in 2U$$

and

$$2u2v = (u + u)(v + v) = uv + uv + uv + uv \in 2U.$$

We conclude that $2U$ is a subring of R.

Moreover, for all $2u \in 2U, r \in R$,

$$[2u, r] = [u + u, r] = [u, r] + [u, r] = 2[u, r] \in 2U.$$

Therefore, $2U$ is a Lie ideal of R. Furthermore, $2U \neq (0)$. By Lemma 1, we conclude that $2U \subseteq Z$ or $2U$ contains a nonzero ideal of R.

If $2U \subseteq Z$, then $U \subseteq Z$, which is a contradiction. Hence $2U$ contains a nonzero ideal of R, and so U contains a nonzero ideal of R, since $2U \subseteq U$.

Theorem 4. Let R be a 2 −torsion free semiprime ring and U be a noncentral square-closed Lie ideal of R. If R admits a multiplicative generalized derivation (F, d) satisfying

$$F([u_1, u_2]) = \pm[u_1, d(u_2)], \text{ for all } u_1, u_2 \in U,$$

then there exists a nonzero ideal I of R and d is commuting on I.

Proof. By Theorem 3, R contains a nonzero ideal I such that $I \subseteq U$. By the hypothesis, we get

$$F([u_1, u_2]) = [u_1, d(u_2)], \text{ for all } u_1, u_2 \in I. \quad (3)$$

Replacing u_1 by $u_1 + u_2$ in Eqn. (3), we get

$$F([u_1, u_2] + [u_2, u_2]) = [u_1, d(u_2)] + [u_2, d(u_2)], \text{ for all } u_1, u_2 \in I. \quad (4)$$

Using Eqn. (4) in the above relation yields that

$$[u_2, d(u_2)] = 0, \text{ for all } u_2 \in I. \quad (5)$$

It means that d is commuting on I.

If we have $F([u_1, u_2]) + [u_1, d(u_2)] = 0$, for all $u_1, u_2 \in U$, applying similar approach above with necessary varitions, we get the required result.

Theorem 5. Let R be a 2 −torsion free semiprime ring and U be a noncentral square-closed Lie ideal of R. If R admits a multiplicative generalized derivation (F, d) satisfying

$$F(u_1 o u_2) = \pm\big(u_1 o d(u_2)\big), \text{ for all } u_1, u_2 \in U,$$

then there exists a nonzero ideal I of R and d is commuting on I.

Proof. By Theorem 3, R contains a nonzero ideal I such that $I \subseteq U$. By the hypothesis, we get

$$F(u_1 o u_2) = \big(u_1 o d(u_2)\big), \text{ for all } u_1, u_2 \in I. \quad (6)$$

Taking u_1 by $u_1 u_2$ in Eqn. (6), we have

$$(u_1 o u_2) d(u_2) = u_1 [u_2, d(u_2)], \text{ for all } u_1, u_2 \in I. \quad (7)$$

Replacing u_1 by $d(u_2) u_1$ and using Eqn. (7), we obtain

$$[d(u_2), u_2] u_1 d(u_2) = 0, \text{ for all } u_1, u_2 \in I. \quad (8)$$

Right multiplying by u_2 to the Eqn. (8), we arrive at

$$[d(u_2), u_2]u_1 d(u_2)u_2 = 0 \text{ , for all } u_1, u_2 \in I. \tag{9}$$

Taking u_1 by u_1u_2 in Eqn. (8), we have

$$[d(u_2), u_2]u_1u_2 d(u_2) = 0, \text{ for all } u_1, u_2 \in I. \tag{10}$$

Combining Eqn. (9) and Eqn. (10), we obtain

$$[d(u_2), u_2]I[d(u_2), u_2] = 0, \text{ for all } u_1, u_2 \in I.$$

Thus, using Lemma 2, we achieved the required result.

Also if we have $F(u_1 o u_2) + u_1 o d(u_2) = 0$ for all $u_1, u_2 \in U$, then using the same techniques as used above with necessary variations we get the required result.

Theorem 6. Let R be a $2-$torsion free semiprime ring and U be a noncentral square-closed Lie ideal of R. If R admits a multiplicative generalized derivation (F, d) satisfying

$$F([u_1, u_2]) = \pm(F(u_2)u_1), \text{ for all } u_1, u_2 \in U,$$

then there exists a nonzero ideal I of R and d is commuting on I.

Proof. By Theorem 3, R contains a nonzero ideal I such that $I \subseteq U$. By the hypothesis, we get

$$F([u_1, u_2]) = F(u_2)u_1, \text{ for all } u_1, u_2 \in I. \tag{11}$$

Replacing u_2 by u_2u_1 in Eqn. (11), we get

$$F([u_1, u_2])u_1 + [u_1, u_2]d(u_1) = F(u_2)u_1^2 + u_2 d(u_1)u_1 \text{ , for all } u_1, u_2 \in I. \tag{12}$$

Right multiplying by u_1 to the Eqn. (12), we arrive at

$$F([u_1, u_2])u_1 = F(u_2)u_1^2, \text{ for all } u_1, u_2 \in I. \tag{13}$$

Using last equation in Eqn. (12), we obtain

$$[u_1, u_2]d(u_1) = u_2 d(u_1)u_1, \text{ for all } u_1, u_2 \in I. \tag{14}$$

Writing $d(u_1)u_2$ instead of u_2 in Eqn. (14) and using Eqn. (14), we have

$$[u_1, d(u_1)]u_2 d(u_1) = 0, \text{ for all } u_1, u_2 \in I. \tag{15}$$

This equation is same as Eqn. (8) in the proof of Theorem 5. Applying the same arguments in the proof of Theorem 5, we get the required result.

On the other hand, it is proved analogously using $F([u_1, u_2]) + (F(u_2)u_1) = 0$, for all $u_1, u_2 \in U$.

By using similar methods in this theorem, the following theorem can be proved.

Theorem 7. Let R be a 2 −torsion free semiprime ring and U be a noncentral square-closed Lie ideal of R. If R admits a multiplicative generalized derivation (F, d) satisfying

$F([u_1, u_2]) = \pm(F(u_1)u_2)$, for all $u_1, u_2 \in U$,

then there exists a nonzero ideal I of R and d is commuting on I.

Theorem 8. Let R be a 2 −torsion free semiprime ring and U be a noncentral square-closed Lie ideal of R. If R admits a multiplicative generalized derivation (F, d) satisfying

$F(u_1 o u_2) = \pm(F(u_2)u_1)$, for all $u_1, u_2 \in U$,

then there exists a nonzero ideal I of R and d is commuting on I.

Proof. By Theorem 3, R contains a nonzero ideal I such that $I \subseteq U$. By the hypothesis, we have

$$F(u_1 o u_2) = F(u_2)u_1, \text{ for all } u_1, u_2 \in I. \tag{16}$$

Taking u_2 by $u_2 u_1$ in Eqn. (16) and using this, we get

$$(u_1 o u_2)d(u_1) = u_2 d(u_1)u_1, \text{ for all } u_1, u_2 \in I. \tag{17}$$

Writing $d(u_1)u_2$ instead of u_2 in Eqn. (17), we obtain

$$d(u_1)(u_1 o u_2)d(u_1) + [u_1, d(u_1)]u_2 d(u_1) = d(u_1)u_2 d(u_1)u_1, \text{ for all } u_1, u_2 \in I. \tag{18}$$

Combining Eqn. (17) and Eqn. (18), we arrive at

$[u_1, d(u_1)]u_2 d(u_1) = 0$, for all $u_1, u_2 \in I$.

This equation is same as Eqn. (8) in the proof of Theorem 5. Applying the same arguments in the proof of Theorem 5, we get the required result.

Also if we have $F(u_1 o u_2) + F(u_2)u_1 = 0$, for all $u_1, u_2 \in U$, then in same way, we can prove the same conclusion.

Similary, in view of Theorem 8, we obtain the following result.

Theorem 9. Let R be a 2 −torsion free semiprime ring and U be a noncentral square-closed Lie ideal of R. If R admits a multiplicative generalized derivation (F, d) satisfying

$$F(u_1 o u_2) = \pm(F(u_1)u_2), \text{ for all } u_1, u_2 \in U,$$

then there exists a nonzero ideal I of R and d is commuting on I.

References

[1] Bresar, M., *On the distance of the composition of two derivations to be the generalized derivations*, The Glasgow Mathematical Journal, 33, 89-93, 1991.

[2] Posner, E.C., *Derivations in Prime Rings*, Proceedings of the American Mathematical Society, 8, 1093-1100, 1957.

[3] Herstein, I.N., *Topics in ring theory*, University of Chicago Press, 1969.

[4] Martindale, W.S., *When are multiplicative maps additive*, Proceedings of the American Mathematical Society, 21, 695-698, 1969.

[5] Daif, M.N., *When is a multiplicative derivation additive*, International Journal of Mathematics and Mathematical Sciences, 14(3), 615-618, 1991.

[6] Goldman, H., Semrl, P., *Multiplicative derivations on C(X)*, Monatshefte für Mathematik, 121(3), 189-197, 1969.

[7] Daif, M. N., Tammam El-Sayiad, M.S., *Multiplicative generalized derivations which are additive*, East-West Journal of Mathematics, 9, 31-37, 1997.

[8] Dhara, B., Ali, S., *On multiplicative (generalized)-derivation in prime and semiprime rings*, Aequationes mathematicae, 86, 65-79, 2013.

[9] Eremita, D., Ilisevic, D., *On additivity of centralizers*, Bulletin of the Australian Mathematical Society, 74, 177-184, 2006.

[10] Ali, A., Dhara, B., Ali, F., *Multiplicative (generalized)-derivations and left ideals in semiprime rings*, Hacettepe Journal of Mathematics and Statistics, 44, 1293-1306, 2015.

[11] Ali, S., Dhara, B., Dar, N.A., Khan, A.N., *On Lie ideals with multiplicative (generalized)-derivations in prime and semiprime rings*, Beiträge zur Algebra und Geometrie, 56, 325-337, 2015.

[12] Koç, E., Gölbaşı, Ö., *Multiplicative generalized derivations on Lie ideals in semiprime rings*, Palastine Journal of Mathematics, 6, 219-227, 2017.

[13] Gölbaşı, Ö., *Multiplicative generalized derivations on ideals in semiprime rings*, Mathematica Slovaca, 66, 1285-1296, 2016.

[14] Huang, S., *Derivations on Lie ideals of semiprime rings*, Gulf Journal of Mathematics, 6(3), 25-32, 2018.

[15] Samman, M.S., Alyamani, N., *Derivations on semiprime ring*, International Journal of Pure and Applied Mathematics, 5(4), 469-477, 2003.

Adıyaman University Journal of Science
https://dergipark.org.tr/en/pub/adyujsci
DergiPark AKADEMİK
ISSN 2147-1630
e-ISSN 2146-586X

Estimating the Parameters of Xgamma Weibull Distribution

Kadir KARAKAYA[1,*], Caner TANIŞ[2]

[1]*Selçuk University, Science Faculty, Department of Statistics, Konya, Turkey*
kkarakaya@selcuk.edu.tr, ORCID: 0000-0002-0781-3587
[2]*Çankırı Karatekin University, Science Faculty, Department of Statistics, Çankırı, Turkey*
canertanis@karatekin.edu.tr, ORCID: 0000-0003-0090-1661

Received: 15.08.2020 **Accepted:** 02.12.2020 **Published:** 30.12. 2020

Abstract

In this paper, we consider a comparison of estimation methods for the parameters of Xgamma Weibull distribution. It is discussed five different estimation methods such as maximum likelihood method, least-squares method, weighted least-squares method, the method of Anderson-Darling and the method of Crámer–von-Mises. We compare these estimators via Monte Carlo simulations according to the biases and mean-squared errors (MSEs). Further, seven real data applications are conducted and Kolmogorov Smirnov goodness of fit test is also calculated for all estimators.

***Keywords*:** Xgamma Weibull distribution; Maximum likelihood method; Least-squares method; Weighted least-squares method; Anderson-Darling method; Crámer–von-Mises estimation method.

Xgamma Weibull Dağılımının Parametre Tahmini

Öz

Bu çalışmada, Xgamma Weibull dağılımının parametre tahmini için tahmin yöntemlerinin kıyaslanması problemi ele alınmıştır. En çok olabilirlik yöntemi, en küçük kareler yöntemi, ağırlıklandırılmış en küçük kareler yöntemi, Anderson-Darling yöntemi ve Crámer–von-Mises

* Corresponding Author DOI: 10.37094/adyujsci.781069

yöntemi olmak üzere beş tahmin yöntemi incelenmiştir. Bu beş tahmin yöntemini yan ve hata kareler ortalaması açısından karşılaştırabilmek için bir Monte Carlo simülasyon çalışması yapılmıştır. Ayrıca yedi gerçek veri uygulaması yapılmış ve tüm tahmin ediciler için Kolmogorov Smirnov uyum iyiliği testi hesaplanmıştır.

Anahtar Kelimeler: Xgamma Weibull dağılımı; En çok olabilirlik yöntemi; En küçük kareler yöntemi; Ağırlıklandırılmış en küçük kareler yöntemi; Anderson-Darling yöntemi; Crámer–von-Mises yöntemi.

1. Introduction

Xgamma Weibull distribution was suggested by Yousof et al. in [1] as an alternative Weibull distribution. We denote Xgamma Weibull distribution as $XGW(\theta,b)$. The probability density function (pdf) and cumulative density function (cdf) of $XGW(\theta,b)$ distribution are

$$f(x;\theta,b)=\frac{b\theta^2}{(1+\theta)}x^{b-1}e^{-\theta x^b}\left(1+\frac{1}{2}\theta x^{2b}\right),I_{(0,\infty)}(x) \tag{1}$$

and

$$F(x;\theta,b)=1-\left(1+\theta+\theta x^b+\frac{\theta^2x^{2b}}{2}\right)\frac{e^{-\theta x^b}}{(1+\theta)}, \tag{2}$$

respectively, where $\theta>0$ is a scale parameter, $b>0$ is a shape parameter and $I_{(0,\infty)}(x)$ is an indicator function. In [1], the authors examined some of the statistical properties of $XGW(\theta,b)$ distribution. Yousof et al. [1] concluded that the shape of failure rate function of $XGW(\theta,b)$ distribution can be increasing, decreasing and bathtub. It was also stated that $XGW(\theta,b)$ distribution can be applied for modelling data in economics, medicine, engineering, reliability etc [1].

It is extensively preferred comparison of the methods of estimation regarding distribution by many authors. It is well-known that the generalized exponential distribution is studied in terms of different estimation methods in [2]. In [3], the authors introduced the generalized Rayleigh distribution and also compared the methods of different estimation for this distribution. The different methods of estimation for half-logistic distribution were compared in [4]. Mazucheli et al. [5] examined different estimation methods for weighted Lindley distribution. Different

methods of estimation for two parameter Rayleigh distribution are discussed in [6]. Peng and Yan [7] obtained maximum likelihood estimators and Bayesian estimators for the parameters of an extended Weibull distribution. A new alternative distribution to Weibull distribution was suggested in [8]. The authors also discussed some properties and different estimation methods such as maximum likelihood, ordinary and weighted least squares, percentile and maximum product spacing this new distribution in [8]. The methods of estimation for log-Kumaraswamy distribution were studied in [9]. Afify et al. [10] considered different methods of estimation for Weibull Marshall-Olkin Lindley distribution.

The main purpose of this paper is to compare five different estimators for the parameters of the $XGW(\theta,b)$ distribution via Monte Carlo simulations and real data applications. Thus, maximum likelihood estimators (MLEs), least square estimators (LSEs), weighted least square estimators (WLSEs), Anderson-Darling estimators (ADEs) and Crámer–von-Mises estimators (CVMEs) are considered for point estimation. The rest of this study is organized as follows: Section 2 introduces five different methods of estimation. A comprehensive Monte Carlo simulation study is presented in order to evaluate the performances of these estimators according to MSE criteria in Section 3. In Section 4, we consider real data illustrations. Finally, concluding remarks are given in Section 5.

2. Point estimations on model parameters

In this section, we focus on five estimators for estimating the unknown parameters of $XGW(\theta,b)$ distribution. For this purpose, we examine the maximum likelihood method, least-squares method, weighted least squares method, the method of Crámer–von-Mises and the method of Anderson-Darling.

Let $X_1, X_2, \ldots, X_n$ be a random sample from the $XGW(\theta,b)$ distribution and $X_{(1)} < X_{(2)} < \ldots < X_{(n)}$ represent the corresponding order statistics. Additionally, $x_{(i)}$ denotes the observed value of $X_{(i)}$. Based on this information the likelihood and log-likelihood function of the $XGW(\theta,b)$ distribution are given, respectively, by

$$L(\boldsymbol{\Psi}) = \prod_{i=1}^{n} \frac{b\theta^2}{(1+\theta)} x_i^{b-1} e^{-\theta x_i^b} \left(1 + \frac{1}{2}\theta x_i^{2b}\right) \tag{3}$$

and

$$\ell(\boldsymbol{\Psi}) = n\log(b) + 2n\log(\theta) - n\log(1+\theta) + (b-1)\sum_{i=1}^{n}\log(x_i) - \sum_{i=1}^{n}\theta x_i^{\,b} + \sum_{i=1}^{n}\log\left(1+\frac{1}{2}\theta x_i^{\,2b}\right) \quad (4)$$

where $\boldsymbol{\Psi} = (\theta, b)$.

Then, MLEs of $\boldsymbol{\Psi}$ is given by

$$\hat{\boldsymbol{\Psi}}_1 = \arg\max_{\boldsymbol{\Psi}} \left\{\ell(\boldsymbol{\Psi})\right\}. \quad (5)$$

Let us define the following functions which are useful to obtain the different type of estimators:

$$Q_{LS}(\boldsymbol{\Psi}) = \sum_{i=1}^{n}\left(\left\{1-\left(1+\theta+\theta x_{(i)}^{\,b}+\frac{\theta^2 x_{(i)}^{\,2b}}{2}\right)\frac{e^{-\theta x_{(i)}^{\,b}}}{(1+\theta)}\right\}-\frac{i}{n+1}\right)^2,$$

$$Q_{WLS}(\boldsymbol{\Psi}) = \sum_{i=1}^{n}\frac{(n+2)(n+1)^2}{i(n-i+1)}\left(\left\{1-\left(1+\theta+\theta x_{(i)}^{\,b}+\frac{\theta^2 x_{(i)}^{\,2b}}{2}\right)\frac{e^{-\theta x_{(i)}^{\,b}}}{(1+\theta)}\right\}-\frac{i}{n+1}\right)^2,$$

$$Q_{CvM}(\boldsymbol{\Psi}) = \frac{1}{12n}+\sum_{i=1}^{n}\left(\left\{1-\left(1+\theta+\theta x_{(i)}^{\,b}+\frac{\theta^2 x_{(i)}^{\,2b}}{2}\right)\frac{e^{-\theta x_{(i)}^{\,b}}}{(1+\theta)}\right\}-\frac{2i-1}{2n}\right)^2$$

and

$$Q_{AD}(\boldsymbol{\Psi}) = -n-\frac{1}{n}\sum_{i=1}^{n}\left((2i-1)\log\left(\left\{1-\left(1+\theta+\theta x_{(i)}^{\,b}+\frac{\theta^2 x_{(i)}^{\,2b}}{2}\right)\frac{e^{-\theta x_{(i)}^{\,b}}}{(1+\theta)}\right\}\right)\right)$$

$$+\frac{1}{n}\sum_{i=1}^{n}\left(\log\left(\left\{\left(1+\theta+\theta x_{(i)}^{\,b}+\frac{\theta^2 x_{(i)}^{\,2b}}{2}\right)\frac{e^{-\theta x_{(i)}^{\,b}}}{(1+\theta)}\right\}\right)\right).$$

The LSEs, WLSEs, CvMEs and ADEs of the parameter $\boldsymbol{\Psi}$ are given, respectively, by

$$\hat{\boldsymbol{\Psi}}_2 = \arg\min_{\boldsymbol{\Psi}} \left\{Q_{LS}(\boldsymbol{\Psi})\right\}, \quad (6)$$

$$\hat{\boldsymbol{\Psi}}_3 = \arg\min_{\boldsymbol{\Psi}} \left\{Q_{WLS}(\boldsymbol{\Psi})\right\}, \quad (7)$$

$$\hat{\boldsymbol{\Psi}}_4 = \arg\min_{\boldsymbol{\Psi}} \left\{Q_{CvM}(\boldsymbol{\Psi})\right\}, \quad (8)$$

$$\hat{\boldsymbol{\Psi}}_5 = \arg\min_{\boldsymbol{\Psi}} \left\{ Q_{AD}\left(\boldsymbol{\Psi}\right) \right\}. \tag{9}$$

All estimators given in Eqn. (5)-(9) can be achieved by optim function in R with BFGS algorithm.

3. Simulation Study

In this section, we consider a Monte Carlo simulation study to interpret the biases and MSEs of MLEs, LSEs, WLSEs, CvMEs and ADEs of XGW distribution parameters are estimated with 5000 trials. The acceptance-rejection algorithm is used to generate the data from $XGW\left(\theta, b\right)$ distribution. BFGS algorithm is carried out to get the five estimates given in (5)-(9). The simulation results are summarized via Figs. 1-6. Table 1 provides six parameter settings for Monte Carlo simulations. In Figs. 1-6, the biases and MSEs of MLEs, LSEs, WLSEs, CVMEs and ADEs are reported.

In the simulation study, the samples of sizes are considered as n=100, 200, 300, 400, 500, 600, 700, 800, 900, 1000.

Table 1: Parameter settings using from simulation study

Situation	θ	b
S1	1.5	0.3
S2	0.9	0.7
S3	0.4	0.6
S4	1.2	0.8
S5	0.75	1.5
S6	1.7	1.8

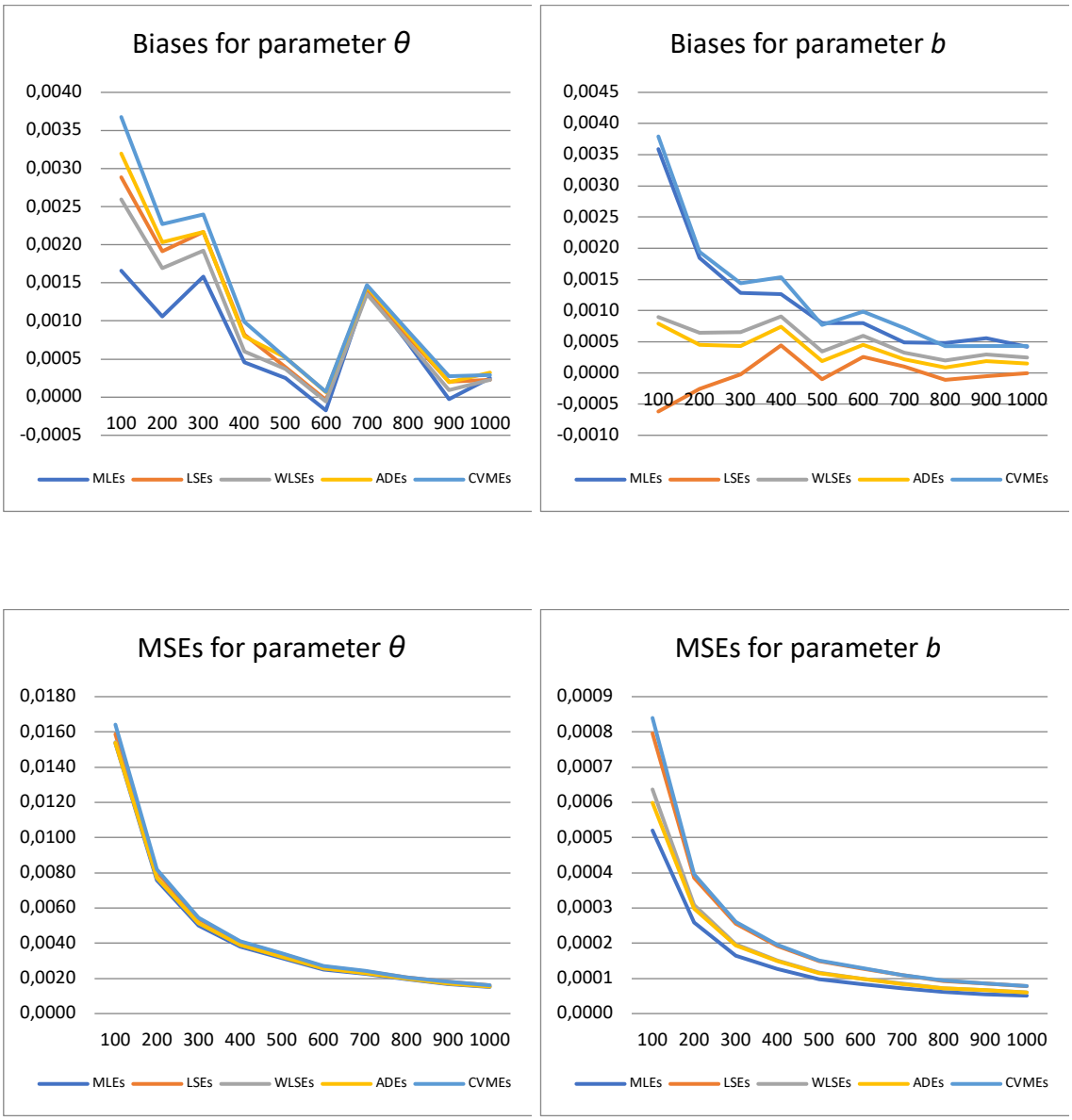

Figure 1: Biases and MSEs for situation S1

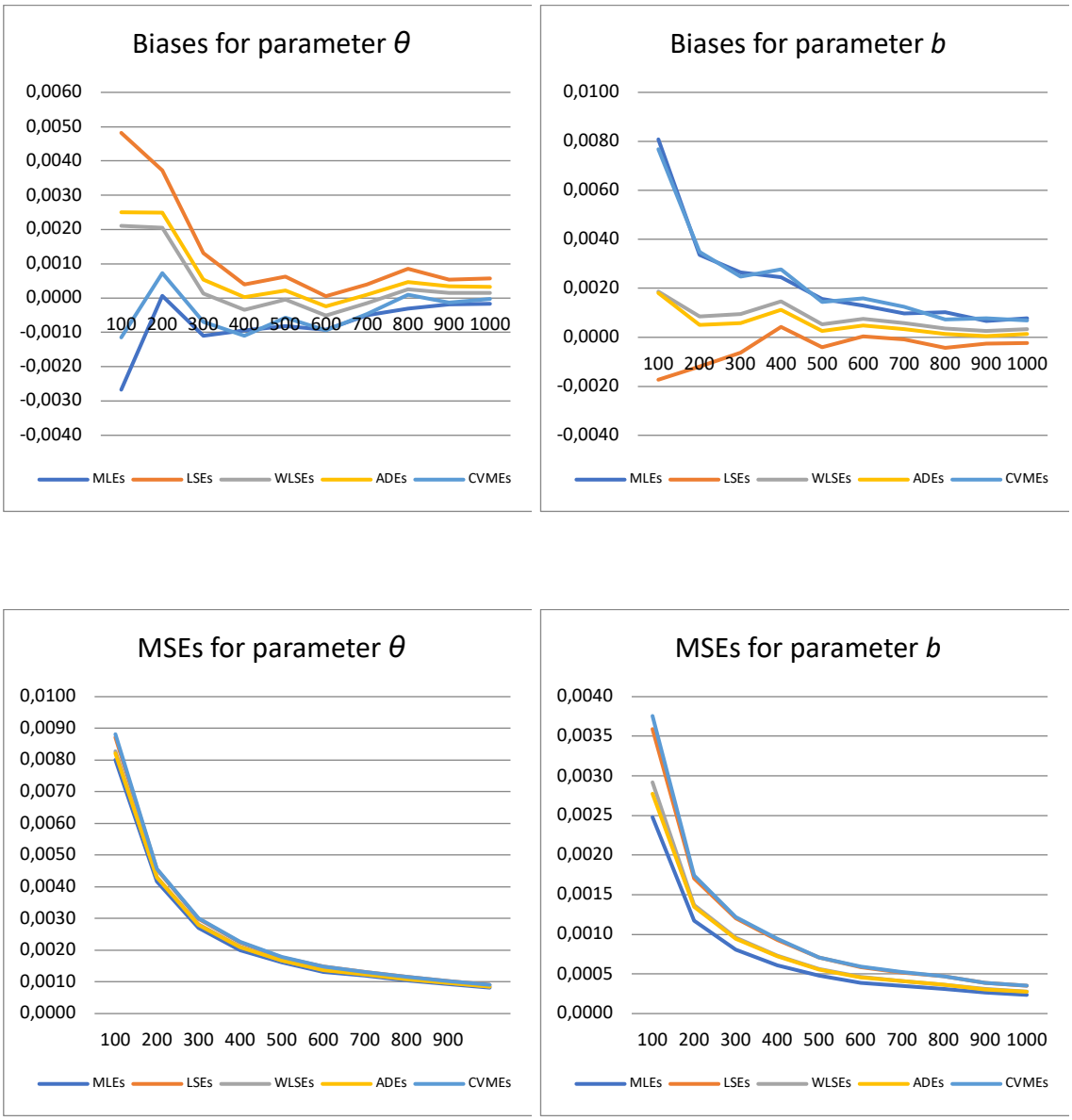

Figure 2: Biases and MSEs for situation S2

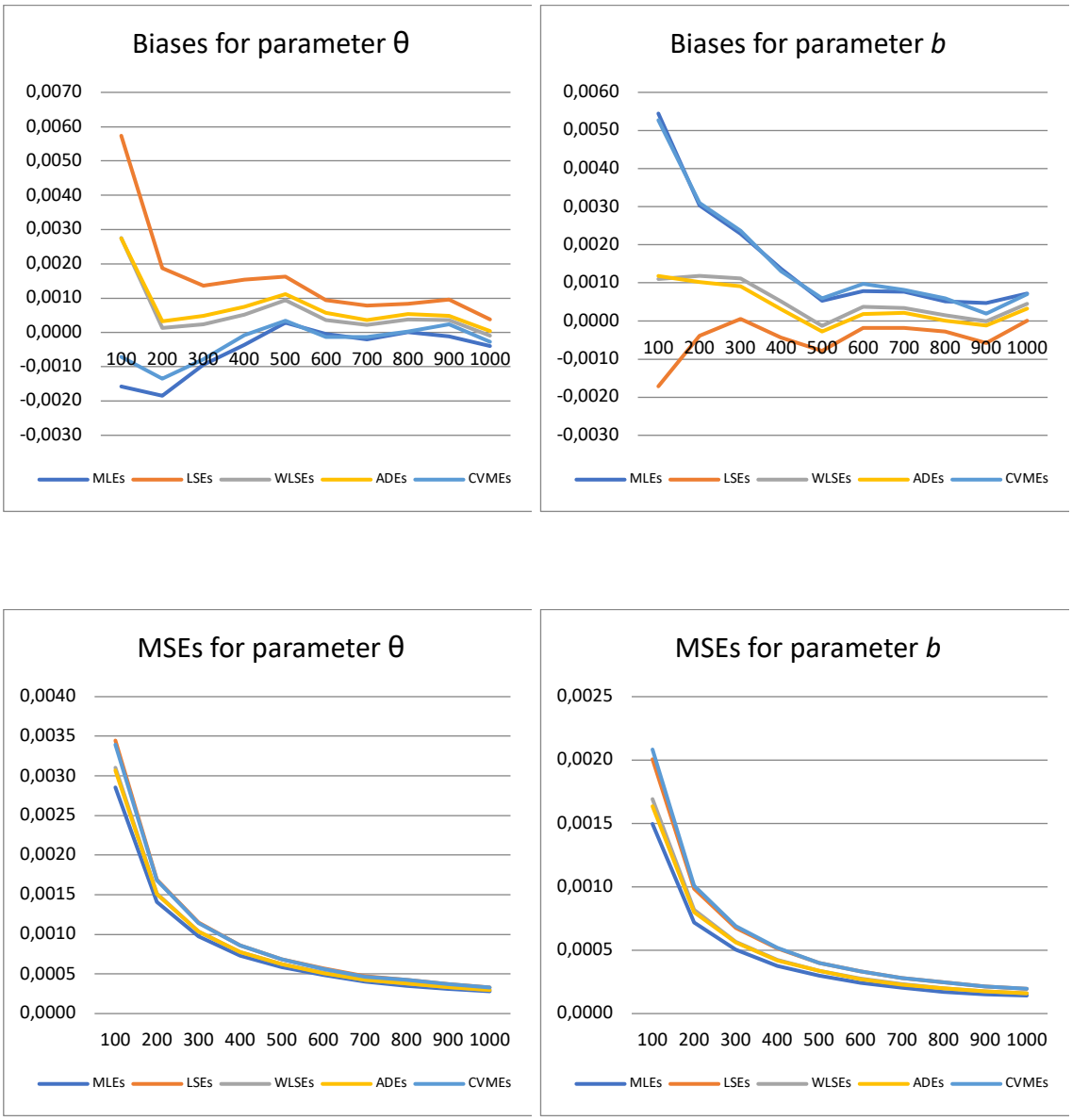

Figure 3: Biases and MSEs for situation S3

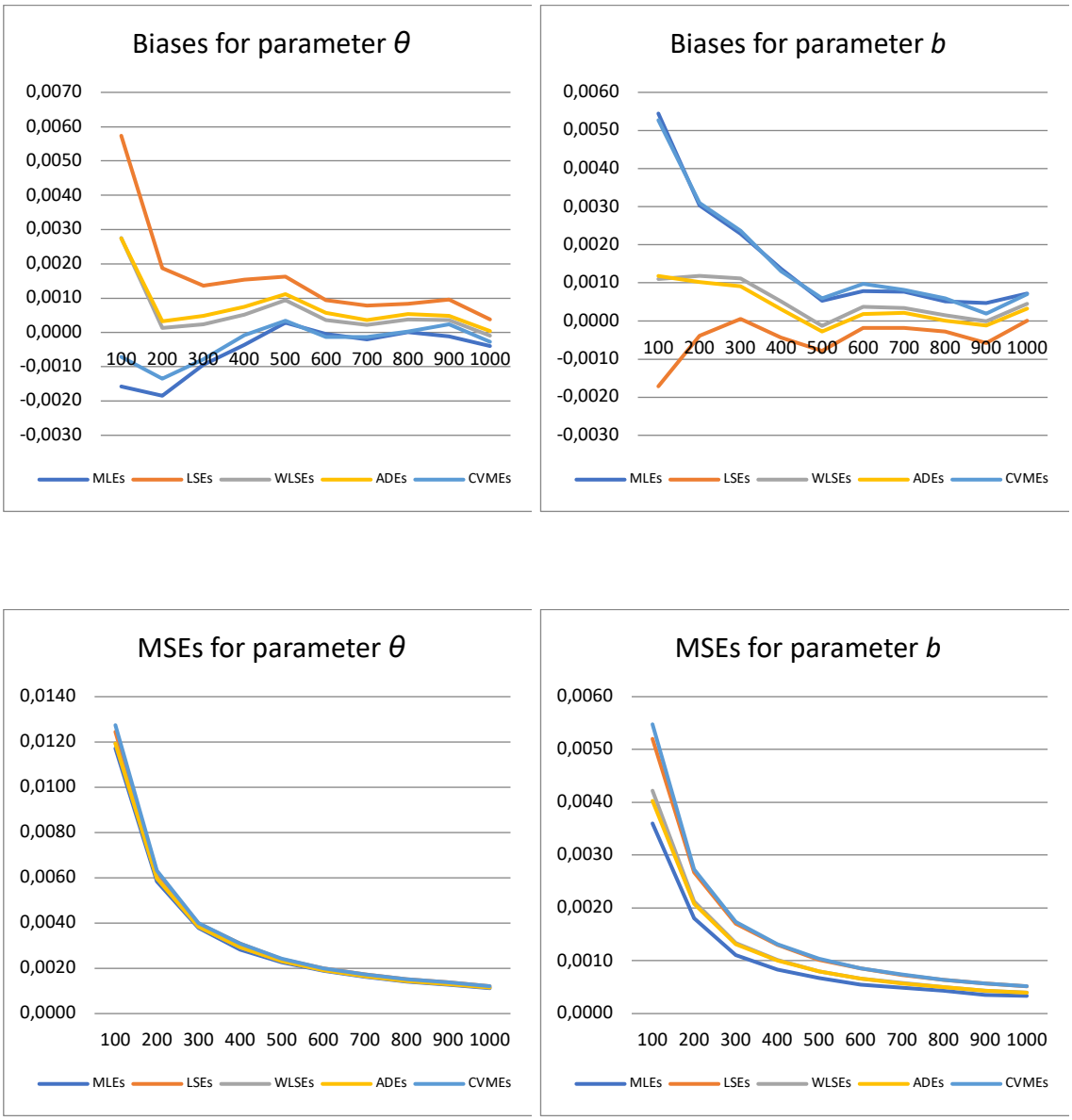

Figure 4: Biases and MSEs for situation S4

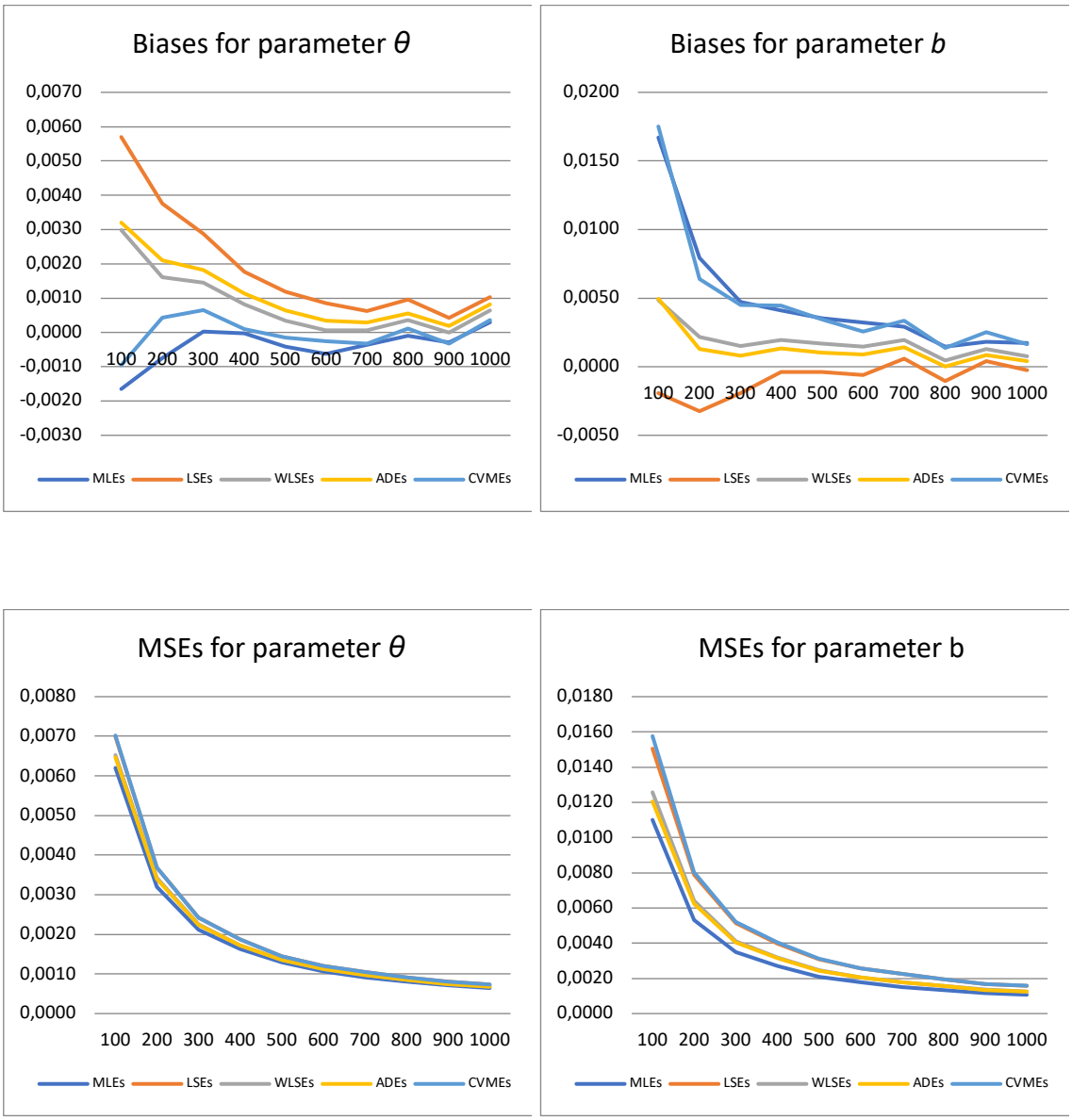

Figure 5: Biases and MSEs for situation S5

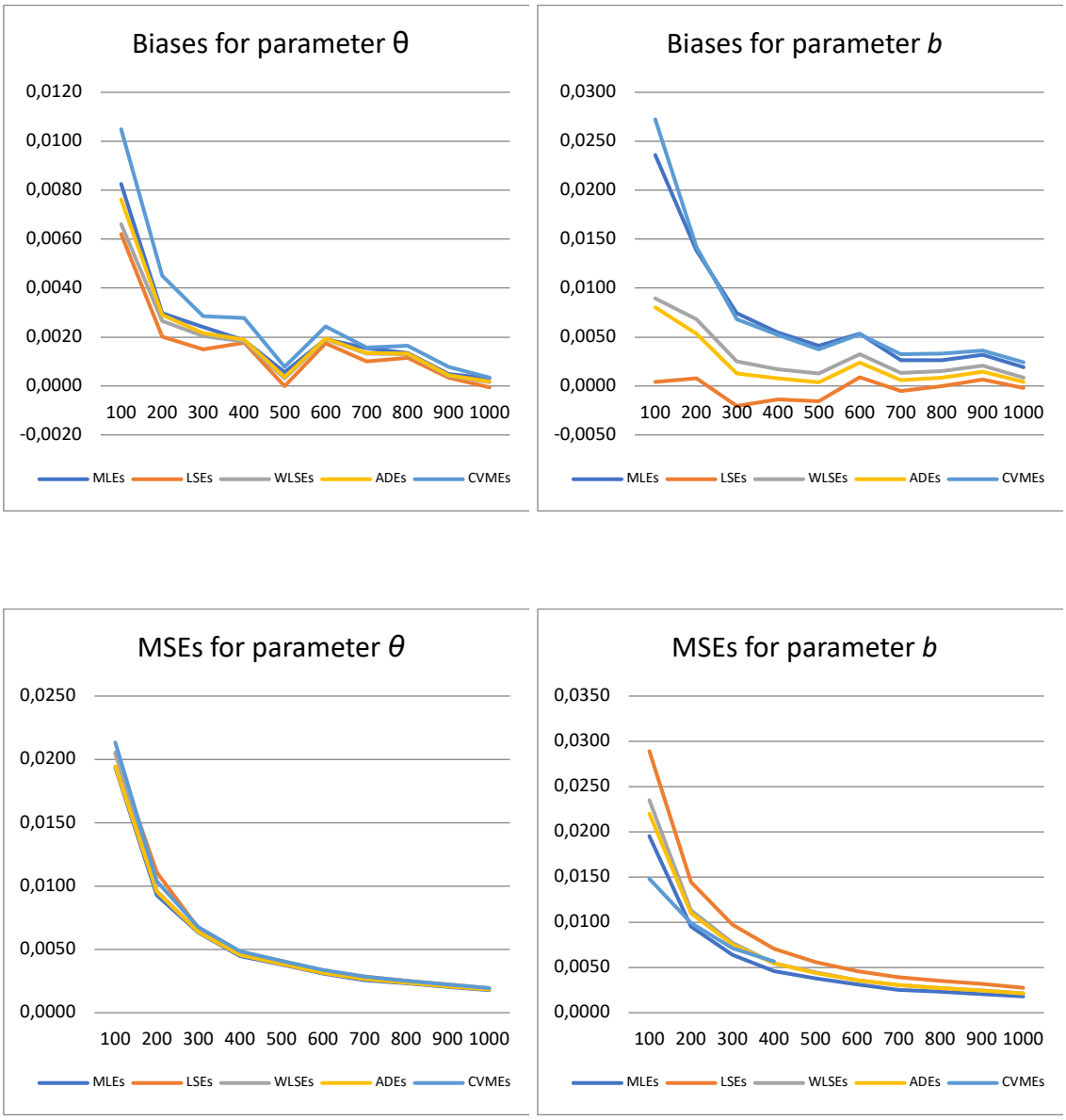

Figure 6: Biases and MSEs for situation S6

From Figs. 1-6, it can be concluded that the biases and MSEs of all estimates are close to zero when the sample of size increases. Also, the best estimator is maximum likelihood estimator for parameter b according to MSE criterion. It is quite difficult to comment on the parameter θ because the MSEs of the estimators are very close to each other. On the other hand, when looking at the values of biases estimators MLEs and LSEs are substantial for the parameter b, while MLEs and CVMEs for the θ parameter draw attention because of their good results. In other words, MLEs and CVMEs for the θ parameter, MLEs and LSEs for the b parameter gave more unbiased results than other estimators.

4. Real Data Applications

In this section, seven real data applications for the XGW distribution are studied. Also, five estimation methods are compared for XGW distribution in this data modelling. The MLEs, LSEs, WLSEs, ADEs and CVMEs of the parameters of XGW distribution are obtained by BFGS algorithm and reported in Table 2. Kolmogorov-Smirnov statistics (KS) and related p values are given in Table 3 for all estimators. From Tables 2-3 it is observed that all estimators nearly give the same results. Therefore, if one will use the XGW distribution in real data modeling, they can use one of the five estimation methods investigated in this paper.

In the following we give the seven real data sets;

Data Set 1 ([11])

65, 156, 100, 134, 16, 108, 121, 4, 39, 143, 56, 26, 22, 1, 1, 5, 65, 56, 65, 17, 7, 16, 22, 3, 4, 2, 3, 8, 4, 3, 30, 4, 43.

Data Set 2 ([12])

0.39, 0.85, 1.08, 1.25, 1.47, 1.57, 1.61, 1.61, 1.69, 1.80, 1.84, 1.87, 1.89, 2.03, 2.03, 2.05, 2.12, 2.35, 2.41, 2.43, 2.48, 2.50, 2.53, 2.55, 2.55, 2.56, 2.59, 2.67, 2.73, 2.74, 2.79, 2.81, 2.82, 2.85, 2.87, 2.88, 2.93, 2.95, 2.96, 2.97, 3.09, 3.11, 3.11, 3.15, 3.15, 3.19, 3.22, 3.22, 3.27, 3.28, 3.31, 3.31, 3.33, 3.39, 3.39, 3.56, 3.60, 3.65, 3.68, 3.70, 3.75, 4.20, 4.38, 4.42, 4.70, 4.90.

Data Set 3 ([13])

1.4, 5.1, 6.3, 10.8, 12.1, 18.5, 19.7, 22.2, 23, 30.6, 37.3, 46.3, 53.9, 59.8, 66.2.

Data Set 4 ([14])

0.77, 1.74, 0.81, 1.20, 1.95, 1.20, 0.47, 1.43, 3.37, 2.20, 3.00, 3.09, 1.51, 2.10, 0.52, 1.62, 1.31, 0.32, 0.59, 0.81, 2.81, 1.87, 1.18, 1.35, 4.75, 2.48, 0.96, 1.89, 0.90, 2.05.

Data Set 5 ([15])

0.3, 0.3, 4.0, 5.0, 5.6, 6.2, 6.3, 6.6, 6.8, 7.4, 7.5, 8.4, 8.4, 10.3, 11.0, 11.8, 12.2, 12.3, 13.5, 14.4, 14.4, 14.8, 15.5, 15.7, 16.2, 16.3, 16.5, 16.8, 17.2, 17.3, 17.5, 17.9, 19.8, 20.4, 20.9, 21.0, 21.0, 21.1, 23.0, 23.4, 23.6, 24.0, 24.0, 27.9, 28.2, 29.1, 30.0, 31.0, 31.0, 32.0, 35.0, 35.0, 37.0, 37.0, 37.0, 38.0, 38.0, 38.0, 39.0, 39.0, 40.0, 40.0, 40.0, 41.0, 41.0, 41.0, 42.0, 43.0, 43.0, 43.0, 44.0, 45.0, 45.0, 46.0, 46.0, 47.0, 48.0, 49.0, 51.0, 51.0, 51.0, 52.0, 54.0, 55.0, 56.0, 57.0, 58.0, 59.0, 60.0, 60.0, 60.0, 61.0, 62.0, 65.0, 65.0, 67.0, 67.0, 68.0, 69.0, 78.0, 80.0,83.0, 88.0, 89.0, 90.0, 93.0, 96.0, 103.0, 105.0, 109.0, 109.0, 111.0, 115.0, 117.0, 125.0, 126.0, 127.0, 129.0, 129.0, 139.0, 154.0.

Data Set 6 ([16])

1.6, 3.5, 4.8, 5.4, 6.0, 6.5, 7.0, 7.3, 7.7, 8.0, 8.4, 2.0, 3.9, 5.0, 5.6, 6.1, 6.5, 7.1, 7.3, 7.8, 8.1, 8.4, 2.6, 4.5, 5.1, 5.8, 6.3, 6.7, 7.3, 7.7, 7.9, 8.3, 8.5, 3.0, 4.6, 5.3, 6.0, 8.7, 8.8, 9.0.

Data Set 7 ([17])

2.247, 2.64, 2.842, 2.908, 3.099, 3.126, 3.245, 3.328, 3.355, 3.383, 3.572, 3.581, 3.681,3.726, 3.727, 3.728, 3.783, 3.785, 3.786, 3.896, 3.912, 3.964, 4.05, 4.063, 4.082,4.111, 4.118, 4.141, 4.216, 4.251, 4.262, 4.326, 4.402, 4.457, 4.466, 4.519, 4.542,4.555, 4.614,4.632, 4.634, 4.636, 4.678, 4.698, 4.738, 4.832, 4.924, 5.043, 5.099, 5.134, 5.359, 5.473, 5.571, 5.684, 5.721, 5.998, 6.06.

Table 2: Parameter estimation for all real data sets based on the all estimators

	MLEs		**LSEs**		**WLSEs**		**ADEs**		**CVMEs**	
Data sets	***θ***	***b***	***θ***	***b***	***θ***	***b***	***θ***	***b***	***θ***	***b***
1	0.5569	0.3696	0.4862	0.4534	0.5306	0.3932	0.5185	0.4131	0.5014	0.4361
2	2.3643	0.2072	2.4633	0.1878	2.4109	0.1989	0.4107	0.1984	2.5094	0.1798
3	0.8379	0.1741	0.7197	0.2421	0.7338	0.2340	0.7856	0.2013	0.7709	0.2100
4	1.5462	0.8248	1.5879	0.8476	1.5987	0.8287	1.5944	0.8277	1.6623	0.8271
5	0.8170	0.1263	0.7874	0.1401	0.7981	0.1348	0.7968	0.1354	0.7951	0.1365
6	2.1022	0.0549	2.0321	0.0587	2.1435	0.0494	2.0243	0.0610	2.0942	0.0524
7	3.1716	0.0267	3.1642	0.0274	3.0961	0.0301	3.1357	0.0284	3.1982	0.0262

Table 3: Kolmogrov-Smirnov statistics and related p value for all real data sets based on the all estimators

	MLEs		**LSEs**		**WLSEs**		**ADEs**		**CVMEs**	
Data sets	***KS***	***p value***	***KS***	***p value***	***KS***	***p value***	***KS***	***p value***	***KS***	***p value***
1	0.1258	0.6723	0.1213	0.7158	0.1152	0.7733	**0.1052**	**0.8584**	0.1143	0.7814
2	0.0718	0.8853	0.0631	0.9551	0.0647	0.9445	0.0661	0.9347	**0.0586**	**0.9769**
3	0.0999	0.9945	0.1051	0.9901	0.0971	0.9961	0.0974	0.9960	**0.0968**	**0.9963**
4	0.0860	0.9793	0.0737	0.9967	**0.0674**	**0.9992**	**0.0674**	**0.9992**	0.0735	0.9968
5	**0.0580**	**0.8095**	0.0613	0.7534	0.0592	0.7887	0.0592	0.7895	0.0611	0.7568
6	0.1092	0.7263	0.1098	0.7202	**0.0934**	**0.8756**	0.1016	0.8031	0.1017	0.8019
7	0.0645	0.9590	0.0557	0.9900	0.0634	0.9647	0.0619	0.9713	**0.0529**	**0.9946**

5. Concluding Remarks

In this study, XGW distribution introduced by [1] is investigated with regard to some point estimations. Five estimators are examined to estimate the two parameters of XGW distribution. A new extension is ensured for the estimation of the parameters for XGW distribution. Monte Carlo simulations are carried out for six different parameter values and different sample sizes. It is eventuated that when the sample of sizes increases, the biases and MSEs of all estimators decreases and approach to zero. The parameter estimates and KS of XGW distribution are obtained using five different estimation methods for seven practical data sets.

References

[1] Yousof, H.M., Korkmaz, M.Ç., Sen, S., *A new two-parameter lifetime model*, Annals of Data Science, 2020, DOI: 10.1007/s40745-019-00203-w.

[2] Gupta, R.D., Kundu, D., *Generalized exponential distribution: different method of estimations*, Journal of Statistical Computation and Simulation, 69(4), 315-337, 2001.

[3] Kundu, D., Raqab, M.Z., *Generalized Rayleigh distribution: different methods of estimations*, Computational statistics & data analysis, 49(1), 187-200, 2005.

[4] Asgharzadeh, A., Rezaie, R., Abdi, M., *Comparisons of methods of estimation for the half-logistic distribution*, Selçuk Journal of Applied Mathematics, 93-108, 2011.

[5] Mazucheli, J., Louzada F., Ghitany M.E., *Comparison of estimation methods for the parameters of the weighted Lindley distribution*, Applied Mathematics and Computation, 220, 463-471, 2013.

[6] Dey, S., Dey, T., Kundu, D., *Two-parameter Rayleigh distribution: different methods of estimation*, American Journal of Mathematical and Management Sciences, 33(1), 55-74, 2014.

[7] Peng, X., Yan, Z., *Estimation and application for a new extended Weibull distribution*, Reliability Engineering & System Safety, 121, 34-42, 2014.

[8] Nassar, M., Afify, A.Z., Dey, S., Kumar, D., *A new extension of Weibull distribution: properties and different methods of estimation*, Journal of Computational and Applied Mathematics, 336, 439-457, 2018.

[9] Taniş, C., Saracoglu, B., *Comparisons of six different estimation methods for log-kumaraswamy distribution*, Thermal Science, 23, 1839-1847, 2019.

[10] Afify, A.Z., Nassar, M., Cordeiro, G. M., Kumar, D., *The Weibull Marshall–Olkin Lindley distribution: properties and estimation*, Journal of Taibah University for Science, 14(1), 192-204, 2020.

[11] Feigl, P., Zelen, M., *Estimation of exponential survival probabilities with concomitant information*, Biometrics 21, 826–38, 1965.

[12] Nichols, M.D., Padgett, W.J., *A bootstrap control chart for Weibull percentiles*, Quality and Reliability Engineering International, 22, 141-151, 2006.

[13] Lawless, J.F., *Statistical models and methods for lifetime data*, Wiley, New York, 2003.

[14] Bjerkedal, T., *Acquisition of resistance in Guinea Piesinfected with different doses of Virulent Tubercle Bacill,* American Journal of Hygiene, 72, 130-148 , 1960.

[15] Lee, E.T., *Statistical methods for survival data analysis*, John Wiley, New York, 1992.

[16] Xu, K., Xie, M., Tang, L.C., Ho, S.L., *Application of neural networks in forecasting engine systems reliability*, Applied Soft Computing, 2(4), 255-268, 2003.

[17] Crowder, M.J., Kimber, A.C., Smith, R.L., Sweeting, T.J. *The statistical analysis of reliability data*, Chapman and Hall, London, 1991.

Adıyaman University Journal of Science
https://dergipark.org.tr/en/pub/adyujsci
DergiPark AKADEMİK
ISSN 2147-1630
e-ISSN 2146-586X

Simpson Type Integral Inequalities for Harmonic Convex Functions via Conformable Fractional Integrals

Zeynep ŞANLI[1,*]

[1]*Department of Mathematics, Faculty of Science, Karadeniz Technical University, Trabzon, Turkey*
zeynep.sanli@ktu.edu.tr, ORCID: 0000-0000-1564-2634

Received: 14.08.2020 **Accepted:** 07.12.2020 **Published:** 30.12.2020

Abstract

Fractional integral operators are very useful in the field of mathematical analysis and optimization theory. The main aim of this investigation is to establish a new Simpson type conformable fractional integral equality for harmonically convex functions. Using this identity, some new results related to Simpson-like type conformable fractional integral inequalities are obtained. Then, some interesting conclusions are attained for some special cases of conformable fractional integrals when $\alpha = 1$.

***Keywords*:** Simpson inequality; Conformable fractional integral; Harmonic convex.

Conformable Kesirli İntegraller Aracılığıyla Harmonik Konveks Fonksiyonlar için Simpson Tipi İntegral Eşitsizlikleri

Öz

Kesirli integral operatörleri matematiksel analiz ve optimizasyon teorisi alanlarında oldukça kullanışlıdır. Bu araştırmanın temel amacı harmonik konveks fonksiyonlar için yeni bir Simpson tipi conformable kesirli integral eşitliği kurmaktır. Bu eşitliği kullanarak Simpson tipi conformable kesirli integral eşitsizlikleri ile ilgili bazı yeni sonuçlar elde edildi. Daha sonra, $\alpha = 1$ olduğunda, conformable kesirli integrallerin bazı özel durumları için ilginç sonuçlara ulaşıldı.

* Corresponding Author DOI: 10.37094/adyujsci.780433

***Anahtar Kelimeler*:** Simpson eşitsizliği; Conformable kesirli integral; Harmonik konveks.

1. Introduction

We will start with the following inequality which is well known in the literature as Simpson's inequality.

Theorem 1. Let $f:[a,b]\to\mathbb{R}$ be a four times continuously differentiable mapping on (a,b) and $\left\|f^{(4)}\right\|_\infty=\sup\left|f^{(4)}(x)\right|<\infty$. Then, the following inequality holds:

$$\left|\int_a^b f(x)dx-\frac{b-a}{3}\left[\frac{f(a)+f(b)}{2}+2f\left(\frac{a+b}{2}\right)\right]\right|\leq\frac{1}{2880}\left\|f^{(4)}\right\|_\infty(b-a)^4. \tag{1}$$

Inequality (1) has been studied by several authors (see [1-11]).

In [12], İşcan gave the definition of harmonically convex functions as follow:

Definition 2. [12] Let $I\subset\mathbb{R}\backslash\{0\}$ be a real interval. A function $f:I\to\mathbb{R}$ is said to be harmonically convex, if

$$f\left(\frac{uv}{tu+(1-t)v}\right)\leq tf(v)+(1-t)f(u), \tag{2}$$

for all $u,v\in I$ and $t\in[0,1]$. If the inequality (2) is reversed, then f is said to be harmonically concave.

Harmonic convex functions are important for mathematical inequalities. Many authors obtained several inequalities for harmonic convex functions [12-15]. The most famous inequality which has been used with harmonic convex functions is Hermite-Hadamard, which is stated as follow:

Theorem 3. [12] Let $f:I\subset\mathbb{R}\backslash\{0\}$ be a hormanically convex function and $u,v\in[a,b]$ with $u<v$. If $f\in L[u,v]$ then the following inequalities hold:

$$f\left(\frac{2uv}{u+v}\right)\leq\frac{uv}{v-u}\int_a^b\frac{f(x)}{x^2}dx\leq\frac{f(u)+f(v)}{2}. \tag{3}$$

The aim of this paper is to establish Simpson type conformable fractional integral inequalities based on harmonically convexity.

2. Preliminaries

In this section, we give some definitions and basic results for later use.

Definition 4. Let $a, b \in \mathbb{R}$ with $a < b$ and $f \in L[a, b]$. The left and right Riemann-Liouville fractional integrals $J_{a+}^{\alpha} f$ and $J_{b-}^{\alpha} f$ order $\alpha > 0$ are defined by

$$J_{a+}^{\alpha} f = \frac{1}{\Gamma(\alpha)} \int_a^x (x-t)^{\alpha-1} f(t) dt, \quad x > a,$$

$$J_{b-}^{\alpha} f = \frac{1}{\Gamma(\alpha)} \int_x^b (t-x)^{\alpha-1} f(t) dt, \quad x < b,$$

respectively, where $\Gamma(\alpha)$ is the Gamma function defined by $\Gamma(\alpha) = \int_0^{\infty} e^{-t} t^{\alpha-1} dt$ (see [16], p.69).

The following definition of conformable fractional integrals can be found in [13, 17, 15].

Definition 5. Let $\alpha \in (n, n+1], n = 0, 1, 2, \ldots, \beta = \alpha - n,\ a,\ b \in \mathbb{R}$ with $a < b$ and $f \in L[a, b]$. The left and right conformable fractional integrals $I_{\alpha}^{a} f$ and ${}^{b}I_{\alpha} f$ order $\alpha > 0$ are defined by

$$I_{\alpha}^{a} f = \frac{1}{\mathrm{n!}} \int_a^x (x-t)^n (t-a)^{\beta-1} f(t) dt, \quad x > a,$$

$${}^{b}I_{\alpha} f = \frac{1}{\mathrm{n!}} \int_x^b (t-x)^n (b-t)^{\beta-1} f(t) dt, \quad x < b,$$

respectively.

It is easily seen that if one takes $\alpha = n + 1$ in the Definition 5 (for the left and right conformable fractional integrals), then the Definition 4 is obtained (the left and right Riemann-Liouville fractional integrals) for $\alpha \in \mathbb{N}$.

3. Main Results

Throughout the paper, we will use the following notations for our results:

$$u_1(t) = \frac{2ab}{(1-t)a + (1+t)b},$$

$$u_2(t) = \frac{2ab}{(1+t)a + (1-t)b},$$

$$H = \frac{2ab}{a+b}.$$

Let's begin the following lemma which will help us to obtain the main results:

Lemma 6. Let $\varphi: I \subset (0, \infty) \to \mathbb{R}$, be a differentiable function on $I^{\circ}, a, b \in I^{\circ}$ and $a < b$. If $\varphi' \in L[a, b]$, then the following equality holds:

$$\frac{1}{6}[\varphi(a)+4\varphi(H)+\varphi(b)]-2^{\alpha-1}\left(\frac{ab}{b-a}\right)^{\alpha}\frac{\Gamma(\alpha+1)}{\Gamma(\alpha-n)}\begin{bmatrix} I_{\alpha}^{\frac{1}{b}}(\varphi\circ\phi)\left(\frac{1}{H}\right) \\ +\quad {}^{\frac{1}{a}}I_{\alpha}\,(\varphi\circ\phi)\left(\frac{1}{H}\right)\end{bmatrix} \tag{4}$$

$$=\frac{b-a}{2ab}\frac{1}{n!}\frac{\Gamma(\alpha+1)}{\Gamma(\alpha-n)}\int_0^1 p(t;\alpha,n)\left[(u_1(t))^2\varphi'\big((u_1(t)\big)-(u_2(t))^2\varphi'\big((u_2(t)\big)\right]dt,$$

where

$$p(t;\alpha,n)=\int_0^1\left(\frac{1}{3}\beta(n+1,\alpha-n)-\frac{1}{3}\beta_t(n+1,\alpha-n)\right)dt$$

and $\phi(x)=\frac{1}{x},\ \alpha>0.$

Proof. We begin by considering the following computations which follow from change of variables and using the definition of the conformable fractional integrals.

$$I_1=\frac{1}{n!}\int_0^1 p(t;\alpha,n)(u_1(t))^2\varphi'\big((u_1(t)\big)dt=\frac{1}{3}\frac{2ab}{a-b}\frac{\Gamma(\alpha-n)}{\Gamma(\alpha+1)}\varphi\big((u_1(t)\big)|_0^1$$

$$-\frac{1}{2.n!}\frac{2ab}{a-b}\begin{pmatrix}\int_0^1\left(\int_0^t x^n(1-x)^{\alpha-n-1}dx\right)\varphi\big((u_1(t)\big)dt \\ -\int_0^1 t^n(1-t)^{\alpha-n-1}\varphi\big((u_1(t)\big)dt\end{pmatrix}$$

$$=\frac{2ab}{a-b}\frac{1}{3}\frac{\Gamma(\alpha-n)}{\Gamma(\alpha+1)}\big(\varphi(a)-\varphi(H)\big)-\frac{1}{2}\frac{2ab}{a-b}\frac{\Gamma(\alpha-n)}{\Gamma(\alpha+1)}\varphi(a)$$

$$+\frac{1}{2}\left(\frac{2ab}{a-b}\right)^{\alpha+1}\quad {}^{\frac{1}{a}}I_{\alpha}\,(\varphi\circ\phi)\left(\frac{1}{H}\right)=\frac{2ab}{a-b}\frac{\Gamma(\alpha-n)}{\Gamma(\alpha+1)}\left(\frac{1}{6}\varphi(a)+\frac{1}{3}\varphi(H)\right)$$

$$-\frac{1}{2}\left(\frac{2ab}{a-b}\right)^{\alpha+1}\quad {}^{\frac{1}{a}}I_{\alpha}\,(\varphi\circ\phi)\left(\frac{1}{H}\right)$$

and similarly

$$I_1=\frac{1}{n!}\int_0^1 p(t;\alpha,n)(u_1(t))^2\varphi'\big((u_1(t)\big)dt$$

$$=\frac{2ab}{b-a}\frac{\Gamma(\alpha-n)}{\Gamma(\alpha+1)}\left(-\frac{1}{6}\varphi(a)-\frac{1}{3}\varphi(H)\right)+\frac{1}{2}\left(\frac{2ab}{b-a}\right)^{\alpha+1}I_{\alpha}^{\frac{1}{b}}(\varphi\circ\phi)\left(\frac{1}{H}\right).$$

Thus, we have

$$\frac{b-a}{2ab}\frac{\Gamma(\alpha+1)}{\Gamma(\alpha-n)}(I_1-I_2)=\frac{1}{6}\ [\varphi(a)+4\varphi(H)+\varphi(b)]$$

$$- 2^{\alpha-1}\left(\frac{ab}{b-a}\right)^{\alpha}\frac{\Gamma(\alpha+1)}{\Gamma(\alpha-n)}\begin{bmatrix} I_{\alpha}^{\frac{1}{b}}(\varphi\circ\phi)\left(\frac{1}{H}\right) \\ +\ {}_{\frac{1}{a}}I_{\alpha}\ (\varphi\circ\phi)\left(\frac{1}{H}\right)\end{bmatrix}.$$

Remark 7. If we take $\alpha = n+1$ in Lemma 6, then we get

$$\frac{1}{6}[\varphi(a)+4\varphi(H)+\varphi(b)] - 2^{\alpha-1}\left(\frac{ab}{b-a}\right)^{\alpha}\Gamma(\alpha+1)\begin{bmatrix} J_{\frac{1}{b}+}^{\alpha}(\varphi\circ\phi)\left(\frac{1}{H}\right) \\ +J_{\frac{1}{a}-}^{\alpha}(\varphi\circ\phi)\left(\frac{1}{H}\right)\end{bmatrix} \tag{5}$$

$$= \frac{b-a}{2ab}\int_0^1\left(\frac{1}{3}-\frac{t^{\alpha}}{2}\right)\left[(u_1(t))^2\varphi'\big((u_1(t)\big) - (u_2(t))^2\varphi'\big((u_2(t)\big)\right]dt.$$

Remark 8. If we take $\alpha = 1$ in Remark 7, then we have

$$\frac{1}{6}[\varphi(a)+4\varphi(H)+\varphi(b)] - \frac{ab}{b-a}\int_a^b\frac{\varphi(x)}{x^2}dx \tag{6}$$

$$= \frac{b-a}{2ab}\int_0^1\left(\frac{1}{3}-\frac{t}{2}\right)\left[(u_1(t))^2\varphi'\big((u_1(t)\big) - (u_2(t))^2\varphi'\big((u_2(t)\big)\right]dt.$$

Theorem 9. Let $\varphi: I\subset(0,\infty)\to\mathbb{R}$, be a differentiable function on I°, $a,b\in I^{\circ}$ and $a<b$. If $\varphi'\in L[a,b]$, and $|\varphi'|$ is harmonic convex function on $[a,b]$, then the following inequality holds:

$$\left|\frac{1}{6}[\varphi(a)+4\varphi(H)+\varphi(b)] - 2^{\alpha-1}\left(\frac{ab}{b-a}\right)^{\alpha}\frac{\Gamma(\alpha+1)}{\Gamma(\alpha-n)}\begin{bmatrix} I_{\alpha}^{\frac{1}{b}}(\varphi\circ\phi)\left(\frac{1}{H}\right) \\ +\ {}_{\frac{1}{a}}I_{\alpha}\ (\varphi\circ\phi)\left(\frac{1}{H}\right)\end{bmatrix}\right| \tag{7}$$

$$\le \frac{b-a}{2ab}\frac{1}{n!}\frac{\Gamma(\alpha+1)}{\Gamma(\alpha-n)}\begin{pmatrix} \left|\varphi'^{(a)|}(\Im_1(t;\alpha,n) + (\Im_2(t;\alpha,n)\right) \\ +|\varphi'(b)|(\Im_3(t;\alpha,n) + (\Im_4(t;\alpha,n))\end{pmatrix},$$

where

$$\Im_1(t;\alpha,n) = \int_0^1|p(t;\alpha,n)|(u_1(t))^2\frac{1+t}{2}dt,$$

$$\Im_2(t;\alpha,n) = \int_0^1|p(t;\alpha,n)|(u_2(t))^2\frac{1-t}{2}dt,$$

$$\Im_3(t;\alpha,n) = \int_0^1|p(t;\alpha,n)|(u_1(t))^2\frac{1-t}{2}dt,$$

$$\Im_4(t;\alpha,n)=\int_0^1|p(t;\alpha,n)|(u_2(t))^2\,\frac{1+t}{2}dt,$$

where $n=0,1,2,\ldots$ and $\alpha\in(n,n+1]$.

Proof. From Lemma 6 and $|\varphi'|$ is harmonic convex, we have

$$\left|\frac{1}{6}[\varphi(a)+4\varphi(H)+\varphi(b)]-2^{\alpha-1}\left(\frac{ab}{b-a}\right)^{\alpha}\frac{\Gamma(\alpha+1)}{\Gamma(\alpha-n)}\begin{bmatrix} I_{\alpha}^{\frac{1}{b}}(\varphi\circ\phi)\left(\frac{1}{H}\right)\\ +\ {}^{\frac{1}{a}}I_{\alpha}\,(\varphi\circ\phi)\left(\frac{1}{H}\right)\end{bmatrix}\right|$$

$$\leq\frac{b-a}{2ab}\frac{1}{n!}\frac{\Gamma(\alpha+1)}{\Gamma(\alpha-n)}\int_0^1|p(t;\alpha,n)|((u_1(t))^2\varphi'(u_1(t))+(u_2(t))^2\varphi'(u_2(t)))dt$$

$$\leq\frac{b-a}{2ab}\frac{1}{n!}\frac{\Gamma(\alpha+1)}{\Gamma(\alpha-n)}\int_0^1|p(t;\alpha,n)|\left((u_1(t))^2\left(\frac{1+t}{2}|\varphi'(a)|+\frac{1-t}{2}|\varphi'(b)|\right)\right.$$

$$\left.+(u_2(t))^2\left(\frac{1-t}{2}|\varphi'(a)\right|+\frac{1+t}{2}|\varphi'(b)|\right)\Bigg)dt$$

$$\leq\frac{b-a}{2ab}\frac{1}{n!}\frac{\Gamma(\alpha+1)}{\Gamma(\alpha-n)}\Big(|\varphi'(a)|\big(\Im_1(t;\alpha,n)+\Im_2(t;\alpha,n)\big)+|\varphi'(b)|\big(\Im_3(t;\alpha,n)$$

$$+\Im_4(t;\alpha,n)\big)\Big).$$

This completes the proof.

Theorem 10. Let $\varphi: I\subset(0,\infty)\to\mathbb{R}$, be a differentiable function on I°, $a,b\in I^{\circ}$ and $a<b$. If $\varphi'\in L[a,b]$, and $|\varphi'|^q$ is harmonic convex function on $[a,b]$ for $q>1$ and $\frac{1}{p}+\frac{1}{p}=1$, then the following inequality holds:

$$\left|\frac{1}{6}[\varphi(a)+4\varphi(H)+\varphi(b)]-2^{\alpha-1}\left(\frac{ab}{b-a}\right)^{\alpha}\frac{\Gamma(\alpha+1)}{\Gamma(\alpha-n)}\begin{bmatrix} I_{\alpha}^{\frac{1}{b}}(\varphi\circ\phi)\left(\frac{1}{H}\right)\\ +\ {}^{\frac{1}{a}}I_{\alpha}\,(\varphi\circ\phi)\left(\frac{1}{H}\right)\end{bmatrix}\right| \tag{8}$$

$$\leq\frac{b-a}{2ab}\frac{1}{n!}\frac{\Gamma(\alpha+1)}{\Gamma(\alpha-n)}\left(\frac{1}{2}\right)^{2q+1}\left(\int_0^1|p(t;\alpha,n)|^p dt\right)^{\frac{1}{p}}$$

$$\times\begin{pmatrix}(\gamma_1(q;a,b)|\varphi'(a)|^q+\gamma_2(q;a,b)|\varphi'(b)|^q)^{\frac{1}{q}}\\ +(\gamma_3(q;a,b)|\varphi'(a)|^q+\gamma_4(q;a,b)|\varphi'(b)|^q)^{\frac{1}{q}}\end{pmatrix},$$

where

$$\gamma_1(q;a,b) = -\frac{\begin{matrix}a^{2q}b^{2q}\left(\left((8b^2-8ab)q-4b^2+8ab\right)e^{2\ln(b+a)q}\right.\\ \left.+\left((2a^2-2b^2)q+b^2-2ab-3a^2\right)e^{2\ln(2b)q}.2^{2q-1}e^{-2\ln(b+a)q-2\ln(2b)q}\right)\end{matrix}}{(b-a)^2(2q^2-3q+1)},$$

$$\gamma_2(q;a,b) = \frac{\begin{matrix}a^{2q}b^{2q}\left(4b^2e^{2\ln(b+a)q}+\left((2b^2-2a^2)q-3b^2-2ab+a^2\right)e^{2\ln(2b)q}\right.\\ \left..2^{2q-1}e^{2\ln(b+a)q-2\ln(2b)q}\right)\end{matrix}}{(b-a)^2(2q^2-3q+1)},$$

$$\gamma_3(q;a,b) = \frac{\begin{matrix}a^{2q}b^{2q}\left(4b^2e^{2\ln(b+a)q}+\left((2a^2-2b^2)q+b^2-2ab-3a^2\right)e^{2\ln(2a)q}\right.\\ \left..2^{2q-1}e^{2\ln(b+a)q-2\ln(2a)q}\right)\end{matrix}}{(b-a)^2(2q^2-3q+1)},$$

$$\gamma_4(q;a,b) = \frac{\begin{matrix}a^{2q}b^{2q}\left(\left((8ab-8a^2)q-8ab+4a^2\right)e^{2\ln(b+a)q}\right.\\ \left.+\left((2a^2-2b^2)q+3b^2+2ab-a^2\right)e^{2\ln(2a)q}.2^{2q-1}e^{-2\ln(b+a)q-2\ln(2a)q}\right)\end{matrix}}{(b-a)^2(2q^2-3q+1)},$$

$n = 0,1,2,\ldots$ *and* $\alpha \in (n, n+1]$.

Proof. From Lemma 6 and using Hölder's integral inequality and the harmonic convexity of $|\varphi'|^q$, we have

$$\left|\frac{1}{6}[\varphi(a)+4\varphi(H)+\varphi(b)] - 2^{\alpha-1}\left(\frac{ab}{b-a}\right)^{\alpha}\frac{\Gamma(\alpha+1)}{\Gamma(\alpha-n)}\left[\begin{matrix}I_{\alpha}^{\frac{1}{b}}(\varphi\circ\phi)\left(\frac{1}{H}\right)\\ +\ {}_{\frac{1}{a}}I_{\alpha}\ (\varphi\circ\phi)\left(\frac{1}{H}\right)\end{matrix}\right]\right|$$

$$\leq \frac{b-a}{2ab}\frac{1}{n!}\frac{\Gamma(\alpha+1)}{\Gamma(\alpha-n)}\left(\int_0^1 |p(t;\alpha,n)|^p dt\right)^{\frac{1}{p}}\left\{\left(\int_0^1 ((u_1(t))^{2q}|\varphi'(u_1(t))|^q dt\right)^{\frac{1}{q}}\right.$$

$$\left.+\left(\int_0^1 ((u_2(t))^{2q}|\varphi'(u_2(t))|^q dt\right)^{\frac{1}{q}}\right\}$$

$$\leq \frac{b-a}{2ab}\frac{1}{n!}\frac{\Gamma(\alpha+1)}{\Gamma(\alpha-n)}\left\{\left(\int_0^1 |p(t;\alpha,n)|^p dt\right)^{\frac{1}{p}}\right.$$

$$\times\left[\left(\int_0^1 ((u_1(t))^{2q}\left[|\varphi'(a)|^q\left(\frac{1+t}{2}\right)+|\varphi'(b)|^q\left(\frac{1-t}{2}\right)\right]dt\right)^{\frac{1}{q}}\right.$$

$$\left.\left.+\left(\int_0^1 ((u_2(t))^{2q}\left[|\varphi'(a)|^q\left(\frac{1-t}{2}\right)+|\varphi'(b)|^q\left(\frac{1+t}{2}\right)\right]dt\right)^{\frac{1}{q}}\right]\right\}$$

$$\leq \frac{b-a}{ab}\frac{1}{n!}\frac{\Gamma(\alpha+1)}{\Gamma(\alpha-n)}\left(\frac{1}{2}\right)^{\frac{1}{2q+1}}\left(\int_0^1 |p(t;\alpha,n)|^p dt\right)^{\frac{1}{p}}$$

$$\times\left[(\gamma_1(q;a,b)|\varphi'(a)|^q+\gamma_2(q;a,b)|\varphi'(b)|^q)^{\frac{1}{q}}\right.$$

$$\left.+(\gamma_3(q;a,b)|\varphi'(a)|^q+\gamma_4(q;a,b)|\varphi'(b)|^q)^{\frac{1}{q}}\right].$$

This completes the proof.

Remark 11. If we take $\alpha = n+1$, after that if we take $\alpha = 1$ in Theorem 10, we obtain the following inequality

$$\left|\frac{1}{6}[\varphi(a)+4\varphi(H)+\varphi(b)]-\frac{ab}{b-a}\int_0^1 \frac{\varphi(x)}{x^2}dx\right|$$

$$\leq \frac{b-a}{12ab}\left(\frac{2^{p+1}+1}{3(p+1)}\right)^{\frac{1}{p}}\left(\frac{1}{4}\right)^{\frac{1}{q}}$$

$$\times\left[(\gamma_1(q;a,b)|\varphi'(a)|^q+\gamma_2(q;a,b)|\varphi'(b)|^q)^{\frac{1}{q}}\right.$$

$$\left.+(\gamma_3(q;a,b)|\varphi'(a)|^q+\gamma_4(q;a,b)|\varphi'(b)|^q)^{\frac{1}{q}}\right]$$

with

$$\int_0^1 \left|\frac{1}{2}t-\frac{1}{3}\right|^p dt = \frac{2^{p+2}+2}{(p+1)6^{p+1}}.$$

Theorem 12. Let $\varphi: I \subset (0,\infty) \to \mathbb{R}$ be a differentiable function on I°, $a, b \in I^{\circ}$ and $a < b$. If $\varphi' \in L[a,b]$ and $|\varphi'|^q$ is harmonic convex function on $[a,b]$ for $q \geq 1$, then the following inequality holds:

$$\left|\frac{1}{6}[\varphi(a)+4\varphi(H)+\varphi(b)] - 2^{\alpha-1}\left(\frac{ab}{b-a}\right)^{\alpha}\frac{\Gamma(\alpha+1)}{\Gamma(\alpha-n)}\left[\begin{matrix} I_{\alpha}^{\frac{1}{b}}(\varphi\circ\phi)\left(\frac{1}{H}\right) \\ + \ {}^{\frac{1}{a}}I_{\alpha}\ (\varphi\circ\phi)\left(\frac{1}{H}\right)\end{matrix}\right]\right| \tag{9}$$

$$\leq \frac{b-a}{2ab}\frac{1}{n!}\frac{\Gamma(\alpha+1)}{\Gamma(\alpha-n)}\left(\int_0^1 |p(t;\alpha,n)|^p dt\right)^{1-\frac{1}{q}}$$

$$\times\left(\begin{matrix}(\zeta_1(q,t;\alpha,n)|\varphi'(a)|^q + \zeta_2(q,t;\alpha,n)|\varphi'(b)|^q)^{\frac{1}{q}} \\ +(\zeta_3(q,t;\alpha,n)|\varphi'(a)|^q + \zeta_4(q,t;\alpha,n)|\varphi'(b)|^q)^{\frac{1}{q}}\end{matrix}\right)$$

where

$$\zeta_1(q,t;\alpha,n) = \int_0^1 |p(t;\alpha,n)|(u_1(t))^{2q}\frac{1+t}{2}dt,$$

$$\zeta_2(q,t;\alpha,n) = \int_0^1 |p(t;\alpha,n)|(u_1(t))^{2q}\frac{1-t}{2}dt,$$

$$\zeta_3(q,t;\alpha,n) = \int_0^1 |p(t;\alpha,n)|(u_2(t))^{2q}\frac{1-t}{2}dt,$$

$$\zeta_4(q,t;\alpha,n) = \int_0^1 |p(t;\alpha,n)|(u_2(t))^{2q}\frac{1-t}{2}dt,$$

$n = 0,1,2,\ldots$ and $\alpha \in (n, n+1]$.

Proof. From Lemma 6 and using the power mean inequality, we see that the following inequality holds:

$$\left|\frac{1}{6}[\varphi(a)+4\varphi(H)+\varphi(b)]-2^{\alpha-1}\left(\frac{ab}{b-a}\right)^{\alpha}\frac{\Gamma(\alpha+1)}{\Gamma(\alpha-n)}\begin{bmatrix} I_{\alpha}^{\frac{1}{b}}(\varphi\circ\phi)\left(\frac{1}{H}\right) \\ + \ {}_{\frac{1}{a}}I_{\alpha}\ (\varphi\circ\phi)\left(\frac{1}{H}\right)\end{bmatrix}\right|$$

$$\leq \frac{b-a}{2ab}\frac{1}{n!}\frac{\Gamma(\alpha+1)}{\Gamma(\alpha-n)}\int_0^1|p(t;\alpha,n)|\left(\left(u_1(t)\right)^2|\varphi'(u_1(t))|\right.$$

$$\left.+\left(u_2(t)\right)^2|\varphi'(u_2(t))|\right)dt$$

$$\leq \frac{b-a}{2.n!}\frac{\Gamma(\alpha+1)}{\Gamma(\alpha-n)}\left\{\left(\int_0^1|p(t;\alpha,n)|^p dt\right)^{1-\frac{1}{q}}\right.$$

$$\times\left[\left(\int_0^1|p(t;\alpha,n)|\left(u_1(t)\right)^{2q}|\varphi'(u_1(t))|^q dt\right)^{\frac{1}{q}}\right]$$

$$\left.+\left(\int_0^1|p(t;\alpha,n)|\left(u_2(t)\right)^{2q}|\varphi'(u_2(t))|^q dt\right)^{\frac{1}{q}}\right\}.$$

By the harmonic convexity of $|\varphi'|^q$ we write

$$\int_0^1|p(t;\alpha,n)|\left(u_1(t)\right)^{2q}|\varphi'(u_1(t))|^q dt$$

$$\leq|\varphi'(a)|^q\int_0^1|p(t;\alpha,n)|\left(u_1(t)\right)^{2q}\frac{1+t}{2}dt$$

$$+|\varphi'(b)|^q\int_0^1|p(t;\alpha,n)|\left(u_1(t)\right)^{2q}\frac{1-t}{2}dt$$

and

$$\int_0^1|p(t;\alpha,n)|\left(u_2(t)\right)^{2q}|\varphi'(u_2(t))|^q dt$$

$$\leq|\varphi'(a)|^q\int_0^1|p(t;\alpha,n)|\left(u_2(t)\right)^{2q}\frac{1-t}{2}dt$$

$$+|\varphi'(b)|^q \int_0^1 |p(t;\alpha,n)|\left(u_2(t)\right)^{2q} \frac{1+t}{2} dt.$$

Using the last two inequalities, we obtain

$$\left|\frac{1}{6}[\varphi(a)+4\varphi(H)+\varphi(b)] - 2^{\alpha-1}\left(\frac{ab}{b-a}\right)^{\alpha}\frac{\Gamma(\alpha+1)}{\Gamma(\alpha-n)}\left[\begin{matrix} I_{\alpha}^{\frac{1}{b}}(\varphi\circ\phi)\left(\frac{1}{H}\right) \\ + \ {}^{\frac{1}{a}}I_{\alpha}\ (\varphi\circ\phi)\left(\frac{1}{H}\right)\end{matrix}\right]\right|$$

$$\leq \frac{b-a}{2ab}\frac{1}{n!}\frac{\Gamma(\alpha+1)}{\Gamma(\alpha-n)}\left(\int_0^1 |p(t;\alpha,n)|dt\right)^{1-\frac{1}{q}}$$

$$\times\left[\left(|\varphi'(a)|^q \int_0^1 |p(t;\alpha,n)|\left(u_1(t)\right)^{2q}\frac{1+t}{2}dt\right.\right.$$

$$\left.+|\varphi'(b)|^q \int_0^1 |p(t;\alpha,n)|\left(u_1(t)\right)^{2q}\frac{1-t}{2}dt\right)^{\frac{1}{q}}$$

$$+\left(|\varphi'(a)|^q \int_0^1 |p(t;\alpha,n)|\left(u_2(t)\right)^{2q}\frac{1+t}{2}dt\right.$$

$$\left.\left.+|\varphi'(b)|^q \int_0^1 |p(t;\alpha,n)|\left(u_2(t)\right)^{2q}\frac{1-t}{2}dt\right)^{\frac{1}{q}}\right].$$

Remark 13. If we take $\alpha = n+1$, after that if we take $\alpha = 1$ in Theorem 12, we obtain the following inequality

$$\left|\tfrac{1}{6}[\varphi(a)+4\varphi(H)+\varphi(b)] - \tfrac{ab}{b-a}\textstyle\int_a^b \frac{\varphi(x)}{x^2}dx\right|$$

$$\leq \frac{b-a}{2ab}\left(\frac{5}{36}\right)^{1-\frac{1}{q}}\left[(\zeta_1(q,t;\alpha,n)|\varphi'(a)|^q + \zeta_2(q,t;\alpha,n)|\varphi'(b)|^q)^{\frac{1}{q}}\right.$$

$$\left.+(\zeta_3(q,t;\alpha,n)|\varphi'(a)|^q + \zeta_4(q,t;\alpha,n)|\varphi'(b)|^q)^{\frac{1}{q}}\right].$$

4. Conclusion

In this paper, by using a new identity of Simpson-like type for conformable fractional integral for harmonic convex functions, we obtained some new Simpson type conformable

fractional integral inequalities. Furthermore, some interesting conclusions were obtained for some special values of α.

References

[1] Alomari, M., Darus, M., Dragomir, S.S., *New inequalities of Simpson's type for s-convex functions with applications,* Research Group in Mathematical Inequalities and Applications Research Report Collection, 12(4), 2009.

[2] Dragomir, S.S., Agarwal, R.P., Cerone, P., *On Simpson's inequality and applications,* Journal of Inequalities and Applications, 5(2), 2000.

[3] Luo, C.Y., Du, T.S., Zhang, Y., *Certain new bounds considering the weighted Simpson-like type inequality and applications,* Journal of Inequalities and Applications, (2018), Article ID 332, 2018.

[4] Matloka, M., *Some inequalities of Simpson type for h-convex functions via fractional integrals,* Abstract and Applied Analysis, (2015), 5 pages, 2015.

[5] Matloka, M., *Weighted Simpson type inequalities for h-convex functions*, Journal of Nonlinear Sciences and Applications, 10, 5570-5780, 2017.

[6] Rashid, S., Akdemir A.O., Jarad, F., Noor, M.A., Noor, K.I., *Simpson's type integral inequalities for k-fractional integrals and their applications,* AIMS Mathematics, 4(4), 1087-1100, 2019.

[7] Sarıkaya, M.Z., Bardak, S., *Generalized Simpson type integral inequalities,* Konuralp Journal of Mathematics, 7, 186-191, 2019.

[8] Sarıkaya, M.Z, Set, E., Özdemir, M.E., *On new inequalities of Simpson's type for functions whose second derivatives absolute values are convex,* Journal of Applied Mathematics, Statistics and Information, 9(1), 37-45, 2013.

[9] Sarıkaya, M.Z, Set, E., Özdemir, M.E., *On new inequalities of Simpson's type for s-convex funcyions,* Computers and Mathematics with Applications, 60, 2191-2199, 2010.

[10] Tunç, M., Göv, E., Balgeçti, S., *Simpson type quantum integral inequalities for convex functions,* Miskolc Mathematical Notes, 19(1), 649-669, 2018.

[11] Zhu, T., Wang, P., Du, T.S., *Some estimates on the weighted Simpson like integral inequalities and their applications,* Journal of Nonlinear Functional Analysis, Article ID 17, 2020.

[12] İşcan, İ., *Hermite-Hadamard type inequalities for harmonically convex functions,* Hacettepe Journal of Mathematics and Statistics, 46(6), 935-942, 2014.

[13] Awan, M.U., Noor, M.A., Mihai, M.V., Noor, K.I., *Inequalities via harmonic convex functions: Conformable fractional calculus approach*, Journal of Mathematical Inequalities, 12(1), 143-153, 2018.

[14] Latif, A.M., Hussein, S., Baloch, M., *Weighted Simpson's type inequalities for HA-convex,* Punjab University Journal of Mathematics, 57(2), 11-24, 2020.

[15] Şanlı, Z., Köroğlu, T., *New conformable fractional Hermite-Hadamard type inequalities for harmonically convex functions,* Journal of Mathematical Analysis, 9(6), 77-79, 2017.

[16] Kılbaş, A.A., Srivastava, H.M., Trujillo, J.J., *Theory and applications of fractional differential equations,* Elsevier, Amsterdam, 2006.

[17] Abdeljawad, T., Yiğit, N., Aktaş, E., Özgen, U., *On conformable fractional calculus*, Journal of Computational and Applied Mathematics, 279, 57-59, 2015.

Adıyaman University Journal of Science
https://dergipark.org.tr/en/pub/adyujsci
DergiPark AKADEMİK
ISSN 2147-1630
e-ISSN 2146-586X

Solitary Wave Solutions of the Coupled Konno-Oono Equation by Using the Functional Variable Method and the Two Variables $\left(\frac{G'}{G},\frac{1}{G}\right)$ -Expansion Method

Serbay DURAN[1,*]

[1]*Adıyaman University, Faculty of Education, Department of Mathematics, Adıyaman, Turkey*
sduran@adiyaman.edu.tr, ORCID: 0000-0002-3585-8061

Received: 18.11.2020 **Accepted:** 10.12.2020 **Published:** 30.12.2020

Abstract

In this work, we investigate solitary wave solutions of the coupled Konno-Oono equation with the aid of the functional variable method (FVM) and the two variables $\left(\frac{G'}{G},\frac{1}{G}\right)$-expansion method. We obtain solitary wave solutions in form of trigonometric function, hyperbolic function and rational function solutions. We also draw two and three-dimensional graphics for some solutions with help of Mathematica 7.

***Keywords*:** Functional variable method; Two variables $\left(\frac{G'}{G},\frac{1}{G}\right)$-expansion method; The coupled Konno-Oono equation; Solitary wave solution; Traveling wave solution.

Birleştirilmiş Konno-Oono Denkleminin Fonksiyonel Değişken Metodu ve İki Değişkenli $\left(\frac{G'}{G},\frac{1}{G}\right)$-Açılım Metodu Yardımıyla Solitary Dalga Çözümleri

Öz

Bu çalışmada, birleştirilmiş Konno-Oono Denkleminin fonksiyonel değişken metodu ve iki değişkenli $\left(\frac{G'}{G},\frac{1}{G}\right)$- açılım metodu yardımıyla solitary dalga çözümlerini araştırdık. Ele

* Corresponding Author DOI: 10.37094/adyujsci.827964

aldığımız denklemin trigonometrik ve hiperbolik ve rasyonel fonksiyon formunda solitary dalga çözümlerini elde ettik. Ayrıca Mathematica 7 yardımıyla bazı çözümlerin iki ve üç boyutlu grafiklerini çizdik.

***Anahtar Kelimeler*:** Fonksiyonel değişken metodu; İki değişkenli $\left(\frac{G'}{G},\frac{1}{G}\right)$-açılım metodu; Birleştirilmiş Konno-Oono denklemi; Solitary Dalga Çözümleri; Hareket eden dalga çözümü.

1. Introduction

Nonlinear partial differential equations (NPDEs) occur in many areas of mathematical physics. These equations are used in mathematical modeling of physical phenomena. The solutions of these equations are very important for the scientists. These solutions offer a lot of information about the character of the nonlinear event. That's why the scientists have focused on these solutions in recent years. The scientists have studied on different methods to obtain these solutions. When the scientists study these methods, they usually reduce the nonlinear event to linear. In doing this reduction, they often consider a nonlinear auxiliary equation. Many analytical methods have emerged thanks to the different choices of auxiliary equations. Another aspect of these methods that differ from each other is the selected solution function. The balancing term is used when writing these solutions. The balancing term is obtained by comparing the nonlinear term with the linear term. The solutions obtained by these methods are generally hyperbolic, trigonometric and rational solutions. Many different versions of these methods have been presented [1-11].

In this study, we implement FVM [12] and the two variables $\left(\frac{G'}{G},\frac{1}{G}\right)$-expansion method [13] to the coupled Konno-Oono equation [14]. There are many studies about the coupled Konno-Oono equation in the literature. For example, Manafian obtained some analytical solutions by the external trial equation method [15]. Bashar found traveling wave solutions by using tanh-function method and extended tanh-function method [16]. Torvattanabun presented the new exact solutions by extended simplest equation method [17]. Inan obtained multiple soliton solutions by improved tanh function method [18].

2. Methods

2.1. Analysis of functional variable method (FVM)

In this part, we present the FVM. Let's consider a given NLPDE for $u(x,t)$ as follows:

$$H(u,u_x,u_t,u_{xx},u_{xt},u_{tt},\dots)=0, \tag{1}$$

where H is a polynomial of its arguments. Using the transformation $u(x,t) = U(\xi),\ \xi = x \pm ct$ where u is the wave speed, then, we have ordinary differential equation (ODE) like

$$Q\left(U, U_{\xi}, U_{\xi\xi}, U_{\xi\xi\xi}, U_{\xi\xi\xi\xi}, \ldots\right) = 0, \tag{2}$$

U is considered as a functional variable in the form

$$U_{\xi} = F(U), \tag{3}$$

and other derivatives of U are

$$U_{\xi\xi} = \frac{1}{2}(F^2)', \tag{4}$$

$$U_{\xi\xi\xi} = \frac{1}{2}(F^2)''\sqrt{F^2}, \tag{5}$$

$$U_{\xi\xi\xi\xi} = \frac{1}{2}[(F^2)''F^2 + (F^2)''(F^2)'], \tag{6}$$

we write Eqn. (2) with respect to U, F and their derivatives as follows:

$$G\left(U, F, F', F'', F''', F^{(4)}, \ldots\right) = 0, \tag{7}$$

Eqn. (7) can be rewritten with respect to F by integration of Eqn. (7) and suitable solutions for the investigated problem can be found by using Eqn. (3).

2.2. Analysis of two Variables $\left(\frac{G'}{G}, \frac{1}{G}\right)$-expansion method

In this part, we present analysis of the two variables $\left(\frac{G'}{G}, \frac{1}{G}\right)$-expansion method [13]. Let's consider the following the second order linear ODE

$$G''(\zeta) + \lambda G(\zeta) = \mu, \tag{8}$$

where $\varphi = \frac{G'}{G}$ and $\psi = \frac{1}{G}$, then, we have

$$\varphi' = -\varphi^2 + \mu\psi - \lambda, \quad \psi' = -\varphi\psi. \tag{9}$$

Step 1. For $\lambda < 0$, the general solutions of Eqn. (8)

$$G(\zeta) = C_1 sinh\left(\sqrt{-\lambda}\,\zeta\right) + C_2 cosh\left(\sqrt{-\lambda}\,\zeta\right) + \frac{\mu}{\lambda}, \tag{10}$$

where C_1 and C_2 are arbitrary constants. Thus, we have

$$\psi^2 = \frac{-\lambda}{\lambda^2\sigma+\mu^2}(\varphi^2 - 2\mu\psi + \lambda), \tag{11}$$

where $\sigma = C_1^2 - C_2^2$.

Step 2. For $\lambda > 0$, the general solutions of Eqn. (8)

$$G(\zeta) = C_1 sin\left(\zeta\sqrt{\lambda}\right) + C_2 cos\left(\zeta\sqrt{\lambda}\right) + \frac{\mu}{\lambda}, \tag{12}$$

and therefore,

$$\psi^2 = \frac{\lambda}{\lambda^2\sigma-\mu^2}(\varphi^2 - 2\mu\psi + \lambda), \tag{13}$$

where $\sigma = C_1^2 + C_2^2$.

Step 3. For $\lambda = 0$, the solutions of Eqn. (8)

$$G(\zeta) = \frac{\mu}{2}\zeta^2 + C_1\zeta + C_2, \tag{14}$$

and therefore,

$$\psi^2 = \frac{1}{C_1^2-2\mu C_2}(\varphi^2 - 2\mu\psi). \tag{15}$$

Now, we show how this method is applied. Thus, let's consider an NLPDE is written by

$$H = \left(u, u_t, u_{x,} u_{xx}, u_{tt}, \ldots\right). \tag{16}$$

If we use transformation $u(x,t) = u(\zeta)$, $\zeta = x - Vt$ then, we yield a nonlinear ODE for $u(\zeta)$

$$H' = (u, u', u'' \ldots) = 0. \tag{17}$$

It can be written the solutions of Eqn. (17) by a polynomial φ and ψ as:

$$u(\zeta) = \sum_{i=0}^{M} a_i\varphi^i + \sum_{i=1}^{M} b_i\varphi^{i-1}\psi, \tag{18}$$

where $a_i(i = 0,1, \ldots, M)$ and $b_i(i = 1, \ldots, M)$ are arbitrary constants to be found later. M is a positive integer that can be concluded through balancing the highest nonlinear terms in Eqn. (17) and the highest order derivative. Substitute Eqn. (18) into Eqn. (17), the Eqn. (17) is written depending on the φ and ψ polynomials. The coefficient of each powers of $\varphi^i\psi^j$ equals zero and it is obtained an equation system for $a_i, b_i, V, \mu, C_1, C_2$ and λ. We calculate this equation system by means of Mathematica 7. Therefore, we find the solutions in relation to the hyperbolic

functions for $\lambda < 0$, the trigonometric functions for $\lambda > 0$ and finally the rational functions for $\lambda = 0$ respectively.

3. Application of FVM and Two Variables $\left(\frac{G'}{G}, \frac{1}{G}\right)$-Expansion Method to Coupled Konno-Oono Equation

Example 1. In this part, we present solitary wave solutions of coupled Konno-Oono equation by using the FVM.

$$\begin{cases} v_t + 2uu_x = 0, \\ u_{xt} - 2uv = 0, \end{cases} \tag{19}$$

where $u = u(x,t)$, $v = v(x,t)$. Using the transformation $u(x,t) = U(\xi)$, $v(x,t) = V(\xi)$, and $\xi = x - wt$, we find that

$$\begin{cases} -wV' + 2UU' = 0, \\ -wU'' - 2UV = 0, \end{cases} \tag{20}$$

where the prime denotes the derivation with respect to ξ. Integrating Eqn. (20), we have

$$\begin{cases} -wV + U^2 + c = 0, \\ -wU'' - 2UV = 0, \end{cases} \tag{21}$$

where c is the integration constant. We have from first equation of Eqn. (21)

$$V = \frac{1}{w}(U^2 + c). \tag{22}$$

If we substitute Eqn. (22) in Eqn. (21), we obtain the following:

$$U'' = -\frac{2}{w^2}U^3 - \frac{2c}{w^2}U. \tag{23}$$

Substituting Eqn. (4) into Eqn. (23) leads to the following equation:

$$F(U) = U' = \sqrt{-\frac{1}{w^2}U^4 - \frac{2c}{w^2}U^2 + h_0}\,, \tag{24}$$

where h_0 is an integration constant. Let be $h_4 = -\frac{1}{w^2}$ and $h_2 = -\frac{2c}{w^2}$. We obtain bell shaped solitary wave solutions of Eqn. (19) by solving Eqn. (24) for $h_0 = 0$ and $h_2 > 0$, $(c < 0), h_4 < 0$,

$$\begin{cases} u(x,t) = \sqrt{-2c}\,\mathrm{Sech}\left(\sqrt{\frac{-2c}{w^2}}(x-wt)\right), \\ v(x,t) = \frac{1}{w}\left(\left(\sqrt{-2c}\,\mathrm{Sech}\left(\sqrt{\frac{-2c}{w^2}}(x-wt)\right)\right)^2 + \mathrm{c}\right). \end{cases} \tag{25}$$

Example 2. In this part, we obtain solitary wave solutions of coupled Konno-Oono equation by using the two variables $\left(\frac{G'}{G}, \frac{1}{G}\right)$-expansion method. If we balance the highest order derivative with the nonlinear term in Eqn. (23), we write solution for Eqn. (23) as

$$U(\xi) = a_0 + a_1\phi(\xi) + b_1\psi(\xi). \tag{26}$$

Substituting Eqn. (26) in Eqn. (23), we have an algebraic system as follows:

$$\begin{gathered} \frac{2ca_0}{w^2} + \frac{2a_0^3}{w^2} = 0, \quad \frac{2cb_1}{w^2} + \lambda b_1 + \frac{6a_0^2 b_1}{w^2} = 0, \quad -\mu b_1 + \frac{6a_0 b_1^2}{w^2} = 0, \\ \frac{2ca_1}{w^2} + 2\lambda a_1 + \frac{6a_0^2 a_1}{w^2} = 0, \; 3\mu a_1 + \frac{12a_0 a_1 b_1}{w^2} = 0, \quad \frac{6a_1 b_1^2}{w^2} = 0, \\ 2b_1 + \frac{6a_1^2 b_1}{w^2} = 0, \; 2a_1 + \frac{2a_1^3}{w^2} = 0, \quad \frac{6a_0 a_1^2}{w^2} = 0, \quad \frac{2b_1^3}{w^2} = 0, \end{gathered} \tag{27}$$

If Eqn. (27) is solved by Mathematica 7, we obtain

$$\mu = 0, \; c = -w^2\lambda, \; a_0 = 0, \; a_1 = -iw, \; b_1 = 0, \; w \neq 0. \tag{28}$$

Case 1. For $\lambda < 0$,

$$\begin{cases} u(x,t) = iw\left(\frac{A_1\sqrt{-\lambda}\,\mathrm{Cosh}\left(\sqrt{-\lambda}\,(x-wt)\right)+A_2\sqrt{-\lambda}\,\mathrm{Sinh}\left(\sqrt{-\lambda}\,(x-wt)\right)}{A_1\mathrm{Sinh}\left(\sqrt{-\lambda}\,(x-wt)\right)+A_2\mathrm{Cosh}\left(\sqrt{-\lambda}\,(x-wt)\right)}\right) \\ v(x,t) = \frac{1}{w}\left(\left(iw\left(\frac{A_1\sqrt{-\lambda}\,\mathrm{Cosh}\left(\sqrt{-\lambda}\,(x-wt)\right)+A_2\sqrt{-\lambda}\,\mathrm{Sinh}\left(\sqrt{-\lambda}\,(x-wt)\right)}{A_1\mathrm{Sinh}\left(\sqrt{-\lambda}\,(x-wt)\right)+A_2\mathrm{Cosh}\left(\sqrt{-\lambda}\,(x-wt)\right)}\right)\right)^2 - w^2\lambda\right), \end{cases} \tag{29}$$

where $\sigma = A_1^2 - A_2^2$.

If we specifically select $\mathrm{A}_1 = 0$, $\mathrm{A}_2 > 0$ in Eqn. (29), we have hyperbolic solitary wave solutions

$$\begin{cases} u(x,t) = iw\sqrt{-\lambda}\,\mathrm{Tanh}\left(\sqrt{-\lambda}\,(x-wt)\right) \\ v(x,t) = \frac{1}{w}\left(\left(iw\sqrt{-\lambda}\,\mathrm{Tanh}\left(\sqrt{-\lambda}\,(x-wt)\right)\right)^2 - w^2\lambda\right), \end{cases} \tag{30}$$

If we specifically select $\mathrm{A}_2 = 0$, $\mathrm{A}_1 > 0$ in Eqn. (29), we obtain hyperbolic solitary wave solutions

$$\begin{cases} u(x,t) = iw\sqrt{-\lambda}\,\mathrm{Coth}\left(\sqrt{-\lambda}\,(x-wt)\right) \\ v(x,t) = \frac{1}{w}\left(\left(iw\sqrt{-\lambda}\,\mathrm{Coth}\left(\sqrt{-\lambda}\,(x-wt)\right)\right)^2 - w^2\lambda\right) \end{cases}. \tag{31}$$

Case 2. For $\lambda > 0$,

$$\begin{cases} u(x,t) = iw\left(\frac{A_1\sqrt{\lambda}\,\mathrm{Cos}\left(\sqrt{\lambda}\,(x-wt)\right)+A_2\sqrt{\lambda}\,\mathrm{Sin}\left(\sqrt{\lambda}\,(x-wt)\right)}{A_1\mathrm{Sin}\left(\sqrt{\lambda}\,(x-wt)\right)+A_2\mathrm{Cos}\left(\sqrt{\lambda}\,(x-wt)\right)}\right) \\ v(x,t) = \frac{1}{w}\left(\left(iw\left(\frac{A_1\sqrt{\lambda}\,\mathrm{Cos}\left(\sqrt{\lambda}\,(x-wt)\right)+A_2\sqrt{\lambda}\,\mathrm{Sin}\left(\sqrt{\lambda}\,(x-wt)\right)}{A_1\mathrm{Sin}\left(\sqrt{\lambda}\,(x-wt)\right)+A_2\mathrm{Cos}\left(\sqrt{\lambda}\,(x-wt)\right)}\right)\right)^2 - w^2\lambda\right) \end{cases}, \tag{32}$$

where $\sigma = A_1^2 + A_2^2$.

If we specifically select $\mathrm{A}_1 = 0$, $\mathrm{A}_2 > 0$ in Eqn. (32), we have trigonometric solitary wave solutions

$$\begin{cases} u(x,t) = iw\sqrt{\lambda}\,\mathrm{Tan}\left(\sqrt{\lambda}\,(x-wt)\right) \\ v(x,t) = \frac{1}{w}\left(\left(iw\sqrt{\lambda}\,\mathrm{Tan}\left(\sqrt{\lambda}\,(x-wt)\right)\right)^2 - w^2\lambda\right) \end{cases}. \tag{33}$$

If we specifically select $\mathrm{A}_2 = 0$, $\mathrm{A}_1 > 0$ in Eqn. (32), we obtain trigonometric solitary wave solutions

$$\begin{cases} u(x,t) = iw\sqrt{\lambda}\,\mathrm{Cot}\left(\sqrt{\lambda}\,(x-wt)\right) \\ v(x,t) = \frac{1}{w}\left(\left(iw\sqrt{\lambda}\,\mathrm{Cot}\left(\sqrt{\lambda}\,(x-wt)\right)\right)^2 - w^2\lambda\right) \end{cases}. \tag{34}$$

Case 3. For $\lambda = 0$, we obtain the rational solutions of Eqn. (19)

$$\begin{cases} u(x,t) = -iw\frac{A_1}{A_1(x-wt)+A_2} \\ v(x,t) = \frac{1}{w}\left(-iw\frac{A_1}{A_1(x-wt)+A_2}\right)^2 \end{cases}, \tag{35}$$

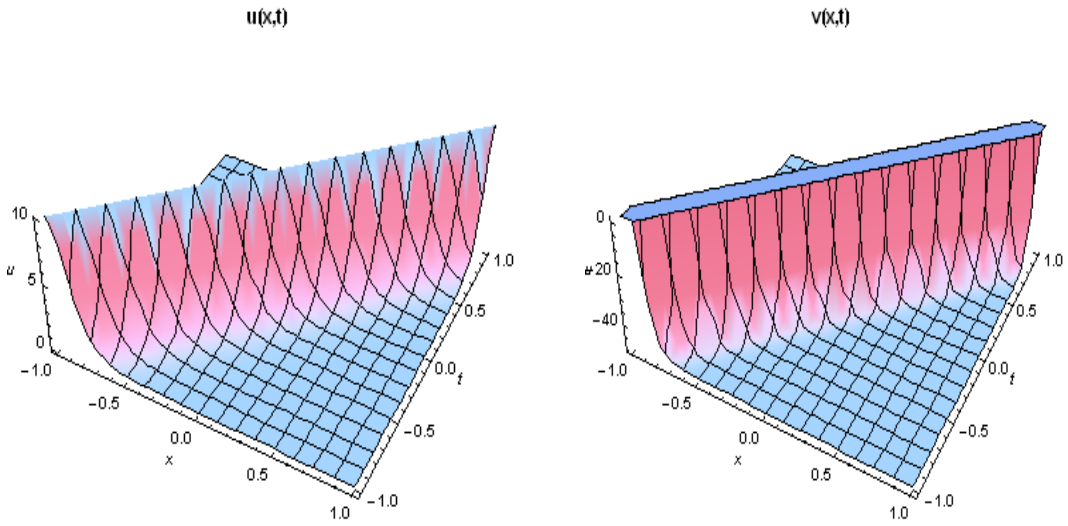

Figure 1: Above set of figures represent smooth bell shaped and singular bell shaped wave solutions of Eqn. (25) for $u(x,t)$ and $v(x,t)$, respectively $(c=-50, w=1)$

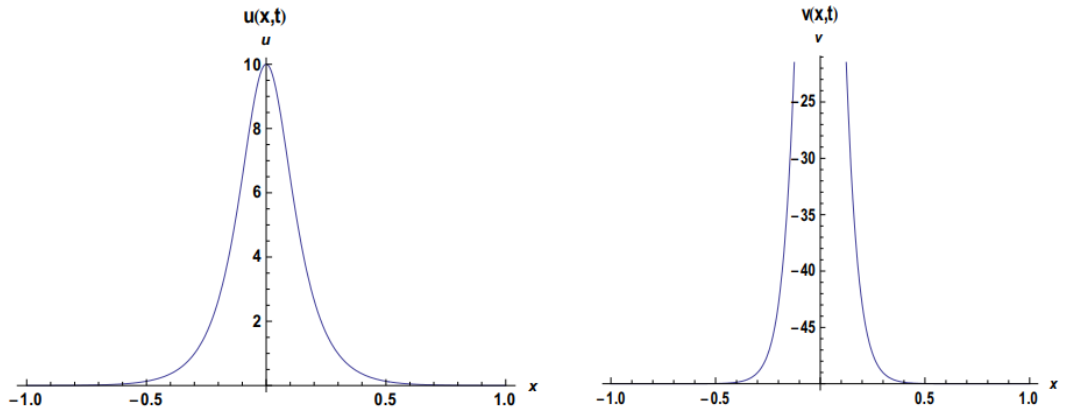

Figure 2: Above set of figures represent smooth bell shaped and singular bell shaped wave solutions of Eqn. (25) for $u(x,t)$ and $v(x,t)$, respectively $(c=-50,\ w=1,\ t=0)$

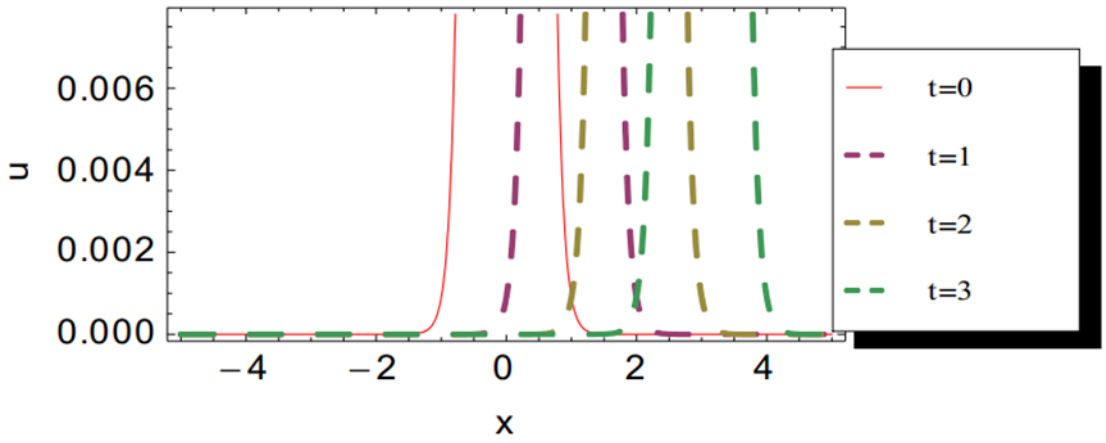

Figure 3: Above figure represent rightward traveling wave solutions of Eqn. (25) for $u(x,t)$ $(c=-50,$ $w=1)$

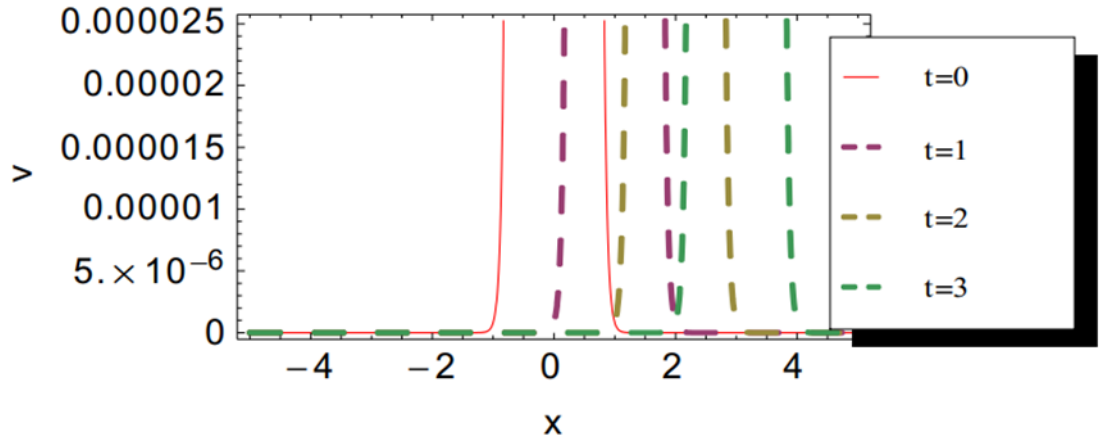

Figure 4: Above figure represent rightward traveling wave solutions of Eqn. (25) for $v(x,t)$ ($c=-50$, $w=1$)

4. Conclusion

In this study, we obtain solitary wave solutions of the coupled Konno-Oono equation by using the FVM and the two variables $\left(\frac{G'}{G},\frac{1}{G}\right)$-expansion method. These methods used in this study can be used to obtain the solutions of many other NPDEs. While we only obtain hyperbolic solution by using FVM for the Eqn. (19), we find hyperbolic, trigonometric and rational solutions by the two variables $\left(\frac{G'}{G},\frac{1}{G}\right)$-expansion method. We have smooth bell shaped and singular bell shaped wave solutions of Eqn. (19) for $u(x,t)$ and $v(x,t)$, respectively in Fig. 1. We draw traveling wave shape in 2D for $u(x,t)$ and $v(x,t)$ at $t=0$ in Fig. 2. We show rightward traveling wave solutions of Eqn. (25) for $u(x,t)$ and $v(x,t)$ at $t=0, t=1, t=2, t=3$, respectively in Fig. 3-4. We checked all the obtained solutions and they indeed satisfied Eqn. (19).

References

[1] Wang, M., Li, X., Zhang, J., *The (G'/G)-expansion method and travelling wave solutions of nonlinear evolution equations in mathematical physics,* Physics Letters A, 372, 417-423, 2008.

[2] Guo, S., Zhou, Y., Zhao, X., *The extended (G'/G)-expansion method and its applications to the Whitham-Broer-Kaup-Like equations and coupled Hirota-Satsuma KdV equations*, Applied Mathematics and Computation, 215, 3214-3221, 2010.

[3] Lü, H.L., Liu, X.Q., Niu, L., *A generalized (G'/G)-expansion method and its applications to nonlinear evolution equations*, Applied Mathematics and Computation, 215, 3811-3816, 2010.

[4] Malfiet, W., *Solitary wave solutions of nonlinear wave equations*, American Journal of Physics, 60, 650-654, 1992.

[5] He, J.H., Wu, X.H., *Exp-function method for nonlinear wave equations*, Chaos, Solitons & Fractals, 30, 700-708, 2006.

[6] Ozpinar, F., Baskonus, H.M., Bulut, H., *On the Complex and Hyperbolic Structures for the (2+1)-Dimensional Boussinesq Water Equation*, Entropy, 17(12), 8267-8277, 2015.

[7] Baskonus, H.M., Askin, M., *Travelling Wave Simulations to the Modified Zakharov-Kuzentsov Model Arising In Plasma Physics*, 6th International Youth Science Forum "LITTERIS ET ARTIBUS", Computing in Science & Engineering, 2016.

[8] Baskonus, H.M., Sulaiman, T.A., Bulut, H., *On the Novel Wave Behaviors to the Coupled Nonlinear Maccari's System with Complex Structure*, Optik, 131, 1036-1043, 2017.

[9] Bulut, H., Sulaiman, T.A., Baskonus, H.M., *New Solitary and Optical Wave Structures to the Korteweg-de Vries Equation with Dual-Power Law Nonlinearity*, Optical and Quantum Electronics, 48, 1-14, 2016.

[10] Gao, W., Baskonus, H. M., Shi, L., *New investigation of bats-hosts-reservoir-people coronavirus model and application to 2019-nCoV system*, Advances in Difference Equations, 391, 1-11, 2020.

[11] Gao, W., Yel, G., Baskonus, H. M., Cattani, C., *Complex solitons in the conformable (2+1)-dimensional Ablowitz-Kaup-Newell-Segur equation*, Aims Mathematics, 5(1), 507–521, 2020.

[12] Zerarka, A., Ouamane, S., *On the functional variable method for finding exact solutions to a class of wave equations*, Applied Mathematics and Computation, 217, 2897–2904, 2010.

[13] Li, L., Li, E., Wang, M., *The (G'/G, 1/G)-expansion method and its application to travelling wave solutions of the Zakharov equations*, Applied Mathematics-A Journal of Chinese Universities, 25, 454–462, 2010.

[14] Konno, K., Oono, H., *New coupled integrable dispersionless equations*, Journal of the Physical Society of Japan, 63, 377–378, 1994.

[15] Manafian, J., Zamanpourand, I., Ranjbaran, A., *On some new analytical solutions for new coupled Konno–Oono equation by the external trial equation method*, Journal of Physics Communications, 2, 015023, 2018.

[16] Bashar, A., Mondal, G., Khan, K., Bekir, A., *Traveling wave solutions of new coupled Konno-Oono equation*, New Trends in Mathematical Sciences, 4, 296-303, 2016.

[17] Torvattanabun, M., Juntakud, P., Saiyun, A., Khansai, N., *The new exact solutions of the new coupled konno-oono equation by using extended simplest equation method*, Applied Mathematical Sciences, 12, 293-301, 2018.

[18] Inan, E., *Multiple soliton solutions of some nonlinear partial differential equations*, Universal Journal of Mathematics and Applications, 1, 273-279, 2018.

Adıyaman University Journal of Science
https://dergipark.org.tr/en/pub/adyujsci
DergiPark AKADEMİK
ISSN 2147-1630
e-ISSN 2146-586X

An Application of Subclasses of Harmonic Univalent Functions Involving Hypergeometric Function

Waggas Galib ATSHAN[1], Enaam Hadi ABD[2,3], Sibel YALÇIN[4,*]

[1]*Department of Mathematics, College of Science, University of Al-Qadisiyah, Diwaniya, Iraq*
waggashnd@gmail.com, waggas.galib@qu.edu.iq, ORCID: 0000-0002-7033-8993
[2]*Department of Computer, College of Science, University of Kerbala, Kerbala, Iraq*
[3]*Department of Mathematics, College of Science, University of Baghdad, Baghdad, Iraq*
enaam_hadi2004@yahoo.com, ORCID: 0000-0003-3580-8379
[4]*Department of Mathematics, Faculty of Arts and Science, Uludağ University, Bursa, Turkey*
syalcin@uludag.edu.tr, ORCID: 0000-0002-0243-8263

Received: 27.01.2020 **Accepted:** 11.12.2020 **Published**: 30.12.2020

Abstract

The main purpose of this paper is to establish connections between various subclasses of harmonic univalent functions by applying certain convolution operator involving hypergeometric functions. We investigate such connections with Goodman-Salagean-Type harmonic univalent functions in the open unit disc U.

***Keywords*:** Univalent function; Uniformly convex; Linear operator; Hadamard product.

Hipergeometrik Fonksiyonu İçeren Harmonik Tek Değerlikli Fonksiyonların Altsınıflarının Bir Uygulaması

Öz

Bu makalenin amacı, hipergeometrik fonksiyonları içeren belirli konvolusyon operatörünü uygulayarak harmonik univalent fonksiyonların çeşitli altsınıfları arasında bağlantılar kurmaktır.

* Corresponding Author DOI: 10.37094/adyujsci.680530

Bu tür bağlantılar açık birim disk U da Goodman-Salagean tipli harmonik univalent fonksiyonları ile araştırılmıştır.

***Anahtar Kelimeler*:** Univalent fonksiyon; Düzgün konveks; Lineer operatör; Hadamard çarpımı.

1. Introduction

Let A denote the class of analytic functions of the form:

$$f(z) = z + \sum_{k=2}^{\infty} a_k z^k \,, (\, a_k \, \geq 0 \,, \mathrm{k} \in N \,), \tag{1}$$

which is univalent in the open unit disc U=$\{z \in C : |z| < 1\}$. Hohlov [1] introduced the convolution operator $H(a,b;c): A \to A$ defined by

$$H(a,b;c)f(z) = zF(a,b;c;z) * f(z),$$

where $F(a,b;c;z)$ is a well-known Gaussian hypergeometric function and defined by

$$F(a,b;c;z) = \sum_{k=0}^{\infty} \frac{(a)_k (b)_k}{(c)_k (1)_k} z^k \;,$$

where a, b, c are complex numbers such that $c \neq 0, -1, -2, \ldots$.

A hypergeometric function $F(a,b;c;z)$ is analytic in U and plays an important role in Geometric Function Theory. See the studies by Branges [2], Ahuja [3], Carleson and Shaffer [4], Owa and Srivastava [5], Miller and Mocanu [6], Ruscheweyh and Singh [7], Srivastava and Manocha [8], and Swaminathan [9].

For a function $f \in A$ given by Eqn. (1) and $g \in A$ defined by

$$g(z) = z + \sum_{k=2}^{\infty} b_k z^k \,,$$

we define the Hadamard product of f and g by

$$(f * g)(z) = z + \sum_{k=2}^{\infty} a_k b_k z^k \qquad , \quad z \in U \,. \tag{2}$$

Let E be the family of all harmonic functions $f = h + \overline{g}$, where

$$h(z) = z + \sum_{k=2}^{\infty} A_k z^k \quad , \qquad g(z) = \sum_{k=1}^{\infty} B_k z^k \quad , \qquad |B_1| < 1 \,, z \in U \tag{3}$$

are in the class A. For complex parameters $a_1, b_1, c_1, a_2, b_2, c_2$ $(c_1, c_2 \neq 0, -1, -2, \ldots)$, we define the functions $\Phi_1 = zF(a_1, b_1; c_1; z)$ and $\Phi_2 = zF(a_2, b_2; c_2; z)$.

Corresponding to these functions, we consider the following convolution operator

$$\Omega \equiv \Omega \begin{pmatrix} a_1, & b_1, & c_1 \\ a_2, & b_2, & c_2 \end{pmatrix} : E \to E ,$$

defined by

$$\Omega \begin{pmatrix} a_1, & b_1, & c_1 \\ a_2, & b_2, & c_2 \end{pmatrix} f = f * \left(\Phi_1 + \overline{\Phi_2}\right) = h * \Phi_1 + \overline{g * \Phi_2}$$

for any function $f = h + \overline{g}$ in E. Letting

$$\Omega \begin{pmatrix} a_1, & b_1, & c_1 \\ a_2, & b_2, & c_2 \end{pmatrix} F(z) = H(z) + \overline{G(z)} ,$$

we have

$$H(z) = z + \sum_{k=2}^{\infty} \frac{(a_1)_{k-1}(b_1)_{k-1}}{(c_1)_{k-1}(1)_{k-1}} A_k z^k ,$$

$$G(z) = \sum_{k=1}^{\infty} \frac{(a_2)_{k-1}(b_2)_{k-1}}{(c_2)_{k-1}(1)_{k-1}} B_k z^k. \tag{4}$$

We observe that

$$\Omega \begin{pmatrix} a_1, & 1, & a_1 \\ a_2, & 1, & a_2 \end{pmatrix} f(z) = f(z) = f(z) * \left(\frac{z}{1-z} + \overline{\frac{z}{1-z}}\right),$$

is the identity mapping.

This convolution operator Ω were defined and studied by the author in [10]. Denote by S_E the subclass of E that are univalent and sense-preserving in U.

Note that $\frac{f - \overline{B_1 f}}{1 - |B_1|^2} \in S_E$ whenever $f \in S_E$. We also let the subclass $S_E^0 \; of \; S_E$

$$S_E^0 = \{f = h + \overline{g} \in S_E : g'(0) = B_1 = 0\} .$$

The classes S_E^0 and S_E were first studied in [11]. Also, we let K_E^0, $S_E^{*,0}$ and C_E^0 denote the subclasses of S_E^0 of harmonic functions which are, respectively, convex, starlike and close-to-convex in U. For definitions and properties of these classes, one may refer to ([11,12]) or [13].

For $0 \le \alpha < 1$, $m \in N$ and $n \in N_0 = \{0,1,...\}$ let

$$N_E(\alpha) = \left\{ f \in E : Re\frac{f'(z)}{z'} \ge \alpha, z = re^{i\theta} \in U \right\},$$

$$G_E(\alpha) = \left\{ f \in E : Re\left\{ \left(1 + \rho e^{i\gamma}\right)\frac{D^m f(z)}{D^n f(z)} - \rho e^{i\gamma} \right\} \ge \alpha, \gamma \in R, z \in U \right\},$$

where $z' = \frac{\partial}{\partial\theta}\left(z = re^{i\theta}\right)$, $f'(z) = \frac{\partial}{\partial\theta} f\left(re^{i\theta}\right)$.

Define $TN_E(\alpha) = N_E(\alpha) \cap T$ and $TG_E(\alpha) = G_E(\alpha) \cap T$, where T consists of the functions $f = h + \overline{g}$ in S_E so that h and g are of the form

$$h(z) = z - \sum_{k=2}^{\infty} |A_k| z^k \quad , \qquad g(z) = \sum_{k=1}^{\infty} |B_k| z^k \quad . \tag{5}$$

The classes $N_E(\alpha)$ and $G_E(\alpha)$ were initially introduced and studied, respectively, in [14, 15]. A function in $G_E(\alpha)$ is called Goodman-Salagean-type harmonic univalent function in U.

In this paper, we will frequently use the notations

$$\Omega(f) = \Omega \begin{pmatrix} a_1, & b_1, & c_1 \\ a_2, & b_2, & c_2 \end{pmatrix} f ,$$

$$D_{k-1} = \frac{(|a_1|)_{k-1}(|b_1|)_{k-1}}{(|c_1|)_{k-1}(1)_{k-1}} \quad , \quad E_{k-1} = \frac{(|a_2|)_{k-1}(|b_2|)_{k-1}}{(|c_2|)_{k-1}(1)_{k-1}} ,$$

and a well-known formula

$$F(a,b;c;1) = \frac{\Gamma(c-a-b)\Gamma(c)}{\Gamma(c-a)\Gamma(c-b)} , Re(c-a-b) > 0.$$

In this paper the main object is to establish some important connections between the classes K_E^0, $S_E^{*,0}$, C_E^0, $N_E(\alpha)$ and $G_E(\alpha)$ by applying the convolution operator.

2. Connections with Goodman-Salagean-type Harmonic Univalent Functions

In order to establish connections between harmonic convex functions, we need following results in Lemma 1 [11], Lemma 2 [15] and Lemma 4 [10].

Lemma 1. If $f = h + \overline{g} \in K_E^0$ where h and g are given by Eqn. (3) with $B_1 = 0$, then

$$|A_n| \leq \frac{n+1}{2} \quad , \quad |B_n| \leq \frac{n-1}{2} .$$

Lemma 2. Let $f = h + \overline{g}$ be given by Eqn. (3). If

$$\sum_{k=2}^{\infty} \left[[(1+\rho)k^m - k^n(\alpha+\rho)]|a_k| + [(1+\rho)k^m - (-1)^{m-n}k^n(\alpha+\rho)]|b_k| \right]$$

$$\leq 1 - \alpha , \tag{6}$$

then f is sense-preserving, Goodman-Salagean-type harmonic univalent functions in U and $f \in G_E(\alpha)$.

Remark 3. In [15], it is also shown that $f = h + \overline{g}$ given by Eqn. (5) is in the family $TG_E(\alpha)$, if and only if the coefficient condition (6) holds. Moreover, if $f \in TG_E(\alpha)$, then

$$|A_k| \leq \frac{1-\alpha}{(1+\rho)k^m - k^n(\alpha+\rho)} \quad , \qquad k \geq 2,$$

$$|B_k| \leq \frac{1-\alpha}{(1+\rho)k^m - (-1)^{m-n}k^n(\alpha+\rho)} \quad , \qquad k \geq 1.$$

Lemma 4. If $a, b, c > 0$, then

(i) $F(a+n, b+n; c+n; 1) = \frac{(c)_n}{(c-a-b-n)_n} F(a, b; c; 1)$,

for $n = 0, 1, 2, 3, \ldots$, $if\ c > a + b + \mathrm{n}$.

(ii) $\sum_{k=2}^{\infty}(k-1)\frac{(a)_{k-1}(b)_{k-1}}{(c)_{k-1}(1)_{k-1}} = \frac{ab}{c-a-b-1} F(a, b; c; 1)$, $if\ c > a + b + 1$.

(iii) $\sum_{k=2}^{\infty}(k-1)^2\frac{(a)_{k-1}(b)_{k-1}}{(c)_{k-1}(1)_{k-1}} = \left[\frac{(a)_2(b)_2}{(c-a-b-2)_2} + \frac{ab}{c-a-b-1}\right] F(a, b; c; 1)$,

if $c > a + b + 2$.

(iv) $\sum_{k=2}^{\infty}(k-1)^3\frac{(a)_{k-1}(b)_{k-1}}{(c)_{k-1}(1)_{k-1}} = \left[\frac{(a)_3(b)_3}{(c-a-b-3)_3} + \frac{3(a)_2(b)_2}{(c-a-b-2)_2} + \frac{ab}{c-a-b-1}\right] F(a, b; c; 1)$,

if $c > a + b + 3$.

Theorem 5. Let $a_i, b_i \in C\backslash\{0\}, c_i \in R$ and $c_i > |a_i| + |b_i| + 2$ for $i = 1, 2$. If for some $\rho(0 \leq \rho \leq 1)$ and $\alpha(0 \leq \alpha < 1)$, when $m = 1, n = 0$ the inequality

$$Q_1F(|a_1|,|b_1|;c_1;1)+R_1F(|a_2|,|b_2|;c_2;1)\leq 4(1-\alpha),$$

is satisfied, then $\Omega(K_E^0)\subset G_E(\alpha)$, where

$$Q_1=(1+\rho)\frac{(|a_1|)_2(|b_1|)_2}{(c_1-|a_1|-|b_1|-2)_2}-(3+2\rho-\alpha)\frac{|a_1b_1|}{(c_1-|a_1|-|b_1|-1)}+2(1-\alpha)$$

$$R_1=(1+\rho)\frac{(|a_2|)_2(|b_2|)_2}{(c_2-|a_2|-|b_2|-2)_2}+(1+2\rho+\alpha)\frac{|a_2b_2|}{(c_2-|a_2|-|b_2|-1)}\ .$$

Proof. Let $f=h+\overline{g}\in K_E^0$ where h and g are of the form Eqn. (3) with $B_1=0$. We need to show that $\Omega(f)=H+\overline{G}\in G_E(\alpha)$, where H and G defined by Eqn. (4) are analytic functions in U. In view of Lemma 2, we need to prove that $P_1\leq 1-\alpha$ where

$$P_1=\sum_{k=2}^{\infty}[(1+\rho)k^m-k^n(\alpha+\rho)]\left|\frac{(a_1)_{k-1}(b_1)_{k-1}}{(c_1)_{k-1}(1)_{k-1}}A_k\right|$$

$$+\sum_{k=2}^{\infty}[(1+\rho)k^m-(-1)^{m-n}k^n(\alpha+\rho)]\left|\frac{(a_2)_{k-1}(b_2)_{k-1}}{(c_2)_{k-1}(1)_{k-1}}B_k\right|.$$

In view of Lemma 1 and Lemma 4, it follows that

$$P_1\leq\frac{1}{2}\sum_{k=2}^{\infty}(k+1)[(1+\rho)k^m-k^n(\alpha+\rho)]D_{k-1}$$

$$+\frac{1}{2}\sum_{k=2}^{\infty}(k-1)[(1+\rho)k^m-(-1)^{m-n}k^n(\alpha+\rho)]\,E_{k-1}$$

$$=\frac{1}{2}\sum_{k=2}^{\infty}[(1+\rho)(k-1)^2-(3+2\rho-\alpha)(k-1)+2(1-\alpha)]D_{k-1}$$

$$+\frac{1}{2}\sum_{k=2}^{\infty}[(1+\rho)(k-1)^2+(1+2\rho+\alpha)(k-1)]\,E_{k-1}$$

$$=\frac{1}{2}Q_1F(|a_1|,|b_1|;c_1;1)+\frac{1}{2}R_1F(|a_2|,|b_2|;c_2;1)-(1-\alpha)\ .$$

Hence $P_1\leq 1-\alpha$ follows from the given condition.

In order to determine connection between $TN_E(\beta)$ and $G_E(\alpha)$, we need the following results in Lemma 6 [14] and Lemma 8 [3] .

Lemma 6. Let $f = h + \overline{g}$ where h and g are given by Eqn. (5) with $B_1 = 0$, and suppose that $0 \leq \beta < 1$. Then

$$f \in TN_E(\beta) \Leftrightarrow \sum_{k=2}^{\infty} k|A_k| + \sum_{k=2}^{\infty} k|B_k| \leq 1 - \beta.$$

Remark 7. If $f \in TN_E(\beta)$, then

$$|A_k| \leq \frac{1-\beta}{k} \quad , \qquad k \geq 2 \quad , \qquad |B_k| \leq \frac{1-\beta}{k} \quad , \qquad k \geq 1.$$

Lemma 8. Let $a, b \in C\backslash\{0\}, a \neq 1, b \neq 1, c \in (0,1) \cup (1,\infty)$ and $c > \max\{0, |a| + |b| - 1\}$. Then

$$\sum_{k=1}^{\infty} \frac{1}{k} \frac{(|a|)_{k-1}(|b|)_{k-1}}{(c)_{k-1}(1)_{k-1}} = \frac{(c - |a| - |b|)}{(|a| - 1)(|b| - 1)} F(|a|, |b|; c; 1) - \frac{(c-1)}{(|a| - 1)(|b| - 1)} .$$

Theorem 9. Let $a_i, b_i \in C\backslash\{0\}, a_i \neq 1, b_i \neq 1, c_i \in R$ and $c_i > \max\{0, |a_i| + |b_i| - 1\}$ for $i = 1, 2$. If for some $\beta (0 \leq \beta < 1)$ and $\alpha (0 \leq \alpha < 1)$, when $m = 1, n = 0$ and $m = 2, n = 0$ and $m = 2, n = 1$ the inequality

$$Q_2 F(|a_1|, |b_1|; c_1; 1) + R_2 F(|a_2|, |b_2|; c_2; 1) \leq \frac{(1-\alpha)(2-\beta)}{(1-\beta)}$$

$$-((\alpha + \rho)) \left[\frac{(c_1 - 1)}{(|a_1| - 1)(|b_1| - 1)} - \frac{(c_2 - 1)}{(|a_2| - 1)(|b_2| - 1)}\right]$$

is satisfied, then $\Omega(TN_E(\beta)) \subset G_E(\alpha)$, where

$$Q_2 = (1 + \rho) - (\alpha + \rho) \frac{(c_1 - |a_1| - |b_1|)}{(|a_1| - 1)(|b_1| - 1)},$$

$$R_2 = (1 + \rho) + (\alpha + \rho) \frac{(c_2 - |a_2| - |b_2|)}{(|a_2| - 1)(|b_2| - 1)} .$$

Proof. Let $f = h + \overline{g} \in TN_E(\beta)$ where h and g are given by Eqn. (5). In view of Lemma 2, it is enough to show that $P_2 \leq 1 - \alpha$ and

$$P_2 = \sum_{k=2}^{\infty} [(1 + \rho)k^m - k^n(\alpha + \rho)] \left| \frac{(a_1)_{k-1}(b_1)_{k-1}}{(c_1)_{k-1}(1)_{k-1}} A_k \right|$$

$$+\sum_{k=1}^{\infty}[(1+\rho)k^m-(-1)^{m-n}k^n(\alpha+\rho)]\left|\frac{(a_2)_{k-1}(b_2)_{k-1}}{(c_2)_{k-1}(1)_{k-1}}B_k\right|.$$

Using Remark 7 and Lemma 8 if $m=1, n=0$. Then

$$P_2 \le (1-\beta)\left(\sum_{k=2}^{\infty}\left[(1+\rho)-\frac{(\alpha+\rho)}{k}\right]D_{k-1}+\sum_{k=1}^{\infty}\left[(1+\rho)+\frac{(\alpha+\rho)}{k}\right]E_{k-1}\right)$$

$$= (1-\beta)\begin{pmatrix} Q_2F(|a_1|,|b_1|;c_1;1)+R_2F(|a_2|,|b_2|;c_2;1) \\ -(1-\alpha)+\dfrac{(\alpha+\rho)(c_1-1)}{(|a_1|-1)(|b_1|-1)}-\dfrac{(\alpha+\rho)(c_2-1)}{(|a_2|-1)(|b_2|-1)}\end{pmatrix}$$

$$\le (1-\alpha)$$

by the given hypothesis.

Now, if $m=2, n=0$, then

$$P_2 \le (1-\beta)\left(\sum_{k=2}^{\infty}\left[(1+\rho)k-\frac{(\alpha+\rho)}{k}\right]D_{k-1}+\sum_{k=1}^{\infty}\left[(1+\rho)k-\frac{(\alpha+\rho)}{k}\right]E_{k-1}\right)$$

$$= (1-\beta)\left(\sum_{k=2}^{\infty}\left[(1+\rho)(k-1)+(1+\rho)-\frac{(\alpha+\rho)}{k}\right]D_{k-1}\right.$$

$$\left.+\sum_{k=1}^{\infty}\left[(1+\rho)(k-1)+(1+\rho)-\frac{(\alpha+\rho)}{k}\right]E_{k-1}\right)$$

$$= (1-\beta)\begin{pmatrix} Q_2F(|a_1|,|b_1|;c_1;1)+R_2F(|a_2|,|b_2|;c_2;1) \\ -(1-\alpha)+\dfrac{(\alpha+\rho)(c_1-1)}{(|a_1|-1)(|b_1|-1)}-\dfrac{(\alpha+\rho)(c_2-1)}{(|a_2|-1)(|b_2|-1)}\end{pmatrix}$$

$$\le (1-\alpha)$$

and

$$Q_2 = (1+\rho)\frac{|a_1b_1|}{(c_1-|a_1|-|b_1|-1)}+(1+\rho)\frac{|a_1b_1|}{(c_1-|a_1|-|b_1|-1)}$$

$$+(\alpha+\rho)\frac{(c_1-|a_1|-|b_1|)}{(|a_1|-1)(|b_1|-1)}$$

$$R_2 = (1+\rho)\frac{|a_2b_2|}{(c_2-|a_2|-|b_2|-1)}+(1+\rho)\frac{|a_1b_1|}{(c_1-|a_1|-|b_1|-1)}$$

$$+(\alpha+\rho)\frac{(c_2-|a_2|-|b_2|)}{(|a_2|-1)(|b_2|-1)}.$$

Finally, if $m=2, n=1$, then

$$P_2 \le (1-\beta)\left(\sum_{k=2}^{\infty}[(1+\rho)k-(\alpha+\rho)]D_{k-1}+\sum_{k=1}^{\infty}[(1+\rho)k+(\alpha+\rho)]\,E_{k-1}\right)$$

$$=(1-\beta)\left(\sum_{k=2}^{\infty}[(1+\rho)(k-1)-(1-\alpha)]D_{k-1}\right.$$

$$\left.+\sum_{k=1}^{\infty}[(1+\rho)(k-1)+(1+2\rho+\alpha)]\,E_{k-1}\right)$$

$$=(1-\beta)\left(Q_2F(|a_1|,|b_1|;c_1;1)+R_2F(|a_2|,|b_2|;c_2;1)-(1-\alpha)\right)$$

$$\le(1-\alpha)$$

and

$$Q_2=(1+\rho)\frac{|a_1b_1|}{(c_1-|a_1|-|b_1|-1)}-(1-\alpha),$$

$$R_2=(1+\rho)\frac{|a_2b_2|}{(c_2-|a_2|-|b_2|-1)}+(1+2\rho+\alpha)\ .$$

We next find connections of the classes $S_E^{*,0}$, C_E^0 and T_E^0 with $G_E(\alpha)$. However, we first need the following result which may be found in [11, 12] or [16] .

Lemma 10. If $f=h+\overline{g}\in C_E^0(S_E^{*,0}, T_E^0)$ where h and g are given by Eqn. (3) with $B_1=0$, then

$$|A_k|\le\frac{(2k+1)(k+1)}{6}\quad,\quad |B_k|\le\frac{(2k-1)(k-1)}{6}\ .$$

Theorem 11. Let $a_i, b_i\in C\backslash\{0\}, c_i\in R$ and $c_i>|a_i|+|b_i|+3$ for $i=1,2$. If for some $\rho(0\le\rho\le1)$ and $\alpha(0\le\alpha<1)$, when $m=1, n=0$ the inequality

$$Q_3F(|a_1|,|b_1|;c_1;1)+R_3F(|a_2|,|b_2|;c_2;1)\le12(1-\alpha),$$

is satisfied, then $\Omega(C_E^0)\subset G_E(\alpha)$, $\Omega(S_E^{*,0})\subset G_E(\alpha)$, $\Omega(T_E^0)\subset G_E(\alpha)$, where

$$Q_3=2(1+\rho)\frac{(|a_1|)_3(|b_1|)_3}{(c_1-|a_1|-|b_1|-3)_3}+(9+7\rho-2\alpha)\frac{(|a_1|)_2(|b_1|)_2}{(c_1-|a_1|-|b_1|-2)_2}$$

$$+(13+6\rho-7\alpha)\frac{|a_1b_1|}{(c_1-|a_1|-|b_1|-1)}+6(1-\alpha)\ ,$$

$$R_3=2(1+\rho)\frac{(|a_2|)_3(|b_2|)_3}{(c_2-|a_2|-|b_2|-3)_3}+(3+\rho-2\alpha)\frac{(|a_2|)_2(|b_2|)_2}{(c_2-|a_2|-|b_2|-2)_2}$$

$$+(1-\alpha)\frac{|a_2b_2|}{(c_2-|a_2|-|b_2|-1)}\ .$$

Proof. Let $f=h+\overline{g}\in C_E^0(S_E^{*,0},T_E^0)$ where h and g are of the form Eqn. (3) with $B_1=0$. We need to prove that $\Omega(f)=H+\overline{G}\in G_E(\alpha)$, where H and G defined by Eqn. (4) are analytic functions in U. In view of Lemma 2, we need to show that $P_3\le 1-\alpha$ where

$$P_3=\sum_{k=2}^{\infty}[(1+\rho)k^m-k^n(\alpha+\rho)]\left|\frac{(a_1)_{k-1}(b_1)_{k-1}}{(c_1)_{k-1}(1)_{k-1}}A_k\right|$$

$$+\sum_{k=2}^{\infty}[(1+\rho)k^m-(-1)^{m-n}k^n(\alpha+\rho)]\left|\frac{(a_2)_{k-1}(b_2)_{k-1}}{(c_2)_{k-1}(1)_{k-1}}B_k\right|.$$

In view of Lemma 4 and Lemma 10, it follows that

$$P_3\le\frac{1}{6}\sum_{k=2}^{\infty}(2k+1)(k+1)[(1+\rho)k-(\alpha+\rho)]D_{k-1}$$

$$+\frac{1}{6}\sum_{k=2}^{\infty}(2k-1)(k-1)[(1+\rho)k+(\alpha+\rho)]\,E_{k-1}$$

$$=\frac{1}{6}\sum_{k=2}^{\infty}\begin{bmatrix}2(1+\rho)(k-1)^3+(9+7\rho-2\alpha)(k-1)^2\\+(13+6\rho-7\alpha)(k-1)+6(1-\alpha)\end{bmatrix}D_{k-1}$$

$$+\frac{1}{6}\sum_{k=2}^{\infty}[2(1+\rho)(k-1)^3+(3+\rho-2\alpha)(k-1)^2+(1-\alpha)(k-1)]\,E_{k-1}$$

$$=\frac{1}{6}Q_3F(|a_1|,|b_1|;c_1;1)+\frac{1}{6}R_3F(|a_2|,|b_2|;c_2;1)-(1-\alpha).$$

Hence $P_3\le 1-\alpha$ follows from the given condition.

In the next theorem, we establish connections between $TG_E(\alpha)$ and $G_E(\alpha)$.

Theorem 12. Let $a_i,b_i\in C\backslash\{0\},c_i\in R$ and $c_i>|a_i|+|b_i|$ for $i=1,2$. If for some $\alpha(0\le\alpha<1)$, when $m=1,\ n=0$ the inequality

$$F(|a_1|,|b_1|;c_1;1)+F(|a_2|,|b_2|;c_2;1)\le 2\ ,$$

is satisfied, then $\Omega(TG_E(\alpha)) \subset G_E(\alpha)$.

Proof. By using Lemma 2 and the definition of P_2 in Theorem 9, we need to prove that $P_2 \leq 1-\alpha$.

By Remark 3, it follows that

$$P_2 = \sum_{k=2}^{\infty}[(1+\rho)k^m - k^n(\alpha+\rho)]\left|\frac{(a_1)_{k-1}(b_1)_{k-1}}{(c_1)_{k-1}(1)_{k-1}}A_k\right| + \sum_{k=1}^{\infty}[(1+\rho)k^m - (-1)^{m-n}k^n(\alpha+\rho)]\left|\frac{(a_2)_{k-1}(b_2)_{k-1}}{(c_2)_{k-1}(1)_{k-1}}B_k\right|$$

$$\leq (1-\alpha)\left(\sum_{k=2}^{\infty}D_{k-1} + \sum_{k=1}^{\infty}E_{k-1}\right)$$

$$= (1-\alpha)\,(F(|a_1|,|b_1|;c_1;1) + F(|a_2|,|b_2|;c_2;1) - 1)$$

$$\leq (1-\alpha).$$

By the given condition, the proof is completed.

In the next results, we establish connections between $TG_E(\alpha)$ and $G_E(\alpha)$. By diluting the restrictions on the complex coefficients of Theorem 12.

Theorem 13. Let $a_1b_1 < 0$, $a_1, b_1 > -1$, $c_1 > \max\{0, a_1+b_1\}$, $a_2, b_2 \in C\backslash\{0\}$ and $c_2 > |a_2| + |b_2|$, then a sufficient condition for $\Omega(TG_E(\alpha)) \subset G_E(\alpha)$ is that

$$F(|a_1|,|b_1|;c_1;1) - F(|a_2|,|b_2|;c_2;1) \geq 0,$$

for any $\rho(0 \leq \rho \leq 1)$ and $\alpha(0 \leq \alpha < 1)$, when $m = 1,\ n = 0$.

Proof. Let $f = h + \overline{g} \in TG_E(\alpha)$ where h and g are of the form Eqn. (5). Then

$$\Omega(f) = z - \sum_{k=2}^{\infty}\frac{(a_1)_{k-1}(b_1)_{k-1}}{(c_1)_{k-1}(1)_{k-1}}|A_k|z^k + \overline{\sum_{k=1}^{\infty}\frac{(a_2)_{k-1}(b_2)_{k-1}}{(c_2)_{k-1}(1)_{k-1}}|B_k|z^k}.$$

This function can be rewritten as

$$\Omega(f) = z + \frac{|a_1b_1|}{c_1}\sum_{k=2}^{\infty}\frac{(a_1+1)_{k-2}(b_1+1)_{k-2}}{(c_1+1)_{k-2}(1)_{k-1}}|A_k|z^k + \overline{\sum_{k=1}^{\infty}\frac{(a_2)_{k-1}(b_2)_{k-1}}{(c_2)_{k-1}(1)_{k-1}}|B_k|z^k}.$$

In view of Lemma 2, we need to show that $P_4 \leq 1$ where

$$P_4 = \frac{|a_1 b_1|}{c_1}\sum_{k=2}^{\infty}\left[\frac{(1+\rho)k-(\alpha+\rho)}{1-\alpha}\right]\frac{(a_1+1)_{k-2}(b_1+1)_{k-2}}{(c_1+1)_{k-2}(1)_{k-1}}|A_k|$$
$$+\sum_{k=1}^{\infty}\left[\frac{(1+\rho)k+(\alpha+\rho)}{1-\alpha}\right]\frac{(a_2)_{k-1}(b_2)_{k-1}}{(c_2)_{k-1}(1)_{k-1}}|B_k|$$

$$\leq \frac{|a_1 b_1|}{c_1}\sum_{k=2}^{\infty}\frac{(a_1+1)_{k-2}(b_1+1)_{k-2}}{(c_1+1)_{k-2}(1)_{k-1}}|A_k| + \sum_{k=1}^{\infty}E_{k-1}$$

$$= \frac{|a_1 b_1|}{a_1 b_1}\sum_{k=1}^{\infty}\frac{(a_1)_k(b_1)_k}{(c_1)_k(1)_{k-1}}|A_k| + \sum_{k=1}^{\infty}E_{k-1}$$

$$= -F(|a_1|,|b_1|;c_1;1) + F(|a_2|,|b_2|;c_2;1) + 1 \leq 1,$$

by the given condition.

In the next theorem, we present condition on the parameters $a_1, a_2, b_1, b_2, c_1, c_2$ and obtain a characterization for operator Ω which maps $TG_E(\alpha)$ onto itself.

Theorem 14. Let $a_i, b_i > 0$, $c_i > a_i + b_i$ $(i = 1,2)$, $\rho(0 \leq \rho \leq 1)$ and $\alpha(0 \leq \alpha < 1)$ when $m = 1, n = 0$ then $\Omega(TG_E(\alpha)) \subset TG_E(\rho,\alpha)$ if and only if

$$F(|a_1|,|b_1|;c_1;1) + F(|a_2|,|b_2|;c_2;1) \leq 2.$$

Proof. Let $f = h + \overline{g} \in TG_E(\rho,\alpha)$ where h and g are of the form Eqn. (5). We need to prove that $\Omega(f) = H + \overline{G} \in TG_E(\rho,\alpha)$, where H and G defined by Eqn. (4) $P_4 \leq 1$, where

$$P_4 = \sum_{k=2}^{\infty}\left[\frac{(1+\rho)k-(\alpha+\rho)}{1-\alpha}\right]\left|\frac{(a_1)_{k-1}(b_1)_{k-1}}{(c_1)_{k-1}(1)_{k-1}}A_k\right|$$
$$+\sum_{k=1}^{\infty}\left[\frac{(1+\rho)k+(\alpha+\rho)}{1-\alpha}\right]\left|\frac{(a_2)_{k-1}(b_2)_{k-1}}{(c_2)_{k-1}(1)_{k-1}}B_k\right|.$$

By using Remark 3, we obtain

$$P_4 \leq \sum_{k=1}^{\infty}D_k + \sum_{k=0}^{\infty}E_k \leq F(|a_1|,|b_1|;c_1;1) + R_3F(|a_2|,|b_2|;c_2;1) - 1.$$

Hence $P_4 \leq 1$ follows from the given condition.

References

[1] Hohlov, Y.E., *Convolution operators preserving univalent functions*, Ukrainian Mathematical Journal, 37, 220-226, 1985.

[2] de Branges, L., *A proof of the Bieberbach conjecture*, Acta Mathematica, 154, 137-152, 1985.

[3] Ahuja, O.P., *Connections between various subclasses of planar harmonic mappings Involving hypergeometric functions* , Applied Mathematics and Computation, 198 (1), 305-316, 2008.

[4] Carleson, B.C., Shaffer, D.B., *Starlike and prestarlike hypergeometric functions*, SIAM Journal on Mathematical Analysis, 15, 737-745, 1984.

[5] Owa, S., Srivastava, H.M., *Univalent and starlike generalized hypergeometric functions*, Canadian Journal of Mathematics, 39, 1057-1077, 1987.

[6] Miller, S., Mocanu, P.T., *Univalence of Gaussian and confluent hypergeometric Functions*, Proceedings of American Mathematical Society, 110(2), 333-342, 1990.

[7] Ruscheweyh, S., Singh, V., *On the order of starlikeness of hypergeometric functions*, Journal of Mathematical Analysis and Applications, 113, 1-11, 1986.

[8] Srivastava, H.M., Manocha, H.L., *A Treatise on Generating Functions*, Ellis Horwood Limited and John Wiley & Sons, New York, Chichester, Toronto, 1984.

[9] Swaminathan, A., *Certain Sufficiency conditions on Gaussian hypergeometric functions*, Journal of Inequalities in Pure and Applied Mathematics, 5(4), Article 83, 1-10, 2004.

[10] Ahuja, O.P., *Planar harmonic convolution operators generated by hypergeometric functions*, Integral Transforms and Special Functions, 18 (3), 165-177, 2007.

[11] Clunie, J., Sheil-Small, T., *Harmonic univalent functions,* Annales Academie Scientiarum Fennice, Series A. I. Mathematica 9, 3-25, 1984.

[12] Ahuja, O.P., *Planar harmonic univalent and related mappings*, Journal of Inequalities in Pure and Applied Mathematics, 6(4) Art. 122, 1-18, 2005.

[13] Duren, P., *Harmonic Mappings in the plane*, Cambridge Tracts in Mathematics, Vol. 156, Cambridge University Press, Cambridge, 2004, ISBN 0-521064121-7.

[14] Ahuja, O.P., Jahangiri J.M., *Noshiro-type harmonic univalent functions*, Scientiae Mathematicae Japonicae, 6(2), 253-259, 2002.

[15] Aghalary, R., *Goodman-Salagean-Type Harmonic Univalent Functions with Varying Arguments*, International Journal of Mathematical Analysis, Vol. 1, no. 22, 1051-1057, 2007.

[16] Wang, X.T., Liang, X.Q., Zhang, Y.L., *Precise coefficient estimates for close-to-convex harmonic univalent mappings*, Journal of Mathematical Analysis and Applications, 263(2), 501-509, 2001.

Adıyaman University Journal of Science
https://dergipark.org.tr/en/pub/adyujsci
DergiPark AKADEMİK
ISSN 2147-1630
e-ISSN 2146-586X

A Probabilistic Atomic Radius Definition: Application to Ground State Hydrogen-Like Atoms

Fatih Mehmet AVCU[1,*], Serkan ALAGÖZ[2]

[1]*Inonu University, Department of Informatics, Malatya, Turkey*
fatih.avcu@inonu.edu.tr, ORCID: 0000-0002-1973-7745
[2]*Inonu University, Department of Physics, Malatya, Turkey*
serkan.alagoz@inonu.edu.tr, ORCID: 0000-0003-2642-8462

Received: 25.05.2020 **Accepted:** 03.12.2020 **Published:** 30.12.2020

Abstract

Several atomic radius concepts were proposed to express size of atoms in chemistry and physics. This study briefly surveys widely used definitions of atomic radiuses and introduces a probabilistic atomic radius concept that is based on the probability measure, which considers probability of the outermost electron to be in a spherical volume that is centered by nucleus of a hydrogen-like atom. Depending on this probability measure, 99% probabilistic atomic radius is calculated for a ground state hydrogen atom and its interpretation for hydrogen-like atomic systems is discussed.

Keywords: Quantum mechanics; Solutions of wave equations; Atomic radius; Bound states.

Olasılıksal Atomik Yarıçap Tanımı: Taban Durumu Hidrojen Benzeri Atomlara Uygulanması

Öz

* Corresponding Author
DOI: 10.37094/adyujsci.742590

Kimya ve Fizik alanında atomların büyüklüğünü ifade etmek için birkaç atom yarıçapı kavramı önerilmiştir. Bu çalışmada, atomik yarıçap tanımları incelenmiş, olasılık ölçüsüne dayanan ve en dıştaki elektronun hidrojen benzeri bir atomun çekirdeği ile merkezlenmiş küresel bir hacimde olma olasılığını dikkate alan olasılıksal bir atomik yarıçap kavramını sunulmuştur. Bu olasılık ölçüsüne bağlı olarak, temel durum hidrojen atomu için %99 olasılık ile atomik yarıçapı hesaplanmış ve bunun hidrojen benzeri atomik sistemler için yorumlanmıştır.

Anahtar Kelimeler: Kuantum Mekaniği; Dalga denklemlerinin çözümleri; Atom yarıçapı; Bağlı durumlar.

1. Introduction

Rutherford–Bohr model, also known as Bohr model, have suggested an atom structure that consists of a nucleus and spinning electrons. This model is relatively primitive model of a hydrogen atom compared to quantum wave mechanics models of atoms. Based on experimental measurements, Bohr atom model suggests that mechanical energy related with energy of atomic electrons should be quantized. According to Bohr's model, electron orbiting around nucleus of atom can be certain particular states of motion, which is called “stationary states” [1]. In other words, the model implies that an electron orbits only at certain distances to nucleus depending on energy state of an atom. Such consideration of an atom allows fundamental definition of an atom radius with respect to distances of electron orbits to nucleus in space. For single electron atoms such as hydrogen, the smallest possible orbit with lowest energy state has an orbital radius, which was called Bohr radius. Then, the Bohr radius became an important physical constant associated with atomic scales and it is approximately equal to the most probable distance between the nucleus and the electron in a hydrogen atom in its ground state. Value of Bohr radius is approximately $a_0 = \frac{\mathrm{h}^2}{mke^2} = 0.0529\, nm \cong 0.53\ A^o$. An important point for Bohr radius is the fact that it is the radial distance to nucleus that has the peak of probability density of an electron [2].

The atomic radius is commonly used in chemistry and physics to assign a size for atoms in spatial domain, and it is generally considered as distance between the nucleus and the boundary of the surrounding cloud of electrons [3]. Experimental value of atomic radius came out in works of X-ray crystallography with a question whether the same radii is valid for atoms of the same element [4]. More experimental data on crystal structures showed that the same atom in different crystal structures could not have the same experimental radii [5].

There is not unique value of atomic radius parameter because it changes depending on the atom’s state and the purpose of measurements or analyses [3]. The main difficulty is that

definition of atomic boundary varies depending on the context of analyses. For example, atomic radius changes depending on several factors: atoms can be isolated or bounded; type of bounding (ionic or covalent) affects atomic boundary considerations and energy states of atoms are effective in atom models. Therefore, several non-equivalent definitions of atomic radius are utilized at various contexts. For ease of atomic radius calculations, atoms were mainly assumed to have a spherical shape and such approximate models are utilized for explanations of several phenomena, such as the density of matter, the diffusion of fluids, arrangement of atoms and ions in crystals and the size and shape of molecules [6]. Such a spherical confinement of hydrogen atom enables investigation of many properties in several studies [7]. A set of empirical atomic radii has been proposed and sum of the atomic radii of two atoms forming a bond in a crystal or molecule is used for estimation of approximate distance between nucleuses of those two atoms [8]. For other atoms and molecules, relationship between atomic radius and chemical properties has been investigated. A recent work indicated existence of a linear relationship between the atomic radius and deposition potentials for lanthanide metals [9]. Another study considered decoding of atomic and ionic radii of transition metals in terms of energy response against changes in electron number. Employing charge sensitivity analysis and the electronegativity equalization principle, authors have presented an interpretation of the electronic structure transformation (electron-following/preceding perspectives) into atomic diameters [10].

This study introduces a probabilistic atomic radius concept, which is based on probability of the outermost electrons to be in the spherical volume that is centered by nucleus. Hence, probability measure is used to express tendency of the outermost electron in a nucleus centered, spherical space volume. Cumulative radial probability density of electron, which is obtained from solution of Schrodinger equation for hydrogen atom, is used and the 99% probability of electron to be existent in this volume is considered for probabilistic atomic radius definition. It is the case that spherical space volume involves 99% of electron cloud, which infers a 99% probability of an electron existence in this spherical volume. The 99% probabilistic atomic radius is defined arithmetically as the radius of such nucleus centered spherical volume that involves the valance electron with a probability of 99%.

2. Brief Survey of Atomic Radius

This section summarizes commonly used atomic radius definitions:

Van der Waals radius is the half of minimum distance between the nuclei of two atoms that are not bound to the same molecule [11]. It is widely used to calculate Van der Waals volume of

atoms. For hydrogen molecules, value of Van der Waals radii is found 0.12 nm. Neutron diffraction experiments can provide an estimate experimental value of Van der Waals radius.

Ionic radius defines a radius for an ion in ionic crystals. Sum of ionic radiuses is utilized to estimate gaps between two adjacent oppositely charged ions [11]. Ions were assumed to be hard spherical bodies with ionic radii. The sum of ionic radii is used to estimate the distance between cations and anions in a crystal lattice. X-ray crystallography is used to estimate ionic radius of ions. Hydrogen ions lose their single electrons and they become a positive charged ion formed only by a proton nucleus without any electron. Therefore, ionic radius is not applicable for hydrogen ions so that it does not contain a valance electron to form space volume.

Covalent radius is the radius that is defined for covalently bounded atoms [6]. The length of covalent bond is estimated by the sum of covalent radii [11]. For Hydrogen with single bond, covalent radius is estimated to be 0.038 nm. X-ray diffraction and rotational spectroscopy are used to estimate experimental value of covalent radius.

Metallic radius is the half distance between the two adjacent metal ions in a metallic structure [6]. It is defined for atoms that can be joined by metallic bonds.

Bohr radius is considered as the most probable distance between the nucleus and the electron in a hydrogen atom in its ground state. Value of Bohr radius was given $a_0 \cong 0.0529$ nm and depending on energy states, radius of hydrogen atom is written by $r_n = a_o n^2$, where principle quantum number n takes 1, 2, 3. Bohr radius of hydrogen atom is considered as a physical constant to scale atomic distances [2].

Critical cage radius is considered according to binding energy of ground state hydrogen atom. A spherical box is assumed to have impenetrable surface and the radius of sphere box reduced until binding energy diminishes [12, 13]. A critical value of the sphere radius at which the binding energy becomes zero is called critical cage radius [7, 12, 13]. Binding energy of ground state of the hydrogen atom is calculated as a function of the sphere radius [13]. For hydrogen in ground state, critical cage radius is found about 1.83 $a_0 = 0.097$ nm [7].

Another probabilistic modeling of atom radius was given corresponding to the maximum of the radial probability function of the valence electron [14-16]. For a hydrogen-like atom, peak of radial probability function is exactly at Bohr radius [14-16]. On the other hand, expected value of radial probability function is accounted as atomic radii. For ground state hydrogen atoms, expected value is calculated as $< r >= 1.5a_0 = 0.0794$ nm [2].

3. Volumetric Probability Distribution of a Particle in Quantum Mechanics

As known, electrons in the hydrogen atom have a spherically symmetric potential, therefore, spherical polar coordinates are used for the time independent solution of Schrodinger wave equation. Schrodinger equation is generally solved for the hydrogen atoms by separating the variables in spherical polar coordinate system as follows [2, 17-19],

$$\psi_{n,l,m_l}(r,\theta,\varphi) = R(r)P(\theta)F(\varphi) \tag{1}$$

where, parameters (r,θ, φ) are components of polar coordinate. Schrodinger equation is generally expressed as [2, 17-19],

$$\frac{-\hbar^2}{2\mu}\frac{1}{r^2\,sin\,\theta}\left[sin\,\theta\frac{\partial}{\partial r}\left(r^2\frac{\partial\psi}{\partial r}\right)+\frac{\partial}{\partial\theta}\left(sin\,\theta\frac{\partial\psi}{\partial\theta}\right)+\frac{1}{sin\,\theta}\frac{\partial^2\psi}{\partial\theta^2}\right]+U(r)\psi(r,\theta,\varphi) = E\psi(r,\theta,\varphi) \tag{2}$$

where, the potential energy is $U(r) = -e^2/4\pi\varepsilon_0 r$ and the parameter E denotes energy of system. The reduced mass is written as $\mu = m_e m_p/(m_e + m_p)$. Solution of this equation is found depending on states of principle quantum number (n), orbital quantum number (l), magnetic quantum number (m_l).

In quantum mechanics, the maximum of square of wave function shows the most likely position where a particle can exist in space [2, 17-19]. Probability of a free particle in a range $x \in [x_1, x_2]$) is expressed as,

$$P(x_1 \le x \le x_2) = \int_{x_2}^{x_2} |\psi(x)|^2 dx \tag{3}$$

where, $\psi(x)$ is normalized wave function of the particle, which satisfies the condition $\int_{-\infty}^{\infty}|\psi(x)|^2dx = 1$ to express a probability density function on space. This condition also infers that the particle definitely exist in an infinite space. The radial probability density is defined as multiplication of the normalized wave function square and a spherical shell volume element $4\pi r dr$ as,

$$dP = |\psi(r)|^2 4\pi r dr \tag{4}$$

When a finite volume of spherical space element, which is bounded in radial range of $r_1 \le r \le r_2$, is considered, volumetric probability density of a particle can be expressed as,

$$P(r_1 \leq r \leq r_2) = \int_{r_2}^{r_2} |\psi(r)|^2 4\pi r dr \tag{5}$$

where, r is the diameter of spherical shell volume. Then, one can express volumetric probability density function of the radial distance r for a particle that is confined into spherical space volume with radius r as,

$$P(r) = \int_0^r |\psi(r)|^2 4\pi r dr \tag{6}$$

This function expresses cumulative radial density function of a valance electron.

4. Probabilistic Atom Radius According to Orbiting Electron Probability

In quantum mechanics, one can mention probability of a particle to exist in space. Since atoms are composed of subatomic particles, probabilistic atomic radius is preferable to consider a spherical volume of atoms, where all building blocks or elements of an atom exist with a high probability in this volume. Even though radial probability density infinitely overlay throughout space, a finite space volume can be represented by a probabilistic boundary, which infers a space volume with a high probability of containing all elements of Bohr atom model (nucleus and electrons). A probability measure of $q \in (0,1)$ can be used to express such probabilistic boundaries or probabilistic confinement of space volumes of an atom. The probability measure q excludes the value of 0 because zero probability infers absence of electrons in space, and it also excludes the value of 1, which infers a definite existence of all elements of atom; however, it is only possible for infinite (unbounded) space volume with an infinite radius in quantum mechanical point of view.

The $q\%$ probabilistic atomic radius (r_q) represents a finite spherical volume around the nucleus of atom, which contains the outermost electron with a probability value of $q\%$. Probabilistic atom radius r_q can be calculated by solving the equation $P(r_q) = q$, which can be expressed by using cumulative radial density function of orbital electrons as

$$\int_0^{r_x} |\psi(r)|^2 4\pi r dr = q \tag{7}$$

This paper particularly considers 99% probabilistic radius ($r_{0.99}$) of hydrogen atom and presents an analysis for atomic radius and volume in quantum mechanical perspective. In order to calculate 99% probabilistic radius, the equation of $P(r_{0.99}) = 0.99$ is solved and $r_{0.99}$ radius is

calculated, numerically. Fig. 1 depicts $r_{0.99}$ probabilistic radius of an atom based on electron probability. In the spherical volume with $r_{0.99}$, valance electron exists with a probability of 99%.

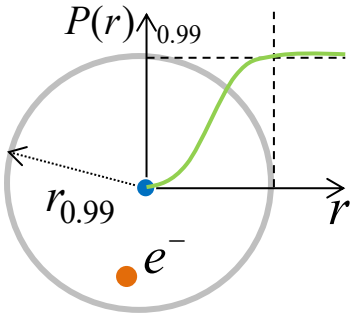

Figure 1: $r_{0.99}$ probabilistic radius of an atom

5. Probabilistic Atomic Radius ($r_{0.99}$) for Single Electron Hydrogen-like Atoms

The radial probability density of an electron for ground state hydrogen atom (the quantum numbers are $n = 1$, $l = 0$, $m_l = 0$ for 1s state) is written by multiplying the square of the normalized wave function, given by

$$\psi_{n,l,m_l}(r,\theta,\varphi) = R(r)P(\theta)F(\varphi) = \frac{2e^{-r/a_0}}{a_0^{3/2}}\frac{1}{\sqrt{2}}\frac{1}{\sqrt{2\pi}} = \frac{e^{-r/a_0}}{\sqrt{\pi}a_0^{3/2}} \tag{8}$$

[2,17-19] and the spherical shell volume element $4\pi r^2$ as follows:

$$dP = [\frac{e^{-r/a_0}}{\sqrt{\pi}a_0^{3/2}}]^2 4\pi r^2 dr = \frac{4}{a_0^3} r^2 e^{-2r/a_0} dr \tag{9}$$

For the probability of electron to be in the spherical volume, the following cumulative radial density function for existence of orbital electron in spherical volume surrounding a hydrogen nucleus is written according to Eqn. (6) as

$$P(r) = \int_0^r [\frac{e^{-r/a_0}}{\sqrt{\pi}a_0^{3/2}}]^2 4\pi r^2 dr \tag{10}$$

where parameter r is radial distance to nucleus of atom. The solution of Eqn. (10) is written by,

$$P(r) = 1 - \frac{1}{a_0^2}(a_0^2 + 2a_0 r + 2r^2)e^{-2r/a_0} \tag{11}$$

where, $a_0$is an atomic unit length, also known as Bohr radius. It is found as $a_0 = \frac{\hbar^2}{mke^2} = 0.0529\ nm \cong 0.53\ A^o$ [1]. 99% probabilistic atom radius ($r_{0.99}$) was defined as the radius of a spherical cage of the nucleus of hydrogen atom, where the electron is found with a probability of 99%. To calculate $r_{0.99}$, the following equation is written by consideration of $P(r_{0.99}) = 0.99$.

$$1 - \frac{1}{a_0^2}(a_0^2 + 2a_0 r_{0.99} + 2r_{0.99}^2)e^{-2r_{0.99}/a_0} = 0.99 \tag{12}$$

This equation can be numerically solved by using the code that is shown in Fig. 2. If numerical calculation is performed by Δr unit increment, error in calculations becomes less than Δr.

```
% Code for numerical calculation of probabilistic atomic radius rq for
ground state hydrogen atoms

% User configurations
a0=0.0529e-9; % Bohr radius in meter unit [m]
dr=0.001; % Unit increment of numerical calculation [m]
ri=(0:dr:1)*1e-9; % Sampled radial distance for numerical [m] calculation
q=0.99; % Sub-index of rq to set cummulative probability

% Calculation of cumulative radial probabilities and rq
P(1)=0;
for i=2:length(ri)
r=ri(i);
P(i)= 1 - (exp(-(2*r)/a0)*(a0^2 + 2*a0*r + 2*r^2))/a0^2
%For calculation of rq (probabilistic atom radius)
if (P(i)-q)*(P(i-1)-q)<0
%rx is assumed at mid-point of unit increment
rq=0.5*(ri(i)+ri(i-1));
end
```

Figure 2: Proposed code for numerical calculation of equation r_q for $q = 0.99$

Fig. 3 shows volumetric probability of electron in ground state (1s) hydrogen atom. According to proposed definition, $P(r_{0.99}) = 0.99$ is numerically solved and the 99% probabilistic atomic radius for isolated, ground state hydrogen atom is found $r_{0.99} \cong 2.2510^{-10}\ m$, which is about 4.2 Bohr radius ($4.2a_0$). In general, hydrogen atom is assumed to have one Bohr radius (a_0) and it coincides to an electron probability of 32% ($P(r_{0.32}) = 0.32$).

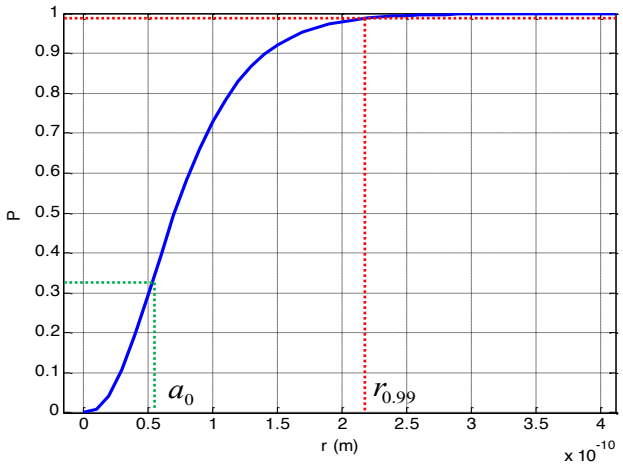

Figure 3: Cumulative probability density of electrons in spherical volume

Fig. 4 shows radial probability density function of ground state electron. The figure shows Bohr radius and the expected value of radial distance $< r >= 3a_0/2$ that is 1.5 times the Bohr radius. Bohr radius appears at a maximum of radial density function. As seen in figures, $r_{0.99} \cong 4.2a_0$ includes a large portion of radial probability density and implies a high probable inclusion of an electron by a spherical volume. The existence probability of the outermost element of atom, namely the valance electron probability, is considered. Bohr radius or expected value of radial distance does not imply a volume with such a high probable of electron existence. Fig. 5 shows two-dimensional (2D) view of atomic volumes in spatial domain, which are drawn corresponding to $r_{0.99}$ and a_0 radiuses. When compared, $r_{0.99}$ radii better represents size of atom in term of quantum mechanical aspects.

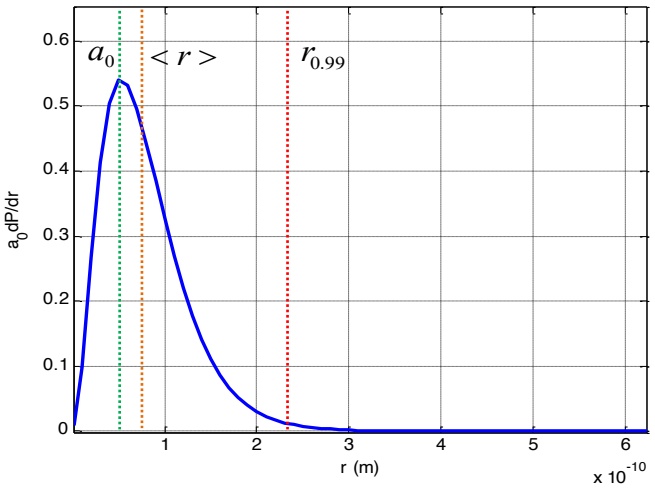

Figure 4: Radial probability density of hydrogen atom and some atomic radiuses

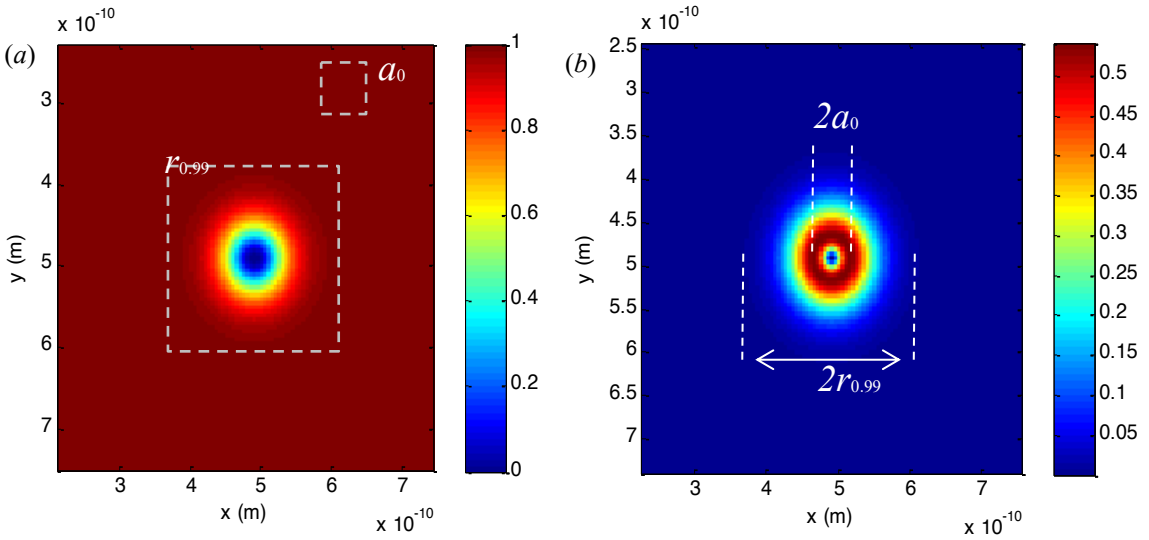

Figure 5: (a) 2D view of cumulative probability density of electrons in spherical volume **(b)** 2D view of radial probability density of hydrogen atom and comparisons of corresponding atomic radiuses

Table 1 compares values of several atomic radius definitions that can be applicable for hydrogen atoms. The $r_{0.99}$ probabilistic atomic radius has the largest value that ensures all fundamental elements (electron and proton) of a ground state hydrogen atom are included with a probability of 0.99 within the spherical space volume. The classes of q% probabilistic atomic radiuses ($r_q, q \in (0,1)$) can be particularly useful when analyzing and modeling quantum mechanical interaction among atoms and expressing their results. This definition can embody an atom in space with its quantum mechanical entity. Besides $r_{0.99}$ radius, Van der Waals radius and Critical cage radius can express a volume of Hydrogen atom with high possibilities of electron existence, which are 83% for Van der Waals radius and 70% for Critical cage radius, respectively.

Table 1: Values of several atomic radius definitions, which are applicable for hydrogen atom

Atomic Radius Definitions	**Values in nm**	**Normalized values (Bohr radius (a_0))**	**Their correspondence to probabilistic atomic radii (q% , r_q)**
Van der Waals radius	0.12	2.26	(83% , $r_{0.83}$)
Covalent radius	0.038	0.71	(17%, $r_{0.17}$)
Critical cage radius	0.097	1.83	(70%, $r_{0.70}$)
Peak probability atomic radius (Maximum of radial probability density)	0.0529	1	(32%, $r_{0.32}$)
Expected value of radial probability density	0.0794	1.5	(57%, $r_{0.57}$)
99% probabilistic atomic radius ($r_{0.99}$)	0.225	4.2	(99%, $r_{0.99}$)

6. Normalization of Spatial Domain according to Radial Probability Factor of Atoms

Another useful application of probabilistic radial distance $r_{0.99}$ is that, space surrounding nucleus of atom can be mapped to radial probability factor $q \in (0,1)$ that allows a normalization

of real distances according to cumulative radial probability of electrons. One of the advantages of this normalization is that it can compensate difficulties in analyses, which are associated with diversity in atomic radius. Use of radial probability factor $q \in (0,1)$ instead of spatial distance metrics allows consideration of a limited-range and common factor $q \in (0,1)$ for analysis of all atoms.

Normalization of spatial radial distance for q radial probability factor of hydrogen atom can be expressed as $d(q) = r/r_q$. Normalization of a spherical space volume can be expressed as $V(q) = (r/r_q)^3$. In this case, atom density can be normalized according to the electron probability as

$$\rho(q) = n/V(q) \tag{13}$$

where n is the number of atoms in the normalized volume $V(q)$ that is for probability factor q. Accordingly, one can analyze interaction between atoms on the bases of radial probability factor $q \in (0,1)$.

7. Conclusion

This study introduces a probabilistic atomic radius model that represents an atom with a nucleus centered spherical space volume according to cumulative radial probabilities of a valance electron. The $r_{0.99}$ probabilistic atomic radius expresses a spherical atom volume that is the most likely to observe a valance electron. This assumes the case that an electron can be found in this spherical volume with 99% probability. For ground state Hydrogen atom, atomic radius $r_{0.99}$ is calculated and its value is compared with values of other substantial atomic radius definitions.

Radius r_q definition allows sizing an atom in a space volume according to probability space of the time independent solutions of Schrödinger wave equation. Particularly, this probabilistic radius concept can contribute to analyze quantum mechanical interactions among atoms depending on a probabilistic radial dimension r, and this atomic radius concept can project the probability space to the real spatial space of atom.

Future studies can address calculation of $r_{0.99}$ values for higher quantum numbers and energy states of hydrogen atoms. While compressing hydrogen atoms, effects of interactions between atoms can be observed experimentally. In analysis of experimental results, changes in phase or properties of various atoms can be elaborated on the bases of probability factor q.

References

[1] Zettili, N., *Quantum mechanics: concepts and applications, 2nd ed.*, 408 pp, Wiley, 2013.

[2] Adamson, A.W., *Advanced inorganic chemistry. By F.A. Cotton and G. Wilkinson,* Inorganic Chemistry, 2 (3), 665–665, 1963.

[3] Bragg, W.L., *The arrangement of atoms in crystals*, Nature, 106 (2675), 725–725, 1921.

[4] Wyckoff, R.W.G., *On the hypothesis of constant atomic radii*, Proceedings of the National Academy of Sciences of the United States of America, 9 (2), 33–38, 1923.

[5] Huggins, M.L., *Atomic radii I,* Physical. Review, 19 (4), 346–353, 1922.

[6] Michels, A., De Boer, J., Bijl, A., *Remarks concerning molecural interaction and their influence on the polarisability*, Physica, 4 (10), 981–994, 1937.

[7] Montgomery, H.E., Sen, K.D., *Electron density and its derivatives at the nucleus for spherically confined hydrogen atom,* International Journal of Quantum Chemistry, 109 (4), 688–692, 2009.

[8] Xu, H., Qu, J., Zhang, M., Yan, Y., Sun, X., Zheng, Y., Qiu, M., Liu L., *The linear relationship derived from the deposition potential of Pb–Ln alloy and atomic radius,* New Journal of Chemistry, 42 (20), 16533–16541, 2018.

[9] Szarek, P., Witkowski, M., Woźniak, A.P., *Unconventional look at the diameters of quantum systems: could the characteristic atomic radius be interpreted as a reactivity measure,* The Journal of Physical Chemistry C, 123 (18), 11572–11580, 2019.

[10] French, S.J., *Nature of the chemical bond. second edition, revised (Pauling, Linus),* Journal of Chemical Education, 17 (11), 551, 1940.

[11] Sommerfeld, A., Welker, H., *Künstliche Grenzbedingungen beim Kepler problem*, Annalen der Physik, 424 (1–2), 56–65, 1938.

[12] Varshni, Y.P., *Critical cage radii for a confined hydrogen atom*, Journal of Physics B: Atomic, Molecular and Optical Physics, 31 (13), 2849–2856, 1998.

[13] Gill, P.M.W., Johnson, B.G., Pople, J.A.A., *Standard grid for density functional calculations*, Chemical Physics Letters, 209 (5), 506–512, 1993.

[14] Gill, P.M.W., Johnson, B.G., Pople, J.A., *Two-electron repulsion integrals over gaussian s functions*, International Journal of Quantum Chemistry, 40 (6), 1991.

[15] Slater, J.C., *Atomic shielding constants*, Physical Review, 36 (1), 57–64, 1930.

[16] Tang, C.L., *Fundamentals of quantum mechanics: for solid state electronics and optics*, Cambridge University Press, 224 pp, 2005.

[17] Griffiths, D.J., Schroeter, D.F., *Introduction to quantum mechanics 3rd ed.*, Cambridge University Press, 495 pp, 2018.

[18] Rogers, G.L.A., *Visual demonstration of the simple quantum theory of the hydrogen atom*, European Journal of Physics, 15 (3), 110–110, 1994.

Adıyaman University Journal of Science
https://dergipark.org.tr/en/pub/adyujsci
DergiPark AKADEMİK
ISSN 2147-1630
e-ISSN 2146-586X

Annealing Effect on Magneto-impedance in CoSiB Wires

Nevzat BAYRİ[1,*], Selçuk ATALAY[2], Veli Serkan KOLAT[3], Tekin İZGİ[4], Melike PEKTAŞ[5]

[1]*Department of Mathematics and Science, Education Faculty, Inonu University, Malatya, Turkey, nevzat.bayri@inonu.edu.tr, ORCID: 0000-0001-7105-7707*
[2]*Physics Department, Science and Arts Faculty, Inonu University, Malatya, Turkey, selcuk.atalay@inonu.edu.tr, ORCID: 0000-0002-8840-7766*
[3]*Physics Department, Science and Arts Faculty, Inonu University, Malatya, Turkey, veli.kolat@inonu.edu.tr ORCID:0000-0002-8864-5051*
[4]*Physics Department, Science and Arts Faculty, Inonu University, Malatya, Turkey, tekin.izgi@inonu.edu.tr, ORCID:0000-0002-4489-905X*
[5]*Physics Department, Science and Arts Faculty, Inonu University, Malatya, Turkey, dr.melikepektas@gmail.com, ORCID:0000-0003-2119-5014*

Received: 21.05.2020 **Accepted:** 03.12.2020 **Published:** 30.12.2020

Abstract

In this study, thermal treatments dependence of Magneto-impedance (MI) effect in $Co_{72.5}Si_{12.5}B_{15}$ wires has been investigated. Wires were annealed at 460 °C for different times (1-400 min). It was found that low time annealed leads to increase in magnetic softness. The largest change in the MI was observed at 1 MHz frequency value. It was determined that maximum MI, coercivity (H_c) and maximum field sensitivity (S) values were 247%, 1.28 A/m and 1.35% per A/m respectively in the wire annealed at 460 °C for 10 minutes. This high MI and field sensitivity value occurring in low annealed time shows that this wire can be used in the design of low magnetic field sensors.

Keywords: Amorphous wire; Magneto-impedance; Coercivity.

CoSiB Tellerin Manyeto-empedansında Isıl İşlem Etkisi

Öz

* Corresponding author DOI: 10.37094/adyujsci.740976

Bu çalışmada $Co_{72.5}Si_{12.5}B_{15}$ tellerde Manyeto-empedans (ME) etkinin ısıl işleme bağlılığı incelenmiştir. Numuneler 460°C'de farklı sürelerde ısıtılmıştır (1-400 dakika). Düşük süreli ısıl işlemlerin manyetik yumuşaklıkta artışa yol açtığı bulunmuştur. MI değerinde en büyük değişim 1MHz frekans değerinde gözlenmiştir. MI, H_c ve maksimum alan hassasiyet (S) değerleri 460 °C'de 10 dakika ısıl işlemde sırasıyla %247, 1.28 A/m ve A/m başına %1.35 olarak belirlenmiştir. Düşük ısıl işlem süresinde ortaya çıkan bu yüksek MI ve alan hassasiyet değeri bu telin düşük manyetik alan sensörlerinin tasarımında kullanılabileceğini göstermektedir.

Anahtar Kelimeler: Amorf tel; Manyetoempedans; Koersivite.

1. Introduction

The magneto impedance (MI) effect in amorphous wire, strip and films has been interesting due to the possible technological applications of these materials. [1-12]. When a magnetic material carrying a low intensity, high frequency alternating current is subjected to an external magnetic field, it exhibits a sharp change in its electrical impedance. This effect is known as the magneto impedance (MI) effect [1, 2]. In sensitive magnetic field sensor designs, besides high MI variation, field sensitivity values have an important place. The field sensitivity value of the MI against the applied external magnetic field is calculated using equation 1 as follows [2].

$$S = d\left(\frac{\Delta Z}{Z}\right)/dH \quad (1)$$

Alloy composition is important in obtaining MI curves. Different domain structures are observed depending on the alloy composition [2]. The domain structure of a material obtained by rapid cooling is determined by the interaction between internal stresses and magnetostriction [2]. Accordingly, the sign and magnitude of the magnetostriction value has an important role in MI effect. Magnetostriction value in amorphous ferromagnetic wires is negative in Fe based wires, positive in Co-based wires and approximately zero in CoFe based wires [2, 13-15]. Depending on the sign and magnitude of the magnetostricrion value, MI curves show single or double peak behaviors.

Different annealing treatment, such as furnace and current has an important role in the exchange of MI data [16-20]. In $Co_{75}Fe_{4.2}Si_8B_{12}Nb_{0.8}$ wires, the change of MI effect with annealing was studied [21]. In this study, while the maximum MI value was observed at a temperature of 450 °C for 25 minutes, it was observed that the value of MI decreased due to the formation of nanocrystalline phases at annealed above 25 minutes. Annealing applied to amorphous materials causes changes in MI effect. Therefore, in this work the thermal treatments dependence of MI effect in $Co_{72.5}Si_{12.5}B_{15}$ wires was investigated.

2. Materials and Methods

The $Co_{72.5}Si_{12.5}B_{15}$ wires produced by the melt spinning technique were cut 10 cm long. Samples were annealed in air in a non-inductive tube furnace at temperature of 460 °C for different times (1-400 min). The M–H curves were obtained using a dc digital system; the coercivity (H_c) was derived from the M–H curves. Sample impedance was measured using HP4294 impedance analyzer and HP4294A probe. MI data were obtained at 100 kHz, 1 MHz, 5 MHz and 10 MHz frequencies with 5 mA constant amplitude ac current. In magneto impedance measurements, solenoid was used for the outer dc magnetic field. The application of the Dc current along the solenoid was controlled by a computer. MI measurement system is given in Fig. 1. The data from the impedance analyzer were collected and averaged by the computer at each step of the magnetic field. The average of the impedance data leads to a large reduction in noise / signal ratio and thus clearer MI effect curves. The MI ratio was calculated from the equation $\Delta Z/Z\ (\%)=100[Z(H) - Z(Hmax)]/Z(Hmax)$, where Zmax is the impedance measured at a magnetic field of $H \approx 7400$ A/m.

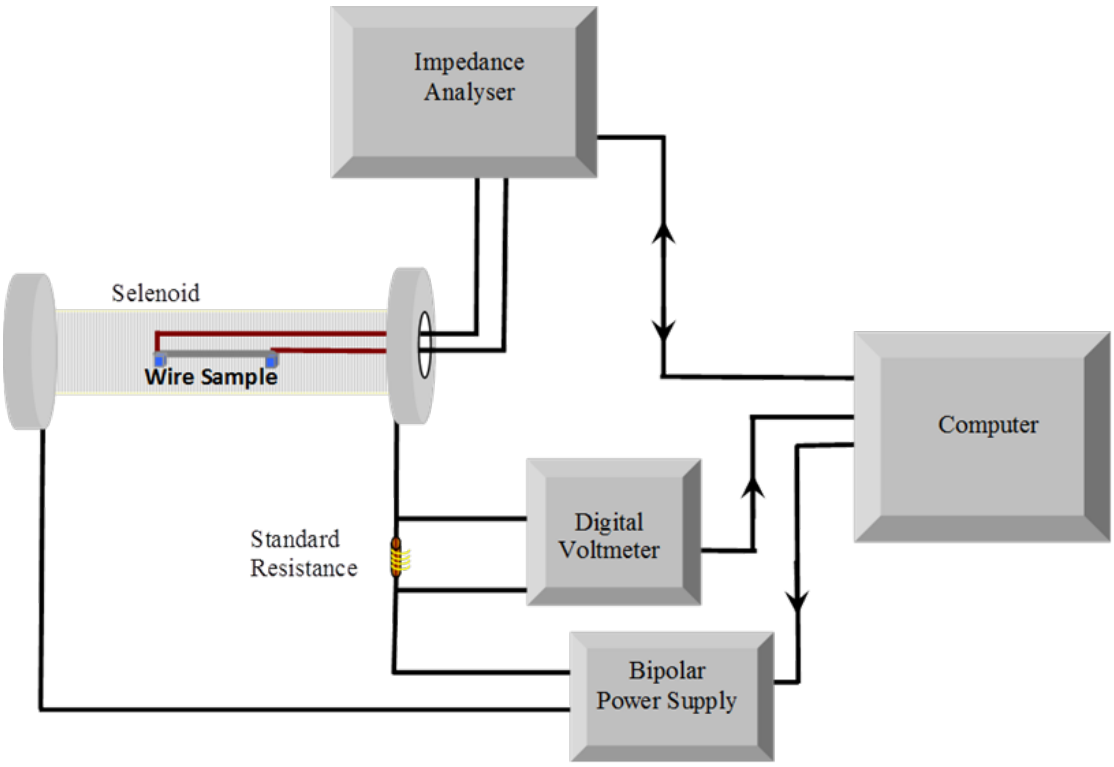

Figure 1: MI measurement system

3. Results

Fig. 2 shows MI curves for the as-received $Co_{72.5}Si_{12.5}B_{15}$ wire at various frequencies. MI values for 100 kHz, 1 MHz, 5 MHz and 10 MHz frequency values were measured as 67%, 149%, 81% and 68%, respectively. Fig. 3 presents the dependence of impedance on magnetic field in as-received and annealed samples in a particular case of 1MHz. Since the as-received CoSiB wire has a negative magnetostriction value, double peak behaviors were observed in the curves. [2, 14].

MI curves of $Co_{72.5}Si_{12.5}B_{15}$ wires, which are as-received and annealed at different times, was shown in Fig. 4. These curves were obtained by applying the frequency of 1 MHz. The highest value in magneto-impedance measurements was obtained on the wire which was annealed at 460 °C for 10 minutes. MI value for this wire was found to be 247%. It was determined that MI values changed with increasing annealed time and after 400 minutes the value decreased to 113%.

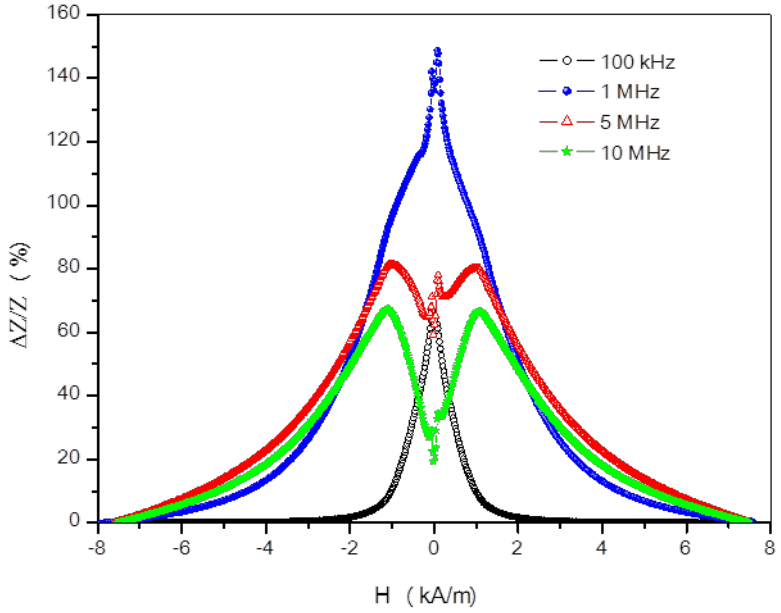

Figure 2: MI curves of as-received $Co_{72.5}Si_{12.5}B_{15}$ wire for different frequency

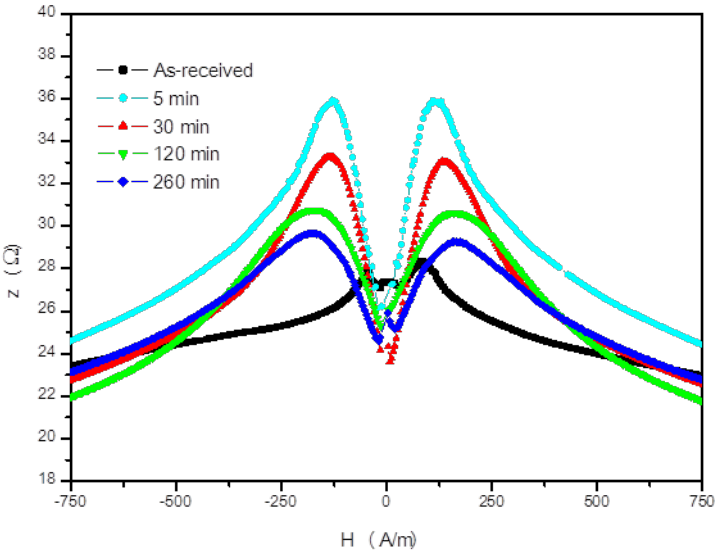

Figure 3: Impedance curves for as-received and annealed samples at 1 MHz

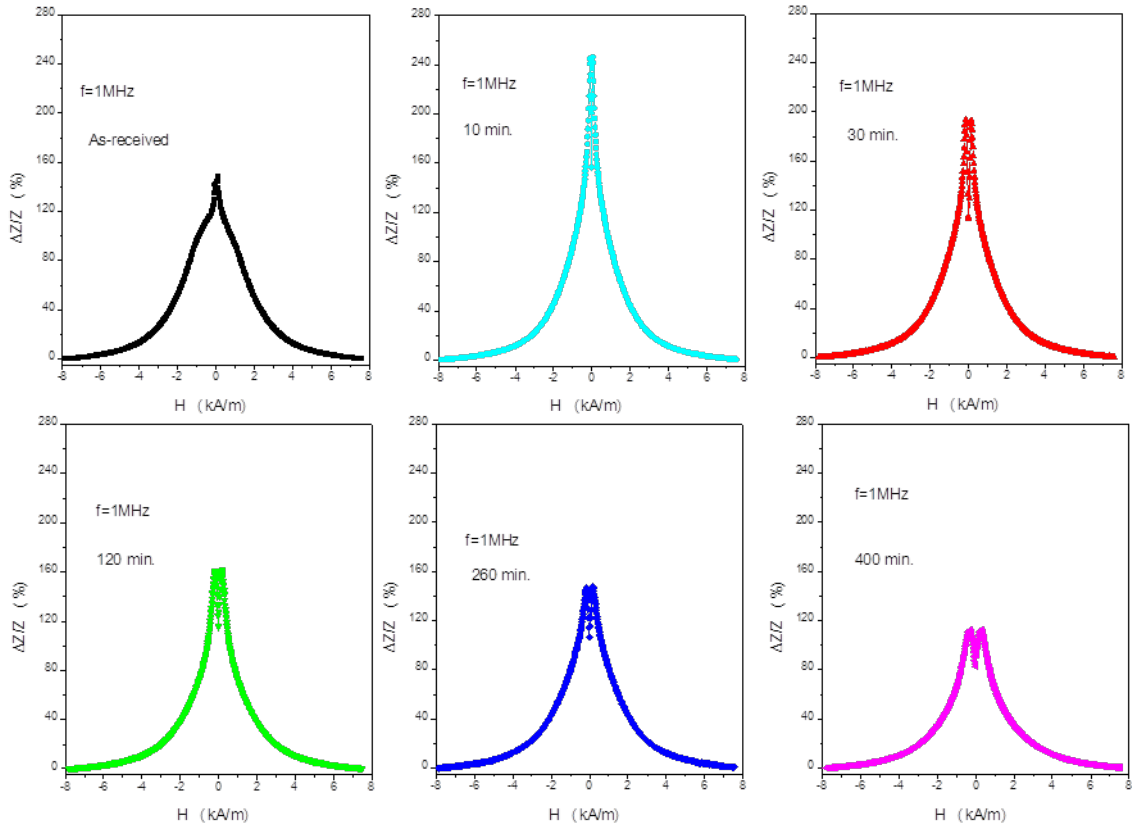

Figure 4: MI curves for as-received and annealed samples at 1 MHz

Fig. 5 shows variation of MI values as a function of annealing time for $Co_{72.5}Si_{12.5}B_{15}$ wires. The curves in Fig. 5 were obtained at the frequency values of 100 kHz, 1 MHz, 5 MHz and 10 MHz.

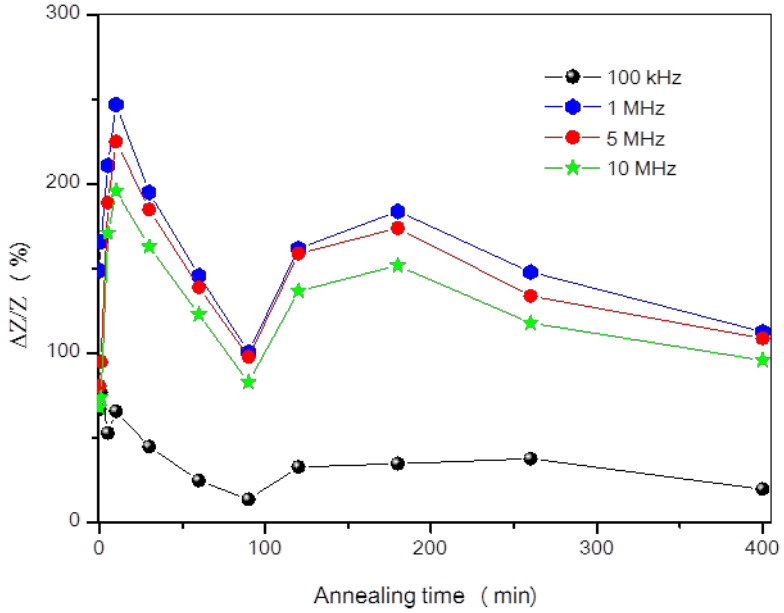

Figure 5: Variation of MI values as a function of annealing time

In the magnetic impedance measurements obtained for all frequency values, the greatest value has been observed on the wire annealed for 10 minutes. MI values were measured as 66%, 247%, 225% and 196% for the frequency values of 100 kHz, 1 MHz, 5 MHz, and 10 MHz respectively. As can be seen from Fig. 5, it is seen that MI values decrease sharply for all frequency values between 10-90 minutes. It was determined that MI values increased up to 180 minutes and decreased during the heat treatments over this time. MI values of $Co_{72.5}Si_{12.5}B_{15}$ wire annealed for 400 minutes. MI values were calculated as 20%, 113%, 109%, and 96% for 100 kHz, 1 MHz, 5 MHz, and 10 MHz frequency values respectively at 400 minutes annealing time.

Fig. 6 shows the magnitude of the MI and H_c values, a function of annealing time for the wires annealed at 460 °C. H_c and magneto-impedance changes were found to be compatible depending on the annealing time.

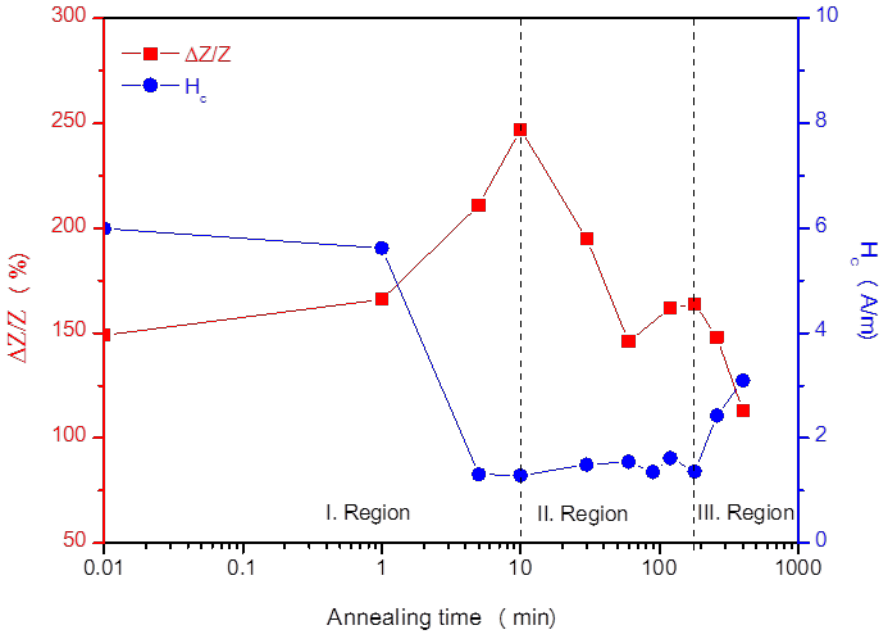

Figure 6: Variation of MI and H_c values with annealing time

Impedance and field sensitivity values (S) at ± 1000 A/m external magnetic field value were plotted in Fig. 7. In Fig. 7 (a), the double peak behavior against the applied external magnetic field is clearly seen. S values were determined as 1.2% per A/m and 1.35% per A/m in the positive and negative magnetic field directions, respectively (Fig. 7 (b)).

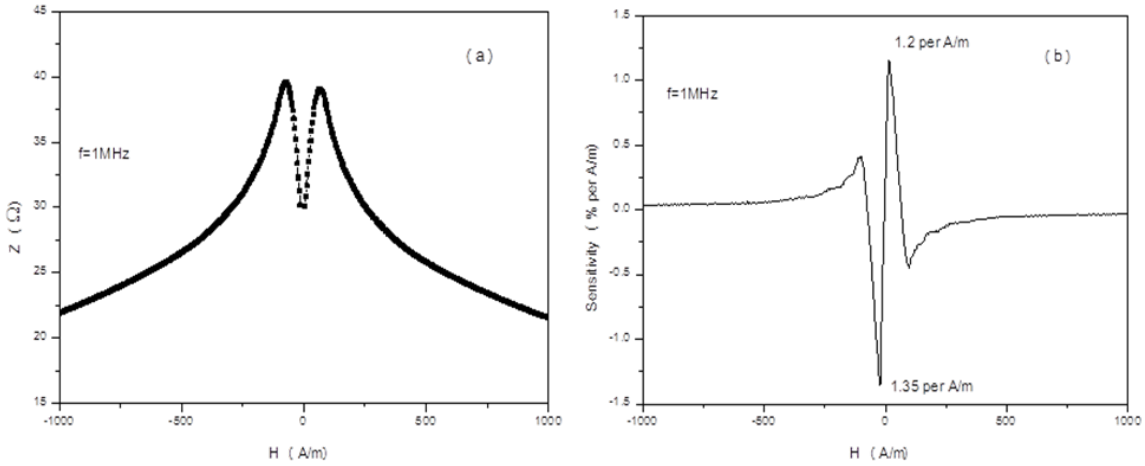

Figure 7: (a) Impedance, (b) field sensitivity values against the applied low field of the wire annealed at 460 C for 10 minutes. (f = 1 MHz)

4. Discussion

The magnetic permeability of the samples has an important role in the interpretation of MI data. The permeability of materials can be related to the skin effect. For a conductor carrying

a sinusoidal alternating current, the penetration or skin depth, d, is given by the well-known expression [22, 23]

$$\delta = \left(\frac{2}{\omega\sigma\mu}\right)^{1/2} \text{and } Z \propto {}^{1}/_{\delta} \quad (2)$$

where σ is the conductivity, ω is the ac current frequency and μ is the permeability.

It is also well-known that the permeability of a magnetic material is proportional to the total anisotropy (K) of a sample. For amorphous and nanocrystalline materials the main contributions to the anisotropy are the magneto-elastic anisotropy (K_{me}), shape anisotropy (K_D) and the magneto-crystalline anisotropy (K_{mcrys}) [4]. The K_D contribution is similar in all samples since the lengths of the as-received and annealed samples are the same. For this reason, K_{me} and K_{mcrys} are considered in the interpretation of the data. The total anisotropy value of the sample is inversely proportional to the impedance value due to magnetic permeability. Bearing this in mind, the effect of the annealing time on (ΔZ/Z) (%) and H_c values can be divided into three regions (see Fig. 6).

As can be seen in Fig. 6, I. Region is low annealed time (up to 10 minutes), II. Region medium annealed time (30-180 minutes) and III. Region shows the annealed time over 180 minutes. In the low annealed time, it was determined that both the H_c value reached a minimum (1.28 A / m) and the magneto impedance value reached a maximum value (247%). Annealing up to 10 min relieves the internal stresses, thus reducing K_{me}, and hence increasing MI values.

In the II. Region, a very small increase in H_c values and a sharp decrease in magneto-impedance value were observed up to 120 minutes of heat treatment. Between 120-180 minutes, a partial increase in magneto impedance value and very small changes in H_c values were determined. This is related to the surface crystallization that occurs in the sample [4, 16]. In longer annealed time, in the III. Region (over 180 minutes), boron phases are formed in the building [21]. Due to the formation of these phases, magneto crystal anisotropy occurs in the amorphous structure and this leads to an increase in the total anisotropy in the sample. Therefore, it was determined that H_c values increased and MI values decreased due to the increase of total anisotropy.

Field sensitivity values are also important in magnetic field sensor designs of samples with high MI variation. In the literature, the field sensitivity value for the as-received $Co_{72.5}Si_{12.5}B_{15}$ wire was calculated as 0.22% per A/m [14]. In our study, S value was determined as approximately 1.35% per A/m in the negative magnetic field region as a result of the low-time annealed (Fig. 7 (b)). This shows that the soft properties resulting from the low-time annealed increase the S value.

5. Conclusion

In this study, we observed that annealing time had a great effect on MI curves of $Co_{72.5}Si_{12.5}B_{15}$ wire. Especially low annealed time has been found to lead to an improvement in the magnetic softness, leading to an increase in MI effect. It was determined that MI and H_c values were 247% and 1.28 A/m in the wire annealed at 460 °C for 10 minutes. In addition, the S value of the wire annealed during this low-time was calculated as 1.35% in the negative magnetic field direction and 1.2% in the positive magnetic field direction per A/m. Maximum MI and S values indicate that this wire is suitable for magnetic field sensor design. When annealed time was over 180 min, nanocrystalline phase growing up improves the magneto crystalline anisotropy and reduces the MI effect.

References

[1] Lenz, J., Edelstein, S., *Magnetic sensors and their applications*, IEEE Sensors Journal, 6(3), 631-64, 2006.

[2] Phan, M.H., Peng, H.X., *Giant magnetoimpedance materials: Fundamentals and applications,* Progress in Materials Science, 53(2), 323-420, 2008.

[3] Kurlyandskaya, G.V., Sanchez, M.L., Hernando, B., Prida, V.M., Gorria, P., Tejedor, M., *Giant-magnetoimpedance-based sensitive element as a model for biosensors,* Applied Physics Letters, 82(18), 3053-3055, 2003.

[4] Kolat, V.S., Bayri, N., Michalik, S., Izgi, T., Atalay, F.E., Gencer, H., Atalay, S., *Magnetic and magnetoimpedance properties of Mn-doped FINEMET*, Journal of Non-Crystalline Solids, 355, 2562-2566, 2009.

[5] Vazquez, M., Knobel, M., Sanchez, M.L., Valenzuela, R., Zhukov, A.P., *Giant magnetoimpedance effect in soft magnetic wires for sensor applications*, Sensors and Actuators A-Physical, 59(1-3), 20-29, 1997.

[6] Velazquez, J., Vazquez, M., Chen, D.X., Hernando, A., *Giant Magnetoimpedance in Nonmagnetostrictive Amorphous Wires*, Physical Review B, 50(22), 16737-16740, 1994.

[7] Zhukov, A., *Design of the magnetic properties of Fe-rich, glass-coated microwires for technical applications*, Advanced Functional Materials, 16(5), 675-680, 2006.

[8] Atalay, F.E., Atalay, S., *Giant magnetoimpedance effect in NiFe/Cu plated wire with various plating thicknesses*, Journal of Alloys and Compounds, 392 (1-2), 322-328, 2005.

[9] Gazda, P., Szewczyk, R., *Novel giant magnetoimpedance magnetic field sensor*, Sensors, 20(3), 691, 2020.

[10] Xiao, S.Q., Liu, Y.H ., Yan, S.S., Dai, Y.Y., Zhang, L., Mei, L.M., *Giant magnetoimpedance and domain structure in FeCuNbSiB films and sandwiched films*, Physical Review B, 61(8), 5734-5739, 2000.

[11] Phan, M.H., Peng, H.X., Wisnom, M.R., Yu, S.C., *Giant magnetoimpedance effect in ultrasoft FeAlSiBCuNb nanocomposites for sensor applications*, Journal of Applied Physics, 98(1), 014316, 2005.

[12] Hernando, B., Sanchez, M.L., Prida, V.M., Tejedor, M., Vazquez, M., *Magnetoimpedance effect in amorphous effect in amorphous and nanocrystalline ribbons*, Journal of Applied Physics, 90(9), 4783-4790, 2001.

[13] Kamruzzaman, M., Rahman, I.Z., Rahman, M.A., *A review on magneto-impedance effect in amorphous magnetic materials*, Journal of Materials Processing Technology, 119(1-3), 312-317, 2001.

[14] Pal, S.K., Panda, A.K., Vazquez, M., Mitra, A., *The effect of magnetoeleastic interaction on the GMI behaviour of Fe-, Co- and Co-Fe-based amorphous wires*, Journal of Materials Processing Technology, 172, 182-187, 2006.

[15] Zhukov, A., Ipatov, A., Talaat, A., Blanco, J.M., Zhukova, V., *Engineering of Magnetic Properties of, Co-and Fe-rich Microwires*, IEEE Transactions on Magnetics, 54(6), 2000707, 2018.

[16] Bayri, N., Kolat, V.S., Atalay, F.E., Atalay, S., *The effect of furnace annealing and surface crystallization on the anisotropy*, ΔE *and magnetoimpedance effects in* $Fe_{71}Cr_7Si_9B_{13}$ *amorphous wires*, Journal of Physics D: Applied Physics, 37, 3067-3072, 2004.

[17] Atalay, S., *Comparative study of magnetoimpedance effect in current and field annealed (Co0.9Fe0.05Ni0.05)(75)Si15B10 amorphous ribbons*, Physica B-Condensed Matter, 368(1-4), 273-278, 2005.

[18] Dzhumazoda, A., Panina, L.V., Nematov, M.G., Yudanov, N.A., Tabarov, F.S., Morchenko, A.T., Ukhasov, A.A., *Influence of Current Annealing on the Temperature Dependences of Magnetoimpedance in Amorphous Microwires*, Technical Physics, 64(7), 990-993, 2019.

[19] Celegato, F., Coisson, M., Olivetti, E., Tiberto, P., Vinai, F., *A study of magnetic properties in CoFeSiB amorphous thin films submitted to furnace annealing*, Physica Status Solidi A-Applications and Materials Science, 205(8), 1745-1748, 2008.

[20] Ghanaatshoar, M., Tehranchi, M.M., Mohseni, S.M., Roozmeh, S.E., Gharehbagh, A.J., *Effect of magnetic field-current annealing on the magnetoimpedance of Co-based ribbons*, Journal of Non-crystalline Solids, 353(8-10), 899-901, 2007.

[21] Shuling, Z., Dawei, X., Jianfei S., *Effect of annealing on the giant magneto-impedance of Co-based Wires*, International Journal of Modern Physics B, 23(6-7), 1265-1269, 2009.

[22] Machado, F.L.A., Rezende, S.M., *A theoretical model for the giant magnetoimpedance in ribbons of amorphous soft-ferromagnetic alloys*, Journal of Applied Physics, 79(8), 6558-6560, 1996.

[23] Panina, L.V., Mohri, K., *Magneto-impedance effect in amorphous wires*, Applied Physics Letter, 65, 1189-1191, 1994.

Supplementary Information File

Adıyaman University Journal of Science
https://dergipark.org.tr/en/pub/adyujsci
ISSN 2147-1630
e-ISSN 2146-586X

Synthesis and Anticancer Activities of Water Soluble Schiff Base Metal Complexes

Burcu SAYGIDEĞER DEMİR[1,*], İlyas GÖNÜL[2], Gizem GÜMÜŞGÖZ ÇELİK[3], Seda İPEKBAYRAK[2], Yasemin SAYGIDEĞER[4]

[1]*Çukurova University, Central Research Laboratory, Adana, Turkey*
burcusaygidemir@gmail.com, ORCID: 0000-0001-5179-0522
[2]*Çukurova University, Arts and Science Faculty, Department of Chemistry, Adana, Turkey*
ilyasgonul01@gmail.com, ORCID: 0000-0002-7697-3613
seda_kzy@hotmail.com, ORCID: 0000-0001-7628-807X
[3]*Gebze Technical University, Faculty of Science, Department of Chemistry, Kocaeli, Turkey*
gizemgumusgozc@gtu.edu.tr, ORCID: 0000-0003-4816-7419
[4]*Çukurova University, Faculty of Medicine, Department of Pulmonry, Adana, Turkey*
yaseminsaygideger@gmail.com, ORCID: 0000-0003-3293-373X

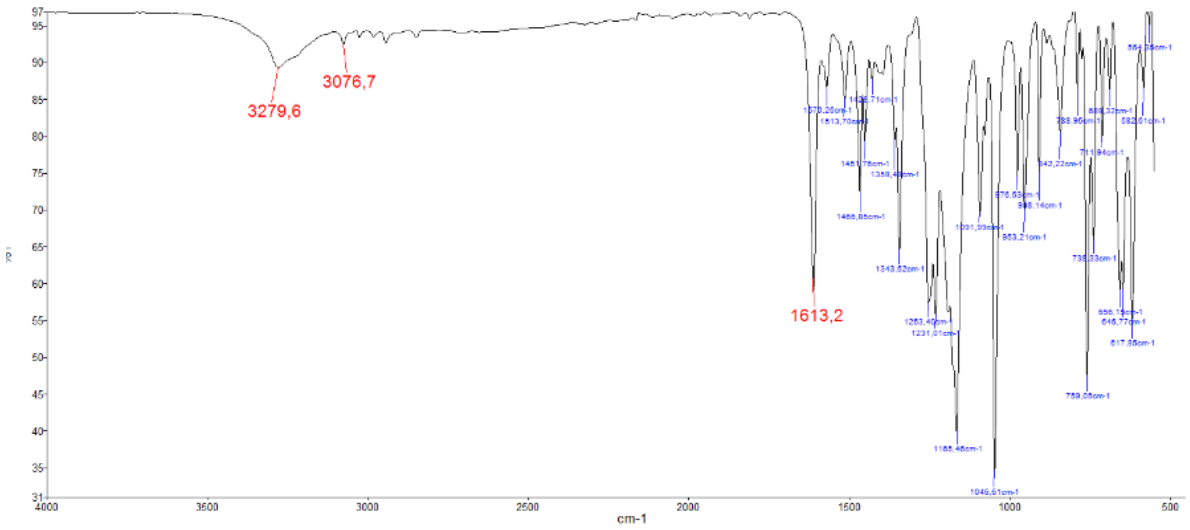

Figure S1: IR Spectrum of Schiff Base Ligand (L)

* Corresponding Author
DOI: 10.37094/adyujsci.738743

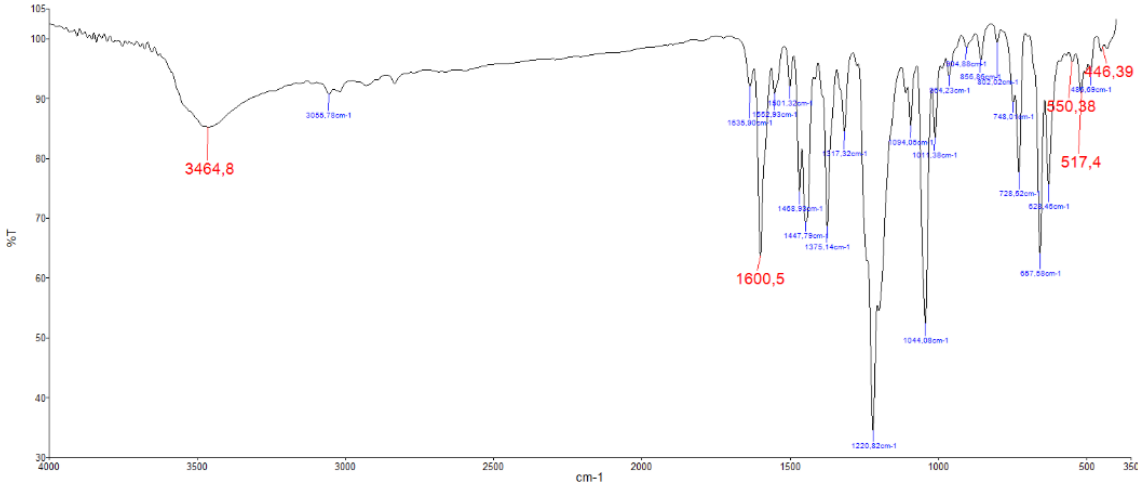

Figure S2: IR Spectrum of L-Cu Complex

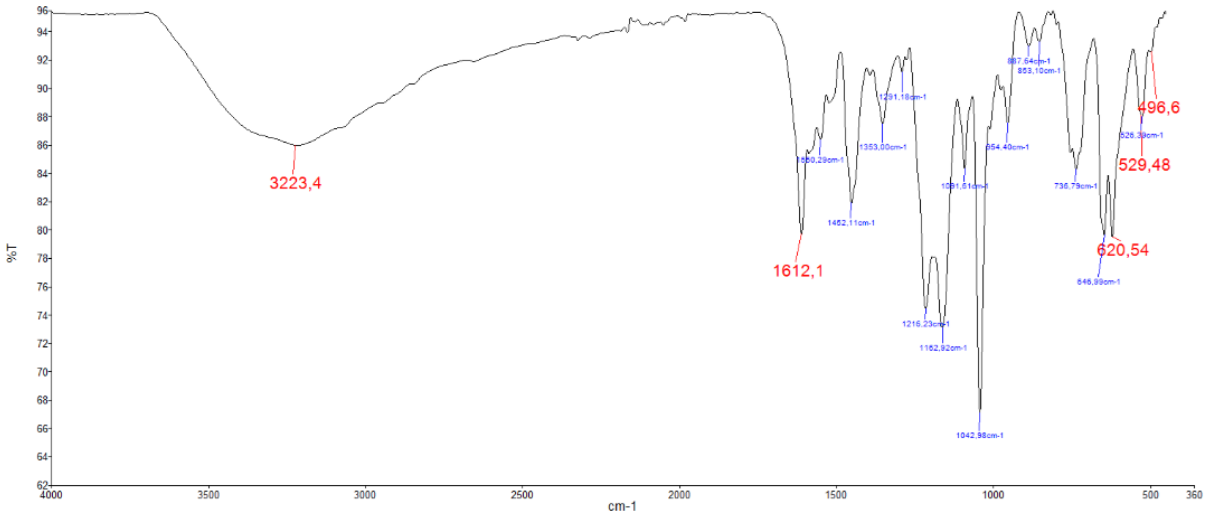

Figure S3: IR Spectrum of L-Ni Complex

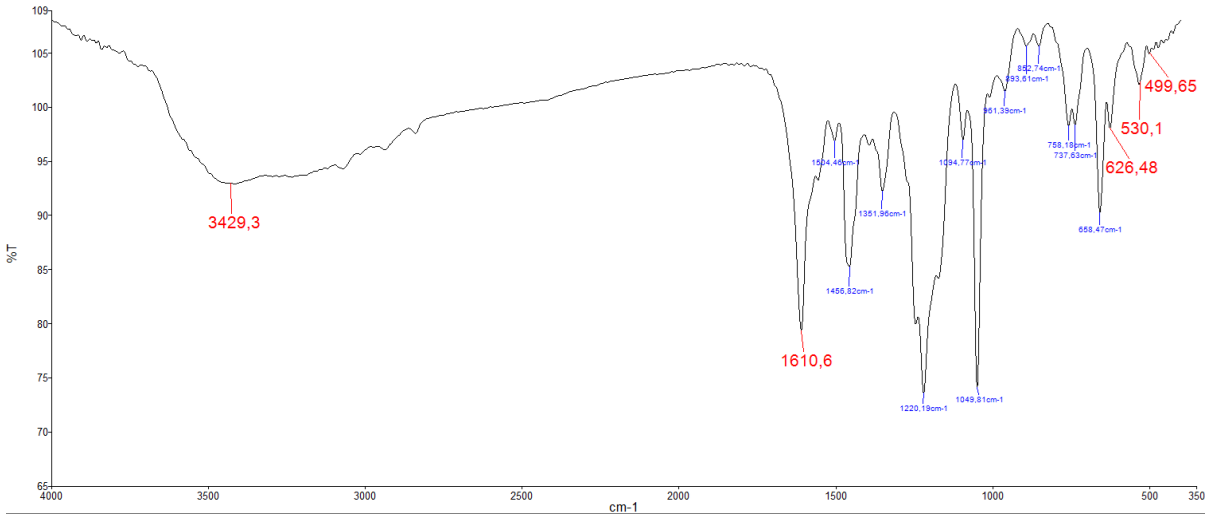

Figure S4: IR Spectrum of L-Zn Complex

* Corresponding Author
DOI: 10.37094/adyujsci.738743

Supplementary Information File

Adıyaman University Journal of Science
https://dergipark.org.tr/en/pub/adyujsci
ISSN 2147-1630
e-ISSN 2146-586X

Rapid and Specific Purification of RNA by PolyUracil Membranes

Canan ARMUTCU[1,*]

[1]*Hacettepe University, Faculty of Science, Department of Chemistry, TR-06800 Ankara, Turkey*
cananarmutcu@hacettepe.edu.tr, ORCID: 0000-0002-0920-2843

Captions

* Corresponding Author
DOI: 10.37094/adyujsci.780049

Supplementary Information File

Mathematical Operations on Experimental Data

Adsorption Isotherms at Equilibrium State

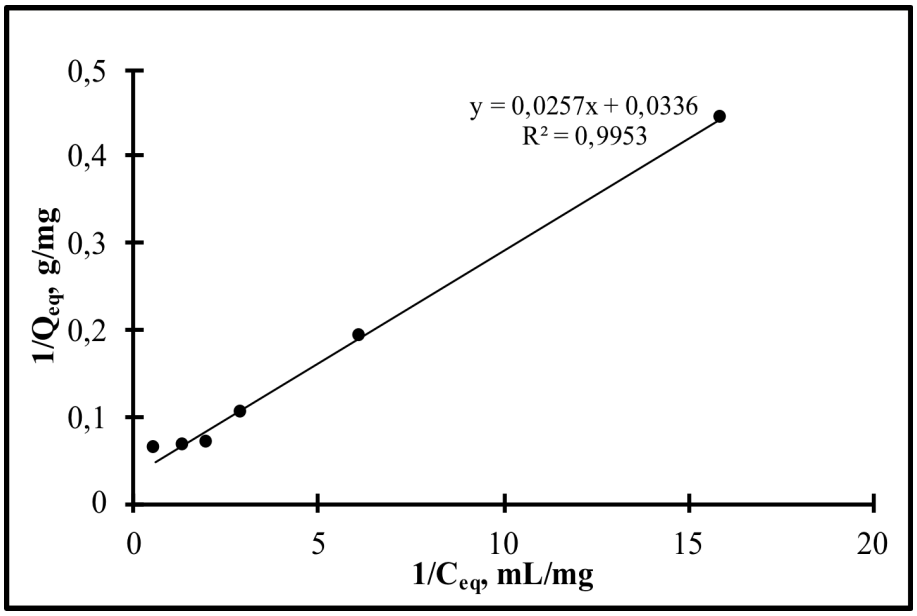

Figure SI-1: Langmuir isotherm.

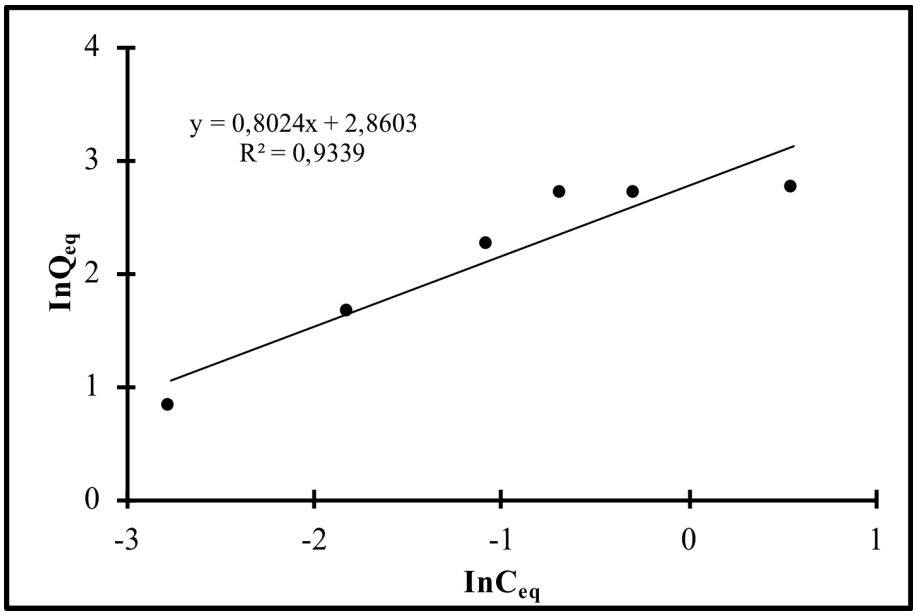

Figure SI-2: Freundlich isotherm.

* Corresponding Author
DOI: 10.37094/adyujsci.780049

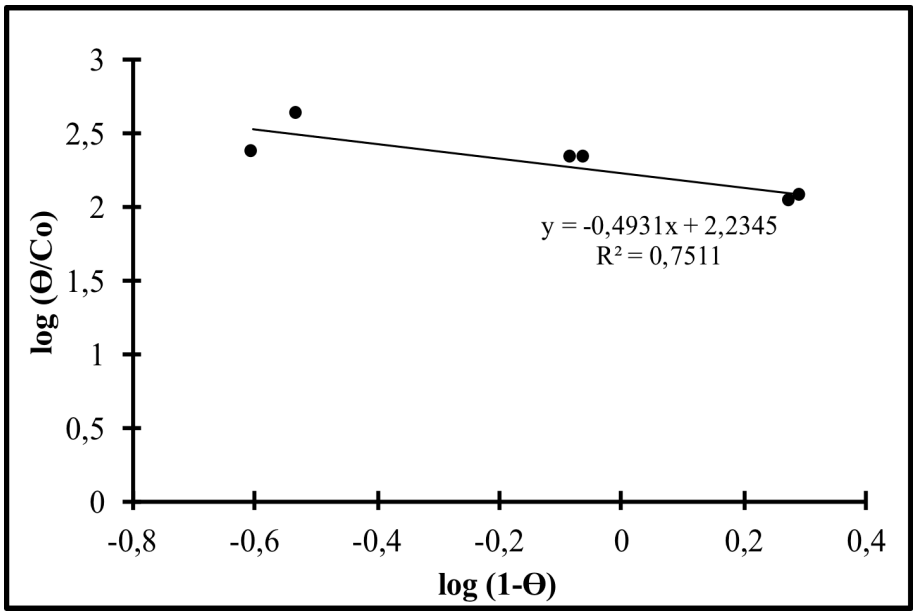

Figure SI-3: Flory-Huggins isotherm.

* Corresponding Author
DOI: 10.37094/adyujsci.780049

Kinetic Modelling

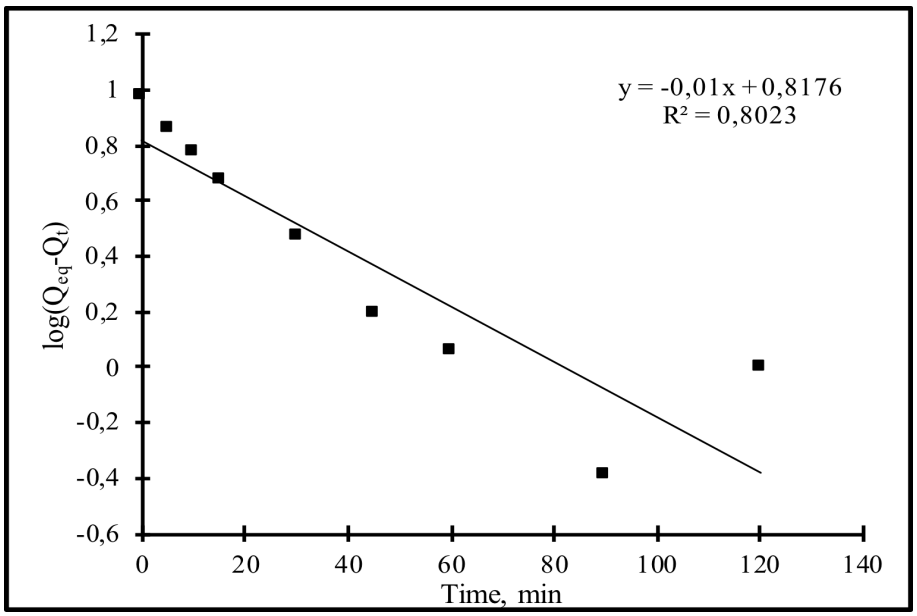

Figure SI-4: First order kinetic model.

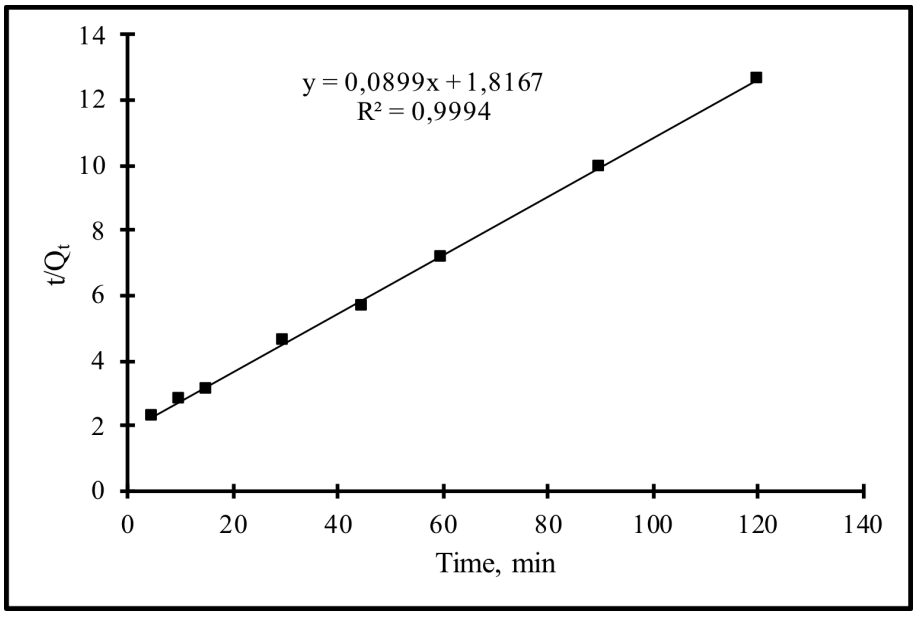

Figure SI-5: Second order kinetic model.

* Corresponding Author
DOI: 10.37094/adyujsci.780049

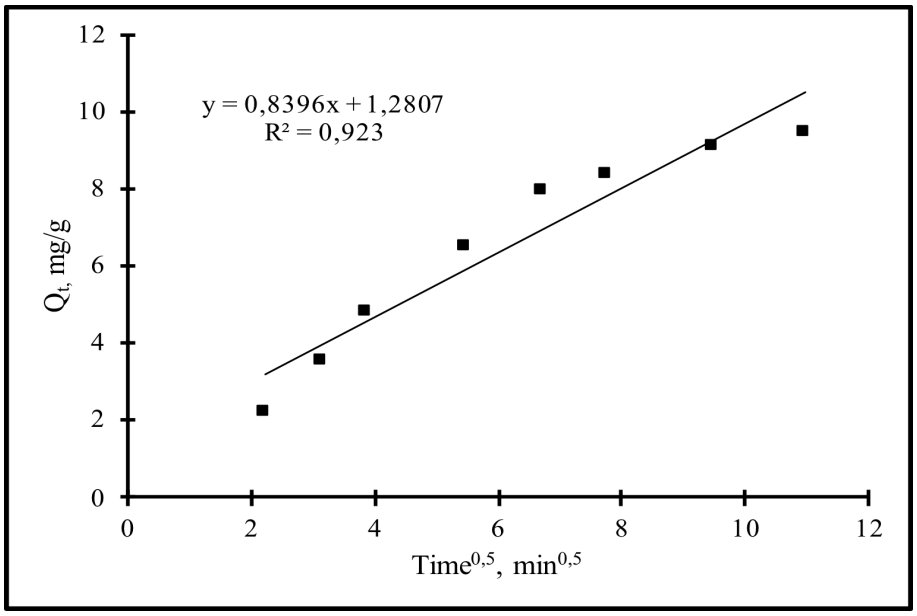

Figure SI-6: Weber-Morris model (intraparticle diffusion).

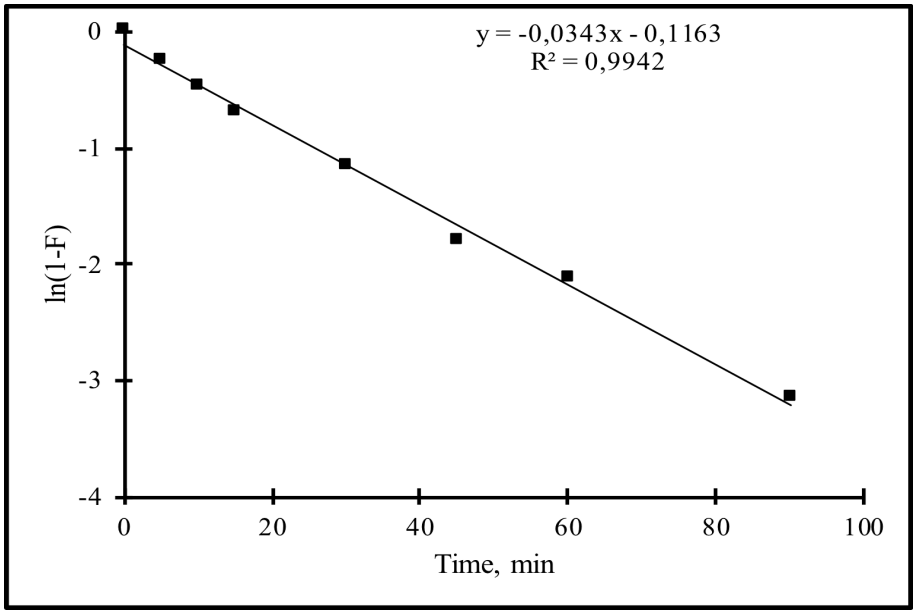

Figure SI-7: Film diffusion model.

* Corresponding Author
DOI: 10.37094/adyujsci.780049